

Transport of very short-lived substances from the Indian Ocean to the stratosphere through the Asian monsoon

Dissertation

for obtaining a binational doctoral degree

at the Faculty of Mathematics and Natural Sciences

of Christian-Albrechts-University Kiel, Germany,

and

the Faculty of Mathematics and Natural Sciences,

Department of Geosciences, Meteorology-Oceanography Section

of University of Oslo, Norway,

submitted by

Alina Fiehn

Kiel, October 2017



Christian-Albrechts-Universität zu Kiel

Mathematisch-
Naturwissenschaftliche Fakultät



**Faculty of Mathematics
and Natural Sciences**
University of Oslo

Supervisor at the University of Kiel: Prof. Dr. Christa A. Marandino
Supervisor at the University of Oslo: Prof. Dr. Kirstin Krüger

Date of Disputation: 03.11.2017

Abstract

Anthropogenic halogenated substances cause the ozone hole above Antarctica through catalytic ozone destruction and depletion of the stratospheric ozone layer, which shields the Earth from harmful ultraviolet radiation. Their emissions were regulated through the Montreal Protocol in 1989. Since the beginning of the 21st century, the amount of chlorine and bromine in the stratosphere from long-lived ozone depleting substances (ODS) has been decreasing and stratospheric ozone has started to increase slowly. Under these circumstances the importance of natural halogenated substances for atmospheric composition and chemistry will increase in the future. Trace-gases with atmospheric lifetimes of less than half a year belong to the so-called very short-lived substances (VSLS). The most important bromine containing VSLS bromoform (CHBr_3 , 17 days lifetime) and dibromomethane (CH_2Br_2 , 150 days) from marine sources currently contribute about 25% to the observed stratospheric bromine loading. In addition, the short-lived VSLS methyl iodide (CH_3I , 3.5 days) contributes to stratospheric iodine levels. Sulfur containing compounds, such as dimethylsulfide (DMS, 1 day), also influence stratospheric ozone. Sulfur supplies the stratospheric aerosol layer, which amplifies heterogeneous chemical ozone depleting reactions under high chlorine levels. DMS is a potential source of sulfur to the stratosphere. VSLS are naturally produced in the oceans by phytoplankton, macro algae, and photochemistry. They are primarily transported to the stratosphere with deep convection in the tropics and mainly enter the stratosphere over the Pacific warm pool in boreal winter and the Asian monsoon region in boreal summer. Major uncertainties still exist with respect to the oceanic emissions of halogenated VSLS from the Indian Ocean and their stratospheric entrainment through the Asian monsoon circulation. This thesis investigates the emissions of VSLS from the Indian Ocean and their transport to the stratosphere with novel combinations of data and modeling.

During the OASIS research cruise on RV Sonne in the subtropical and tropical West Indian Ocean in July and August 2014, the emissions of DMS, CH_3I , CHBr_3 , and CH_2Br_2 were determined for the Indian Ocean. These are the first open Indian Ocean observations of CHBr_3 and CH_2Br_2 . In this thesis, the Lagrangian particle dispersion model Flexpart with ERA-Interim meteorological fields is used to simulate high resolution transport of oceanic emissions from the Indian Ocean to the stratosphere with different modeling approaches and for different regions, seasons, and years.

In the first manuscript, the transport pathways of measurement-based halogenated VSLs emissions from the tropical and subtropical West Indian Ocean to the stratosphere during Asian summer monsoon is investigated from 2000-2015. During OASIS in 2014, we observed average emissions of CH_3I , high emissions of CHBr_3 , and very high emissions of CHBr_2 in the subtropical and tropical West Indian Ocean, especially south of Madagascar and in the open ocean upwelling between 10°S - 5°S . The transport to the stratosphere is more efficient than above the tropical Atlantic, but less efficient than in the West Pacific during previous cruises. There are two main transport pathways from the West Indian Ocean to the stratosphere during the summer monsoon. The tropical deep convection around the equator is more relevant for the shorter-lived VSLs such as CH_3I , while the monsoon convection over India and the Bay of Bengal and the Asian monsoon anticyclone transport mainly longer-lived VSLs like CHBr_3 and CH_2Br_2 to the stratosphere. Over the 16 years, interannual variability and a small increase in transport through the Asian summer monsoon is found.

The second manuscript reports about DMS emission measurements with the eddy-covariance technique from the same Indian Ocean research cruise in July-August 2014. The transport of DMS emissions in the troposphere and their influence on aerosol and cloud formation is investigated. A positive correlation between DMS emissions and satellite aerosol products indicate a local influence of marine DMS emissions on atmospheric aerosol formation, which impact the radiative budget.

After these two studies for the Asian summer season, the third manuscript considers the influence of the large seasonal differences of the Asian monsoon circulation. Therefore, the intra- and interannual variability of transport from the tropical West Indian Ocean to the stratosphere and its causes is investigated from 2000-2015. The pronounced annual cycle of VSLs entrainment is driven by the shifting monsoon winds. The transport efficiency to the stratosphere is enhanced by high local sea surface temperatures in the tropical West Indian Ocean all year round. It can also be enhanced during boreal spring by El Niño events and during boreal fall by La Niña events in the central and eastern equatorial Pacific through changes in the Walker circulation. Intra- and interannual variability of transport efficiency to the stratosphere is larger for VSLs with shorter lifetimes.

Due to the pronounced annual cycle in transport efficiency found in the third paper, seasonal and regional variations in the VSLs emissions from the Indian Ocean are assumed to influence their stratospheric entrainment as well. Thus, the focus of the fourth

manuscript is to investigate the influence of annually vs. monthly resolved oceanic VSLS emissions on stratospheric delivery seasons and regions. This manuscript contains a process study for CHBr_3 emissions and their transport from the tropical Indian Ocean and West Pacific to the stratosphere in 2014. The main oceanic source regions for stratospheric CHBr_3 are the Bay of Bengal and the Arabian Sea during boreal summer. The main stratospheric entrainment occurs during the same season over the southern tip of the Indian subcontinent. Using annual emissions, the highest CHBr_3 volume mixing ratio at the tropopause is simulated above the tropical central Indian Ocean in boreal spring, while monthly emissions have a maximum in boreal summer in the Asian monsoon anticyclone. This seasonal and regional difference shows the importance of resolving seasonal and regional variations of emissions for the Indian Ocean in modeling efforts.

At the end of this thesis, I calculate the contribution of VSLS from the Indian Ocean to total tropical VSLS emissions from different emission inventories. The Indian Ocean contribution of the three VSLS CHBr_3 , CH_2Br_2 , and DMS is higher than tropical averages, while CH_3I emissions are slightly lower. Furthermore, the contribution of these emissions to total stratospheric bromine, iodine, and sulfur from VSLS is estimated. The relative contributions from the Indian Ocean to the stratospheric abundances are always higher than the tropical average contribution. The Indian Ocean is an important source region for VSLS to the troposphere and stratosphere because of high emissions and efficient upward transport through the Asian monsoon especially during boreal summer.

Zusammenfassung

Anthropogene halogenierte Substanzen verursachen das Ozonloch über der Antarktis durch katalytische Ozonzerstörung und einen Schwund der stratosphärischen Ozonschicht, welche die Erde vor schadhafter ultravioletter Strahlung schützt. Seit 1989 reguliert das Montrealer Protokoll die Emissionen von langlebigen halogenierten Fluorchlorkohlenwasserstoffen. Seit dem Beginn des 21. Jahrhundert sinkt die atmosphärische Konzentration von Chlor und Brom aus den langlebigen anthropogenen Substanzen und das stratosphärische Ozon nimmt langsam wieder zu. Unter diesen Voraussetzungen wird die Bedeutung natürlicher halogenhaltiger Substanzen, vor allem sehr kurzlebiger Substanzen (engl. very short-lived substances, VSLS) mit atmosphärischen Lebenszeiten kürzer als ein halbes Jahr, für die Zusammensetzung und Chemie der Atmosphäre in der Zukunft zunehmen. Momentan beträgt der Beitrag von VSLS zum stratosphärischen Brom etwa 25%. Die beiden wichtigsten bromierten VSLS sind Bromoform (CHBr_3 , 17 Tage Lebenszeit) und Dibrommethan (CH_2Br_2 , 150 Tage). Weiterhin wird ein stratosphärischer Eintrag von Methyljodid (CH_3I , 3,5 Tage) und schwefelhaltigem Dimethylsulfid (DMS, 1 Tag) vermutet. Schwefel verstärkt die heterogene chemische Ozonzerstörung bei hohem Chlorgehalt in der Stratosphäre. VSLS werden im Ozean auf natürlichem Wege von Phytoplankton, Makroalgen und durch chemische Reaktionen produziert. Sie werden in tropischen Gebieten mit hochreichender Konvektion in die Stratosphäre eingetragen, hauptsächlich über dem tropischen Westpazifik im borealen Winter und der asiatischen Monsunzirkulation im borealen Sommer. Die Unsicherheiten bezüglich der VSLS-Emissionen aus dem Indischen Ozean und des Transportes durch den asiatischen Monsun in die Stratosphäre sind groß. Diese Arbeit untersucht erstmalig VSLS Emissionen aus dem Indischen Ozean und ihren Transport in die Stratosphäre mit einer neuartigen Kombination aus Daten und Modellierung.

Während der OASIS Forschungsfahrt auf dem Forschungsschiff Sonne im subtropischen und tropischen westlichen Indischen Ozean im Juli und August 2014 wurden die Emissionen von CH_3I und DMS und zum ersten Mal von CHBr_3 und CH_2Br_2 im offenen Indischen Ozean ermittelt. In dieser Arbeit wird das Lagrangsche Partikeldispersionsmodell Flexpart mit ERA-Interim verwendet, um den hochaufgelösten

Transport der ozeanischen Emissionen in die Stratosphäre mit verschiedenen Modellansätzen und für verschiedene Regionen, Saisons und Jahre zu modellieren.

Im ersten Manuskript werden die Transportwege der halogenierten VSLs aus dem subtropischen und tropischen Westindik im asiatischen Sommermonsun zwischen 2000-2015 bestimmt. Die aus den Messungen während OASIS in 2014 abgeleiteten Emissionen waren durchschnittlich für CH_3I , hoch für CHBr_3 und sehr hoch für CH_2Br_2 , insbesondere südlich von Madagaskar und im ozeanischen Auftriebsgebiet zwischen 10°S - 5°S . Der Transport in die Stratosphäre ist effizienter als im tropischen Atlantik, aber weniger effizient als im Westpazifik während vorhergehender Forschungsfahrten. Zwei Haupttransportwege in die Stratosphäre wurden durch die Simulationen diagnostiziert. Die hochreichende tropische Konvektion um den Äquator ist wichtiger für den Transport des kurzlebigen VSLs CH_3I , während die Monsunkonvektion über Indien und der Bucht von Bengalen und die asiatische Monsunantizyklone hauptsächlich die längerlebigen VSLs CHBr_3 und CH_2Br_2 in die Stratosphäre transportieren. Die Eintragszeitserie zeigt interannuale Variabilität und einen leichten Anstieg der Transporteffizienz vom tropischen Westindik in die Stratosphäre über die 16 Jahre.

Im zweiten Manuskript werden DMS-Emissionsmessungen mit der Eddy-Kovarianz Methode von der gleichen Fahrt im Indik präsentiert. Der Transport der DMS-Emissionen in der Troposphäre während des Sommermonsuns und ihr Einfluss auf Aerosolbildung wird untersucht. Die positive Korrelation zwischen DMS-Emissionen und Aerosolprodukten von Satellitenmessungen bestätigt den lokalen Einfluss von marinen Spurengasen auf atmosphärische Aerosole.

Nachdem die ersten beiden Studien lediglich den Transport während der borealen Sommermonate betrachten, beschäftigt sich das dritte Manuskript mit den Einflüssen der starken saisonalen Unterschiede in der asiatischen Monsunregion. Hier werden die intra- und interannuale Variabilität des Transportes vom tropischen Westindik in die Stratosphäre und ihre Ursachen im Zeitraum von 2000-2015 untersucht. Es gibt, einen ausgeprägten Jahresgang im stratosphärischen Eintrag getrieben von den wechselnden Monsunwinden. Die Transporteffizienz in die Stratosphäre wird das ganze Jahr über durch hohe lokale Meeresoberflächentemperaturen im tropischen Westindik verstärkt. Im borealen Frühling wird der Eintrag außerdem durch El Niño- und im borealen Herbst durch La Niña-Verhältnisse im zentralen und östlichen äquatorialen Pazifik intensiviert. Die intra- und interannuale Variabilität der Transporteffizienz in die Stratosphäre ist höher je kürzer die Lebenszeit der VSLs ist.

Aufgrund des starken Jahresganges in der Transporteffizienz sollte eine Saisonalität der Emissionen aus dem Indischen Ozean auch den stratosphärischen Eintrag beeinflussen. Deshalb liegt der Fokus des vierten Manuskriptes auf den Auswirkungen von jährlich und monatlich aufgelösten VLSL Emissionen auf die Saison und Region des Eintrages in die Stratosphäre. Das Manuskript enthält eine Prozessstudie für CHBr_3 -Emissionen aus dem tropischen Indik und Westpazifik und ihren Transport in die Stratosphäre in 2014. Das in die Stratosphäre eingetragene CHBr_3 kommt im borealen Sommer hauptsächlich aus der Bucht von Bengalen und dem Arabischen Meer. Der Eintrag in die Stratosphäre aus dem tropischen Indischen Ozean und Westpazifik ist über der südlichen Spitze von Indien konzentriert, ebenfalls im borealen Sommer. Werden jährliche Emissionen verwendet, so sind die simulierten CHBr_3 Mischungsverhältnisse an der Tropopause im borealen Frühling am höchsten. Monatliche Emissionen führen zu einem Maximum der Mischungsverhältnisse in der asiatischen Monsunantizyklone im borealen Sommer. Dieser saisonale und regionale Unterschied zeigt die Bedeutung der saisonalen und regionalen Auflösung der Emissionen aus dem tropischen Indischen Ozean für Modellstudien.

Am Ende der Doktorarbeit berechne ich den Beitrag der VLSL Emissionen aus dem tropischen Indischen Ozean zu den gesamten tropischen Emissionen aus verschiedenen Emissionsinventaren. Der Beitrag des Indik zu Emissionen der drei VLSL CHBr_3 , CH_2Br_2 und DMS ist höher als im tropischen Mittel, während CH_3I Emissionen etwas weniger als im Durchschnitt beitragen. Ich schätze außerdem den Beitrag dieser Emissionen zum gesamten stratosphärischen Brom, Iod und Schwefel aus VLSL ab. Der relative Beitrag des Indischen Ozeans zu stratosphärischen Konzentrationen ist für alle VLSL höher als der mittlere tropische Beitrag. Der Indische Ozean ist eine wichtige Quellregion für VLSL für die Troposphäre und Stratosphäre aufgrund der starken Emissionen und dem effizienten Transport in die Stratosphäre durch den Asiatischen Monsun besonders im borealen Sommer.

Manuscript Contributions

This thesis is based on the following manuscripts:

1. Manuscript 1: Delivery of halogenated VSLS to the stratosphere

Fiehn, A.; Quack, B.; Hepach, H.; Fuhlbrügge, S.; Tegtmeier, S.; Toohey, M.; Atlas, E.; and Krüger, K.: Delivery of halogenated very short-lived substances from the west Indian Ocean to the stratosphere during the Asian summer monsoon, *Atmos. Chem. Phys.*, 17, 6723-6741, <https://doi.org/10.5194/acp-17-6723-2017>, 2017.

My contribution: I designed the model experiments together with K. Krüger and B. Quack and I carried them out. I was involved in the VSLS measurements and analyses made during the OASIS cruise. I analyzed and interpreted the meteorological cruise data. I prepared the manuscript with help from K. Krüger and B. Quack with contributions from all co-authors.

2. Manuscript 2: The influence of air-sea fluxes on atmospheric aerosols

Zavarsky, A.; Booge, D.; Fiehn, A.; Krüger, K.; Atlas, E.; and Marandino, C.: The influence of air-sea fluxes on atmospheric aerosols during the summer monsoon over the Indian Ocean, under review at *Geophysical Research Letters*.

My contribution: I calculated the air mass back- and forward trajectories with Flexpart/ERA-Interim and helped writing and reviewing the manuscript.

3. Manuscript 3: Variability of VSLS transport to the stratosphere

Fiehn, A.; Quack, B.; Marandino, C. A.; Krüger, K.: Variability of VSLS transport from the West Indian Ocean to the stratosphere, under review at *Journal of Geophysical Research: Atmospheres*.

My contribution: I designed the model simulations with help from all co-authors and carried them out. I analysed the model data and wrote the manuscript with contributions from all co-authors.

4. Manuscript 4: Influence of seasonally resolved emissions

Fiehn, A.; Quack, B.; Stemmler, I.; Ziska, F.; and Krüger, K.: Influence of seasonally resolved emissions on the transport of bromoform from the Indian Ocean to the stratosphere, *Atmos. Chem. Phys.*, in preparation.

My contribution: I created the emission fields with advice from B. Quack. All co-authors designed the model experiments and I carried out the FLEXPART

calculations. I analyzed the model output and wrote the manuscript with contributions from all co-authors.

In addition, I contributed to the following publication through dispersion modelling with Flexpart:

Fuhlbrügge, S., Quack, B., Atlas, E., Fiehn, A., Hepach, H., and Krüger, K.: Meteorological constraints on oceanic halocarbons above the Peruvian upwelling, *Atmos. Chem. Phys.*, 16, 12205-12217, <https://doi.org/10.5194/acp-16-12205-2016>, 2016.

Contents

1	Introduction.....	3
1.1	Asian monsoon and the Indian Ocean	5
1.1.1	General circulation of the atmosphere	5
1.1.2	Asian monsoon circulation.....	7
1.1.3	Asian monsoon variability and trends	10
1.1.4	Transport of surface air to the stratosphere.....	14
1.1.5	Indian Ocean circulation	17
1.2	Very short-lived substances and their transport to the stratosphere	18
1.2.1	Marine production	18
1.2.2	Air-sea gas exchange.....	19
1.2.3	VSLs emission estimates	21
1.2.4	Atmospheric degradation and lifetimes.....	23
1.2.5	VSLs entrainment to the stratosphere.....	24
1.2.6	Impacts of VSLs on the stratosphere	26
2	Research Questions	29
3	Results.....	33
3.1	Manuscript 1	33
3.2	Manuscript 2	65
3.3	Manuscript 3	85
3.4	Manuscript 4	129
4	Summary, Conclusions, and Outlook	173
5	References.....	183
6	List of Figures	195
7	List of Tables	197
8	List of Abbreviations	199
	Curriculum Vitae	203
	Danksagung.....	205
	Eidesstattliche Erklärung	207

1 Introduction

The ozone hole above Antarctica was first discovered in 1984 (Chubachi, 1984; Farman et al., 1985). It occurs in southern hemispheric spring and is connected with catalytic depletion of the stratospheric ozone layer involving anthropogenic chloro- and bromofluorocarbons (Molina et al., 1974; Wofsy et al., 1975). The stratospheric ozone layer protects the Earth's surface from harmful ultraviolet (UV) radiation originating from the sun. This radiation impacts physiological and developmental processes in plants and increases the incidence of skin cancer, eye diseases, and infectious diseases in humans and animals (Van der Leun et al., 1995). Anthropogenic ozone depleting substances (ODS) cause a reduction of the stratospheric ozone abundances which is small around the equator, larger in the midlatitudes and most pronounced at the poles in spring. ODS have been widely used as refrigerants, propellants, solvents, extinguishers, fumigants, and cleaning agents before they were banned when the Montreal Protocol entered into force in 1989. Because of the long lifetimes of the major chlorofluorocarbons (CFC-11 around 50 years, CFC-12 around 100 years), their abundances in the atmosphere are decreasing slowly and a recovery of the global ozone level to 1960 values is projected for approximately the middle of the 21st century (WMO, 2014).

Beside the depletion of the ozone layer by ODS, there is also a contribution of natural chlorinated, brominated, and iodinated substances to ozone destruction. Bromine is important for ozone chemistry despite much lower stratospheric abundances than chlorine, since it is about 60 times more efficient at destroying ozone than chlorine (Sinnhuber et al., 2009). Iodine is more than 100 times as efficient as chlorine in depleting ozone (Ko et al., 2003). The impact of natural long-lived halogenated substances, mainly methyl chloride (CH_3Cl) and methyl bromide (CH_3Br), on the ozone layer is relatively well known (WMO, 2014). The role of shorter-lived bromine containing compounds in ozone depletion is, however, less certain. Recent balloon-borne stratospheric bromine measurements revealed a discrepancy between measured bromine abundances and those, that could be accounted for by long-lived gases (Dorf et al., 2006). The missing stratospheric bromine source is attributed to natural marine derived substances with lifetimes in the order of days to half a year, which are called very short-lived substances (VSLS) (Law et al., 2006). The two natural oceanic compounds bromoform (CHBr_3) and dibromomethane (CH_2Br_2) are estimated to contribute ~76% to VSLS bromine ($\text{Br}_y^{\text{VSLS}}$)

in the stratosphere using a top down approach (Hossaini et al., 2012). The natural oceanic VSLs methyl iodide (CH_3I) delivers small amounts of iodine to stratosphere, when it is emitted in regions with active convection (Solomon et al., 1994; Tegtmeier et al., 2013).

Polar ozone depletion occurs by heterogeneous reactions involving chlorine on the surface of polar stratospheric clouds, which mainly consist of sulfuric acid aerosols (Solomon et al., 2015). These aerosols are also the major constituents of the stratospheric background aerosol layer (Junge et al., 1961), which impacts Earth's radiative budget by cooling the surface climate (Solomon et al., 2011). The stratospheric background aerosol layer is supplied by long-lived natural substances from the ocean e.g. carbonyl sulfide (Crutzen, 1976; Kremser et al., 2016) and anthropogenic sulfur compounds such as sulfur dioxide (Myhre et al., 2004; Solomon et al., 2011; Sheng et al., 2015). Volcanic eruptions can significantly contribute to stratospheric sulfur (Mossop, 1964) over timescales of a few months to years. Oceanic DMS, the major biogenic sulfur carrier to the atmosphere (Liss et al., 2014), may despite its very short lifetime of around one day directly contribute to stratospheric sulfur in regions of pronounced tropical deep convection like the tropical West Pacific (Marandino et al., 2013). Furthermore, it contributes through the atmospheric conversion to carbonyl sulfide (Barnes et al., 1994) and subsequent entrainment to the stratosphere.

These very short-lived halogen and sulfur containing substances are naturally produced by phytoplankton and macroalgae (Moore et al., 1994; Carpenter et al., 1999; Stefels, 2000; Quack et al., 2003) and are emitted to the atmosphere when they are oversaturated in the surface ocean. The emissions of VSLs vary spatially and temporally and depend on the concentrations in ocean and atmosphere, as well as on physical parameters like sea surface temperature, salinity, and wind speed (Quack et al., 2003). VSLs are mainly transported to the stratosphere through fast uplift with deep convection in the tropics. The main entrainment regions of tropospheric air to the stratosphere, the so-called "stratospheric fountain", are the Pacific warm pool in boreal winter and the Asian monsoon in boreal summer (Newell et al., 1981). After entering the stratosphere, air is transported from the tropics toward the winter pole with the Brewer-Dobson circulation (Brewer, 1949; Dobson, 1956). Tropical oceanic surface sources of VSLs matter for the ozone cycle in the atmosphere and ozone depletion in midlatitudes and polar regions of the stratosphere (Oman et al., 2016; Fernandez et al., 2017).

Major uncertainties still exist with regard to the sources and strength of the highly variable VSLs emissions from the oceans and their transport to the stratosphere.

Especially emissions from the Indian Ocean, which is the most rapidly warming ocean basin in current climate change (Roxy et al., 2014), are poorly constrained due to very sparse data coverage in this ocean basin (Lana et al., 2011; Ziska et al., 2013). Furthermore, the Asian monsoon as important gateway for tropospheric air to the stratosphere (Fueglistaler et al., 2005) has not been studied in detail as a VLSL pathway with observations or models. Thus, it is important to investigate the emissions and transport processes of VLSL in the Asian monsoon region in order to calculate the contribution of natural halocarbons and sulfur under present-day conditions. Only by understanding the current situation can we begin to predict the influence of these natural compounds on the stratosphere in a future climate, which will likely include a slowing of the Asian monsoon circulation (Christensen et al., 2013).

The relative importance of natural halogenated compounds for ozone depletion will change in the future since the stratospheric chlorine abundances are declining due to the regulation of ODS emissions through the Montreal protocol. The ozone depletion efficiency of bromine will decrease with the future stratospheric abundance of chlorine and thus the chlorine-bromine ozone destruction cycle will become less efficient (Yang et al., 2014). Taking this depletion efficiency decrease into account, Tegtmeier et al. (2015) projected the ozone depletion potential of CHBr_3 to increase until 2100 due to enhanced emissions and larger convective mass flux. Furthermore, the emissions of CHBr_3 are projected to increase, if oceanic concentrations remain the same (Ziska et al., 2017). However, it is unclear what will happen to ocean concentrations in a future climate, as they depend on oceanic biological activity (Stemmler et al., 2015). The impact of future climate scenarios on oceanic biology is highly debated (Richardson et al., 2016; Roxy et al., 2016). Thus, projections of future VLSL influence on ozone are still inconclusive and detailed emission and transport studies are needed to reduce the existing uncertainties.

1.1 Asian monsoon and the Indian Ocean

1.1.1 General circulation of the atmosphere

The general circulation of the atmosphere depicts the mean global flow in the atmosphere averaged with time. The circulation is driven by the differential heating from the sun between the equator and the poles and further influenced by the rotation of the earth and the distribution of continents and oceans. The difference in incoming solar energy

between the equator and the poles causes a surface pressure gradient with low pressure at the equator and high pressure at the poles. This gradient accelerates surface air parcels towards the equator. They are deflected to the right on the northern hemisphere and to the left on the southern hemisphere due to the Coriolis effect, a result of the rotation of the earth and their movement away from the rotation axis. The movement toward the equator of surface air is interrupted by the deflected air masses in the midlatitudes, where westerly winds prevail. A circulation cell, called the Hadley cell, exists between the equator and the subtropics on each hemisphere (Figure 1). In these cells air parcels rise around the equator, flow towards the poles in the upper troposphere, descend in the subtropics and converge toward the center at the surface. The resulting tropical easterly winds at the surface are the trade winds and the temperature inversion occurring due to the descending air masses is called trade inversion. The low pressure center, called the intertropical convergence zone (ITCZ), is marked by rising air masses and intense rainfall. The position of the ITCZ and the accompanying rainfall shift over the year as the latitude of maximum incoming solar radiation moves towards the summer hemisphere of the Earth. On average, it is located around 5°N, but over the Indian Ocean its mean position is south of the equator (Schneider et al., 2014).

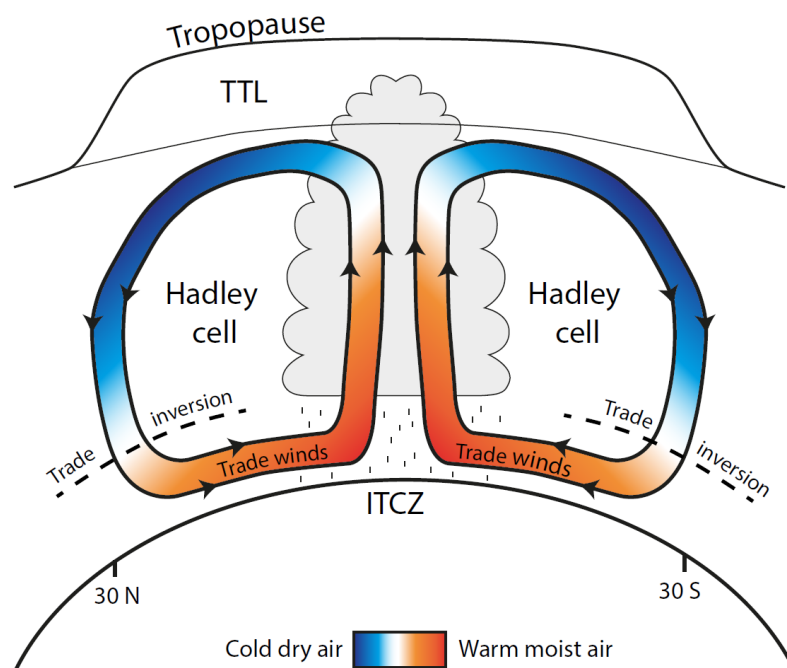


Figure 1: Schematic of the Hadley circulation. Abbreviations: TTL – Tropical tropopause layer, ITCZ – Intertropical convergence zone.

1.1.2 Asian monsoon circulation

The Asian monsoon dominates the atmospheric circulation above the Indian Ocean. The term monsoon refers to a seasonal shift in the prevailing surface winds. This shift is often accompanied by a change in the precipitation regime from a rainy season with onshore flow to a dry season with offshore flow (Krishnamurti et al., 2013). Ramage (1971) defined monsoon regions by a shift in the surface winds of at least 120° between January and July. More recent definitions include a local difference between summer and winter precipitation (called annual range; Wang et al., 2006; Figure 2) and the normalized seasonality in the wind field (Li et al., 2003). The monsoon has been described as a global-scale persistent overturning of the atmosphere that varies with the time of year (Trenberth et al., 2000). It can be divided into three regional monsoons, which are summarized under the term global monsoon: The American, the African, and the Asian-Australian monsoon.

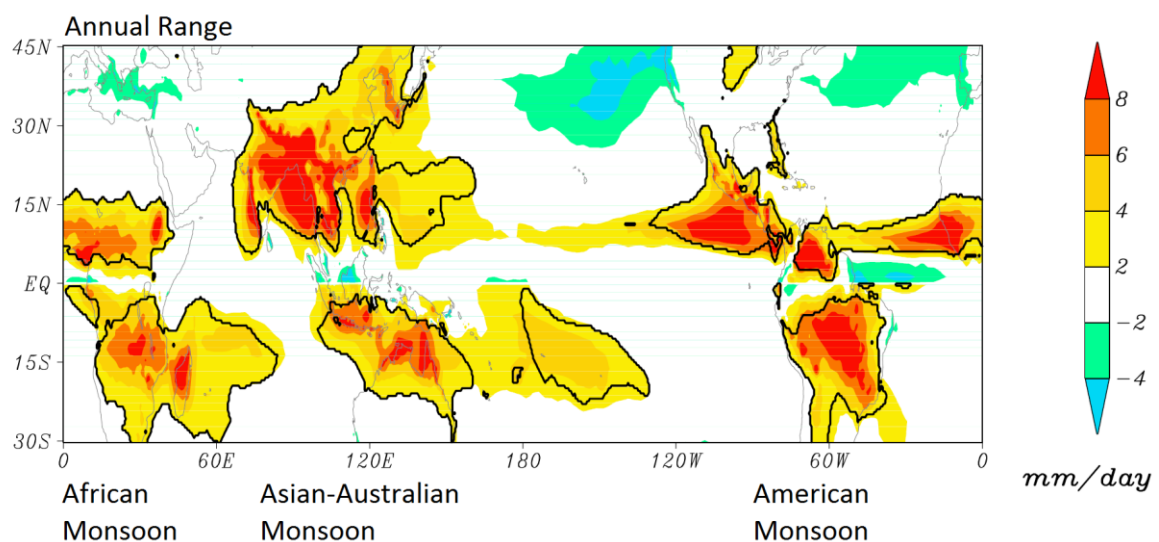


Figure 2: Annual range (difference between summer and winter precipitation) and global monsoon domain (delineated by the bold line) after the definition of Wang et al. (2006).

Webster (1987) suggested the monsoon to be a planetary scale moist sea-breeze modified by the Coriolis force. Satellite observations showed that the monsoon is also part of the planetary rain band connected with the ITCZ, only the amplitude of displacement from the equator is larger in monsoon regions (Sikka et al., 1980). Seasonally reversing winds are associated with large-scale heat sources and sinks. The Asian summer monsoon heat source first comes from the warm Indian subcontinent and is then intensified by the heavy rainfalls over India, Indochina, and China and the associated convective heating. Additionally, the elevated grounds of the Tibetan Plateau

absorb solar radiation and release it back into the atmosphere through sensible and latent heat fluxes above the sea level, meaning that the large-scale meridional temperature gradient also exists over significant depth in the troposphere. The boreal summer heat sink lies in the southern Indian Ocean between 30°S and 60°S and the southern part of the South China Sea (Krishnamurti et al., 2013). The temperature difference creates the Monsoon Low pressure system on the Asian continent and the Mascarene High above the ocean (Figure 3). The seasonal displacement of the ITCZ is amplified by these pressure systems. The global monsoons mainly respond to the net heating on planetary scales, but the regional monsoons depend on the distribution of land and ocean, as well as sea surface temperature (SST) gradients and topography (Webster, 1987). The uneven distribution of land and ocean between northern and southern hemisphere and the high altitude of the Himalaya create a pressure gradient that makes the Asian monsoon the most pronounced monsoon. The Asian monsoon is often divided into the Indian monsoon, also called South Asian monsoon, and the East Asian monsoon. These monsoons are two separate but interactive monsoon sub-systems (Wang et al., 2001).

The Indian summer monsoon surface winds develop above the southern Indian Ocean as southeast (SE) trades, flow across the equator and onto the Indian subcontinent as the Somali Jet and southwest (SW) monsoon, bringing moisture toward the convective centers over northern India and the Bay of Bengal (Figure 3).

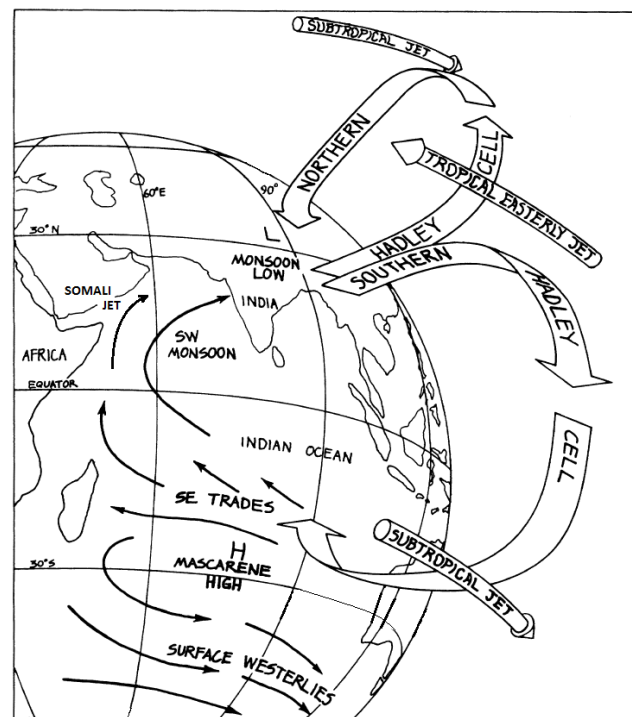


Figure 3: Schematic of the major circulation of the surface winds, the Hadley cell, and the jets of the Indian summer monsoon (after Meehl, 1987).

The release of latent heat from the convection establishes an upper tropospheric high pressure system with anticyclonic circulation above the Asian continent (Figure 4a). This pressure system, called Asian monsoon anticyclone, is flanked by the subtropical jet in the north and the Tropical Easterly Jet (TEJ) in the south (Dunkerton, 1995) (Figure 4b).

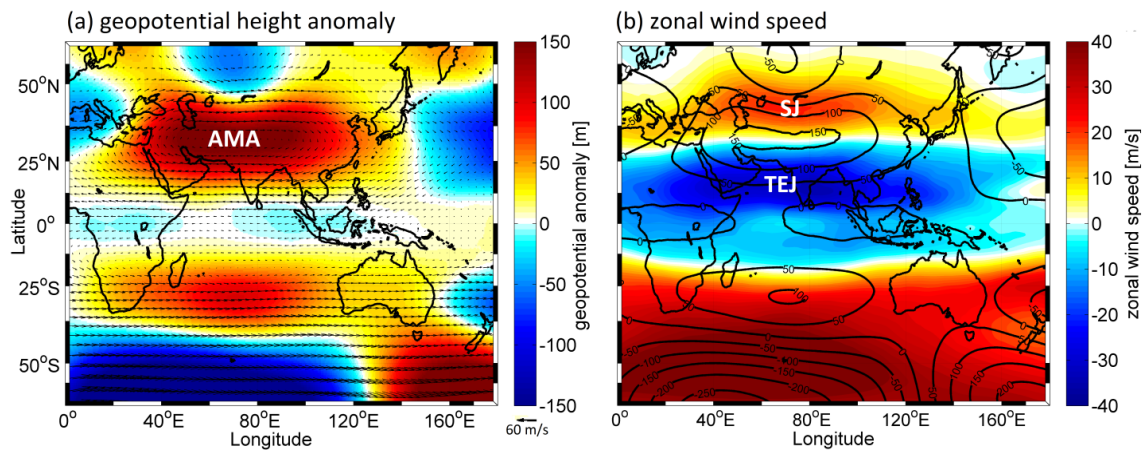


Figure 4: ERA-Interim monthly fields for July 2014 at 100 hPa for (a) geopotential height anomaly with wind arrows and (b) zonal wind speed with geopotential height anomaly contours. Abbreviations: Asian monsoon anticyclone (AMA), subtropical jet (SJ), Tropical Easterly Jet (TEJ).

The winter monsoon over Asia is characterized by northeasterly offshore winds both in India and East Asia and little rainfall over the continents. The ITCZ and accompanying rainfall over the Indian Ocean is located to the south of the equator. Figure 5 depicts the annual movement of main precipitation over the Indian Ocean. Note that some deep convection and rain remains around the equator, when the main convection center moves to the northern hemisphere in boreal summer.

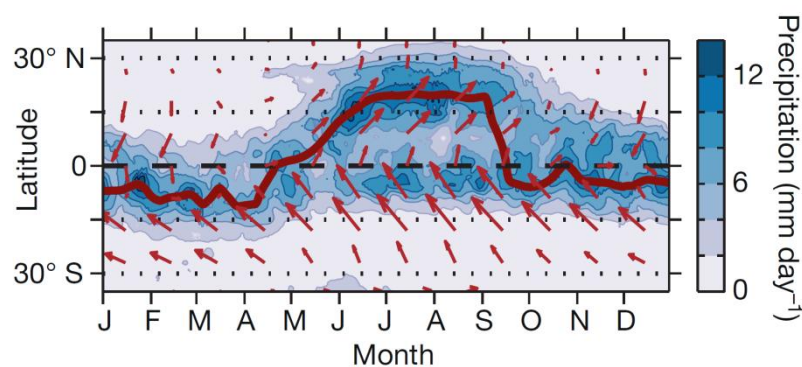


Figure 5: Annual shift of main rainfall and surface winds over the Indian Ocean. The red line marks the ITCZ (precipitation maxima) (Schneider et al., 2014).

1.1.3 Asian monsoon variability and trends

The Asian monsoon experiences variability on different time scales, from intraseasonal over interannual to inter-decadal and additionally long-term trends driven by changes and variability in the oceans and the atmospheric circulation. This thesis determines the seasonal and interannual variability in transport of VSLs from the ocean to the stratosphere via the Asian monsoon circulation. The seasonal variability is mainly driven by the strong annual cycle of the Asian monsoon. Interannual variability in the Asian monsoon exists and is connected to other oceanic or atmospheric phenomena acting on interannual scales in the tropics. Furthermore, this thesis briefly investigates short-term (15-year time period) changes in transport to the stratosphere, which may be caused by changes in the monsoon circulation and its drivers. These changes may impact the stratospheric delivery of VSLs and, thus, influence stratospheric composition and chemistry.

The variability of the Asian monsoon is expressed by certain physical parameters like rainfall and wind speed at different locations or heights. Some of the most important indices for the Asian and Indian monsoon are:

- All-India Rainfall Index (AIRI): sum of rainfall over the Indian continent during June to September (Parthasarathy et al., 1994),
- Extended Indian monsoon rainfall (EIMR): sum of rainfall including adjacent oceans covering 70° – 110° E, 10° – 30° N during June to August,
- Webster Yang Index (WYI): broad-scale South Asian summer monsoon index, vertical shear of zonal wind anomalies between 850 hPa and 200 hPa during JJA, (40° – 110° E, 0° – 20° N) defined in Webster et al. (1992),
- Indian Monsoon Index (IMI): dynamical index for the Indian monsoon, horizontal shear of zonal wind between a southern region (40° – 80° E, 5° – 15° N) and a northern region (70° – 90° E, 20° – 30° N) at 850 hPa (Wang et al., 1999; Wang et al., 2001).

In my thesis, I use the AIRI and IMI to investigate seasonal variability of atmospheric transport through the Indian monsoon. The characteristics of a pronounced Indian summer monsoon include a strong Mascarene high over the southern subtropical Indian Ocean, a distinct land-sea thermal gradient and a resulting enhanced cross-equatorial flow with increased moisture transport towards India (Webster et al., 2003).

Interannual variability in the tropics, especially the Indian and Pacific Ocean, is modulated by coupled ocean-atmosphere phenomena. These often also influence each other. The phenomena discussed here are the El Niño-Southern Oscillation (ENSO), the Indian Ocean Dipole (IOD), the Tropospheric Biennial Oscillation (TBO), and the Pacific Decadal Oscillation (PDO). A map of the areas, where indices for these phenomena and the IMI are defined, can be found in Manuscript 3 (Sect. 3.3).

El Niño-Southern Oscillation (ENSO)

The main interannual influence on the Asian monsoon is through ENSO (Webster et al., 1992; Ju et al., 1995) (Figure 6). It is a coupled ocean-atmosphere phenomena in the equatorial Pacific, with remote influences around the globe. The easterly trade winds over the Pacific push warm surface waters towards the west inducing an SST gradient of about 5°C between the West Pacific warm pool and the East Pacific. The movement of water mass also causes sea level differences around 0.5 m between the east and the west, an inclination of the thermocline, the border between warm surface and cold bottom water, and upwelling of cold bottom water along the South American coast. This upwelling is increased by the offshore Ekman transport induced by the southerly winds along the South American coast. The equatorial easterly winds above the Pacific are part of the atmospheric Walker circulation (Walker, 1924). It is an earth encompassing zonal circulation in the tropics with atmospheric upwelling over the warm continents, downwelling over the oceans, and compensating horizontal easterly or westerly winds at the surface and in the upper troposphere.

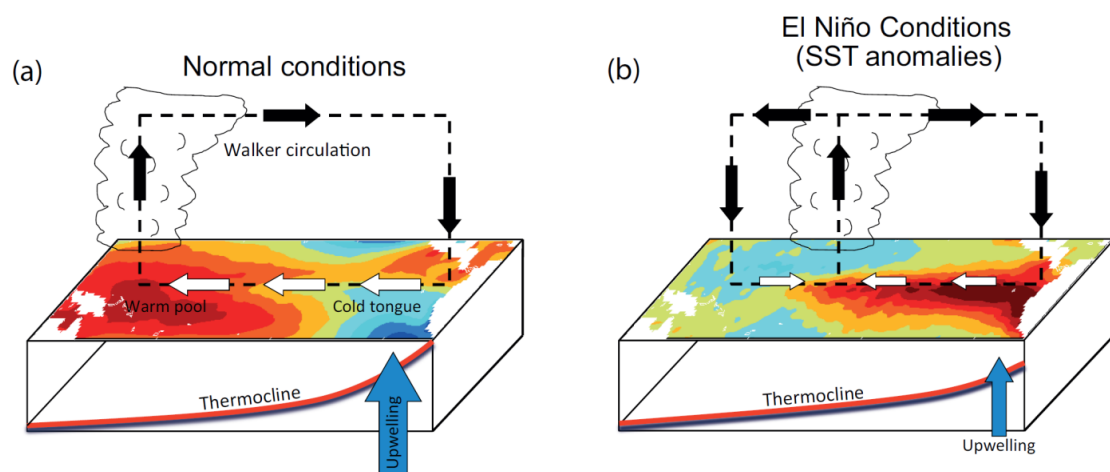


Figure 6: (a) West Pacific SST, Walker cell and upwelling during ENSO neutral conditions. (b) West Pacific SST anomalies, Walker cells and reduced upwelling during El Niño conditions (Christensen et al., 2013).

The state of the Pacific Ocean is sustained by the positive Bjerknes feedback (Bjerknes, 1969): The SST difference across the equatorial Pacific limits convection to the West Pacific, which creates a pressure gradient strengthening the easterly winds. The variation of the pressure gradient between the East and the West Pacific is called the Southern Oscillation and is the atmospheric part of the coupled phenomena. Perturbations to this ocean-atmosphere feedback weaken the whole system and cause large variability known as ENSO. If, for example, the trade winds are weakened due to westerly wind bursts originating in the Indian Ocean, less water is displaced to the West Pacific, the East Pacific warms and the oceanic upwelling along the South American coast is reduced. This is called an El Niño (Spanish: Christ Child) event, because it is observed around Christmas time in boreal winter. The opposite event (La Niña, the girl) supports stronger than normal trade winds, lower temperatures in the East Pacific and enhanced oceanic upwelling. El Niño events occur every 3-7 years and can be described by SST anomalies in the equatorial Pacific in different regions (Nino3: 150°–90°W, 5°S–5°N; Nino4: 160°E–150°W, 5°S–5°N). The influence of ENSO on the Asian monsoon is mainly through its modulation of the Walker circulation (Ju et al., 1995; Wang et al., 2001, Figure 6, Manuscript 3), but also due to a basin wide warming during El Niño in the adjacent Indian Ocean (Schott et al., 2009). For the Indian monsoon, a developing El Niño generally means less summer monsoon rainfall and vice versa for La Niña (Wang et al., 2001) (Figure 7). This connection and its influence on VSLs transport to the stratosphere are described in more detail in Manuscript 3 (Sect. 3.3).

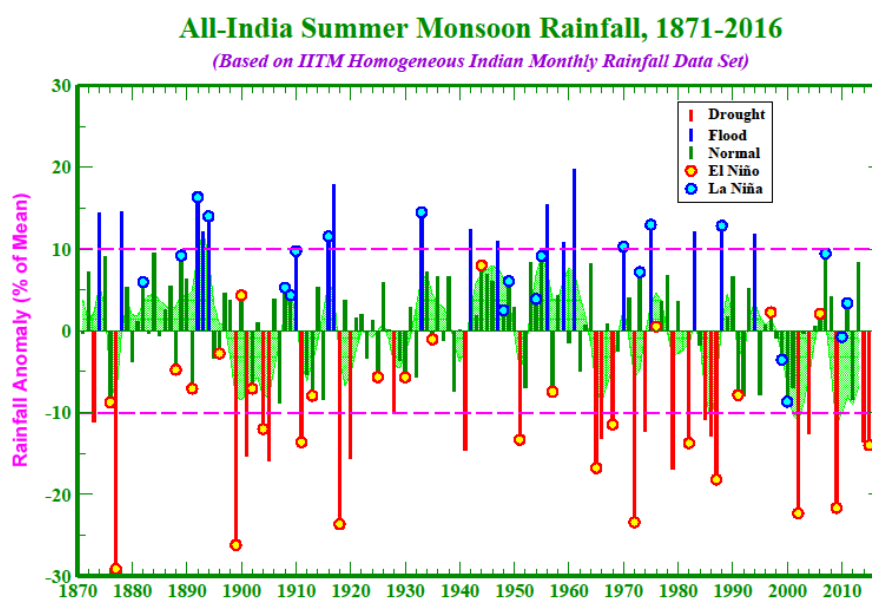


Figure 7: Time series of All-India Summer (JJA) monsoon rainfall and ENSO events (Kothawale et al., 2016).

Indian Ocean Dipole (IOD)

The IOD describes the SST anomaly between the West and East Indian Ocean, which has been shown to influence convection and rainfall in that basin (Figure 8). The Dipole Mode Index (DMI), used to describe the IOD, is defined as the SST difference between a western (50°E - 70°E , 10°S - 10°N) and an eastern (90°E - 110°E , 10°S - 0°) area in the Indian Ocean (Saji et al., 1999). A positive IOD event (a colder eastern Indian Ocean) during boreal summer suppresses deep convection in that region, enhances northward moisture transport toward the monsoon convection and causes more monsoon rainfall (Behera et al., 1999; Ashok et al., 2001).

The tropical circulation has the tendency that a relatively strong Indian monsoon is followed by a relatively weak one, and vice versa. This phenomena is called the Tropical Biennial Oscillation (TBO, Meehl et al., 2002). ENSO, the IOD, and the TBO are all tied together by the Walker circulation over the Indian and Pacific Ocean in the atmosphere (Meehl et al., 2002). The Pacific Decadal Oscillation describes the recurring SST pattern in the Pacific, with anomalies poleward of 20°N (Mantua et al., 2002). On a longer than interannual time scale, the PDO has a similar impact on the Indian summer monsoon rainfall as ENSO, with a negative PDO phase related to an increase in summer monsoon rainfall and vice versa (Krishnan et al., 2003).

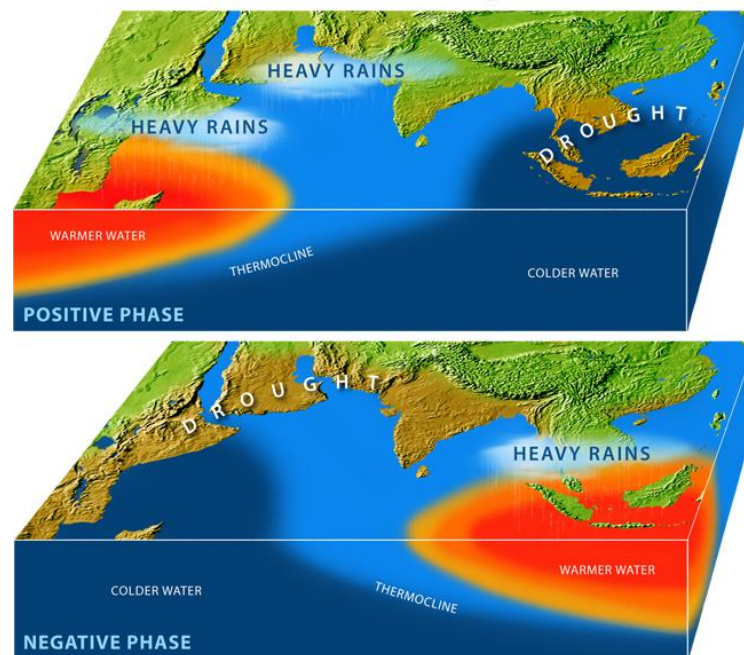


Figure 8: Sea surface temperature anomalies and rainfall patterns during positive and negative Indian Ocean Dipole events (Illustration by Paul E. Oberlander, 2017, Woods Hole Oceanographic Institution).

The Asian monsoon circulation has experienced long-term changes due to greenhouse gas induced global warming in the last decades (Christensen et al., 2013). The Indian Ocean has been warming for over a century, at a rate faster than any other ocean basin (Roxy et al., 2014). This warming decreases the land-sea thermal gradient, which drives the Indian monsoon, and thus slows down the monsoon circulation as observed from 1905-2012, resulting in less rainfall over the central-east and northern regions of India (Roxy et al., 2015). This decrease in rainfall is part of a dipole structure with an increase over the core monsoon region of Pakistan caused by more northward moisture transport over the Arabian Sea and less over the Bay of Bengal from 1951-2012 (Latif et al., 2016). These changes could be due to a 2°-3° westward shift of the whole Asian monsoon circulation system between 1970 and 2015 (Preethi et al., 2016). These recent studies also report a slowing down of the circulation over the Bay of Bengal, which could result in less convection and upward transport.

1.1.4 Transport of surface air to the stratosphere through the Asian monsoon

The delivery of surface air to the stratosphere depends on fast vertical transport, which is mainly realized in enhanced deep convection in the tropics. Generally air masses are lifted into the lower tropical tropopause layer (TTL) through convective processes and then ascend more slowly through the upper part of the TTL into the stratosphere (Figure 9, Path #3). The TTL is a layer of transition between the convective troposphere and the slow ascent of the Brewer-Dobson circulation in the stratosphere. Different definitions for the TTL exist (Folkins et al., 1999; Gettelman et al., 2002; Fueglistaler et al., 2009; Carpenter et al., 2014). Here, the definition as the layer between the level of maximum convective outflow (~12 km altitude, 345 K potential temperature) and the cold-point tropopause (CPT, ~17 km, 380K) is used (Carpenter et al., 2014). The level of zero radiative heating (LZRH) marks the transition from clear-sky radiative cooling to clear-sky radiative heating and the boundary between the lower and upper TTL. Deep convection rapidly transports boundary level air masses up to the level of maximum convective outflow, typically between 12 and 14 km (Folkins et al., 2005). Air masses that are detrained below the LZRH mostly descend back into the mid-troposphere with the large-scale subsidence (Figure 9, Path #2). Air detrained above the LZRH can ascend through the upper TTL and reach the stratosphere. The residence time in the upper TTL

for northern hemispheric winter lies within 15-75 days (Krüger et al., 2009). The residence times in the TTL vary in space and time and are influenced by the location of entry and the horizontal transport through upwelling and downwelling regions (Tzella et al., 2011; Bergman et al., 2012). Overshooting deep convection that transports air masses directly above the tropopause essentially reduces residence times in the TTL (Pommereau, 2010). However, the contribution of this transport pathway to troposphere-to-stratosphere transport is still uncertain (Liu et al., 2005; Vernier et al., 2011; Takahashi et al., 2014). Additionally, horizontal two-way exchange between the TTL and the extratropical lower stratosphere is also possible (Holton et al., 1995; Levine et al., 2007; Ploeger et al., 2012).

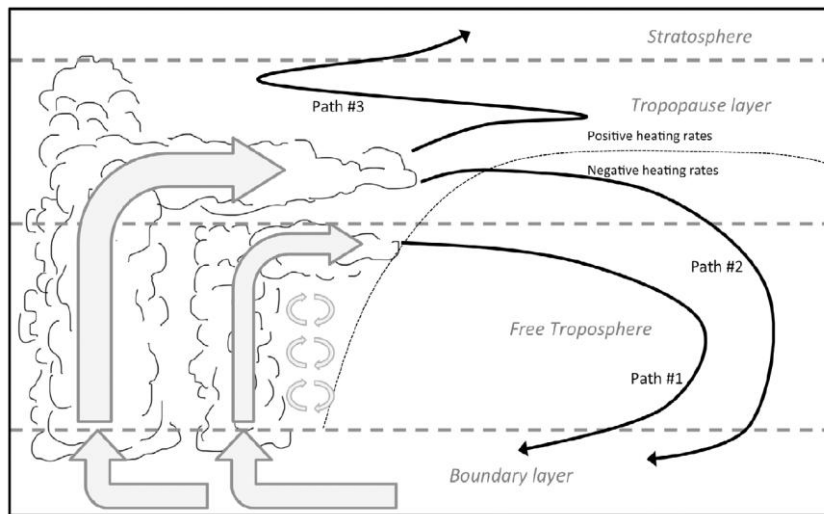


Figure 9: Schematic of vertical transport pathways in the tropics (Bergman et al., 2012).

Preferred regions of air mass transport to the stratosphere appear in conjunction with strong and fast convection above the Maritime Continent in boreal winter (Bergman et al., 2012), the Indian monsoon region (Devasthale et al., 2010) and Southeast Asia (Wright et al., 2011) in boreal summer. Above the tropical Indian Ocean, transport to the stratosphere is strongly influenced by the Asian monsoon circulation and its seasonality and interannual variability.

Stratospheric entrainment of boundary layer trace gases and volcanic aerosols has been detected in connection with the Asian monsoon (Randel et al., 2010; Bourassa et al., 2012). Chemistry climate models support the importance of this pathway for stratospheric delivery (Pan et al., 2016). The Asian monsoon anticyclone in the upper troposphere/lower stratosphere (UTLS) confines boundary layer air masses that have been lifted with the monsoon convection (Park et al., 2009). Furthermore, boundary layer source regions of anticyclonic air have been a topic of recent research. Bergman et al. (2013) identified a slender mid tropospheric vertical conduit connecting India and the

Tibetan Plateau with the anticyclone. The importance of deep convective updrafts for the delivery to the tropopause was identified (Figure 10). This conduit is very persistent and efficient during the Asian summer monsoon. Chen et al. (2012) found the west Pacific Ocean and the Bay of Bengal to be important boundary layer sources for stratospheric entrainment in the Asian summer monsoon area. Vogel et al. (2015) showed that different boundary source regions contribute to the anticyclone related to intraseasonal variation of the summer monsoon associated with the north-south movement of the anticyclone.

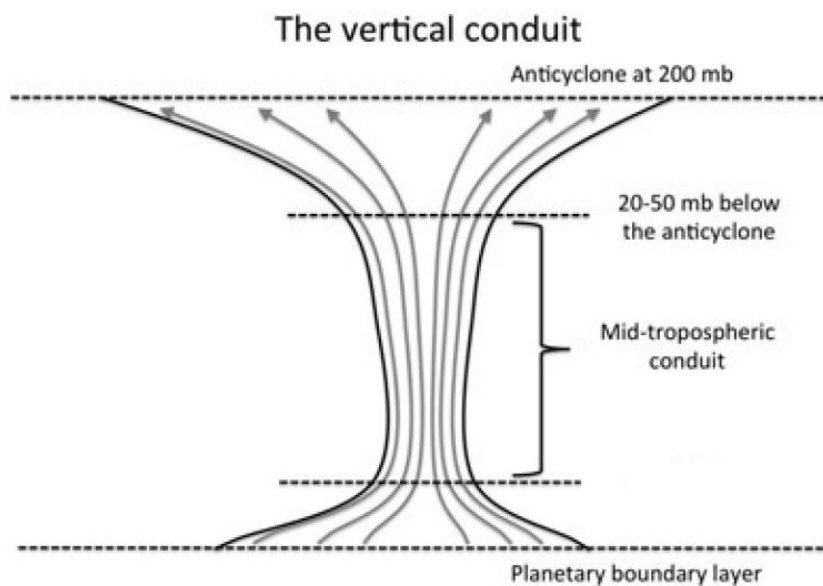


Figure 10: The vertical conduit of boundary layer air masses to the Asian monsoon anticyclone (after Bergman et al., 2013).

From the anticyclone, air masses can be entrained into the stratosphere via slow vertical lifting in the tropics or through quasi-isentropic two way entrainment into the extratropical lowermost stratosphere (Vogel et al., 2015; Garny et al., 2016; Müller et al., 2016). A Lagrangian transport model driven by ERA-Interim inferred that Asian monsoon anticyclonic air contributes up to 5% of the air mass fraction in the confined tropical upwelling in the stratosphere, called the tropical pipe, and 15% to the extratropical lowermost stratosphere (Ploeger et al., 2017).

The boreal winter season is less important for stratospheric entrainment through the Asian monsoon than the summer monsoon season (Pan et al., 2016). The ITCZ resides slightly south of the equator over the Indian Ocean during this time (Schneider et al., 2014). The convection during this season is weaker, but directly over the Indian Ocean, a potential source region for VSLS.

1.1.5 Indian Ocean circulation

The interaction of the tropical Indian Ocean with the atmosphere plays an important role in shaping climate on regional and global scales. The Indian Ocean differs from the Atlantic and Pacific Oceans in several aspects, including the northward boundary of the Asian continent and the low latitude exchange of ocean waters with the Pacific through the Indonesian Through Flow (ITF, Figure 11). The Indian Ocean and the Asian continent drive the strongest monsoon in the world, which exerts an important impact on the Indian Ocean seasonal cycle through a reversal of the monsoon winds.

The Indian Ocean lacks the steady equatorial easterly winds that occur over the Atlantic and Pacific. As a result, there is, in contrast to the other oceans, no climatological mean equatorial upwelling along its eastern boundary. Instead, upwelling occurs along the coast of Africa and Arabian Peninsula, maybe east and west of the tip of India, and south of the equator in the West Indian Ocean (green in Figure 11). These upwelling regimes are connected to the shallow “equatorial roll”, which does not exist in other oceans. During the summer monsoon, this roll emerges from the mean southward Ekman transport across the tropical Indian Ocean (red arrows in Figure 11).

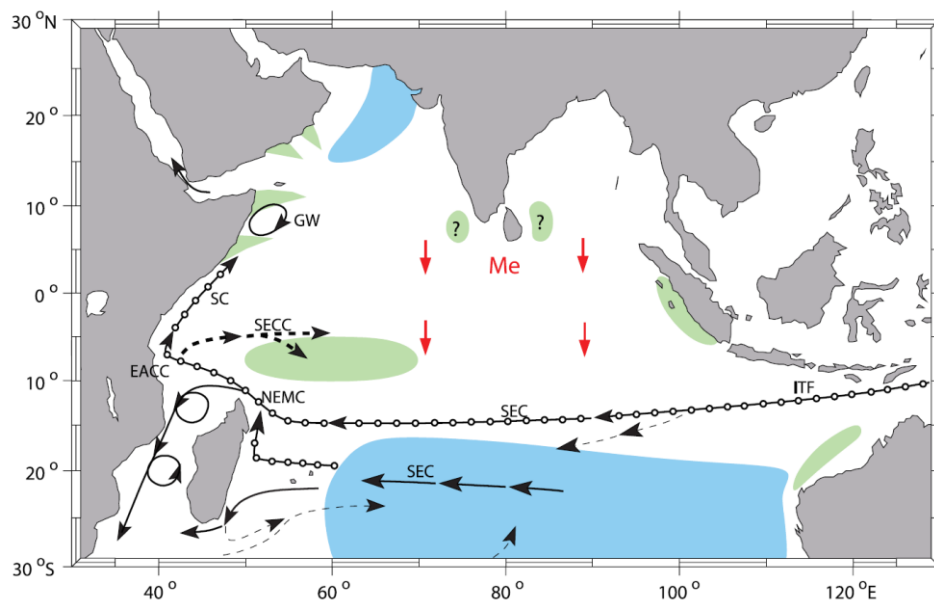


Figure 11: Indian Ocean currents during boreal summer partaking in the equatorial roll circulation and areas of upwelling (green shading) and downwelling (blue shading). Light dashed stream paths stand for upper layer inflow into downwelling area, dotted for thermocline Somali Current supply, solid for Southern Hemisphere thermocline flow, and heavy dashed for the supply route of the subtropical cell. Abbreviations: Indian Through Flow (ITF), Southern Equatorial Current (SEC), Northeast Madagascar Current (NEMC), East African Coastal Current (EACC), South Equatorial Counter Current (SECC), Somali Current (SC), Great Whirl (GW), Mean Ekman Transport (Me) (Schott et al., 2009).

The wind stress is directed to the north along the equator causing the Ekman driven current to subduct and form the equatorial roll. The water wells up again south of the equator forming the Seychelles-Chagos-thermocline ridge (Schott et al., 2009). Furthermore, the atmospheric Somali Jet of the Asian summer monsoon causes strong coastal upwelling of bottom water along the Somali coast (Bruce, 1973).

1.2 Very short-lived substances and their transport to the stratosphere

VSLs are gases that have atmospheric lifetimes of less than half a year after they have been emitted to the atmosphere (Law et al., 2006). This thesis focuses on the four VSLs bromoform (CHBr_3), dibromomethane (CH_2Br_2), methyl iodide (CH_3I) and dimethyl sulfide (DMS).

1.2.1 Marine production

The four VSLs discussed in this thesis have their main sources in the oceans. The production of bromocarbons in the ocean is not yet fully understood, but production pathways have been identified. The two bromocarbons CHBr_3 and CH_2Br_2 have biological and chemical production pathways. Macroalgal formation of bromocarbons has been investigated in the field and laboratory (Gschwend et al., 1985; Carpenter et al., 2000). There is also a source of bromocarbons from phytoplankton in the open ocean (Quack et al., 2004). Several phytoplankton pigments and groups have been related to CHBr_3 and CH_2Br_2 production (Moore et al., 1995b; Quack et al., 2007; Hughes et al., 2013), while they are poor proxies for bromocarbon production (Abrahamsson et al., 2004; Ordóñez et al., 2012; Stemmler et al., 2015). Incubation studies of phytoplankton confirmed the production of bromocarbons from bromoperoxidase enzymes (Tokarczyk et al., 1994; Moore et al., 1996). Furthermore, anthropogenic sources of CHBr_3 and CH_2Br_2 need to be considered. The compounds are formed during the chlorination and ozonization of drinking, sea, and waste water for disinfection and cooling water in power plants to prevent biofouling (Fogelqvist et al., 1982; Fogelqvist et al., 1991; Jenner et al., 1997). Generally, the sources can be divided in coastal and open ocean sources, with macroalgae and anthropogenic production dominating the coastal sources, which yield higher concentrations than phytoplankton in the open ocean (Quack et al., 2003).

For CH₃I production, small biological sources were detected from kelp macroalgae (Lovelock, 1975; Gschwend et al., 1985), phytoplankton (Moore et al., 1996; Scarratt et al., 1999), and bacterial production (Amachi et al., 2001; Hughes et al., 2011). Through incubation experiments also a photochemical source of CH₃I was detected (Moore et al., 1994; Shi et al., 2014). The inclusion of photochemical production in the ocean closed the gap in the global atmospheric CH₃I budget (Bell et al., 2002).

DMS is formed in the ocean from its precursor dimethylsulfoniopropiate (DMSP), which is produced by phytoplankton (Stefels, 2000). DMSP is released to the water and about 1-10% degrades enzymatically into DMS (e.g. Bates et al., 1994; Liss et al., 2014). The production of DMS has been studied in the field (e.g. Simó et al., 2002) and modeled with biogeochemical coupled ocean atmosphere models (e.g. Kloster et al., 2006).

1.2.2 Air-sea gas exchange

Air-sea gas exchange is the main source of organic bromine, iodine and sulfur to the atmosphere. Most of the organic bromine is delivered to the atmosphere in the form of CHBr₃ and CH₂Br₂ (Penkett et al., 1985; Hossaini et al., 2012), while CH₃I contributes significantly to atmospheric iodine (Saiz-Lopez et al., 2012). DMS is an important carrier of sulfur from the ocean to the atmosphere (Liss et al., 2014).

Gases which are produced in the ocean are dissolved in sea water. When they are supersaturated in the oceanic surface layer with respect to the marine atmospheric boundary layer, they are emitted to the atmosphere to achieve equilibrium. They can also be taken up from the atmosphere in the case of undersaturation in the surface ocean. The strength of emissions is influenced by wind, waves, rain, turbulence, bubbles and surface films on very small scales. So far, direct flux measurements using the eddy-covariance technique were only applied to some gases e.g. carbon dioxide (CO₂) (McGillis et al., 2001), oxygenated volatile organic compounds (OVOCs) (Yang et al., 2013), and DMS fluxes (Blomquist et al., 2006; Marandino et al., 2007; Miller et al., 2009). For halocarbons, this method is not available yet.

Currently, air-sea exchange is mainly calculated using parameterizations of exchange rates across the air-sea interface based on wind speed and concentration measurements in the ocean and atmosphere. These estimations are subject to many uncertainties (Wanninkhof et al., 2009) as described in the following. A flux is defined as the product of the transfer velocity k and the concentration gradient Δc (Eq. 1).

$$F = k \cdot \Delta c = k_w \cdot \left(c_w - \frac{c_a}{H} \right) \quad (1)$$

Here, Δc describes the grade of under- or oversaturation of the gas in the ocean and, thus, the direction of the flux and k determines the rate of exchange. The most commonly used simple conceptual model for air-sea exchange is the two layer model (Liss et al., 1974) (Figure 12). In the model, the turbulent atmospheric and oceanic boundary layers, where compounds are well-mixed and concentrations are homogeneous, are separated from the interface by two diffusive layers, one on each side of the interface. In the diffusive layers turbulence is suppressed and transport is realized only through molecular diffusion. This creates concentration gradients and imposes a resistance to the exchange from the air and from the water side, which can be parameterized.

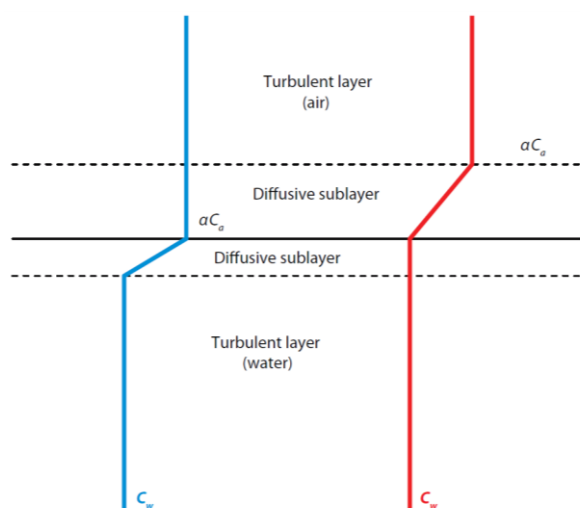


Figure 12: Two layer model of air-sea gas exchange from Liss et al. (1974), displayed in Wanninkhof et al. (2009). Abbreviations: concentration in water (c_w), concentration in air (c_a), Ostwald solubility coefficient (a).

The resistances depend on the solubility of the gas in water, which is described by Henry's Law. The Henry's Law constants (H) and their dependence on temperature were investigated by Moore and coworkers for halocarbons (Moore et al., 1995a; Moore et al., 1995b) and by De Bruyn et al. (1995) for DMS. For gases with low solubility, the air-side resistance is much higher than the water-side resistance, which results in the use of the transfer velocity in water k_w and the concentrations of water c_w and air c_a in Eq. 1. There are several parameterizations available for the transfer velocity. Since the bulk air and water concentrations are measured in the turbulent layers, the transfer velocity correlates with wind speed, which determines the turbulence that drives the exchange. Additionally, the Schmidt Number (Sc) is used to describe the resistance of molecular diffusion in the water. Nightingale et al. (2000) developed a parameterization for the transfer velocity (k_{600}) based on the wind speed at 10 m above the surface (u_{10}) and a Schmidt number of 600 for CO_2 at 20°C in fresh water.

$$k_{600} = 0.222 u_{10}^2 + 0.333 u_{10} \quad (2)$$

The wind speed at 10 m height (u_{10}) is used for this parameterization. The Schmidt number has to be adapted for the different compounds. A compound-specific transfer coefficients k_w is determined through an exponential relation like in Quack et al. (2003):

$$k_w = k_{600} \cdot \left(\frac{600}{Sc}\right)^{\frac{1}{2}} \quad (3)$$

The spread between the different parameterizations of the transfer velocity k_w is large, especially at high wind speeds. Nightingale et al. (2000) provide an estimate around the mean of known parameterizations (Lennartz et al., 2015). This bulk flux calculation method is a simplified approach to describe the more complicated real world and, thus, includes uncertainties through for example the negligence of effects of rain, bubbles, and surfactants.

1.2.3 VSLs emission estimates

Global estimates of VSLs emissions from the oceans vary strongly due to sparse observation data and the high spatial and temporal variability of emissions. Additionally the short lifetimes in the atmosphere make it difficult to accurately model emissions from atmospheric measurements. The first global emission estimates were made for CHBr_3 and assumed homogeneous emissions (Penkett, WMO 1998, Dvortsov 1999, Carpenter and Liss 2000, Nielsen and Douglas 2001). Afterwards the geographical distribution of emissions was added and estimates were extrapolated from oceanic and atmospheric measurements, the so-called bottom-up approach (Quack et al., 2003; Smythe-Wright et al., 2005; Yokouchi et al., 2005; Butler et al., 2007). When atmospheric modeling became available and chemistry was included into the models, emissions were also inferred from observed atmospheric mixing ratios through a top-down approach (Warwick et al., 2006; Kerkweg et al., 2008; Liang et al., 2010; Pyle et al., 2011). Ordóñez et al. (2012) coupled tropical emissions to chlorophyll a (Chl a) concentrations in the surface ocean and created an emission inventory that included seasonality. This is a rough approach, because the correlation with Chl a is mostly weak, since bromocarbon production appears more related to phytoplankton production, influenced by the phytoplankton species and the state of the bloom (Carpenter et al., 2009; Liu et al., 2011; Hepach et al., 2014; Hepach et al., 2015). All other previously described emission inventories only report annual mean emissions. Ziska et al. (2013) created a CHBr_3 , CH_2Br_2 , and CH_3I emission

climatology from the HalOcAt database (<https://halocat.geomar.de/>) of limited oceanic and atmospheric halocarbon observations between 1989 and 2011 including seasonal and interannual variability through the physical parameters. Recently, halocarbon production in the ocean was modeled with ocean biogeochemical models to infer if models can reproduce observed emission patterns (Stemmler et al., 2013; Stemmler et al., 2015). The spread between the emission inventories is large and emissions in undersampled regions remain uncertain. It is hard to accurately model the stratospheric entrainment of halogenated VSLs from uncertain global estimates.

For DMS the data basis is better. Over the open ocean, DMS is hypothesized to be the most important precursor for non-sea salt sulfate aerosols, which influence climate through direct negative radiative forcing (Myhre et al., 2013) and serve as cloud condensation nuclei (Glasow et al., 2004). The formulation of a possible climate feedback mechanism, the CLAW-hypothesis, involving the DMS influence on clouds (Charlson et al., 1987) started a large number of field observations and modeling studies (e.g. Kloster et al., 2006; Marandino et al., 2013; Zindler et al., 2013), which led to an improved understanding of DMS sources to the atmosphere, although the feedback mechanism has not been verified yet. The result is a monthly resolved emission estimate for the global ocean (Lana et al., 2011). Nonetheless, there are many oceanic regions that are still undersampled and the IO is one notable example where the total emissions remain uncertain.

The observations of halogenated VSLs from the Indian Ocean are too sparse to be conclusive (Ziska et al., 2013), but single observations and modeling studies show a high potential for large emissions. High oceanic concentrations in the Arabian Sea and Bay of Bengal (Yamamoto et al., 2001; Roy et al., 2011), as well as modeling studies using atmospheric measurements (Liang et al., 2014), suggest high emissions for the Indian Ocean. For DMS, several observations exist from the Indian Ocean, but still far less than from other ocean basins (Lana et al., 2011). The predicted DMS emissions from the Indian Ocean are high. The Indian Ocean is a region with need for observations of VSLs in the atmosphere and water. The emissions from the Indian Ocean could be important for stratospheric ozone chemistry, if an efficient pathway from the boundary layer to the stratosphere through the Asian summer monsoon existed.

1.2.4 Atmospheric degradation and lifetimes

The atmospheric abundances of VSLS depend on oceanic emissions, transport processes and the degradation of these substances in the atmosphere. Their atmospheric mixing ratios are highly variable because of the short lifetimes and the spatial and temporal variation of emissions. Mixing ratios are high close to the emission sources and rapidly decrease with distance. A VSLS is defined as a substance with an atmospheric lifetime of less than half a year. The lifetime is defined as the time in which the amount of substance has degraded to $1/e$.

The brominated VSLS CHBr_3 and CH_2Br_2 degrade into soluble substances through reaction with the hydroxyl radical (OH) or photolysis (McGivern et al., 2002). For CHBr_3 the main degradation reaction is photolysis and the main products are CBr_2O and CHBrO . These further react to HBr, HOBr, or BrO, which are summarized under Br_y . CH_2Br_2 is mainly oxidized with OH or Cl radicals and also contribute to Br_y . The Br_y in the atmosphere can be washed out with rain (Hossaini et al., 2010). It can also react with ozone both in the troposphere or stratosphere or lead to particle formation (Yang et al., 2005; Saiz-Lopez et al., 2012). Atmospheric CH_3I is photolyzed rapidly in the atmosphere into CH_2I radicals and iodine atoms (Saiz-Lopez et al., 2012). Iodine reacts with ozone to iodine oxide (IO). I and IO together are called active iodine (IO_x). They take part in the tropospheric ozone cycle (Vogt et al., 1999; Saiz-Lopez et al., 2012) and contribute to ozone depletion in the stratosphere (Solomon et al., 1994). Atmospheric active iodine can also form aerosols (O'Dowd et al., 2002) and ultrafine particles (Saiz-Lopez et al., 2012). Atmospheric DMS is degraded even faster than the halocarbons. It is mainly oxidized with OH into methyl sulfonic acid (MSA) or sulfur dioxide (SO_2) (see e.g. Hoffmann et al., 2016, for more details). SO_2 can create H_2SO_4 , which condenses on existing particles or creates new ones, while MSA mainly condenses on existing particles adding to their mass but suppressing new particle formation.

Lifetime estimates of VSLS result from observations, laboratory experiments, and modeling the degradation processes in chemistry models. The lifetimes vary with height, latitude, and season and are therefore often modeled as lifetime profiles (Hossaini et al., 2010) (Figure 13). The most recent summary of lifetime estimates for halocarbons is given by Carpenter et al. (2014) and summarized in Table 1. The lifetime of DMS has been estimated from laboratory studies and observations (Barnes et al., 2006; Osthoff et al., 2009).

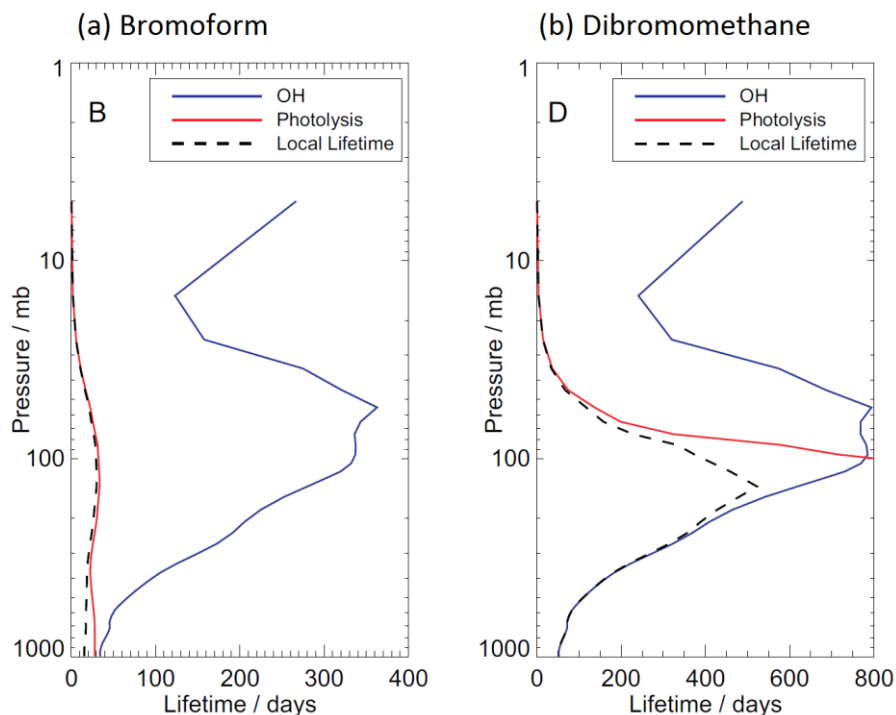


Figure 13: Annual tropical ($\pm 20^\circ$) atmospheric lifetime profiles of (a) CHBr_3 and (b) CH_2Br_2 calculated from a chemistry transport model (Hossaini et al., 2010).

Table 1: Tropical atmospheric lifetimes of VSLs at different altitudes for halogenated VSLs (Carpenter et al., 2014) and for DMS (Barnes et al., 2006; Osthoff et al., 2009).

Compound	Atmospheric lifetimes	
	Boundary layer	10 km
CHBr_3	15 d	17 d
CH_2Br_2	94 d	150 d
CH_3I	4.0 d	3.5 d
DMS	11 min – 46 h	11 min – 46 h

1.2.5 VSLs entrainment to the stratosphere

After emission from the oceans, VSLs can be transported to stratosphere. Transport processes are important for the injection of oceanic VSLs to the stratosphere, because their lifetimes are comparable to transport timescales in the troposphere. Thus, the transport of VSLs to the stratosphere occurs primarily in the tropics and is connected with fast convection and ascent of air masses through the TTL (Figure 9).

The total injection of halogen from VSLs to the stratosphere comprises source gas injection (SGI) and product gas injection (PGI) (Ko et al., 2003). The injection, summed up in Table 2, is estimated from observations, model studies, and a combination of both.

Table 2: Delivery of bromine, iodine, and sulfur from VSLs to the stratosphere.

Element	Source gas injection	Product gas injection	Total injection
Bromine ¹	0.7-3.4 ppt	1.1-4.3 ppt	5 (2-8) ppt
Iodine ¹	<0.05 ppt	<0.1 ppt	<0.15 ppt
Sulfur from DMS ²	4.4 Gg S yr ⁻¹	-	-

¹ (Carpenter et al., 2014); ² (Sheng et al., 2015)

For bromine, the main contributors to stratospheric $\text{Br}_y^{\text{VSLs}}$ are CHBr_3 and CH_2Br_2 (Hossaini et al., 2012). They have been observed in the TTL and around the tropopause with balloon-borne instruments (Brinckmann et al., 2012) and several aircraft campaigns (summary in Carpenter et al., 2014). Oceanic emission estimates and chemistry climate and transport models are used to infer SGI and PGI. These models require a sound treatment of oceanic emissions: A use of different VSLs emission scenarios (Liang et al., 2010; Ordóñez et al., 2012; Ziska et al., 2013) can lead to a difference in the SGI with a factor of ~ 2 (Hossaini et al., 2013). Furthermore, the geographical distribution of OH fields strongly influences the lifetime of source gases that are less affected by photolysis e.g. CH_2Br_2 (Rex et al., 2014). The parameterization of convection and the boundary layer parameters affects the total amount of source gases delivered to the tropopause also with a factor of two between different models (Hossaini et al., 2016). Previous model studies used prescribed lifetimes for VSLs degradation without temporal or regional variations (Sinnhuber et al., 2006; Warwick et al., 2006; Aschmann et al., 2009; Hossaini et al., 2010). Current atmospheric chemistry climate and transport models include an online calculation of degradation and account for product gases and dehydration processes (Aschmann et al., 2011; Hossaini et al., 2012; Aschmann et al., 2013; Liang et al., 2014; Hossaini et al., 2016). The SGI of bromine is derived from direct observations (see list in Montzka et al., 2010), while brominated product gas observations are rare and therefore have to mainly be obtained from model simulations with high uncertainties in wash-out processes (Carpenter et al., 2014). Brominated VSLs are estimated to contribute 1.1-4.3 pptv from product gases to stratospheric bromine abundances, mainly from CHBr_3

and CH_2Br_2 degradation, while 0-0.3 ppt Br come from minor brominated VSLs not considered in the studies mentioned above, such as CHBr_2Cl , CHBrCl_2 , and CH_2BrCl . For the total $\text{Br}_y^{\text{VSLs}}$ entrainment, the most recent estimate has a large range from 2-8 ppt and is thus still uncertain with a factor of four (Carpenter et al., 2014).

For oceanic iodine entrainment to the stratosphere, CH_3I is the most important source gas (Solomon et al., 1994). Aircraft measurements revealed abundances of 0.1 ppt in the TTL and 0.05 ppt at the tropopause (campaigns mentioned in: Bell et al., 2002; Aschmann et al., 2009; Tegtmeier et al., 2013). These estimates were confirmed by modeling studies (Donner et al., 2007; Aschmann et al., 2009; Tegtmeier et al., 2013). Iodine product gases are summed up as total organic iodine I_y and include IO, OIO, and iodine, which are products of CH_3I degradation. They have been observed from solar occultation spectra recorded with balloon-borne Differential Optical Absorption Spectroscopy (DOAS) instruments in the UTLS (Bösch et al., 2003; Butz et al., 2009).

Oceanic sulfur delivery to the stratosphere from DMS is highest in regions of intense vertical transport because of the very short lifetime of around one day (Marandino et al., 2013). Sheng et al. (2015) simulated the DMS entrainment to the stratosphere with 4.4 Gg S yr^{-1} . Although this contribution of DMS source gas to the stratospheric aerosol layer is only 2% of the total contribution of sulfur to stratospheric aerosols, there is also a conversion of DMS to SO_2 in the tropical middle and upper troposphere (Chatfield et al., 1984), which contributes about one third to the stratospheric aerosol SO_2 contribution of 28% (Sheng et al., 2015).

1.2.6 Impacts of VSLs on the stratosphere

This thesis considers natural VSLs from the ocean containing bromine, iodine, and sulfur. Halogens in the stratosphere, including bromine, iodine, and chlorine, mainly influence the ozone layer and therefore the UV-B radiation on the surface, while sulfur supplies the stratospheric aerosol layer, which has an influence on climate, and contributes to ozone depletion (Solomon et al., 2015).

Bromine and iodine in the stratosphere serve as catalyst in ozone depletion (Sect. 1), and especially combined chlorine-bromine and chlorine-iodine reactions are efficient at destroying ozone (Solomon et al., 1994; Salawitch et al., 2005). The stratospheric chlorine abundances mainly result from anthropogenic ODS and the long-lived natural compound methyl chloride (Figure 14).

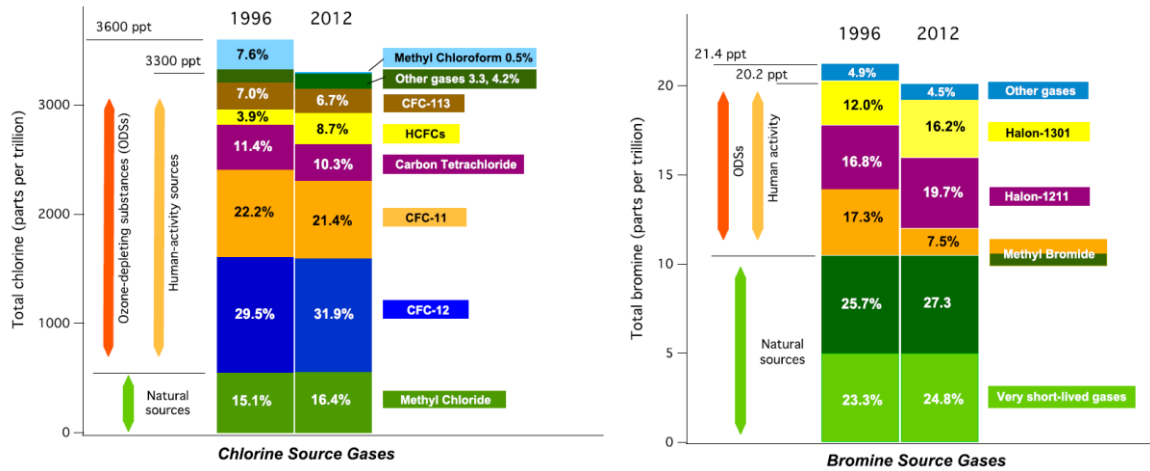


Figure 14: The contribution of different chlorinated and brominated source gases to stratospheric halogen for 1996 and 2012 (WMO, 2014).

Stratospheric bromine originates mainly from the long-lived anthropogenic or natural methyl bromide and anthropogenic halons, but there is also a contribution of about 25% from natural VSLs (Dorf et al., 2006; Carpenter et al., 2014) (Figure 14 and 15). The contribution of $\text{Br}_y^{\text{VSLs}}$ to stratospheric ozone depletion has been modeled with different chemistry climate and transport models. Modeling studies of past stratospheric ozone abundances including VSLs generally achieve a better agreement with observations than models without VSLs (Salawitch et al., 2005; Sinnhuber et al., 2009). These models report a global decrease in stratospheric ozone due to VSLs, which is strongest around the South Pole (Braesicke et al., 2013; Yang et al., 2014; Hossaini et al., 2015; Sinnhuber et al., 2015; Fernandez et al., 2017). $\text{Br}_y^{\text{VSLs}}$ mainly destroys ozone in the lower stratosphere, because all bromine atoms become immediately available for ozone depletion upon entering the stratosphere (Salawitch et al., 2005). Some studies predict a later recovery of the ozone hole to 1980 values if VSLs are included in model simulations (Yang et al., 2014; Oman et al., 2016), while others simulate a deeper and larger current ozone hole, but no delay of the recovery (Fernandez et al., 2017). The natural $\text{Br}_y^{\text{VSLs}}$ ozone chemistry is predicted to dominate Antarctic ozone destruction by the end of the 21st century (Fernandez et al., 2017).

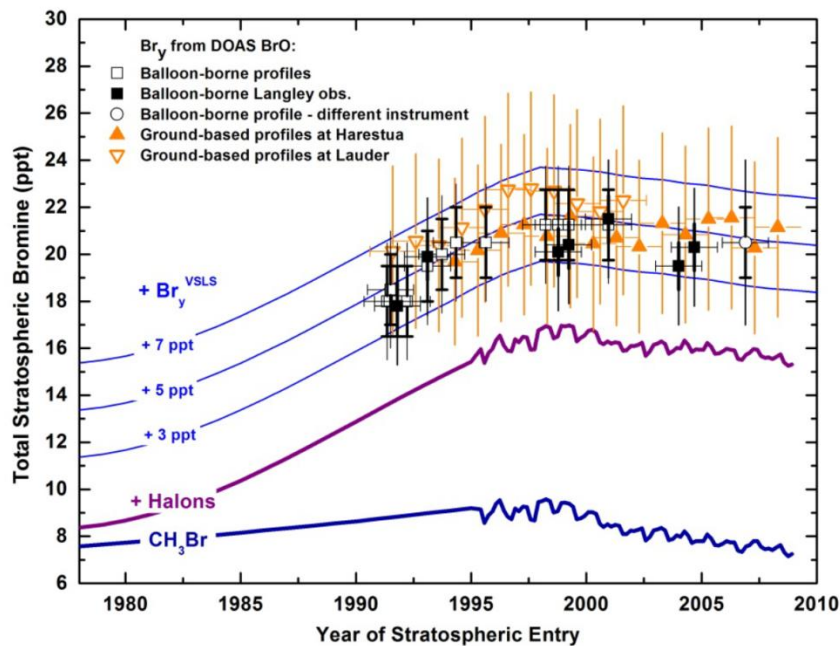


Figure 15: Total stratospheric bromine measurements and estimated contribution of CH_3Br , Halons, and VLS bromine (update from Dorf et al., 2006; in Carpenter et al., 2014).

Iodine in the atmosphere mainly originates from the oceans (Saiz-Lopez et al., 2012). Balloon-borne measurements suggest very low stratospheric abundances of iodine (Bösch et al., 2003) so that iodine is considered a very minor sink for ozone (Carpenter et al., 2014). Amounts between 0.01 - 0.03 pptv have been observed and modeled in the TTL and over 17 km height above the East Pacific (Tegtmeier et al., 2013). Hossaini et al. (2015) modeled the contribution of different VLS to annual global ozone depletion with a chemistry transport model and inferred a contribution of 85% from bromine, 4% from chlorine, and less than 1% from iodine considering natural and anthropogenic VLS.

Stratospheric sulfur mainly influences the temperature of the surface climate as the main component of the Junge aerosol layer. It forms sulfuric acid aerosols (Crutzen, 1976; Kremser et al., 2016), which reflect sunlight (Junge et al., 1961) and cool the surface temperature globally (Solomon et al., 2011). The increase of sulfur supply to the stratosphere since the 2000s is estimated to have reduced the greenhouse gas induced climate warming by 0.05°C (Solomon et al., 2011). At the spring pole sulfur forms polar stratospheric clouds, whose surface acts as a catalyst for heterogeneous ozone destruction (Solomon et al., 2015). The contribution of DMS to stratospheric sulfur and its role in ozone destruction is uncertain.

2 Research Questions

Halogens and sulfur from natural oceanic very short-lived substances (VSLS) contribute to ozone depletion in the stratosphere and influence the radiative budget, which impacts climate. It is crucial to determine and understand their current contribution to ozone depletion, to project their influence under a warming climate and a changing anthropogenic influence. To date, substantial uncertainty exists in the magnitude, distribution, and variability of their emissions, their exact transport mechanisms into the stratosphere and, hence, their absolute contribution to the stratospheric halogen and sulfur loading. VSLS emissions from the Indian Ocean have especially high uncertainties. While the entrainment of tropospheric air to the stratosphere has been widely studied, the mechanisms of stratospheric entrainment through the Asian monsoon are under current investigation. **In particular, there are no studies focusing on the combination of VSLS transport from the Indian Ocean to the stratosphere and the Asian monsoon.** Lagrangian transport models are a good tool in diagnosing transport pathways and timescales in the atmosphere, but in order to determine the strength of stratospheric injection of certain compounds, they need a good representation of spatial and temporal varying emissions, meteorological input fields, and small scale parameterizations (i.e., boundary layer, convection).

The aim of this thesis is to investigate marine VSLS emissions from the Indian Ocean and their transport to the stratosphere through the Asian monsoon. The results are based on unique VSLS observations from the OASIS cruise in the western subtropical and tropical Indian Ocean from South Africa to the Maldives in July and August 2014 on RV Sonne. The transport is modeled with the Lagrangian particle dispersion model FLEXPART based on ERA-Interim reanalysis and different VSLS emission inventories. The overarching research question of this thesis is:

How important are oceanic VSLS emissions from the Indian Ocean for their stratospheric loading?

Indian Ocean emissions of VSLS are uncertain due to sparse or total lack of measurements in this region. During the OASIS cruise, we measured the halogenated VSLS CHBr_3 and CH_2Br_2 for the first time and added to previous CH_3I and DMS measurements in the West Indian Ocean and the atmosphere above. The VSLS emissions and their transport in the atmosphere during the Asian summer monsoon are addressed in

the first two manuscripts: “Delivery of halogenated very short-lived substances from the west Indian Ocean to the stratosphere during the Asian summer monsoon” (Fiehn et al., 2017, ACP) and “The influence of air-sea fluxes on atmospheric aerosols during the summer monsoon over the Indian Ocean” (Zavarsky et al., under review at GRL).

Additional research questions for these two manuscripts are:

- How strong are VSLs emissions from the West Indian Ocean?
- What are the transport pathways in the atmosphere above the West Indian Ocean during Asian summer monsoon?

The Asian monsoon and the Indian Ocean have a distinct seasonal cycle in wind, atmospheric convection, precipitation, ocean currents, and biological activity. Furthermore, there are interannual variations of ocean temperatures, strength of the monsoon, and associated rainfall. Thus, we expect a strong annual cycle and interannual variations in the stratospheric delivery of VSLs which is addressed in the third manuscript “Variability of VSLs transport from the West Indian Ocean to the stratosphere” by Fiehn et al. (under review, JGR Atmospheres) through the following research questions:

- How large is the intra- and interannual variability of VSLs transport from the West Indian Ocean to the stratosphere?
- Which is the main stratospheric entrainment season from the West Indian Ocean?
- What causes the variability of VSLs transport to the stratosphere above the Indian Ocean?

The first three manuscripts focus on the West Indian Ocean, the region of the OASIS cruise, where we obtained new observations. The last manuscript, “Influence of seasonally resolved emissions on the transport of bromoform from the Indian Ocean to the stratosphere” (Fiehn et al., to be submitted) investigates the importance of seasonally resolved VSLs emissions and transport over the whole tropical Indian Ocean and Asian monsoon region including the tropical West Pacific. In this process study, we compiled two bottom-up CHBr_3 emission inventories for the year 2104, one based on an annual mean extrapolation of surface water and air observations and the other on biogeochemical ocean modeling resolving the annual cycle in emissions. The FLEXPART/ERA-Interim calculations focus on the strong seasonality in both emissions and transport and their

impact on stratospheric delivery. Taking into account a large area, tropical Indian Ocean and West Pacific, allows us to determine key source regions that supply CHBr_3 to the stratosphere and the locations and seasons where the CHBr_3 reaches the stratosphere. The application of both annual and monthly emissions illuminates the necessary temporal resolution for a better representation of stratospheric VSLs entrainment. The research questions for this fourth manuscript are:

- Which are the main source regions in the Indian Ocean/West Pacific for stratospheric CHBr_3 and where does it enter the stratosphere?
- What is the influence of the annual vs. monthly representation of CHBr_3 emissions on stratospheric entrainment through the Asian monsoon?

The answers to these seven questions are given explicitly in the four manuscripts (Section 3) and are summarized in Section 4. This latter section also contains a conclusion over VSLs entrainment from the Indian Ocean to the stratosphere and an outlook on possible future studies to address the uncertainties in the stratospheric halogen and sulfur loading from VSLs.

3 Results

3.1 Manuscript 1

Fiehn, A.; Quack, B.; Hepach, H.; Fuhlbrügge, S.; Tegtmeier, S.; Toohey, M.; Atlas, E.; and Krüger, K.: Delivery of halogenated very short-lived substances from the west Indian Ocean to the stratosphere during the Asian summer monsoon, *Atmos. Chem. Phys.*, 17, 6723-6741, <https://doi.org/10.5194/acp-17-6723-2017>, 2017.



Delivery of halogenated very short-lived substances from the west Indian Ocean to the stratosphere during the Asian summer monsoon

Alina Fiehn^{1,2}, Birgit Quack¹, Helmke Hepach^{1,a}, Steffen Fuhlbrügge¹, Susann Tegtmeier¹, Matthew Toohey¹, Elliot Atlas³, and Kirstin Krüger²

¹GEOMAR Helmholtz Centre for Ocean Research Kiel, Kiel, Germany

²Meteorology and Oceanography Section, Department of Geosciences, University of Oslo, Oslo, Norway

³Rosenstiel School of Marine and Atmospheric Science, University of Miami, Miami, USA

^anow at: Environment Department, University of York, York, UK

Correspondence to: Kirstin Krüger (kkrueger@geo.uio.no)

Received: 5 January 2017 – Discussion started: 11 January 2017

Revised: 21 April 2017 – Accepted: 2 May 2017 – Published: 8 June 2017

Abstract. Halogenated very short-lived substances (VSLs) are naturally produced in the ocean and emitted to the atmosphere. When transported to the stratosphere, these compounds can have a significant influence on the ozone layer and climate. During a research cruise on RV *Sonne* in the subtropical and tropical west Indian Ocean in July and August 2014, we measured the VSLs, methyl iodide (CH₃I) and for the first time bromoform (CHBr₃) and dibromomethane (CH₂Br₂), in surface seawater and the marine atmosphere to derive their emission strengths. Using the Lagrangian particle dispersion model FLEXPART with ERA-Interim meteorological fields, we calculated the direct contribution of observed VSL emissions to the stratospheric halogen burden during the Asian summer monsoon. Furthermore, we compare the in situ calculations with the interannual variability of transport from a larger area of the west Indian Ocean surface to the stratosphere for July 2000–2015. We found that the west Indian Ocean is a strong source for CHBr₃ (910 pmol m⁻² h⁻¹), very strong source for CH₂Br₂ (930 pmol m⁻² h⁻¹), and an average source for CH₃I (460 pmol m⁻² h⁻¹). The atmospheric transport from the tropical west Indian Ocean surface to the stratosphere experiences two main pathways. On very short timescales, especially relevant for the shortest-lived compound CH₃I (3.5 days lifetime), convection above the Indian Ocean lifts oceanic air masses and VSLs towards the tropopause. On a longer timescale, the Asian summer monsoon circulation transports oceanic VSLs towards India and the Bay of Bengal, where they are lifted with the monsoon convection and

reach stratospheric levels in the southeastern part of the Asian monsoon anticyclone. This transport pathway is more important for the longer-lived brominated compounds (17 and 150 days lifetime for CHBr₃ and CH₂Br₂). The entrainment of CHBr₃ and CH₃I from the west Indian Ocean to the stratosphere during the Asian summer monsoon is lower than from previous cruises in the tropical west Pacific Ocean during boreal autumn and early winter but higher than from the tropical Atlantic during boreal summer. In contrast, the projected CH₂Br₂ entrainment was very high because of the high emissions during the west Indian Ocean cruise. The 16-year July time series shows highest interannual variability for the shortest-lived CH₃I and lowest for the longest-lived CH₂Br₂. During this time period, a small increase in VSL entrainment from the west Indian Ocean through the Asian monsoon to the stratosphere is found. Overall, this study confirms that the subtropical and tropical west Indian Ocean is an important source region of halogenated VSLs, especially CH₂Br₂, to the troposphere and stratosphere during the Asian summer monsoon.

1 Introduction

Natural halogenated volatile organic compounds in the ocean originate from chemical and biological sources like phytoplankton and macroalgae (Carpenter et al., 1999; Quack and Wallace, 2003; Moore and Zafiriou, 1994; Hughes et al., 2011). When emitted to the atmosphere, the halogenated very

short-lived substances (VSLs) have atmospheric lifetimes of less than half a year (Law et al., 2006). Current estimates of tropical tropospheric lifetimes are 3.5, 17, and 150 days for methyl iodide (CH_3I), bromoform (CHBr_3), and dibromomethane (CH_2Br_2), respectively (Carpenter et al., 2014). VSLs can be transported to the stratosphere by tropical deep convection, where they contribute to the halogen burden, take part in ozone depletion, and thus impact the climate (Solomon et al., 1994; Dvortsov et al., 1999; Hossaini et al., 2015).

CHBr_3 is an important biogenic VSL due to its large oceanic emissions and because it carries three bromine atoms per molecule into the atmosphere (Quack and Wallace, 2003; Hossaini et al., 2012). CH_2Br_2 has a longer lifetime than CHBr_3 and thus a higher potential for stratospheric entrainment. CH_3I is an important carrier of organic iodine from the ocean to the atmosphere and the most abundant organic iodine compound in the atmosphere (Manley et al., 1992; Moore and Groszko, 1999; Yokouchi et al., 2008). Despite its very short atmospheric lifetime, it can deliver iodine to the stratosphere in tropical regions (Solomon et al., 1994; Tegtmeier et al., 2013). Ship-based observations showed that bromocarbon emissions near coasts and in oceanic upwelling regions are generally higher than in the open ocean, because of macroalgal growth near coasts (Carpenter et al., 1999) and enhanced primary production in upwelling regions (Quack et al., 2007), while coastal anthropogenic sources also need to be considered (Quack and Wallace, 2003; Fuhlbrügge et al., 2016b). Measurements of VSLs in the global oceans are sparse and the data show large variability. Thus, attempts at creating observation-based global emission estimates and climatologies (bottom-up approach; Quack and Wallace, 2003; Butler et al., 2007; Palmer and Reason, 2009; Ziska et al., 2013), modeling the global distribution of halogenated VSL emissions from atmospheric abundances (the top-down approach; Warwick et al., 2006; Liang et al., 2010; Ordóñez et al., 2012), and biogeochemical modeling of oceanic concentrations (Hense and Quack, 2009; Stemmler et al., 2013, 2015) are subject to large uncertainties (Carpenter et al., 2014). Global modeled top-down estimates (Warwick et al., 2006; Liang et al., 2010; Ordóñez et al., 2012) yield higher emissions than bottom-up estimates (Ziska et al., 2013; Stemmler et al., 2013, 2015), which may indicate the importance of localized emission hot spots underrepresented in current bottom-up estimates.

The amount of oceanic bromine from VSLs entrained into the stratosphere is estimated to be 2–8 ppt, which is 10–40 % of the currently observed stratospheric bromine loading (Dorf et al., 2006; Carpenter et al., 2014). This wide range results mainly from uncertainties in tropospheric degradation and removal, transport processes, and especially from the spatial and temporal emission variability of halogenated VSL (Carpenter et al., 2014; Hossaini et al., 2016). Analyzing the time period 1993–2012, Hossaini et al. (2016) found no clear long-term transport-driven trend in the stratospheric

injection of oceanic bromine sources during a multi-model intercomparison.

Transport processes strongly impact stratospheric injections of VSLs, because their lifetimes are comparable to tropospheric transport timescales from the ocean to the stratosphere. The main entrance region of tropospheric air into the stratosphere is above the tropical west Pacific. Another active region lies above the Asian monsoon region during the boreal summer (Newell and Gould-Stewart, 1981), when the Asian monsoon circulation provides an efficient transport pathway from the atmospheric boundary layer to the lower stratosphere (Park et al., 2009; Randel et al., 2010). Above India and the Bay of Bengal, convection lifts boundary layer air rapidly into the upper troposphere (Park et al., 2009; Lawrence and Lelieveld, 2010). As a response to the persistent deep convection, an anticyclone forms in the upper troposphere and lower stratosphere above Central, South, and East Asia (Hoskins and Rodwell, 1995). This so-called Asian monsoon anticyclone confines the air masses that have been lifted to this level within the anticyclonic circulation (Park et al., 2007; Randel et al., 2010). For the period 1951–2015, a decreasing trend in rainfall and thus convection has been reported over northeastern India, which was caused by a weakening northward moisture transport over the Bay of Bengal (Latif et al., 2016).

Chemical transport studies in the Asian monsoon region have mostly focused on water vapor entrainment to the stratosphere (Gettelman et al., 2004; James et al., 2008) or on the transport of anthropogenic pollution (Park et al., 2009). The chemical composition and source regions for air masses in the Asian monsoon anticyclone have been the topic of more recent studies (Bergman et al., 2013; Vogel et al., 2015; Yan and Bian, 2015). Chen et al. (2012) investigated air mass boundary layer sources and stratospheric entrainment regions based on a climatological domain-filling Lagrangian study in the Asian summer monsoon area. The west Pacific Ocean and the Bay of Bengal are found to be important source regions, while maximum stratospheric entrainment occurred above the tropical west Indian Ocean.

The Asian monsoon circulation could be an important pathway for the stratospheric entrainment of oceanic VSLs (Hossaini et al., 2016), because the steady southwest monsoon winds in the lower troposphere during boreal summer deliver oceanic air masses from the tropical Indian Ocean towards India and the Bay of Bengal (Lawrence and Lelieveld, 2010), where they are lifted by the monsoon convection and the Asian monsoon anticyclone. However, little is known about the emission strength of VSLs from the Indian Ocean and their transport pathways. A few measurements in the Bay of Bengal (Yamamoto et al., 2001) and Arabian Sea (Roy et al., 2011) as well as global source estimates suggest that the Indian Ocean might be a considerable source (Liang et al., 2010; Ziska et al., 2013). No bromocarbon data are available for the equatorial and southern Indian Ocean, yet, but CH_3I , which has been measured around the Mascarene Plateau,

showed high oceanic concentrations (Smythe-Wright et al., 2005). Liang et al. (2014) use a chemistry climate model for the years 1960 to 2010 and modeled that the tropical Indian Ocean delivers more bromine to the stratosphere than the tropical Pacific because of its higher atmospheric surface concentrations based on the global top-down emission estimate by Liang et al. (2010).

In this study, we show surface ocean concentrations and atmospheric mixing ratios of the halogenated VSLs CH_3I , and for the first time for CHBr_3 and CH_2Br_2 , in the subtropical and tropical west Indian Ocean during the Asian summer monsoon. We use the Lagrangian particle dispersion model FLEXPART to investigate the atmospheric transport pathways of observation-based oceanic VSLs emissions to the stratosphere.

Our questions for this study are as follow: is the tropical Indian Ocean a source for atmospheric VSLs? What is the transport pathway from the west Indian Ocean to the stratosphere during the Asian summer monsoon? How many VSLs are delivered from the west Indian Ocean to the stratosphere during the Asian summer monsoon? How large is the interannual variability of this VSLs entrainment?

In Sect. 2, we describe the cruise data and the transport model simulations. In Sect. 3, the results from the cruise measurements and trajectory calculations are shown and discussed. Then, the spatial and interannual variability of transport is presented in Sect. 4. In Sect. 5, we address uncertainties before summarizing the results and concluding in Sect. 6.

2 Data and methods

2.1 Observations during the cruise

During two consecutive research cruises in the west Indian Ocean, we observed meteorological, oceanographic, and biogeochemical conditions, including atmospheric mixing ratios and oceanic concentrations of halogenated VSLs. The two cruises on RV *Sonne*, SO234-2 from 8 to 19 July 2014 (Durban, South Africa to Port Louis, Mauritius) and SO235 from 23 July to 7 August 2014 (Port Louis, Mauritius to Malé, Maldives), were conducted within the SPACES (Science Partnerships for the Assessment of Complex Earth System Processes) and OASIS (Organic very short-lived Substances and their air sea exchange from the Indian Ocean to the Stratosphere) research projects. Cruise SO234-2 was an international training and capacity building program for students from Germany and southern African countries, whereas SO235 was purely scientifically oriented. The cruise tracks covered subtropical waters, coastal and shelf areas, and the tropical open west Indian Ocean and were designed to cover biologically productive and nonproductive regions (Fig. 1). In the following, we will refer to the combined cruises as the “OASIS cruise”.

We collected meteorological data from ship-based sensors including surface air temperature (SAT), relative humidity, air pressure, wind speed and direction taken every second at about 25 m height on RV *Sonne*. Sea surface temperature (SST) and salinity were measured in the ship's hydrographic shaft at 5 m depth. We averaged all parameters to 10 min intervals for our investigations.

During the cruise, we launched 95 radiosondes and thus obtained high-resolution atmospheric profiles of temperature, wind, and humidity. During the first half of the cruise, regular radiosondes were launched at 00:00 and 12:00 UTC and additionally at 06:00 and 18:00 UTC during the 48 h station (16–18 June 2014; Fig. 1). During the second half of the cruise, the launches were always performed at standard UTC times (00:00, 06:00, 12:00, 18:00 UTC) and every 3 h during the diurnal stations (26 and 28 June, 3 August 2014). For the regular launches, we used GRAW DFM-09 radiosondes, and for the six ozonesonde launches we used DFM-97. The collected radiosonde data was delivered in near real time to the Global Telecommunication System (GTS) to improve meteorological reanalyses (e.g., European Centre for Medium-Range Weather Forecasts, ECMWF, Re-Analysis Interim, ERA-Interim) and operational forecast models (e.g., opECMWF, operational ECMWF) in the subtropical and tropical west Indian Ocean.

Trace gas emissions are generally well mixed within the marine atmospheric boundary layer (MABL) on timescales of an hour or less by convection and turbulence (Stull, 1988). We determined the stable layer that defines the top of the MABL with the practical approach described in Seibert et al. (2000). From the radiosonde ascent we computed the vertical gradient of virtual potential temperature, which indicates the stable layer at the top of the MABL with positive values. A detailed description of our method can be found in Fuhlbrügge et al. (2013).

We collected a total of 213 air samples with a 3-hourly resolution at about 20 m height above sea level. These samples were pressurized to 2 atm in pre-cleaned stainless steel canisters with a metal bellows pump, and they were analyzed within 6 months after the cruise. Details about the analysis, the instrumental precision, the preparation of the samples, and the use of standard gases are described in Schaufli et al. (1999), Montzka et al. (2003), and Fuhlbrügge et al. (2013).

We collected overall 154 water samples, spaced about every 3 h, from the hydrographic shaft of RV *Sonne* at a depth of 5 m. The samples were then analyzed for halogenated compounds using a purge and trap system onboard, which was attached to a gas chromatograph with an electron capture detector. An analytical reproducibility of 10 % was determined from measuring duplicate water samples. Calibration was performed with a liquid mixed-compound standard prepared in methanol. Details of the procedure can be found in Hepach et al. (2016).

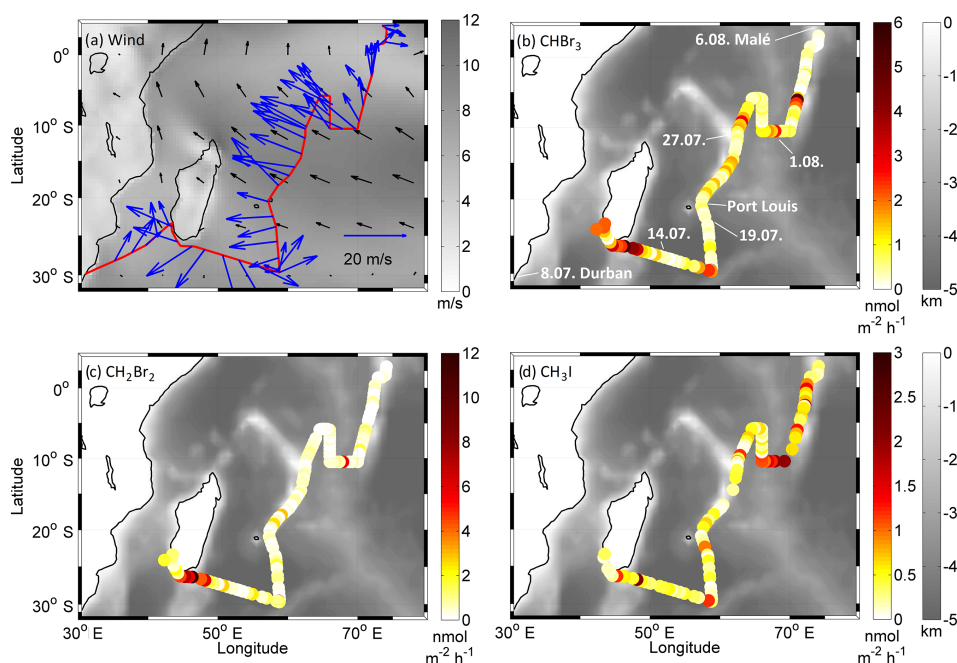


Figure 1. (a) July 2014 average wind speed (gray shading) and direction (black) from ERA-Interim and 10 min mean wind speed (blue arrows) from ship sensors; (b) CHBr_3 , (c) CH_2Br_2 , and (d) CH_3I emissions derived from OASIS cruise on July–August 2014 and bathymetry.

The sea–air flux (F) of the VSLs was calculated from the transfer coefficient (k_w) and the concentration gradient (Δc) according to Eq. (1). The gradient is between the water concentration (c_w) and the theoretical equilibrium water concentration (c_{atm}/H), which is derived from the atmospheric concentration (c_{atm}). We use Henry’s law constants (H) of Moore and coworkers (Moore et al., 1995a, b).

$$F = k_w \cdot \Delta c = k_w \cdot \left(c_w - \frac{c_{\text{atm}}}{H} \right) \quad (1)$$

Compound-specific transfer coefficients were determined using the air–sea gas exchange parameterization of Nightingale et al. (2000) and by applying a Schmidt number (Sc) for the different compounds as in Quack and Wallace (2003) (Eq. 2).

$$k_w = k \cdot \frac{Sc^{-\frac{1}{2}}}{600} \quad (2)$$

Nightingale et al. (2000) determined the transfer coefficient (k) as a function of the wind speed at 10 m height (u_{10}): $k = 2u_{10}^2 + 3u_{10}$. This wind speed is derived from a logarithmic wind profile using the von Kármán constant ($\kappa = 0.41$), the neutral drag coefficient (C_d) from Garratt (1977), and the 10 min average of the wind speed ($u(z)$) measured at $z = 25$ m during the cruise (Eq. 3):

$$u_{10} = u(z) \frac{\kappa \sqrt{C_d}}{\kappa \sqrt{C_d} + \log \frac{z}{z_0}} \quad (3)$$

2.2 Trajectory calculations

For our trajectory calculations, we use the Lagrangian particle dispersion model FLEXPART of the Norwegian Institute for Air Research in the Atmosphere and Climate Department (Stohl et al., 2005), which has been evaluated in previous studies (Stohl et al., 1998; Stohl and Trickl, 1999). The model includes moist convection and turbulence parameterizations in the atmospheric boundary layer and free troposphere (Stohl and Thomson, 1999; Forster et al., 2007). In this study, we employ the most recently released version 9.2 of FLEXPART, modified to incorporate lifetime profiles. We use the ECMWF reanalysis product ERA-Interim (Dee et al., 2011) with a horizontal resolution of $1^\circ \times 1^\circ$ and 60 vertical model levels as meteorological input fields, providing air temperature, winds, boundary layer height, specific humidity, and convective and large scale precipitation with a 6-hourly temporal resolution. The vertical winds in hybrid coordinates were calculated mass-consistently from spectral data by the pre-processor (Stohl et al., 2005). We record the transport model output every 6 h.

We ran the FLEXPART model with three different setups, which are described in Table 1. These configurations are designated as (1) OASIS back (backward trajectories), (2) OASIS (forward trajectories), and (3) Indian Ocean (regional forward trajectories).

We calculated OASIS backward trajectories from the 12:00 UTC locations of RV *Sonne* during the cruise. These trajectories are later used to determine the source regions of air masses investigated along the cruise track.

Table 1. FLEXPART experimental setups including experiment name, mode, start location and time, runtime, and number of trajectories.

Experiment name	Mode	Start location	Start time	Runtime	Number of trajectories
OASIS back	Backward; air mass	along ship track	12:00 UTC, every day during cruise	10 days	50 per cruise day
OASIS	Forward; VSLs	0.0002° × 0.0002° on emission measurements	±30 min from measurement time	10 days (CH ₃ I), 3 months (CHBr ₃), 1.5 years (CH ₂ Br ₂)	10 000 per measurements
Indian Ocean	Forward; VSLs tracers	1° × 1° grid at sea surface; 50–80° E, 20° S–10° N	Every day from 1–31 July 2000–2015	3 months	29 791 × 16 years

With the OASIS setup, we study the transport of oceanic CHBr₃, CH₂Br₂, and CH₃I emissions from the measurement locations into the stratosphere similar to what was carried out in the corresponding study by Tegtmeier et al. (2012). At every position along the cruise track at which emissions were calculated (Sect. 2.1), we release a mass of the compound equal to a release from 0.0002° × 0.0002° in 1 h. The mass is evenly distributed among 10 000 trajectories. During transport, CHBr₃ and CH₂Br₂ mass is depleted according to atmospheric lifetime profiles from Hossaini et al. (2010) based on chemistry transport model simulations including VSLs chemistry. CH₃I decays by applying a uniform vertical lifetime of 3.5 days (Sect. 1). The mass on all trajectories that reaches a height of 17 km is summed and assumed to be entrained into the stratosphere. This threshold height represents the average cold point tropopause (CPT) height during the cruise (see Fig. S1 in the Supplement) and also for the whole tropics (Munchak and Pan, 2014). The influence of the entrainment height criteria is further discussed in Sect. 4. For intercomparison with other ocean basins, we employed exactly the same model setup of transport simulations (including lifetimes) and the same emission calculation method for three previous corresponding cruises in the tropics: the TransBrom campaign in the west Pacific in 2009 (introduction to special issue: Krüger and Quack, 2013), the SHIVA campaign in the South China and Sulu seas in 2011 (Fuhlbrügge et al., 2016a), and the MSM18/3 cruise in the equatorial Atlantic cold tongue (Hepach et al., 2015).

The transport calculations based on the measured emissions from OASIS give insight into the contribution of oceanic emissions to the stratosphere during the Asian summer monsoon. However, transport and emissions in the OASIS study are localized in space and time and could thus be very different for different areas and years. In order to investigate the transport from the west Indian Ocean basin to the stratosphere and its interannual variability under the influence of the Asian summer monsoon circulation (Indian Ocean setup), we calculate trajectories from a large region of the tropical west Indian Ocean surface for the years 2000–2015. Trajectories are uniformly started within the release

area (50–80° E, 20° S–10° N), covering the tropical west Indian Ocean, once every day during the month of July in 2000–2015. The run time is set to 3 months, which covers the period from July to October. We then calculate the fraction (q) of each VSLs tracer that reaches the stratosphere during the transit time (tt), assuming an exponential decay of the tracer (Eq. 4) according to the tropical tropospheric lifetimes (lt) of 17, 150, and 3.5 days for CHBr₃, CH₂Br₂, and CH₃I, respectively (Carpenter et al., 2014).

$$q = e^{-\frac{tt}{lt}} \quad (4)$$

We use the term “VSLs tracer” to distinguish from the calculations used in the OASIS setup, where actual VSLs emissions experience decay according to a vertical lifetime profile (uniform for CH₃I). The use of VSLs tracers allows us to evaluate one model run for different compounds with varying lifetimes. This Indian Ocean setup provides information on the preferred pathways from the west Indian Ocean to the stratosphere for different transport timescales and on their interannual variability. This variability is quantified by the coefficient of variation (CV), which is defined as the ratio of the standard deviation to the mean entrainment. The correlations of the interannual variations between different regions of stratospheric entrainment are given by the correlation coefficient (r) by Pearson (1895). We calculated the p value to determine the 95 % significance level of the correlations.

3 The Indian Ocean cruise: OASIS

3.1 Atmospheric circulation

SST and SAT during the OASIS cruise generally increase from the south towards the equator (Fig. 2a). The SST is on average 1.5 °C higher than the SAT, which benefits convection. Minimum SSTs of 18 °C were measured from 14 to 17 July 2014 in the open subtropical Indian Ocean (30° S, 59° E), and maximum SSTs of 29 °C were measured around the equator.

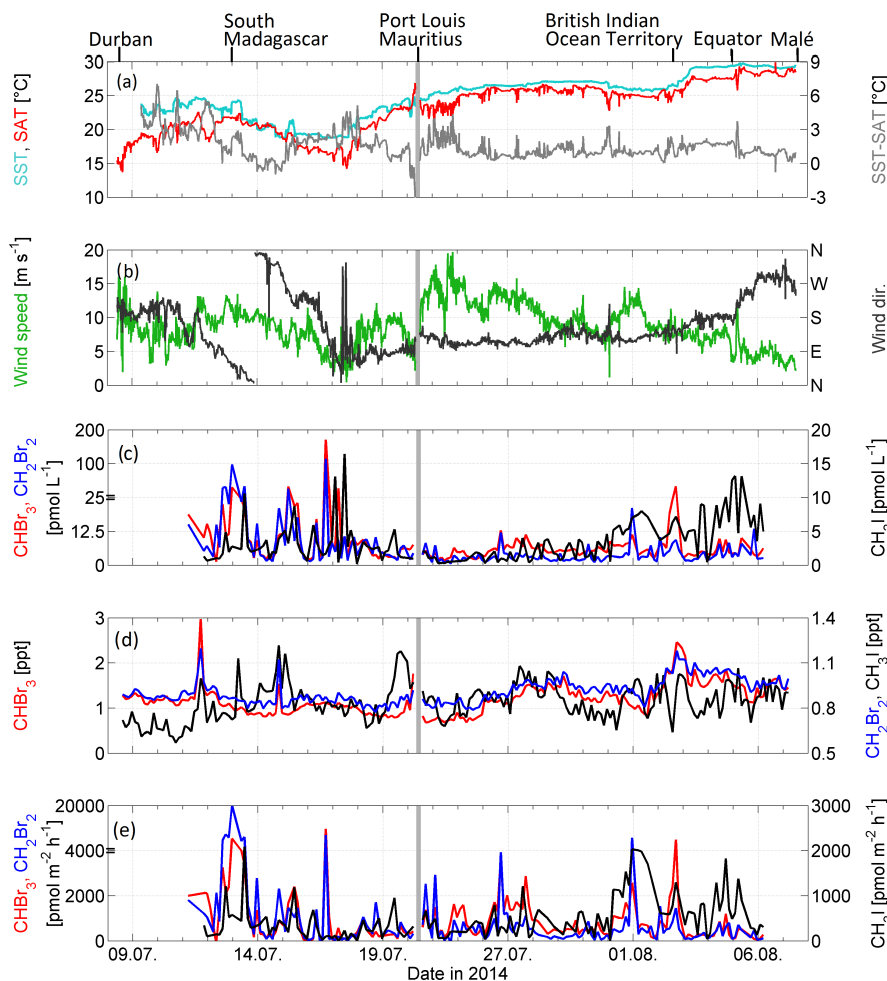


Figure 2. (a) Surface air temperature (SAT), sea surface temperature (SST), and (b) wind speed and direction measured by ship sensors during the OASIS cruise in the Indian Ocean. (c) Water concentration; (d) atmospheric mixing ratio; and (e) emission of CHBr₃, CH₂Br₂, and CH₃I. The gray line denotes the harbor stop at Port Louis, Mauritius, 20–23 July 2014. Also note the nonlinear left y axes in (c) and (e).

The overall mean wind speed was 8.1 m s^{-1} , with lower wind speeds in the subtropics and close to the equator (5 m s^{-1}) and higher wind speeds (up to 15 m s^{-1}) in the trade wind region (23 July to 5 August, $20\text{--}5^\circ \text{ S}$; Fig. 2b). The mean wind direction during the cruise was southeast. While the wind direction showed large variability in the subtropics, southeasterly trade winds dominated between Mauritius and the equator. North of the equator the wind direction changed to westerly winds. Our in situ ship wind measurements deviate from the mean July wind field from ERA-Interim during the first part of the cruise south of Mauritius (Fig. 1a) due to the influence of a developing low-pressure system (not shown). The steady trade winds during the second part of the cruise are well reflected in the July mean wind field from ERA-Interim. Surface winds from in situ ship measurements, radiosondes, and time-varying ERA-Interim data show good agreement (Fig. S2).

Air masses sampled during the cruise originate mainly from the open ocean (Fig. 3a). Trajectories started between South Africa and Mauritius generally come from the south. An influence of terrestrial sources is possible close to South Africa and Madagascar. From Mauritius to the Maldives, the trajectories originate from the southeast open Indian Ocean. The analysis of air samples reveal no recent fresh anthropogenic input, indicated by the very low levels of short-lived trace gas contaminants, e.g., butane (lifetime 2.5 days; Finlayson-Pitts and Pitts, 2000), in this region (not shown).

3.2 VSLs observations and oceanic emissions

CHBr₃, CH₂Br₂, and CH₃I surface ocean concentrations, atmospheric mixing ratios, and emissions for the OASIS cruise are plotted as time series in Fig. 2c–e and are summarized in Table 2.

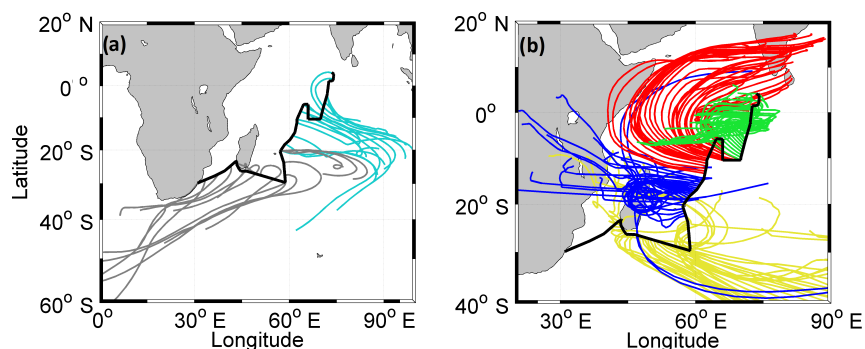


Figure 3. (a) FLEXPART 5-day backward trajectories for OASIS backward setup, averaged for $n = 50$ trajectories, starting from ship positions daily at 12:00 UTC between 8 July and 7 August 2014. The Southern Ocean (gray) and the open Indian Ocean (turquoise) are source regions for air measured during the cruise. (b) FLEXPART 10-day forward trajectories for OASIS setup, averaged for $n = 1000$ trajectories, starting at the ship positions of simultaneous VSLs measurements. Trajectories are colored according to their transport regimes: Westerlies (yellow), Transition (blue), Monsoon Circulation (red), and Local Convection (green).

Table 2. CHBr_3 , CH_2Br_2 , and CH_3I water concentrations, atmospheric mixing ratios, and calculated emissions for the OASIS Indian Ocean cruise. The table lists the average value of all measurements and 1 SD. The brackets give the range of measurements.

VSLs	Water concentration (pmol L^{-1})	Air mixing ratio (ppt)	Emission ($\text{pmol m}^{-2} \text{h}^{-1}$)
CHBr_3	8.4 ± 14.2 [1.3–33.4]	1.20 ± 0.35 [0.68–2.97]	910 ± 1160 [–100–9630]
CH_2Br_2	6.7 ± 12.6 [0.6–114.3]	0.91 ± 0.08 [0.77–1.20]	930 ± 2000 [–70–19 960]
CH_3I	3.4 ± 3.1 [0.2–16.4]	0.84 ± 0.12 [0.57–1.22]	460 ± 430 [5–2090]

CHBr_3 concentrations in the surface ocean range from 1.3 to 33.4 pmol L^{-1} , with an average of all measurements of 8.4 ± 14.2 (1σ) pmol L^{-1} . The standard deviation (σ) is used as a measure of the variability in the measurements during the cruise. We measured large water concentrations of $>10 \text{ pmol L}^{-1}$ close to coasts and shelf regions and in the open Indian Ocean between 5 and 10° S (27 July–2 August). Oceanic concentrations of CH_2Br_2 are smaller, with a mean of $6.7 \pm 12.6 \text{ pmol L}^{-1}$, but show a similar distribution to CHBr_3 concentrations. High concentrations were measured southeast of Madagascar, when we passed the southern stretch of the East Madagascar Current. Oceanic upwelling occurs along the eddy-rich, shallow region south of Madagascar, which leads to locally enhanced phytoplankton growth (Quartly et al., 2006). It is possible that an upwelling of elevated CH_2Br_2 concentrations from the deeper ocean could have occurred in a similar way as was observed for the equatorial upwelling in the Atlantic (Hepach et al., 2015). CH_3I oceanic concentrations range from 0.2 to 16.4 pmol L^{-1} , with a mean of $3.4 \pm 3.1 \text{ pmol L}^{-1}$. They were elevated ($5\text{--}12 \text{ pmol L}^{-1}$) during the last part of the

cruise (August 3–6, 2014) around the equator. In the region of the Mascarene Plateau, to the west of our cruise, Smythe-Wright et al. (2005) detected much larger CH_3I concentrations between 20 and 40 pmol L^{-1} during June–July 2002.

Atmospheric mixing ratios of CHBr_3 during the OASIS cruise (Fig. 2d, Table 2) show an overall mean of 1.20 ± 0.35 ppt. Elevated mixing ratios of >2 ppt are found in three locations: south of Madagascar, in Port Louis, and close to the British Indian Ocean Territory. The first two probably have terrestrial or coastal sources, because they do not coincide with high oceanic CHBr_3 concentrations, but backward trajectories pass land. Close to the British Indian Ocean Territory, oceanic concentrations and atmospheric mixing ratios are elevated, which suggests a local oceanic source. Atmospheric mixing ratios of CH_2Br_2 vary little around the average of 0.91 ppt and show a similar pattern to the CHBr_3 mixing ratios. CH_3I (0.84 ± 0.12 ppt) mixing ratios reveal pronounced variations and surpass 1 ppt in some locations. These atmospheric mixing ratios above the open ocean are much lower than the average of 12 pptv Smythe-Wright et al. (2005) reported around the Mascarene Plateau.

We calculated oceanic emissions from the synchronized measurements of surface water concentration and atmospheric mixing ratio as described in Sect. 2.1 (Figs. 2e and 1). Strong emissions are caused by high oceanic concentrations, high wind speeds, or a combination of both. The OASIS emission strength of CHBr_3 ranges from -100 to $9630 \text{ pmol m}^{-2} \text{h}^{-1}$, with high mean emissions of $910 \pm 1160 \text{ pmol m}^{-2} \text{h}^{-1}$; this is caused by moderate water concentrations and relatively high wind speeds. We derive the strongest emissions south of Madagascar and in the trade wind regime from 5 to 10° S above the open ocean upwelling region of the Seychelles-Chagos-thermocline ridge (Schott et al., 2009), where we also observed enhanced phytoplankton growth (not shown here). CH_2Br_2 emissions (with an overall mean of $930 \pm 2000 \text{ pmol m}^{-2} \text{h}^{-1}$) were by

far strongest south of Madagascar, with a single maximum of up to $20\,000\text{ pmol m}^{-2}\text{ h}^{-1}$. Here, we experienced very high oceanic concentrations and high wind speeds due to the passage of a low-pressure system south of the ship track during 11–17 July 2014. CH_3I emissions ($460 \pm 430\text{ pmol m}^{-2}\text{ h}^{-1}$) had a pronounced maximum of $2090\text{ pmol m}^{-2}\text{ h}^{-1}$ around 10° S and 70° E (31 July–1 August), in accordance with high wind speeds and oceanic concentrations being elevated close to the above-mentioned open ocean upwelling observed between 5 and 10° S .

During the first part of the cruise, we recorded low mean atmospheric mixing ratios of CHBr_3 and CH_2Br_2 , despite high local oceanic concentrations and emissions especially south of Madagascar. In connection with a high and well-ventilated MABL (Fig. S1), this indicates that the strong sources south of Madagascar are highly localized. The occasional enhancement of the brominated VSLs in some air samples underlines the patchiness of the sources in this region. During the second part of the cruise, the atmospheric mixing ratios of CHBr_3 and CH_2Br_2 increased from south to north and in the direction of the wind maximizing close to the equator (Fig. 2d). The emissions were strong between Mauritius and the equator (Fig. 2e). This suggests that the air around the equator was enriched by the advection of the oceanic emissions with the trade winds from south to north. We assume that the bromocarbons accumulate because of the steady wind directions and the suppression of mixing into the free troposphere due to the top of the MABL and the trade inversion layer (Fig. S1, 27 July–2 August) acting as transport barriers for VSLs as was observed for the Peruvian upwelling (Fuhlbrügge et al., 2016a).

3.3 Comparison of OASIS VSL emissions with other oceanic regions

Average emissions of the three VSLs from OASIS and other tropical cruises and modeling studies are summarized in Table 3. We compare with cruises and open ocean estimates, since OASIS mainly covered open ocean regions and only small coastal areas close to Madagascar, the British Indian Ocean Territory, and the Maldives.

The average CHBr_3 emission during the OASIS campaign ($910\text{ pmol m}^{-2}\text{ h}^{-1}$) was larger than during most campaigns in tropical regions: 1.5 times larger than during TransBrom in the subtropical and tropical west Pacific (Tegtmeier et al., 2012), 1.2 times larger than during DRIVE in the tropical northeast Atlantic (Hepach et al., 2014), and 1.5 times larger than during MSM18/3 in the Atlantic equatorial upwelling (Hepach et al., 2015). Only the SHIVA campaign in the South China and Sulu seas yielded larger CHBr_3 emissions of $1486\text{ pmol m}^{-2}\text{ h}^{-1}$ because of very high oceanic concentrations close to the coast (Fuhlbrügge et al., 2016b). The global open ocean estimate by Quack and Wallace (2003) is one-third smaller than our measured values in the west Indian Ocean. The bottom-up emission climatology by Ziska

et al. (2013) estimates smaller values for the Indian Ocean, based on measurements from other oceanic basins due to a lack of available Indian Ocean in situ measurements. With their top-down approach, Warwick et al. (2006), Liang et al. (2010), and Ordóñez et al. (2012) derived CHBr_3 emissions in the range of $580\text{--}956\text{ pmol m}^{-2}\text{ h}^{-1}$ for the tropical ocean. Stemmler et al. (2014) modeled very low CHBr_3 emissions around $200\text{ pmol m}^{-2}\text{ h}^{-1}$ for the equatorial Indian Ocean with their biogeochemical ocean model.

Average CH_2Br_2 emissions from the OASIS cruise ($930\text{ pmol m}^{-2}\text{ h}^{-1}$) are 2–6 times larger than the average cruise emissions listed in Table 3: TransBrom, DRIVE, MSM18/3, SHIVA, and M91. This is caused by the generally high oceanic concentrations during OASIS, with the largest values south of Madagascar. The mean emissions from the west Indian Ocean are also much stronger than the tropical ocean estimates from Butler et al. (2007) and the global open ocean estimate from Yokouchi et al. (2008) and Carpenter et al. (2009). The top-down model approach by Liang et al. (2010) yielded the weakest emissions at only $81\text{ pmol m}^{-2}\text{ h}^{-1}$. The Ziska et al. (2013) climatology shows maximum equatorial Indian Ocean CH_2Br_2 emission values of around $500\text{ pmol m}^{-2}\text{ h}^{-1}$.

The average CH_3I emissions during OASIS ($460\text{ pmol m}^{-2}\text{ h}^{-1}$) were in the range of previously observed and estimated values from 254 to $625\text{ pmol m}^{-2}\text{ h}^{-1}$ (Table 3). For the highly productive Peruvian upwelling, Hepach et al. (2016) calculated much larger emissions of $954\text{ pmol m}^{-2}\text{ h}^{-1}$. The coupled ocean–atmosphere model of Bell et al. (2002) produced average global emissions of $670\text{ pmol m}^{-2}\text{ h}^{-1}$, while Stemmler et al. (2013) modeled CH_3I emissions of around $500\text{ pmol m}^{-2}\text{ h}^{-1}$ for the tropical Atlantic with their biogeochemical ocean model. The Ziska et al. (2013) climatology shows Indian Ocean CH_3I emissions of around $500\text{ pmol m}^{-2}\text{ h}^{-1}$.

In general, the emissions during the OASIS cruise in the subtropical and tropical west Indian Ocean were as strong as or stronger than in other tropical open ocean cruises or studies. CH_2Br_2 emissions during the OASIS cruise were especially stronger than any previous emissions estimates. The west Indian Ocean seems to be a region with significant contribution to the global open ocean VSL emissions, especially in the boreal summer when wind speeds are high because of the southwest monsoon circulation.

3.4 VSL entrainment to the stratosphere during OASIS

The OASIS forward trajectories released at the locations of the VSL measurements show the transport pathway of the air masses from their sample points along the cruise track (Fig. 3b). The mean of all 10 000 trajectories from each release can be grouped into four regimes according to transport direction: Westerlies, Transition, Monsoon Circulation, and Local Convection. The air masses in the Westerlies regime

Table 3. CHBr₃, CH₂Br₂, and CH₃I mean emissions (pmol m⁻² h⁻¹) for several cruises and observational and model-based climatological studies. Abbreviations: IO, Indian Ocean; OLS, ordinary least squares method.

Study	Cruise, region	CHBr ₃	CH ₂ Br ₂	CH ₃ I
	OASIS, west IO	910	930	460
Chuck et al. (2005)	ANT XVIII/1, tropical Atlantic	125		625
Tegtmeier et al. (2012, 2013)	TransBrom, west Pacific Ocean	608	164	320
Hepach et al. (2014)	DRIVE, tropical Atlantic	787	341	254
Hepach et al. (2015)	MSM 18/3, equatorial Atlantic	644	187	425
Hepach et al. (2016)	M91, peruvian upwelling	130	273	954
Fuhlbrügge et al. (2016b)	SHIVA, South China Sea	1486	405	433
Quack and Wallace (2003)	Global open ocean	625		
Yokouchi et al. (2005)	Global open ocean		119	
Butler et al. (2007)	Tropical ocean	379	108	541
Carpenter et al. (2009)	Atlantic open ocean	367	158	
Bell et al. (2002)	Global ocean			670
Warwick et al. (2006)	Tropics, Scenario 5	580		
Liang et al. (2010)	Tropics, open ocean, Scenario A	854	81	
Ordoñez et al. (2012)	Tropics	956		
Ziska et al. (2013)	IO equator (OLS)	≈ 500	≈ 500	≈ 250
Ziska et al. (2013)	IO subtropics (OLS)	≈ 250	≈ 250	≈ 500
Stemmler et al. (2013)	Tropical Atlantic Ocean			≈ 500
Stemmler et al. (2015)	IO equator	≈ 200		

are transported to the southeast Indian Ocean, and the air masses from the Transition regime propagate towards Madagascar and Africa. FLEXPART calculations reveal that both transport regimes lift air masses up to a mean height of about 5.3 km after 1 month (not shown here). The trajectories of the Monsoon Circulation regime first travel with the southeasterly trade winds and then with the southwesterly monsoon winds. The trajectories stay relatively close to the ocean surface (below 3 km) until they reach the Bay of Bengal, where they are rapidly lifted to the upper troposphere. On average they reach a height of 7.9 km after 1 month, which reveals that this is the regime with the most convection. The trajectories of the Local Convection regime mainly experience rapid uplift around the equator. After 1 month this group has reached a mean height of 7.2 km. The different uplifts are reflected in the vertical distribution of bromoform in each transport regime (Fig. S3).

The absolute entrainment of oceanic VSLs to the stratosphere depends on the emission strength as well as the transport efficiency (Fig. 4). This efficiency is defined as the ratio between entrained and emitted VSLs. It depends on the transit time, defined as the time an air parcel needs to be transported from the ocean surface to 17 km height, and the lifetime of the compound. For stratospheric entrainment the transit time must be on the order of the lifetime of a compound or shorter. If the transit time is considerably larger than the lifetime, most of the compound decays before reaching the stratosphere. In the following, we will use the expressions VSLs' transit time, which is the transit time including loss processes of the VSL in the atmosphere during the trans-

port, and transit half-life, which is the time after which half of the total amount of entrained tracer has been entrained above 17 km. We also calculated the relative emission and entrainment by regime. Table 4 displays the absolute and relative emissions and entrainment, the transport efficiency, and the transit half-life for the whole cruise and the four regimes.

The mean sea surface release of CHBr₃ in FLEXPART is 0.43 μmol (on 0.0002° × 0.0002° h⁻¹) during the cruise, and the mean entrainment to the stratosphere is 5.5 nmol, resulting in a mean transport efficiency of 1.3 %. CH₂Br₂ has a higher transport efficiency of 5.5 %, with mean emissions of 0.43 μmol (on 0.0002° × 0.0002° h⁻¹) and very high stratospheric entrainment of 23.6 nmol. CH₃I has a low transport efficiency of 0.3 %, with mean emissions of 0.22 μmol (on 0.0002° × 0.0002° h⁻¹) and stratospheric entrainment of 0.7 nmol.

The four transport regimes show different transport efficiencies for CHBr₃, CH₂Br₂, and CH₃I to the stratosphere. The two most efficient regimes, transporting CHBr₃ and CH₃I to the stratosphere during the OASIS cruise, were the Monsoon Circulation and the Local Convection regime.

The transport efficiency for all three compounds is highest in the Local Convection regime (CHBr₃ ~ 3 %, CH₂Br₂ ~ 9 %, and CH₃I ~ 1 %), because this regime has the shortest transit half-life for all three VSLs. For CH₃I, the compound with the shortest lifetime, the fast transport plays the largest role, and thus this regime is by far the most efficient.

For CHBr₃, the regime with most absolute and relative stratospheric entrainment (11 nmol, 57 %) is the Monsoon Circulation regime because of the high emissions in the

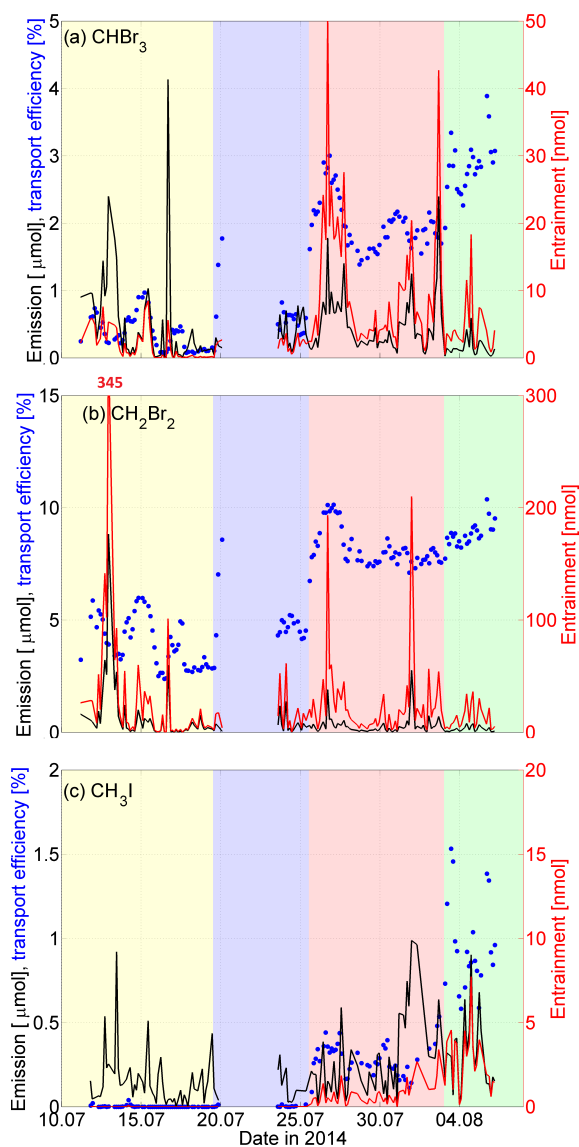


Figure 4. CHBr_3 , CH_2Br_2 , and CH_3I emission entrainment at 17 km and transport efficiency for measurements from the OASIS cruise. The background shading highlights the transport regimes: Westerlies (yellow), Transition (blue), Monsoon Circulation (red), and Local Convection (green).

source region and the high transport efficiency. Although the CHBr_3 emissions are as high in the Westerlies regime, the entrainment is small (2 nmol, 9 %) because of a low transport efficiency due to slow transport visible in the long transit half-life. The Local Convection regime has the highest transport efficiency, but emissions were low, resulting in less entrainment (4 nmol, 23 %) than in the Monsoon Circulation regime. The absolute entrainment of CH_2Br_2 strongly depends on the strength of emission, because the transport efficiency is relatively similar for all transport regimes due to the long lifetime of the compound. Most entrained CH_2Br_2 comes from the Westerlies regime (29 nmol, 35 %),

where sources especially south of Madagascar were extremely strong. Although these emissions occur in the subtropics, they reach 17 km mainly in the tropics (Fig. S4). The transport efficiency of 4 % still allows a large amount of 345 nmol CH_2Br_2 to enter the stratosphere from the maximum emissions at 23:00 UTC on 12 July 2014 (Fig. 4). The CH_3I absolute entrainment (2.8 nmol, 79 %) is highest in the Local Convection regime because of both the highest emissions and highest transport efficiency (Table 4).

3.5 Comparison of VSLS entrainment to the stratosphere with other oceanic regions

A comparison of the subtropical and tropical Indian Ocean contribution to the stratosphere with other tropical ocean regions, applying the same emission calculation and model setup (Sect. 2.2) for CHBr_3 , is shown in Table 5. Though the western Pacific TransBrom cruise had lower bromoform emission rates compared to OASIS, stratospheric entrainment was greater for the western Pacific region compared to the Indian Ocean. This difference was caused by a higher transport efficiency of 4.4 % in the west Pacific influenced by tropical cyclone activity in October 2009 (Krüger and Quack, 2013). Tegtmeier et al. (2012) obtained a higher transport efficiency of 5 % for TransBrom using a previous FLEXPART model (version 8.0). During the SHIVA campaign in the South China Sea, high oceanic concentrations of bromoform produced mean emission rates that were higher than during OASIS. The SHIVA calculations show even higher transport efficiencies of 7.9 %, which lead to an entrainment of 48.4 nmol CHBr_3 (Table 5), because of the strong convective activity in that region during the time (Fuhlbrügge et al., 2016b). The MSM18/3 cruise in the equatorial Atlantic (Hepach et al., 2015) has the smallest emissions, entrainment, and a transport efficiency of 0.9 % (Table 5). Overall, the comparison indicates that more CHBr_3 was entrained to the stratosphere from the tropical west Pacific than from the tropical west Indian Ocean during the Asian summer monsoon using available in situ emissions and 6-hourly meteorological fields. This is in contrast to the study by Liang et al. (2014), who determined with a chemistry climate model climatology that emissions from the tropical Indian Ocean deliver more brominated VSLSs into the stratosphere than tropical west Pacific emissions.

CH_2Br_2 entrainment to the stratosphere for the TransBrom ship campaign was ~ 8 nmol with transport efficiencies of 15 % (Tegtmeier et al., 2012). This is much higher than the Indian Ocean transport efficiency of 6.4 %, but the absolute entrainment of 23.6 nmol CH_2Br_2 we calculated for the OASIS cruise (Table 4) is much higher than during TransBrom, because of the very strong CH_2Br_2 emissions during OASIS.

Tegtmeier et al. (2013) investigated CH_3I entrainment to the stratosphere for three tropical ship campaigns: SHIVA and TransBrom in the tropical west Pacific and DRIVE in the tropical northeast Atlantic. They used a CH_3I lifetime

Table 4. Mean FLEXPART emission, entrainment at 17 km, transport efficiency, and transit half-life for CHBr₃, CH₂Br₂ and CH₃I for the mean and different transport regimes of the OASIS cruise.

VLS	Transport regime	FLEXPART emission (μmol)	Emissions by regime (%)	Transport efficiency (%)	FLEXPART entrainment (nmol)	Entrainment by regime (%)	Transit half-life (days)
CHBr ₃	Cruise mean	0.43	–	1.3	5.5	–	21
	Westerlies	0.49	32	0.4	1.83	9	32
	Transition	0.36	24	0.6	2.05	11	24
	Monsoon Circulation	0.51	34	2.1	10.70	57	15
	Local Convection	0.15	10	2.9	4.31	23	10
CH ₂ Br ₂	Cruise mean	0.43	–	5.5	23.6	–	86
	Westerlies	0.71	48	4.0	28.8	35	112
	Transition	0.32	22	4.9	15.0	19	114
	Monsoon Circulation	0.31	21	8.2	26.2	31	63
	Local Convection	0.14	9	8.8	12.7	15	57
CH ₃ I	Cruise mean	0.22	–	0.3	0.7	–	6
	Westerlies	0.15	18	0.0	0.00	0	9
	Transition	0.11	13	0.0	0.00	0	9
	Monsoon Circulation	0.28	33	0.3	0.74	21	7
	Local Convection	0.31	36	1.0	2.77	79	1

Table 5. CHBr₃ entrainment at 17 km for different ocean regions using the same transfer coefficient for the emission calculations and FLEXPART model setup (Sect. 2.2). The table lists the average value and 1 SD. The brackets give the range of single calculations.

Ocean region	Campaign information	FLEXPART emission (nmol)	FLEXPART entrainment (nmol)	Transport efficiency (%)
West Indian Ocean	OASIS, Jul 2014, this study	430 ± 520 [4–4130]	5.5 ± 7.5 [0.0–50.1]	1.4 ± 1.0 [0.1–3.9]
Open west Pacific	TransBrom, Oct 2009, Krüger and Quack (2013)	190 ± 300 [0–5680]	7.1 ± 10.4 [0.0–61.8]	4.4 ± 1.6 [1.9–8.8]
Coastal west Pacific	SHIVA, Nov 2011, Fuhlbrügge et al. (2016b)	610 ± 720 [1–5680]	48.4 ± 52.1 [0.7–250.1]	7.9 ± 3.7 [3.2–20.2]
Equatorial Atlantic	MSM18/3, Jun 2011, Hepach et al. (2015)	320 ± 400 [2–1910]	2.7 ± 3.2 [0.0–14.2]	0.9 ± 0.2 [0.5–1.4]

profile between 2 and 3 days. The transport efficiencies were 4, 1, and 0.1 %, respectively. The OASIS Indian Ocean mean transport efficiency for CH₃I (0.3 %, Table 4), applying a uniform lifetime profile of 3.5 days, is lower than in the west Pacific but higher than in the Atlantic.

Uncertainties of VLS emissions and the modeling of their transport to the stratosphere will be further discussed in Sect. 5.

4 General transport from west Indian Ocean to the stratosphere

4.1 Spatial variability of stratospheric entrainment

We calculate the entrainment at 17 km for CHBr₃, CH₂Br₂, and CH₃I tracers by weighting the trajectories from the west Indian Ocean release region for July 2000–2015 with the transit-time-dependent atmospheric decay plotted in Fig. 5. A summary of transport efficiency, transit half-life, and entrainment correlations for all three VLSs can be found in Table 6.

The distribution of VLS transit times shows that the shorter the lifetime of a compound is, the more important the transport on short timescales is (Fig. 5). For CHBr₃, CH₂Br₂,

Table 6. Entrainment of CHBr₃, CH₂Br₂, and CH₃I tracer at 17 km altitude through different transport regimes from the west Indian Ocean release box. Correlations with significance of more than 95 % are marked in bold. (Note, transit half-lives differ from Table 4 because of the different model setups.)

Tracer	Transport regime	Mean transport efficiency (%)	Transit half-life (days)	Interannual correlation with Total entrainment	Interannual correlation with Local Convection entrainment
CHBr ₃	Total	1.86	8.5	1.00	0.45
	Local Convection	0.24	1.8	0.45	1.00
	Monsoon Circulation	0.50	6.0	0.54	−0.20
CH ₂ Br ₂	Total	5.88	27.2	1.00	0.24
	Local Convection	0.32	2.4	0.24	1.00
	Monsoon Circulation	1.11	13.3	0.56	−0.06
CH ₃ I	Total	0.42	1.9	1.00	0.91
	Local Convection	0.17	1.2	0.91	1.00
	Monsoon Circulation	0.09	1.0	−0.06	−0.31

and CH₃I tracers, the transit half-lives are 8.5, 27.2, and 1.9 days, respectively (Table 6). For the two bromocarbons, the transit time distribution shows two maxima, one for the 0–2 days bin and the second between 4–10 days for CHBr₃ and 6–12 days for CH₂Br₂. CH₃I tracer entrainment occurs mainly on timescales up to 2 days (Fig. 5).

The stratospheric entrainment regions during the Asian summer monsoon between 2000 and 2015 are displayed at the locations where the trajectories first reach 17 km (Fig. 6). The VLS tracers show two main entrainment regions. Enhanced entrainment occurs above the Bay of Bengal and northern India in the southeastern part of the Asian monsoon anticyclone and is connected to the Monsoon Circulation transport regime (Sect. 3.4). The second entrainment region is above the tropical west Indian Ocean and belongs to the Local Convection regime. We define these two regions to enclose the core entrainment and to be evenly sized in grid space (colored boxes in Fig. 6).

The larger west Indian Ocean release area and longer time series analysis (Table 6) confirms the results of our OASIS analysis (Table 4). The longer-lived VLS tracers (CHBr₃ and CH₂Br₂) are mainly entrained through the Monsoon Circulation regime, while the Local Convection regime is more important for the shortest-lived tracer (CH₃I).

Chen et al. (2012) also identified these two stratospheric entrainment regions, analyzing the air transport from the atmospheric boundary layer to the tropopause layer in the Asian Summer monsoon region for a 9-year climatology. Additionally, they registered entrainment over the west Pacific Ocean, but the Local Convection entrainment above the central Indian Ocean was by far the strongest. Similar to our VLS transit times, the study of Chen et al. (2012) found very short transport timescales of 0–1 days in the equatorial west Indian Ocean, while transit times above the Bay of Bengal and northern India were between 3 and 9 days.

4.2 Interannual variability of stratospheric entrainment

The time series of stratospheric entrainment from the west Indian Ocean to the stratosphere shows interannual variability for all three VLS tracers (Fig. 7). Overall, July 2014 revealed high entrainment for CHBr₃ and CH₂Br₂ tracers and low entrainment for CH₃I tracer. The coefficient of variation (CV) for total entrainment is 0.13, 0.09, and 0.21 for CHBr₃, CH₂Br₂ and CH₃I, respectively. Thus, the shortest-lived compound CH₃I has the strongest interannual variation, and the longest-lived CH₂Br₂ has the weakest variation.

In order to analyze which transport regime has a stronger influence on the total entrainment variability, we correlated the interannual entrainment time series of total entrainment with the entrainment in the Monsoon Circulation and Local Convection regimes (Table 6). Interannual variability of CHBr₃ and CH₂Br₂ tracer entrainment results mainly from variability in the Monsoon Circulation regime ($r = 0.54$ and $r = 0.56$, respectively). In contrast, the interannual variability of CH₃I tracer entrainment is highly correlated with the Local Convection regime variability ($r = 0.91$). The high variability of total CH₃I entrainment (CV = 0.21) implies that interannual variation in convection is larger than in the monsoon circulation. The interannual time series of the Monsoon Circulation and Local Convection regime reveal a weak inverse correlation for all three compounds, suggesting that more entrainment in one regime is related to less entrainment in the other (Fig. 7).

The interannual time series of total VLS tracer entrainment displays a small increase over time. This increase is independent of the chosen entrainment height (between 13 and 18 km, Fig. S5) and is visible in the analysis for all three tracers. The increase is strongest for CHBr₃ and weaker for the other two compounds. It arises mainly from an increase

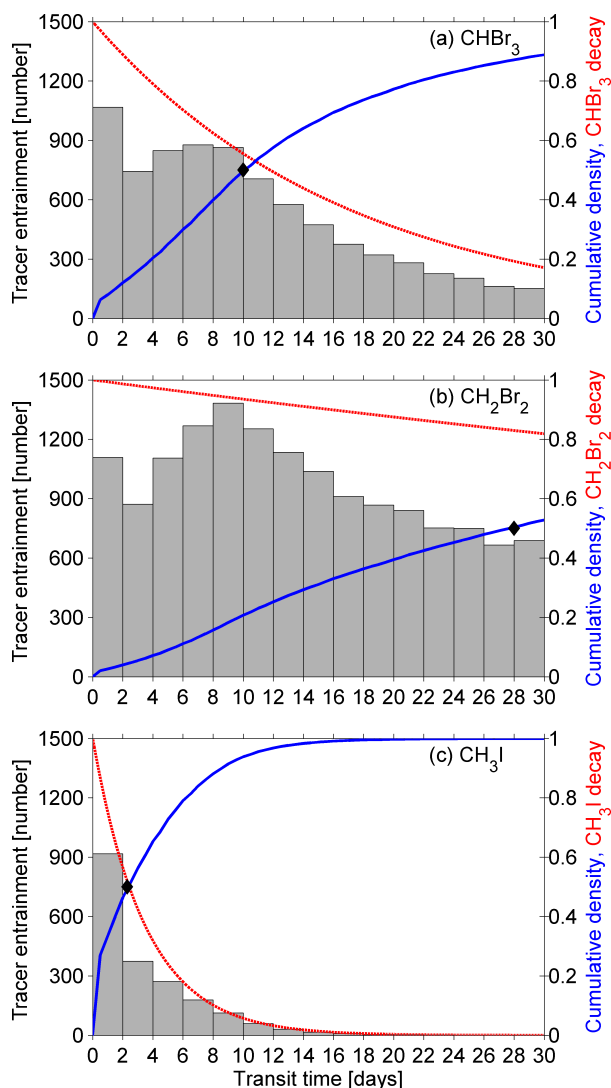


Figure 5. VLSL transit time distribution for entrainment at 17 km of (a) CHBr_3 , (b) CH_2Br_2 , and (c) CH_3I tracers released in July 2000–2015. Entrained tracer per time interval of 2 days is given as number (gray bars). The blue line gives the cumulative distribution and denotes the transit half-life. The red line shows the decay of the tracers during the transport simulation. The black diamond denotes the transit half-life.

in entrainment in the Monsoon Circulation regime (Fig. 7). Analyzing changes of rainfall revealed an increase in precipitation over northeastern India for the time interval of our transport study (Latif et al., 2016; Preethi et al., 2016). This indicates an increase in convection in our Monsoon Circulation regime over the years from 2000 to 2015, which can explain the increase in stratospheric entrainment. However, for the long time period from the 1950s to the 2010s the same authors found a decrease of precipitation over the above-mentioned area, potentially impacting the VLSL entrainment to the stratosphere.

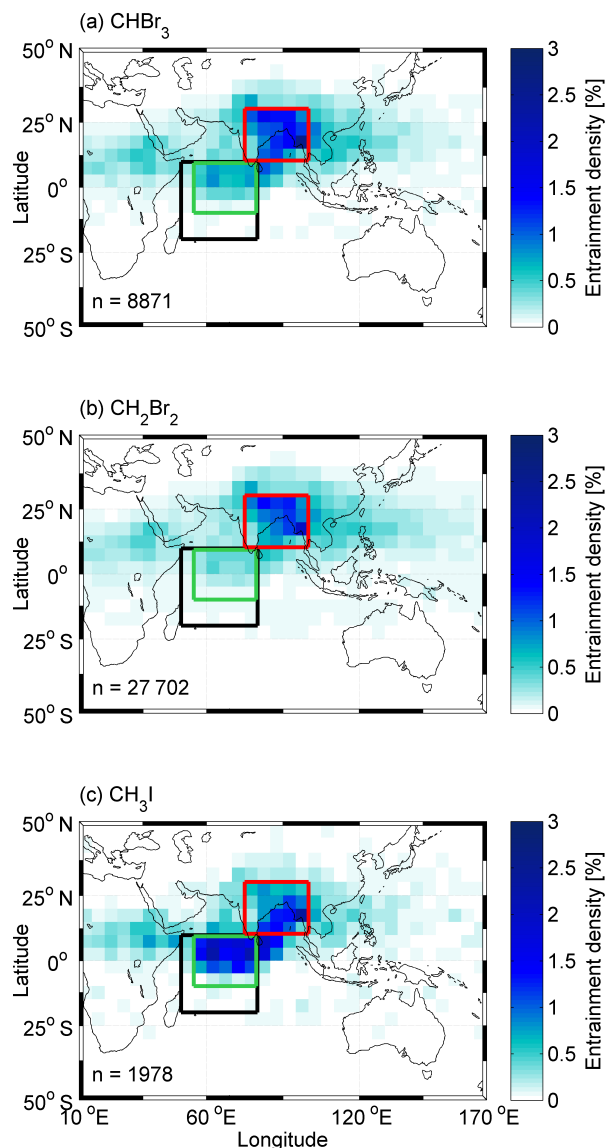


Figure 6. Density at 17 km of (a) CHBr_3 , (b) CH_2Br_2 , and (c) CH_3I tracer on a $5^\circ \times 5^\circ$ grid that is released from the west Indian Ocean surface (black box) in July 2000–2015. Colored boxes show the entrainment regions of the Local Convection (green) and Monsoon Circulation (red) regimes.

In a follow-up study we will investigate the influence of the seasonal cycle of the Asian monsoon circulation and interannual influences through atmospheric circulation patterns on the west Indian Ocean VLSL entrainment to the stratosphere in more detail.

5 Uncertainties in the analysis

This study confirms that the subtropical and tropical west Indian Ocean is a source region of oceanic halogenated VLSLs to the stratosphere during the Asian summer mon-

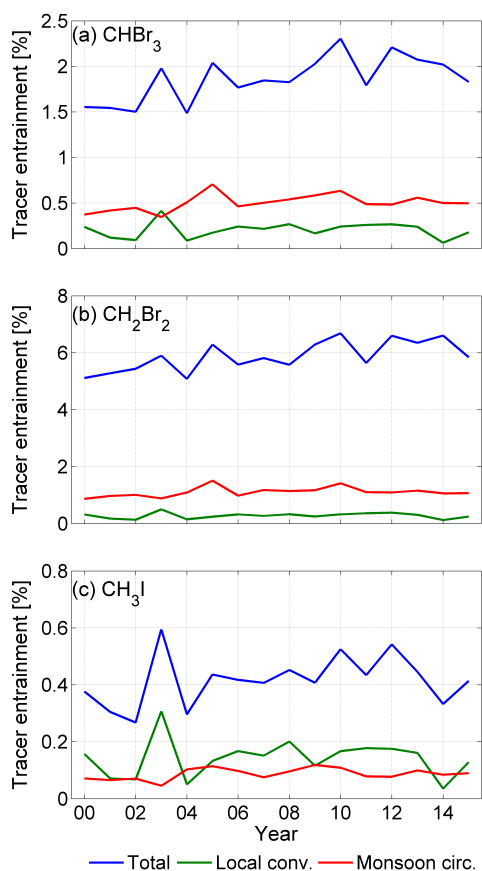


Figure 7. (a) CHBr₃, (b) CH₂Br₂, and (c) CH₃I tracer entrainment at 17 km from trajectories released from the west Indian Ocean surface box in July 2000–2015. The entrainment is evaluated for three regions: Total, Local Convection, and Monsoon Circulation (see Fig. 6).

soon. The amount of VSLSs entrained depends on the emission strength, the lifetime of the compound, and the transport of trajectories in the regime, which have been quantified in this study.

However, uncertainties of this study are present in various aspects of the analysis. The uncertainties result from the calculation of VSLS emissions, the FLEXPART transport using ERA-Interim reanalysis fields, and the definition of entrainment to the stratosphere.

The calculation of VSLS emissions from the concentration gradient between the ocean at 5 m depth and the atmosphere at 20 m height is subject to measurement uncertainties and a possible different concentration gradient directly at the air–sea interface. Additionally, the applied wind-speed-based parameterization for air–sea flux, which represents a reasonable mean of the published parameterizations, is uncertain by more than a factor of two (Lennartz et al., 2015). Both factors may lead to a systematic flux under- or overestimation in our study.

A vital part of this study is the meteorological reanalysis data from ERA-Interim and the FLEXPART model for determining the VSLS transport. With delivery of our radiosonde launches to the GTS we have improved the data coverage over the Indian Ocean for the time in our study and thus the quality of meteorological reanalysis. Indeed, horizontal wind speed and direction from ship sensors and sondes agree well with the ERA-Interim data (Fig. S2). As the scale of tropical convection is below the state-of-the-art grid scale of global atmospheric models, it is not sufficiently resolved and must be parameterized. The Lagrangian model FLEXPART uses a convection scheme, described and evaluated by Forster et al. (2007), to account for vertical transport. Using FLEXPART trajectories with ERA-Interim reanalysis, Fuhlbrügge et al. (2016b) were able to simulate VSLS mixing ratios from the surface to the free troposphere up to 11 km above the tropical west Pacific in very good agreement with corresponding aircraft measurements applying a simple source-loss approach. Tegtmeier et al. (2013) showed that the FLEXPART distribution of oceanic CH₃I in the tropics agrees well with adjacent upper tropospheric and lower stratospheric aircraft measurements, thus increasing our confidence in the FLEXPART convection scheme and ERA-Interim velocities. Testing different FLEXPART model versions (8.0 and 9.2) for stratospheric entrainment of CHBr₃ (not shown) has revealed only a slightly lower stratospheric entrainment of 0.2 % with the more recent model version 9.2 used in this study here.

Another uncertainty in the location and variability of entrained trajectories may result from the definition of stratospheric entrainment (Sect. 2.2). For the tropics, the cold point tropopause is commonly used as the boundary between the troposphere and the stratosphere (Carpenter et al., 2014). The average measured CPT height during OASIS was 17 km (Fig. S1), but it can be up to 17.6 km high within the Asian monsoon anticyclone during the boreal summer season (Munchak and Pan, 2014). To test the sensitivity of our results with regard to the entrainment height, we analyzed entrained trajectories at several different tropical levels in the upper troposphere/lower stratosphere (UTLS; 13, 15, 17, and 18 km altitude, Fig. S6). As described in Sect. 3.4, we can follow the preferred transport pathways by the migration of maximum density at the intersecting UTLS levels. Analyzing the influence of the application of different UTLS entrainment levels reveals an overall good agreement of interannual variability and long-term changes (Figs. S5 and S6).

6 Summary and conclusion

During the OASIS research cruise in the subtropical and tropical west Indian Ocean in July and August 2014, we conducted simultaneous measurements of the halogenated very short-lived substances, methyl iodide (CH₃I) and for the first time of bromoform (CHBr₃) and dibromomethane

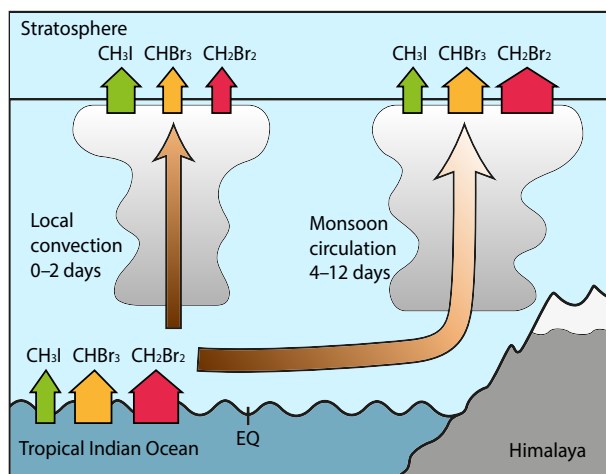


Figure 8. Schematic illustration of emission, transport pathways and timescales, and entrainment of CH₃I, CHBr₃, and CH₂Br₂ tracer from the tropical west Indian Ocean to the stratosphere during the Asian summer monsoon.

(CH₂Br₂), in surface seawater and the marine atmosphere. Based on these measurements, we calculated high emissions of CHBr₃ of $910 \pm 1160 \text{ pmol m}^{-2} \text{ h}^{-1}$ caused by high oceanic concentrations south of Madagascar and moderate concentrations combined with high wind speeds (up to 15 ms^{-1}) in the trade wind regime above the open west Indian Ocean. The average CHBr₃ emissions were at the higher end of previously reported values of the tropical oceans. CH₂Br₂ emissions of $930 \pm 2000 \text{ pmol m}^{-2} \text{ h}^{-1}$ were also especially high south of Madagascar and on average higher than reported from cruises in other tropical regions, from global observational and model-based climatologies. CH₃I emissions ($460 \pm 430 \text{ pmol m}^{-2} \text{ h}^{-1}$) were highest around the equator but in the range of previously reported emission rates from subtropical and tropical ocean regions.

The stratospheric entrainment of these three VSLs from the west Indian Ocean during the Asian summer monsoon depends on the strength of emissions and the timescale of the transport to the stratosphere in comparison to the lifetime of the compound. The entrainment of the shortest-lived compound CH₃I (3.5 days) depends mainly on fast transport. The entrainment of CH₂Br₂ strongly depends on the emission strength, because the transport efficiency is relatively similar for all transport regimes due to the long lifetime of the compound (150 days). CHBr₃ (17 days lifetime) entrainment is influenced by both oceanic emissions and fast transport.

During the OASIS cruise we found four transport regimes with different VSL emission strengths and transport efficiencies. The Monsoon Circulation and the Local Convection regime were the most efficient for VSL entrainment into the stratosphere. These two have different source regions, VSL transit times, stratospheric entrainment regions, and interannual variations summarized in Fig. 8.

In the Monsoon Circulation regime, the oceanic VSL transport pathway begins south of the equator and follows the near-surface winds to India and the Bay of Bengal, where monsoon convection rapidly lifts them into the upper troposphere. The VSLs ascend further within the Asian monsoon anticyclone, being entrained to stratospheric levels in its southeastern part. The transport to the stratosphere in this regime is effective for CHBr₃ and CH₂Br₂ (2 and 8 % transport efficiency, respectively) but less effective for CH₃I (0.3 %), as its lifetime is shorter than the transport timescale. Absolute CHBr₃ entrainment from the OASIS cruise was strongest in the Monsoon Circulation regime because of strong emissions in the source region. The Indian Ocean setup showed that it is generally the preferred regime for the entrainment of VSLs with longer lifetimes during the boreal summer, because many trajectories follow this transport pathway. Mean transit half-lives from the west Indian Ocean surface to 17 km height are 6 days for CHBr₃ and 13 days for CH₂Br₂.

In the Local Convection regime, VSLs are transported upwards by convection above the tropical west Indian Ocean and entrained to the stratosphere in the vicinity of the equator. VSL transit times are short (0–2 days), and thus we found the highest transport efficiencies for CHBr₃, CH₂Br₂, and CH₃I in this region (3, 9, and 1 %). The Local Convection regime is responsible for most of the stratospheric entrainment of CH₃I from the OASIS cruise. The Indian Ocean transport study supports this finding.

CH₂Br₂ transport efficiency is similar for all regimes of the OASIS cruise, because its lifetime is longer than the transport timescale from ocean to stratosphere in the tropics. Absolute entrainment of CH₂Br₂ thus strongly depends on the strength of emissions, and these were very high during OASIS, especially south of Madagascar.

In comparison to other corresponding cruises, the Monsoon Circulation and Local Convection regime in the tropical west Indian Ocean show more entrainment of CHBr₃ and CH₃I than the tropical Atlantic but less than the tropical west Pacific Ocean. CH₂Br₂ entrainment from the west Indian Ocean was higher than from previous corresponding cruises in other tropical oceans due to the very high emissions.

A 16-year time series (2000–2015) of VSL tracer entrainment from the west Indian Ocean to the stratosphere through the monsoon circulation during July reveals the strongest interannual variability for CH₃I, the shortest-lived compound, which seems to be connected to the interannual variation in convection above the west Indian Ocean. The weakest variations were found for CH₂Br₂, the longest-lived compound, whose entrainment hardly depends on the local atmospheric circulation. The time series of entrainment to the stratosphere shows an overall increase for all three compounds, which is likely connected to a reported increase in precipitation and convection over northeastern India during this time period. For CHBr₃, whose transport is mostly associated with the

changing Asian summer monsoon circulation, the increase is stronger than for the other two compounds.

Overall, the OASIS measurements confirm that during boreal summer the subtropical and tropical west Indian Ocean is an important source for VSLs, especially of CH₂Br₂, with pronounced hot spots. This study demonstrates that the VSL delivery from the west Indian Ocean surface to the stratosphere depends on the regional strength of emissions and the transit time in preferred transport regimes. Changes in the Asian summer monsoon circulation likely impact the VSL entrainment to the stratosphere.

Data availability. The underlying data will be available at the open-access library Pangaea (<http://www.pangaea.de>).

The Supplement related to this article is available online at <https://doi.org/10.5194/acp-17-6723-2017-supplement>.

Author contributions. A. Fiehn, K. Krüger, and B. Quack designed the experiments, and A. Fiehn carried them out. K. Krüger was the cruise leader; all authors were involved in the VSL measurements and analyses taken during the OASIS cruise. A. Fiehn, K. Krüger, and B. Quack prepared the manuscript with contributions from all co-authors.

Competing interests. The authors declare that they have no conflict of interest.

Acknowledgements. This study was supported by BMBF grant SONNE 03G0235A. We acknowledge the authorities of Madagascar, Mauritius, the United Kingdom, and the Maldives for the permissions to work in their territorial waters. We would also like to thank the captain and crew of RV *Sonne* as well as the student participants during SPACES for their help and cooperation. We thank the European Centre for Medium-Range Weather Forecasts (ECMWF) for the provision of ERA-Interim reanalysis data and the FLEXPART development team for the Lagrangian particle dispersion model used in this publication. Part of the FLEXPART simulations was performed on resources provided by UNINETT Sigma2 – the National Infrastructure for High Performance Computing and Data Storage in Norway. E. Atlas acknowledges support from the NASA Upper Atmosphere Research Program grant no. NNX13AH20G. Additional thanks go to the editor, J.-U. Groöf, and the two anonymous reviewers for their helpful comments.

The article processing charges for this open-access publication were covered by a Research Centre of the Helmholtz Association.

Edited by: J.-U. Groöf

Reviewed by: two anonymous referees

References

- Bell, N., Hsu, L., Jacob, D. J., Schultz, M. G., Blake, D. R., Butler, J. H., King, D. B., Lobert, J. M., and Maier-Reimer, E.: Methyl iodide: Atmospheric budget and use as a tracer of marine convection in global models, *J. Geophys. Res.-Atmos.*, 107, 1–12, <https://doi.org/10.1029/2001jd001151>, 2002.
- Bergman, J. W., Fierli, F., Jensen, E. J., Honomichl, S., and Pan, L. L.: Boundary layer sources for the Asian anticyclone: Regional contributions to a vertical conduit, *J. Geophys. Res.-Atmos.*, 118, 2560–2575, <https://doi.org/10.1002/jgrd.50142>, 2013.
- Butler, J. H., King, D. B., Lobert, J. M., Montzka, S. A., Yvon-Lewis, S. A., Hall, B. D., Warwick, N. J., Mondeel, D. J., Aydin, M., and Elkins, J. W.: Oceanic distributions and emissions of short-lived halocarbons, *Global Biogeochem. Cy.*, 21, GB1023, <https://doi.org/10.1029/2006gb002732>, 2007.
- Carpenter, L. J., Sturges, W. T., Penkett, S. A., Liss, P. S., Alicke, B., Hebestreit, K., and Platt, U.: Short-lived alkyl iodides and bromides at Mace Head, Ireland: Links to biogenic sources and halogen oxide production, *J. Geophys. Res.-Atmos.*, 104, 1679–1689, <https://doi.org/10.1029/98jd02746>, 1999.
- Carpenter, L. J., Jones, C. E., Dunk, R. M., Hornsby, K. E., and Woeltjen, J.: Air-sea fluxes of biogenic bromine from the tropical and North Atlantic Ocean, *Atmos. Chem. Phys.*, 9, 1805–1816, <https://doi.org/10.5194/acp-9-1805-2009>, 2009.
- Carpenter, L. J., Reimann, S., Burkholder, J. B., Clerbaux, C., Hall, B. D., Hossaini, R., Laube, J. C., and Yvon-Lewis, S. A.: Ozone-Depleting Substances (ODSs) and other gases of interest to the Montreal Protocol, in: Scientific Assessment of Ozone Depletion: 2014. Global Ozone Research and monitoring Project – Report N. 55, World Meteorological Organization, Geneva, Switzerland, 2014.
- Chen, B., Xu, X. D., Yang, S., and Zhao, T. L.: Climatological perspectives of air transport from atmospheric boundary layer to tropopause layer over Asian monsoon regions during boreal summer inferred from Lagrangian approach, *Atmos. Chem. Phys.*, 12, 5827–5839, <https://doi.org/10.5194/acp-12-5827-2012>.
- Dee, D. P., Uppala, S. M., Simmons, A. J., Berrisford, P., Poli, P., Kobayashi, S., Andrae, U., Balmaseda, M. A., Balsamo, G., Bauer, P., Bechtold, P., Beljaars, A. C. M., van de Berg, L., Bidlot, J., Bormann, N., Delsol, C., Dragani, R., Fuentes, M., Geer, A. J., Haimberger, L., Healy, S. B., Hersbach, H., Hólm, E. V., Isaksen, I., Kållberg, P., Köhler, M., Matricardi, M., McNally, A. P., Monge-Sanz, B. M., Morcrette, J. J., Park, B. K., Peubey, C., de Rosnay, P., Tavolato, C., Thépaut, J. N., and Vitart, F.: The ERA-Interim reanalysis: configuration and performance of the data assimilation system, *Q. J. Roy. Meteor. Soc.*, 137, 553–597, <https://doi.org/10.1002/qj.828>, 2011.
- Dorf, M., Bösch, H., Butz, A., Camy-Peyret, C., Chipperfield, M. P., Engel, A., Goutail, F., Grunow, K., Hendrick, F., Hrechanyy, S., Naujokat, B., Pommerehne, J. P., Van Roozendael, M., Sioris, C., Strohm, F., Weidner, F., and Pfeilsticker, K.: Balloon-borne stratospheric BrO measurements: comparison with Envisat/SCIAMACHY BrO limb profiles, *Atmos. Chem. Phys.*, 6, 2483–2501, <https://doi.org/10.5194/acp-6-2483-2006>, 2006.
- Dvortsov, V. L., Geller, M. A., Solomon, S., Schauffler, S. M., Atlas, E. L., and Blake, D. R.: Rethinking reactive halogen budgets in the midlatitude lower stratosphere, *Geophys. Res. Lett.*, 26, 1699–1702, <https://doi.org/10.1029/1999gl900309>, 1999.

- Finlayson-Pitts, B. and Pitts, J.: Chemistry of the upper and lower atmosphere: Theory, experiments and applications, Academic, US, 2000.
- Forster, C., Stohl, A., and Seibert, P.: Parameterization of convective transport in a Lagrangian particle dispersion model and its evaluation, *J. Appl. Meteorol. Climatol.*, 46, 403–422, <https://doi.org/10.1175/JAM2470.1>, 2007.
- Fuhlbrügge, S., Krüger, K., Quack, B., Atlas, E., Hepach, H., and Ziska, F.: Impact of the marine atmospheric boundary layer conditions on VLSL abundances in the eastern tropical and subtropical North Atlantic Ocean, *Atmos. Chem. Phys.*, 13, 6345–6357, <https://doi.org/10.5194/acp-13-6345-2013>, 2013.
- Fuhlbrügge, S., Quack, B., Atlas, E., Fiehn, A., Hepach, H., and Krüger, K.: Meteorological constraints on oceanic halocarbons above the Peruvian upwelling, *Atmos. Chem. Phys.*, 16, 12205–12217, <https://doi.org/10.5194/acp-16-12205-2016>, 2016a.
- Fuhlbrügge, S., Quack, B., Tegtmeier, S., Atlas, E., Hepach, H., Shi, Q., Raimund, S., and Krüger, K.: The contribution of oceanic halocarbons to marine and free tropospheric air over the tropical West Pacific, *Atmos. Chem. Phys.*, 16, 7569–7585, <https://doi.org/10.5194/acp-16-7569-2016>, 2016b.
- Garratt, J. R.: Review of Drag Coefficients over Oceans and Continents, *Month. Weather Rev.*, 105, 915–929, [https://doi.org/10.1175/1520-0493\(1977\)105<0915%3ARODCOO>2.0.CO%3B2](https://doi.org/10.1175/1520-0493(1977)105<0915%3ARODCOO>2.0.CO%3B2), 1977.
- Gottelmann, A., Kinnison, D., Dunkerton, T. J., and Brasseur, G. P.: Impact of monsoon circulations on the upper troposphere and lower stratosphere, *J. Geophys. Res.*, 109, D22101, <https://doi.org/10.1029/2004jd004878>, 2004.
- Hense, I. and Quack, B.: Modelling the vertical distribution of bromoform in the upper water column of the tropical Atlantic Ocean, *Biogeosciences*, 6, 535–544, <https://doi.org/10.5194/bg-6-535-2009>, 2009.
- Hepach, H., Quack, B., Ziska, F., Fuhlbrügge, S., Atlas, E., Krüger, K., Peeken, I., and Wallace, D. W. R.: Drivers of diel and regional variations of halocarbon emissions from the tropical North East Atlantic, *Atmos. Chem. Phys.*, 14, 1255–1275, <https://doi.org/10.5194/acp-14-1255-2014>, 2014.
- Hepach, H., Quack, B., Raimund, S., Fischer, T., Atlas, E. L., and Bracher, A.: Halocarbon emissions and sources in the equatorial Atlantic Cold Tongue, *Biogeosciences*, 12, 6369–6387, <https://doi.org/10.5194/bg-12-6369-2015>, 2015.
- Hepach, H., Quack, B., Tegtmeier, S., Engel, A., Bracher, A., Fuhlbrügge, S., Galgani, L., Atlas, E. L., Lampel, J., Frieß, U., and Krüger, K.: Biogenic halocarbons from the Peruvian upwelling region as tropospheric halogen source, *Atmos. Chem. Phys.*, 16, 12219–12237, <https://doi.org/10.5194/acp-16-12219-2016>, 2016.
- Hoskins, B. J. and Rodwell, M. J.: A Model of the Asian Summer Monsoon. Part I: The Global Scale, *J. Atmos. Sci.*, 52, 1329–1340, [https://doi.org/10.1175/1520-0469\(1995\)052<1329:AMOTAS>2.0.CO;2](https://doi.org/10.1175/1520-0469(1995)052<1329:AMOTAS>2.0.CO;2), 1995.
- Hossaini, R., Chipperfield, M. P., Monge-Sanz, B. M., Richards, N. A. D., Atlas, E., and Blake, D. R.: Bromoform and dibromomethane in the tropics: a 3-D model study of chemistry and transport, *Atmos. Chem. Phys.*, 10, 719–735, <https://doi.org/10.5194/acp-10-719-2010>, 2010.
- Hossaini, R., Chipperfield, M. P., Feng, W., Breider, T. J., Atlas, E., Montzka, S. A., Miller, B. R., Moore, F., and Elkins, J.: The contribution of natural and anthropogenic very short-lived species to stratospheric bromine, *Atmos. Chem. Phys.*, 12, 371–380, <https://doi.org/10.5194/acp-12-371-2012>, 2012.
- Hossaini, R., Chipperfield, M. P., Montzka, S. A., Rap, A., Dhomse, S., and Feng, W.: Efficiency of short-lived halogens at influencing climate through depletion of stratospheric ozone, *Nat. Geosci.*, 8, 186–190, <https://doi.org/10.1038/ngeo2363>, 2015.
- Hossaini, R., Patra, P. K., Leeson, A. A., Krysztofiak, G., Abraham, N. L., Andrews, S. J., Archibald, A. T., Aschmann, J., Atlas, E. L., Belikov, D. A., Bönisch, H., Carpenter, L. J., Dhomse, S., Dorf, M., Engel, A., Feng, W., Fuhlbrügge, S., Griffiths, P. T., Harris, N. R. P., Hommel, R., Keber, T., Krüger, K., Lennartz, S. T., Maksyutov, S., Mantle, H., Mills, G. P., Miller, B., Montzka, S. A., Moore, F., Navarro, M. A., Oram, D. E., Pfeilsticker, K., Pyle, J. A., Quack, B., Robinson, A. D., Saikawa, E., Saiz-Lopez, A., Sala, S., Sinnhuber, B.-M., Taguchi, S., Tegtmeier, S., Lidster, R. T., Wilson, C., and Ziska, F.: A multi-model intercomparison of halogenated very short-lived substances (TransCom-VLSL): linking oceanic emissions and tropospheric transport for a reconciled estimate of the stratospheric source gas injection of bromine, *Atmos. Chem. Phys.*, 16, 9163–9187, <https://doi.org/10.5194/acp-16-9163-2016>, 2016.
- Hughes, C., Franklin, D. J., and Malin, G.: Iodomethane production by two important marine cyanobacteria: *Prochlorococcus marinus* (CCMP 2389) and *Synechococcus* sp. (CCMP 2370), *Mar. Chem.*, 125, 19–25, <https://doi.org/10.1016/j.marchem.2011.01.007>, 2011.
- James, R., Bonazzola, M., Legras, B., Surbled, K., and Fueglistaler, S.: Water vapor transport and dehydration above convective outflow during Asian monsoon, *Geophys. Res. Lett.*, 35, L20810, <https://doi.org/10.1029/2008gl035441>, 2008.
- Krüger, K. and Quack, B.: Introduction to special issue: the Trans-Brom Sonne expedition in the tropical West Pacific, *Atmos. Chem. Phys.*, 13, 9439–9446, <https://doi.org/10.5194/acp-13-9439-2013>, 2013.
- Latif, M., Syed, F. S., and Hannachi, A.: Rainfall trends in the South Asian summer monsoon and its related large-scale dynamics with focus over Pakistan, *Clim. Dynam.*, 1–doi:17, 10.1007/s00382-016-3284-3, 2016.
- Law, K. S., Sturges, W. T., Blake, D. R., Blake, N. J., Burkeholder, J. B., Butler, J. H., Cox, R. A., Haynes, P. H., Ko, M. K. W., Kreher, K., Mari, C., Pfeilsticker, K., Plane, J. M. C., Salawitch, R. J., Schiller, C., Sinnhuber, B. M., von Glasow, R., Warwick, N. J., Wuebbles, D. J., and Yvon-Lewis, S. A.: Halogenated Very Short-Lived Substances, in: Scientific Assessment of Ozone Depletion: 2006. Global Ozone Research and Monitoring Project – Report No. 50, World Meteorological Organization, Geneva, Switzerland, 2006.
- Lawrence, M. G. and Lelieveld, J.: Atmospheric pollutant outflow from southern Asia: a review, *Atmos. Chem. Phys.*, 10, 9463–9466, <https://doi.org/10.5194/acpd-10-9463-2010>, 2010.
- Lennartz, S. T., Krysztofiak, G., Marandino, C. A., Sinnhuber, B. M., Tegtmeier, S., Ziska, F., Hossaini, R., Krüger, K., Montzka, S. A., Atlas, E., Oram, D. E., Keber, T., Bönisch, H., and Quack, B.: Modelling marine emissions and atmospheric distributions of halocarbons and dimethyl sulfide: the influence of prescribed water concentration vs. prescribed emissions, *Atmos. Chem. Phys.*, 15, 11753–11772, <https://doi.org/10.5194/acp-15-11753-2015>, 2015.

- Liang, Q., Stolarski, R. S., Kawa, S. R., Nielsen, J. E., Douglass, A. R., Rodriguez, J. M., Blake, D. R., Atlas, E. L., and Ott, L. E.: Finding the missing stratospheric bromine: a global modeling study of CHBr_3 and CH_2Br_2 , *Atmos. Chem. Phys.*, 10, 2269–2286, <https://doi.org/10.5194/acp-10-2269-2010>, 2010.
- Liang, Q., Atlas, E., Blake, D., Dorf, M., Pfeilsticker, K., and Schauffler, S.: Convective transport of very short lived bromocarbons to the stratosphere, *Atmos. Chem. Phys.*, 14, 5781–5792, <https://doi.org/10.5194/acp-14-5781-2014>, 2014.
- Manley, S. L., Goodwin, K., and North, W. J.: Laboratory production of bromoform, methylene bromide, and methyl iodide by macroalgae and distribution in nearshore southern California waters, *Limnol. Oceanogr.*, 37, 1652–1650, 1992.
- Montzka, S., Butler, J., Hall, B., Mondeel, D., and Elkins, J.: A decline in tropospheric organic bromine, *Geophys. Res. Lett.*, 30, 1826, <https://doi.org/10.1029/2003GL017745>, 2003.
- Moore, R. M. and Zafiriou, O. C.: Photochemical production of methyl iodide in seawater, *J. Geophys. Res.-Atmos.*, 99, 16415–16420, <https://doi.org/10.1029/94jd00786>, 1994.
- Moore, R. M., Geen, C. E., and Tait, V. K.: Determination of Henry's Law constants for a suite of naturally occurring halogenated methanes in seawater, *Chemosphere*, 30, 1183–1191, [https://doi.org/10.1016/0045-6535\(95\)00009-W](https://doi.org/10.1016/0045-6535(95)00009-W), 1995a.
- Moore, R. M., Tokarczyk, R., Tait, V. K., Poulin, M., and Geen, C.: Marine phytoplankton as a natural source of volatile organohalogenes, in: *Naturally-Produced Organohalogenes*, edited by: Grinnvall, A. and de Leer, E. W. B., Springer Netherlands, Dordrecht, 283–294, 1995b.
- Moore, R. M. and Groszko, W.: Methyl iodide distribution in the ocean and fluxes to the atmosphere, *J. Geophys. Res.-Ocean.*, 104, 11163–11171, <https://doi.org/10.1029/1998jc900073>, 1999.
- Munchak, L. A. and Pan, L. L.: Separation of the lapse rate and the cold point tropopause in the tropics and the resulting impact on cloud top-tropopause relationships, *J. Geophys. Res.-Atmos.*, 119, 7963–7978, <https://doi.org/10.1002/2013jd021189>, 2014.
- Newell, R. E. and Gould-Stewart, S.: A Stratospheric Fountain?, *J. Atmos. Sci.*, 38, 2789–2796, [https://doi.org/10.1175/1520-0469\(1981\)038<2789:ASF>2.0.CO;2](https://doi.org/10.1175/1520-0469(1981)038<2789:ASF>2.0.CO;2), 1981.
- Nightingale, P., Malin, G., Law, C., Watson, A., Liss, P., Liddicoat, M., Boutin, J., and Upstill-Goddard, R.: In situ evaluation of air-sea gas exchange parameterizations using novel conservative and volatile tracers, *Global Biogeochem. Cy.*, 14, 373–387, <https://doi.org/10.1029/1999GB900091>, 2000.
- Ordóñez, C., Lamarque, J. F., Tilmes, S., Kinnison, D. E., Atlas, E. L., Blake, D. R., Sousa Santos, G., Brasseur, G., and Saiz-Lopez, A.: Bromine and iodine chemistry in a global chemistry-climate model: description and evaluation of very short-lived oceanic sources, *Atmos. Chem. Phys.*, 12, 1423–1447, <https://doi.org/10.5194/acp-12-1423-2012>, 2012.
- Palmer, C. J. and Reason, C. J.: Relationships of surface bromoform concentrations with mixed layer depth and salinity in the tropical oceans, *Global Biogeochem. Cy.*, 23, GB2014, <https://doi.org/10.1029/2008gb003338>, 2009.
- Park, M., Randel, W. J., Gettelman, A., Massie, S. T., and Jiang, J. H.: Transport above the Asian summer monsoon anticyclone inferred from Aura Microwave Limb Sounder tracers, *J. Geophys. Res.*, 112, D16309, <https://doi.org/10.1029/2006jd008294>, 2007.
- Park, M., Randel, W. J., Emmons, L. K., and Livesey, N. J.: Transport pathways of carbon monoxide in the Asian summer monsoon diagnosed from Model of Ozone and Related Tracers (MOZART), *J. Geophys. Res.-Atmos.*, 114, D08303, <https://doi.org/10.1029/2008JD010621>, 2009.
- Pearson, K.: Note on Regression and Inheritance in the Case of Two Parents, *P. R. Soc. London*, 58, 240–242, 1895.
- Preethi, B., Mujumdar, M., Kripalani, R. H., Prabhu, A., and Krishnan, R.: Recent trends and tele-connections among South and East Asian summer monsoons in a warming environment, *Clim. Dynam.*, 48, 2489–2505, <https://doi.org/10.1007/s00382-016-3218-0>, 2016.
- Quack, B. and Wallace, D. W. R.: Air-sea flux of bromoform: Controls, rates, and implications, *Global Biogeochem. Cy.*, 17, p. 1023, <https://doi.org/10.1029/2002gb001890>, 2003.
- Quack, B., Atlas, E., Petrick, G., and Wallace, D. W. R.: Bromoform and dibromomethane above the Mauritanian upwelling: Atmospheric distributions and oceanic emissions, *J. Geophys. Res.*, 112, D09312, <https://doi.org/10.1029/2006jd007614>, 2007.
- Quartly, G. D., Buck, J. J. H., Srokosz, M. A., and Coward, A. C.: Eddies around Madagascar – The retroreflection re-considered, *J. Mar. Syst.*, 63, 115–129, <https://doi.org/10.1016/j.jmarsys.2006.06.001>, 2006.
- Randel, W. J., Park, M., Emmons, L., Kinnison, D., Bernath, P., Walker, K. A., Boone, C., and Pumphrey, H.: Asian monsoon transport of pollution to the stratosphere, *Science*, 328, 611–613, <https://doi.org/10.1126/science.1182274>, 2010.
- Roy, R., Pratihary, A., Narvenkar, G., Mochemadkar, S., Gauns, M., and Naqvi, S. W. A.: The relationship between volatile halocarbons and phytoplankton pigments during a *Trichodesmium* bloom in the coastal eastern Arabian Sea, *Estuarine, Coast. Shelf Sci.*, 95, 110–118, <https://doi.org/10.1016/j.ecss.2011.08.025>, 2011.
- Schauffler, S., Atlas, E., Blake, D., Flocke, F., Lueb, R., Lee-Taylor, J., Stroud, V., and Travniczek, W.: Distributions of brominated organic compounds in the troposphere and lower stratosphere, *J. Geophys. Res.-Atmos.*, 104, 21513–21535, <https://doi.org/10.1029/1999JD900197>, 1999.
- Schott, F. A., Xie, S.-P., and McCreary, J. P.: Indian Ocean circulation and climate variability, *Rev. Geophys.*, 47, RG1002, <https://doi.org/10.1029/2007rg000245>, 2009.
- Seibert, P., Beyrich, F., Gryning, S., Joffre, S., Rasmussen, A., and Tercier, P.: Review and intercomparison of operational methods for the determination of the mixing height, *Atmos. Environ.*, 34, 1001–1027, [https://doi.org/10.1016/S1352-2310\(99\)00349-0](https://doi.org/10.1016/S1352-2310(99)00349-0), 2000.
- Smythe-Wright, D., Boswell, S. M., Lucas, C. H., New, A. L., and Varney, M. S.: Halocarbon and dimethyl sulphide studies around the Mascarene Plateau, *Philos. T. R. Soc. A*, 363, 169–185, <https://doi.org/10.1098/rsta.2004.1485>, 2005.
- Solomon, S., Garcia, R. R., and Ravishankara, A. R.: On the role of iodine in ozone depletion, *J. Geophys. Res.-Atmos.*, 99, 20491–20499, <https://doi.org/10.1029/94jd02028>, 1994.
- Stemmler, I., Rothe, M., Hense, I., and Hepach, H.: Numerical modelling of methyl iodide in the eastern tropical Atlantic, *Biogeosciences*, 10, 4211–4225, <https://doi.org/10.5194/bg-10-4211-2013>, 2013.
- Stemmler, I., Hense, I., and Quack, B.: Marine sources of bromoform in the global open ocean – global patterns and emissions, *Biogeosciences*, 12, 1967–1981, <https://doi.org/10.5194/bg-12-1967-2015>, 2015.

- Stohl, A. and Thomson, D.: A density correction for Lagrangian particle dispersion models, *Bound.-Lay. Meteorol.*, 90, 155–167, <https://doi.org/10.1023/A:1001741110696>, 1999.
- Stohl, A. and Trickl, T.: A textbook example of long-range transport: Simultaneous observation of ozone maxima of stratospheric and North American origin in the free troposphere over Europe, *J. Geophys. Res.-Atmos.*, 104, 30445–30462, <https://doi.org/10.1029/1999JD900803>, 1999.
- Stohl, A., Hittenberger, M., and Wotawa, G.: Validation of the Lagrangian particle dispersion model FLEXPART against large-scale tracer experiment data, *Atmos. Environ.*, 32, 4245–4264, [https://doi.org/10.1016/S1352-2310\(98\)00184-8](https://doi.org/10.1016/S1352-2310(98)00184-8), 1998.
- Stohl, A., Forster, C., Frank, A., Seibert, P., and Wotawa, G.: Technical note: The Lagrangian particle dispersion model FLEXPART version 6.2, *Atmos. Chem. Phys.*, 5, 2461–2474, <https://doi.org/10.5194/acp-5-2461-2005>, 2005.
- Stull, R.: *An Introduction to Boundary Layer Meteorology*, Kluwer Academic Publishers, Dordrecht, 1988.
- Tegtmeier, S., Krüger, K., Quack, B., Atlas, E. L., Pisso, I., Stohl, A., and Yang, X.: Emission and transport of bromocarbons: from the West Pacific ocean into the stratosphere, *Atmos. Chem. Phys.*, 12, 10633–10648, <https://doi.org/10.5194/acp-12-10633-2012>, 2012.
- Tegtmeier, S., Krüger, K., Quack, B., Atlas, E., Blake, D. R., Boenisch, H., Engel, A., Hepach, H., Hossaini, R., Navarro, M. A., Raimund, S., Sala, S., Shi, Q., and Ziska, F.: The contribution of oceanic methyl iodide to stratospheric iodine, *Atmos. Chem. Phys.*, 13, 11869–11886, <https://doi.org/10.5194/acp-13-11869-2013>, 2013.
- Vogel, B., Günther, G., Müller, R., Groß, J. U., and Riese, M.: Impact of different Asian source regions on the composition of the Asian monsoon anticyclone and on the extratropical lowermost stratosphere, *Atmos. Chem. Phys.*, 15, 13699–13716, <https://doi.org/10.5194/acp-15-13699-2015>, 2015.
- Warwick, N. J., Pyle, J. A., Carver, G. D., Yang, X., Savage, N. H., O'Connor, F. M., and Cox, R. A.: Global modeling of biogenic bromocarbons, *J. Geophys. Res.-Atmos.*, 111, D18311, <https://doi.org/10.1029/2006jd007264>, 2006.
- Yamamoto, H., Yokouchi, Y., Otsuki, A., and Itoh, H.: Depth profiles of volatile halogenated hydrocarbons in seawater in the Bay of Bengal, *Chemosphere*, 45, 371–377, [https://doi.org/10.1016/S0045-6535\(00\)00541-5](https://doi.org/10.1016/S0045-6535(00)00541-5), 2001.
- Yan, R. and Bian, J.: Tracing the boundary layer sources of carbon monoxide in the Asian summer monsoon anticyclone using WRF-Chem, *Adv. Atmos. Sci.*, 32, 943–951, <https://doi.org/10.1007/s00376-014-4130-3>, 2015.
- Yokouchi, Y., Osada, K., Wada, M., Hasebe, F., Agama, M., Murakami, R., Mukai, H., Nojiri, Y., Inuzuka, Y., Toom-Sauntry, D., and Fraser, P.: Global distribution and seasonal concentration change of methyl iodide in the atmosphere, *J. Geophys. Res.-Atmos.*, 113, D18311, <https://doi.org/10.1029/2008jd009861>, 2008.
- Ziska, F., Quack, B., Abrahamsson, K., Archer, S. D., Atlas, E., Bell, T., Butler, J. H., Carpenter, L. J., Jones, C. E., Harris, N. R. P., Hepach, H., Heumann, K. G., Hughes, C., Kuss, J., Krüger, K., Liss, P., Moore, R. M., Orlikowska, A., Raimund, S., Reeves, C. E., Reifenhäuser, W., Robinson, A. D., Schall, C., Tanhua, T., Tegtmeier, S., Turner, S., Wang, L., Wallace, D., Williams, J., Yamamoto, H., Yvon-Lewis, S., and Yokouchi, Y.: Global sea-to-air flux climatology for bromoform, dibromomethane and methyl iodide, *Atmos. Chem. Phys.*, 13, 8915–8934, <https://doi.org/10.5194/acp-13-8915-2013>, 2013.

Supplement of Atmos. Chem. Phys., 17, 6723–6741, 2017
<https://doi.org/10.5194/acp-17-6723-2017-supplement>
© Author(s) 2017. This work is distributed under
the Creative Commons Attribution 3.0 License.



Supplement of

Delivery of halogenated very short-lived substances from the west Indian Ocean to the stratosphere during the Asian summer monsoon

Alina Fiehn et al.

Correspondence to: Kirstin Krüger (kkrueger@geo.uio.no)

The copyright of individual parts of the supplement might differ from the CC BY 3.0 License.

The analysis of the radiosonde profiles of temperature, relative humidity, zonal wind, and the calculated gradient of the virtual potential temperature (Fig. S1) reveals a clear separation between subtropical and tropical circulation. The first part of the cruise shows high relative humidity in the Marine Atmospheric Boundary Layer (MABL), but very low in the rest of the troposphere (Fig. S1b), which revealed that there was low convective activity transporting water vapor upward in the subtropics. During the second, tropical part of the cruise, a temperature inversion layer, called trade inversion, exists at about 2.5 km height between July 24 and August 4, 2014, which we associate with the dry descending air masses of the lateral monsoon (Webster et al., 1998) and the Hadley Cell in the subtropics. The temperature inversion coincides with the upper boundary of a humid layer, indicating that it suppresses convection and exchange through this layer. The MABL upper boundary was below the inversion, and acted as a weaker transport barrier than the inversion, indicated by the lower values in the gradient of the virtual potential temperature, a measure for atmospheric stability, at 1 km height than at 3 km height (Fig. S1d).

Close to the equator, we find enhanced relative humidity in the middle and upper troposphere, which is a sign of enhanced convective activity. The winds north of the equator belong to the southwesterly monsoon winds, which transport West Indian Ocean air masses towards India. Close to the equator, a strong easterly jet, just below the tropopause, is visible. This relates to the upper part of the transverse monsoon circulation (Webster et al., 1998).

References

Webster, P.J., V. O. Magaña, T. N. Palmer, J. Shukla, R. A. Tomas, M. Yanai, T. Yasunari, Monsoons: Processes, predictability, and the prospects for prediction, *J. Geophys. Res.*, 103, 14451–14510, <https://doi.org/10.1029/97JC02719>, 1998.

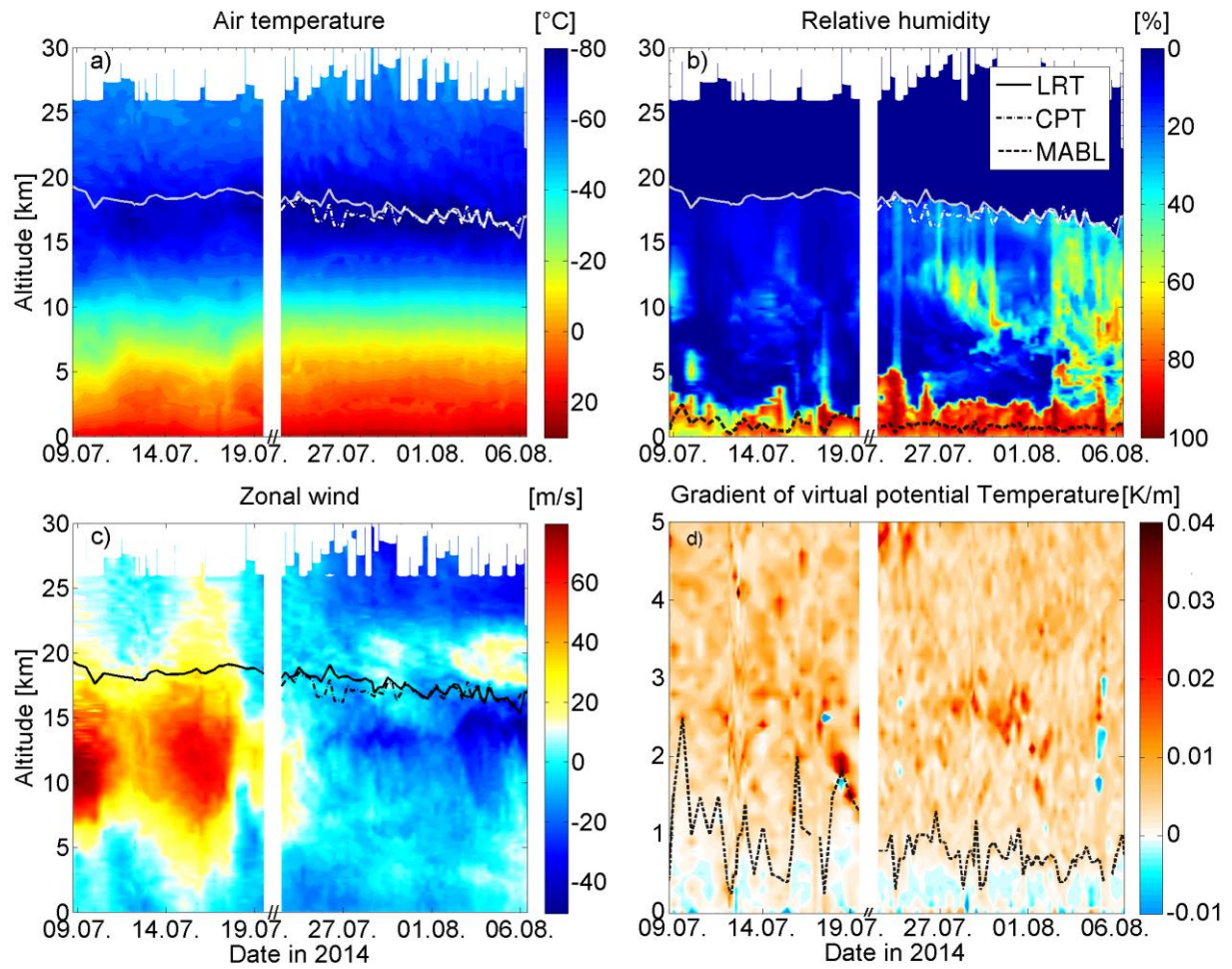


Figure S1: Radiosonde profiles of temperature, relative humidity, zonal winds and gradient of virtual potential temperature as time series for the OASIS cruise. The white gap denotes the harbor stop at Port Louis, Mauritius. LRT: lapse rate tropopause, CPT: cold point tropopause, MABL: marine atmospheric boundary layer.

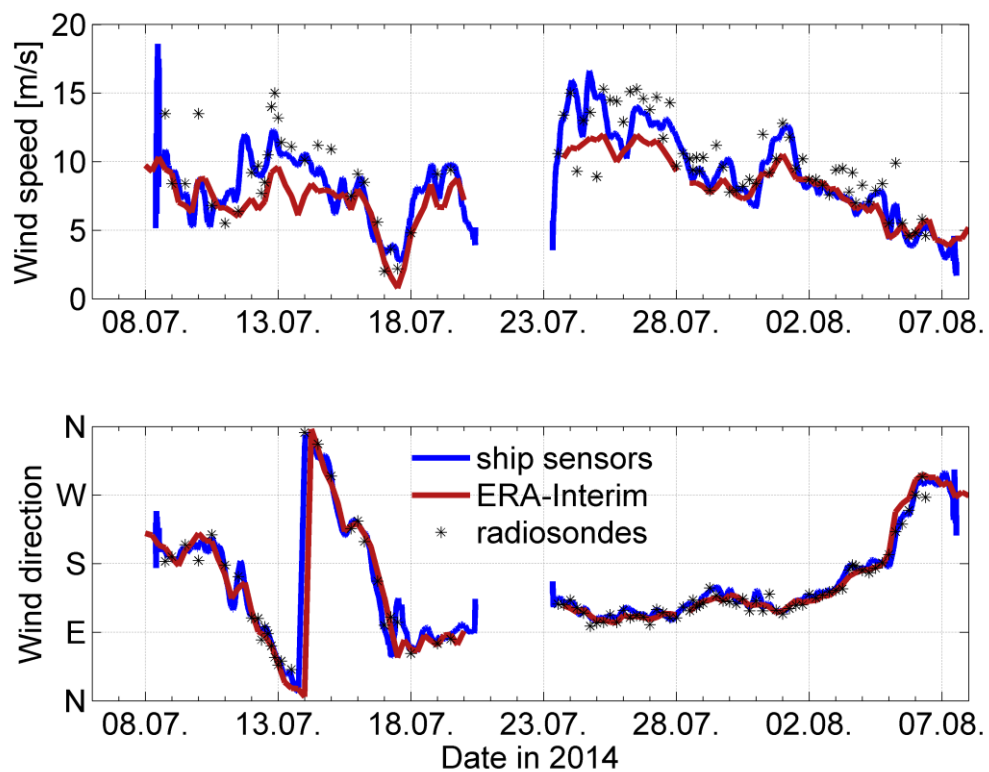


Figure S2: Wind speed and wind direction during the OASIS cruise from ship sensors and ERA-Interim reanalysis data (both as 6 hour mean) and radiosondes launched from the ship (as instantaneous measurement).

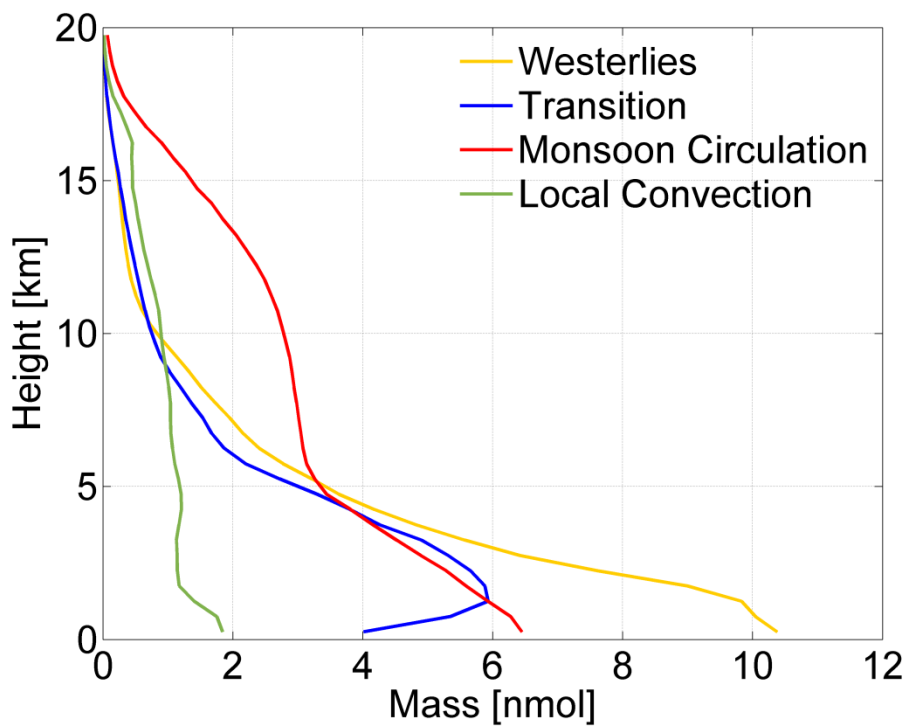


Figure S3: Time-averaged vertical distribution of bromoform in the four transport regimes (Figure 3b).

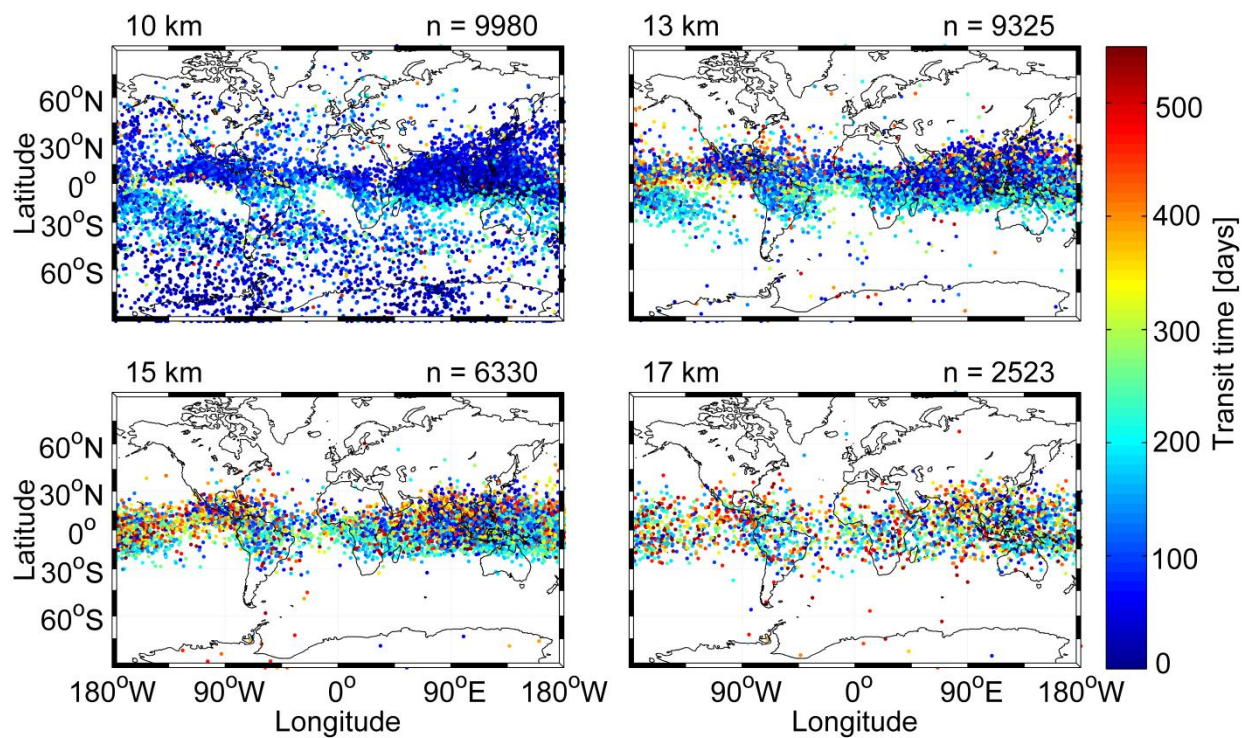


Figure S4: Trajectory positions and transit time at different altitudes for the 10.000 trajectories of the simulation of the CH₂Br₂ measurement on 23 UTC July 12, 2014.

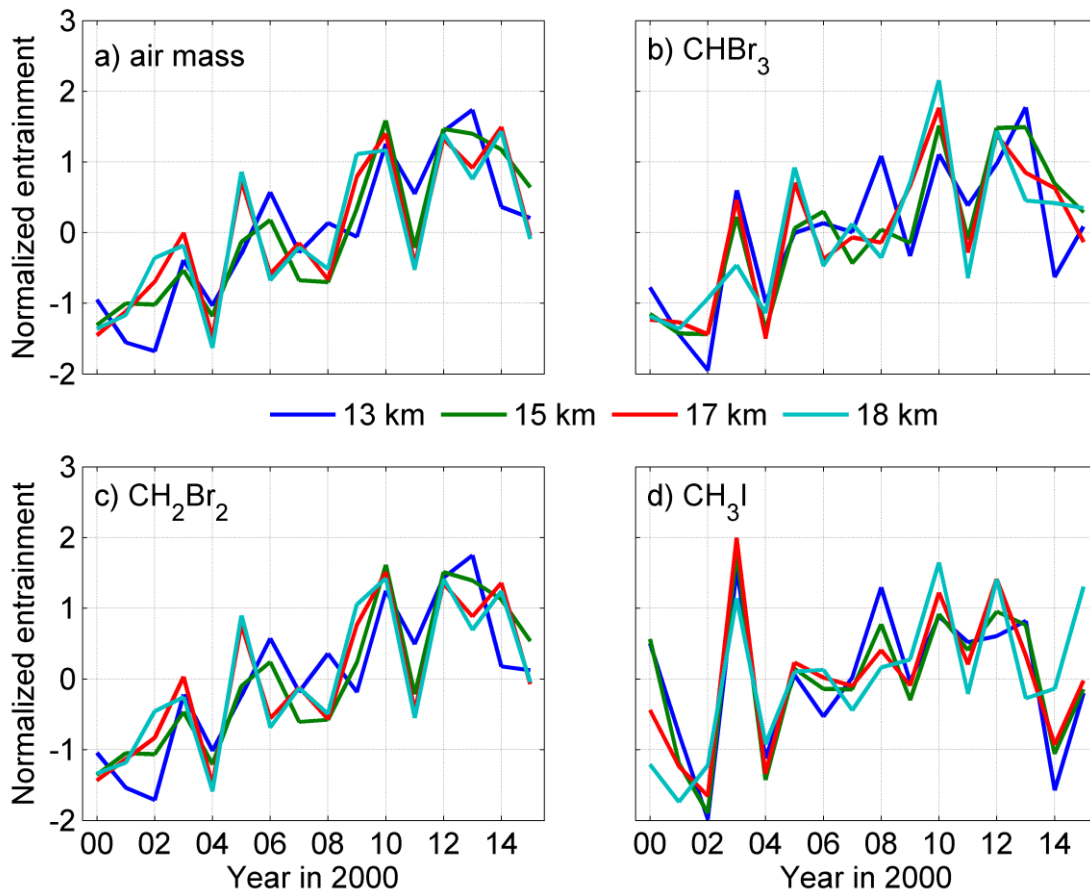


Figure S5: Normalized entrainment strength of air mass and VSL tracers from the *Indian Ocean FLEXPART* setup at different heights released every day during July 2000-2015.

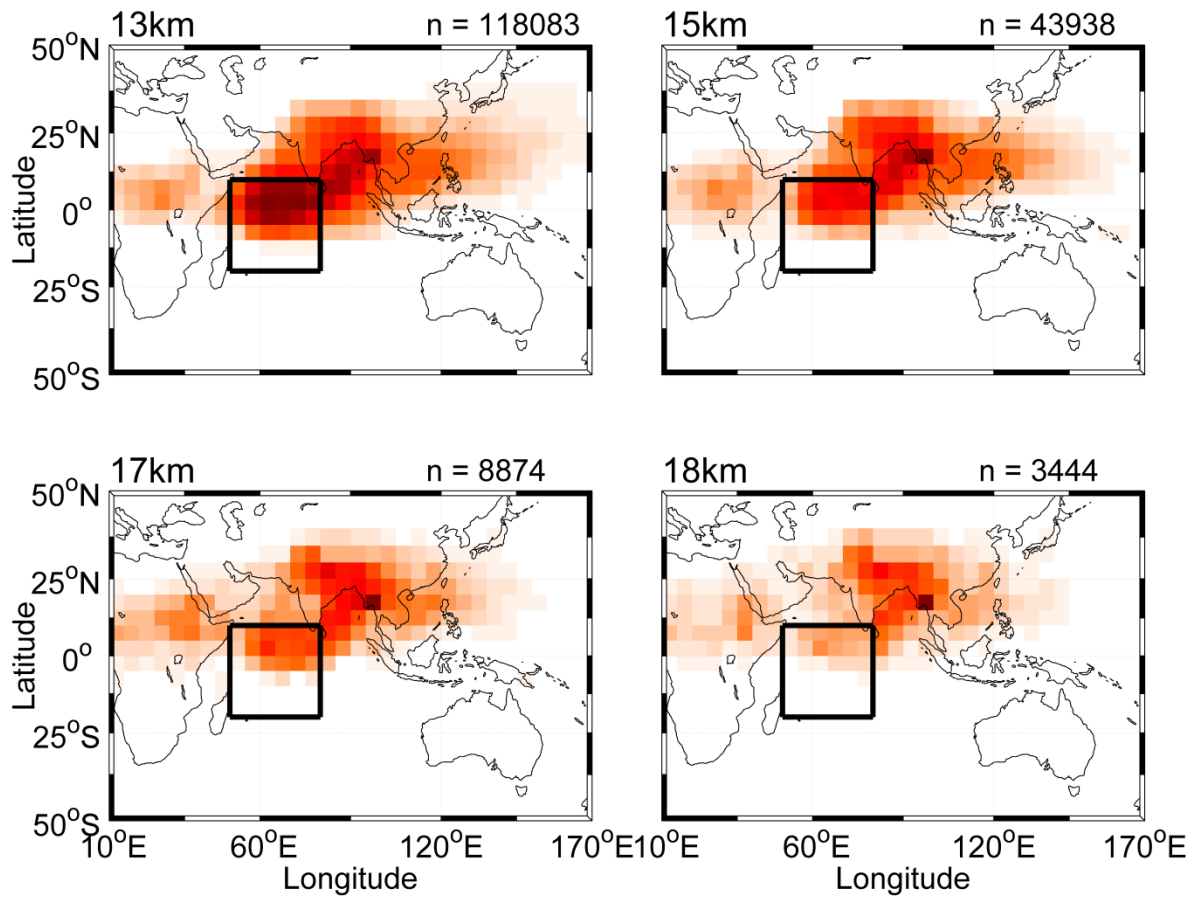


Figure S6: Entrainment regions for CHBr_3 tracer at different heights for daily releases in July 2000-2015 from the west Indian Ocean release box (black rectangle). The height is noted in the upper left corner, while the total entrainment number is noted as n .

3.2 Manuscript 2

Zavarsky, A.; Booge, D.; Fiehn, A.; Krüger, K.; Atlas, E.; and Marandino, C.: The influence of air-sea fluxes on atmospheric aerosols during the summer monsoon over the Indian Ocean, under review at Geophysical Research Letters.

1 **The influence of air-sea fluxes on atmospheric aerosols during**
2 **the summer monsoon over the Indian Ocean**

3 **Alex Zavorsky^{1*}, Dennis Booge¹, Alina Fiehn^{1,2}, Kirstin Krüger², Elliot Atlas³ and Christa**
4 **Marandino¹**

5 ¹GEOMAR Helmholtz Centre for Ocean Research Kiel, Kiel, Germany

6 ²University of Oslo, Oslo, Norway

7 ³University of Miami, Miami, USA

8 **Key Points:**

- 9 • First eddy covariance measurements of DMS in the Western Tropical Indian Ocean
- 10 • Western tropical Indian Ocean DMS hotspot confirmed
- 11 • Clear linkage of reduced sulfur source gases and remotely sensed aerosol end prod-
- 12 ucts

*Independent Researcher, Metzstraße 8, 24116 Kiel Germany

Corresponding author: Alex Zavorsky, alexz@mailbox.org

Abstract

During the summer monsoon, the western tropical Indian Ocean is predicted to be a hotspot for dimethylsulfide (DMS) emissions, the major marine sulfur source to the atmosphere and an important aerosol precursor. Other aerosol relevant fluxes, such as isoprene and sea salt fluxes, should also be enhanced, due to the steady strong winds during the monsoon. In addition, marine air masses dominate the area during the summer monsoon, excluding the influence of continentally derived pollutants. During the SO234-2/235 cruise in the western tropical Indian Ocean from July-August, 2014, directly measured eddy covariance DMS fluxes confirm that the area is a large source of sulfur to the atmosphere (cruise average $9.1 \mu\text{molm}^{-2}\text{d}^{-1}$). The directly measured fluxes, as well as computed isoprene and sea salt fluxes, were combined with Flexpart back- and forward trajectories to track the emissions in space and time. The fluxes show a significant positive correlation with satellite aerosol products from MODIS-Terra and Suomi-NPP, indicating a local influence of marine emissions on atmospheric aerosol properties.

1 Introduction

The CLAW hypothesis [Charlson *et al.*, 1987], still heavily debated in the scientific community [Quinn and Bates, 2011], describes a feedback process connecting oceanic production to cloud formation, which influences Earth's albedo and as a consequence oceanic production. One of the main steps of the CLAW hypothesis is the formation of aerosols and cloud condensation nuclei (CCN) in the marine boundary layer (MBL). The original publication, proposed dimethylsulfide (DMS) to be the key source of CCN and driver of the feedback. DMS is produced by phytoplankton in the ocean and then released into the atmosphere, where it is one of the major sulfur sources [Quinn and Bates, 2011]. In the atmosphere it undergoes oxidation to either sulfur dioxide (SO_2), sulfuric acid (H_2SO_4) or methane sulfonic acid (MSA) and subsequently forms CCN through homogeneous or heterogeneous nucleation. In more recent years other CCN sources, for instance sea salt, primary organic aerosols (POA) and other biogenic trace gases such as isoprene, have come into focus. Quinn and Bates [2011] argue that only 40-50 % of the MBL-CCN can be attributed to sulfur emissions and, depending on the region, up to 60 % can be attributed to sea salt aerosols. The quantitative impact of sea salt, POA and isoprene is still unclear. Furthermore, Quinn and Bates [2011] claim that most of the DMS derived CCN are actually formed in the free troposphere and then entrained into the boundary layer again. This

45 would mean a regional decoupling of the DMS emissions and the formation of CCN and
46 clouds, which is in opposition to the CLAW feedback. As pointed out by *Green and Hat-*
47 *ton* [2014] and *Vallina et al.* [2006] most studies still lack the temporal and spatial cover-
48 age to give a significant answer to the importance of DMS in the CCN forming process in
49 the MBL. In contrast to the arguments of *Quinn and Bates* [2011], *Lana et al.* [2012] per-
50 formed a satellite based correlation-study, connecting DMS- and sea salt-emissions with
51 the MODIS (Moderate Resolution Imaging Spectroradiometer)-derived CCN number con-
52 centrations. They found a rather uniform positive correlation for DMS-CCN (with some
53 areas of weak correlation at the boundaries of the tropics). For sea salt-CCN the correla-
54 tion depended on latitude: The tropics exhibited a positive correlation, all other latitudes
55 exhibited a negative correlation. These findings provide a basis for further investigation
56 but no studies have correlated air-sea fluxes with aerosol products on regional level or
57 multi-day timescales.

58 According to the Lana climatology [*Lana et al.*, 2011], the western tropical Indian
59 Ocean (WTIO) is a hotspot for DMS flux during the months July and August. The ef-
60 flux is one of the highest worldwide ($63.32 \mu\text{molm}^{-2}\text{d}^{-1}$, [*Lana et al.*, 2011]). The WTIO
61 is associated with marine influenced air masses during the boreal summer [*Rhoads et al.*,
62 1997]. Biological productivity, especially in the upwelling areas of the WTIO (off north
63 east Africa and the north Arabian Sea), is strongly correlated with the monsoon seasonal
64 cycle [*Yoder et al.*, 1993]. This production influences the DMS concentration in the sur-
65 face water and, together with steady strong winds, enhances gas transfer.

66 Thus, the WTIO could be an important source of sulfur to the atmosphere and the
67 SO234-2/235 cruise provides the opportunity to study DMS-CCN correlations. We focus
68 on linking source gases and aerosol products in order to confirm the *Lana et al.* [2012]
69 correlations. We use an improved approach, as our DMS fluxes were directly measured,
70 coupled to the atmospheric transport model Flexpart and their transformation was studied
71 on regional scale above the WTIO.

72 **2 Methods**

73 We performed direct eddy covariance DMS flux measurements aboard the RV Sonne
74 sailing from Durban, SA to Port Louis, MU (SO234-2, 8 July - 20 July 2014) and from
75 Port Louis, MU to Malé, MV (SO235, 23 July - 8 August 2014) (Figure 1). Addition-
76 ally, we recorded DMS and isoprene surface water and air concentrations. Basic meteoro-

logical observations were done by the ship's automated weather station. For the span of the cruise, back- and forward trajectories were calculated using the Flexpart model [Stohl *et al.*, 2005], Figure 2). Aerosol satellite data from MODIS-Terra and Suomi-NPP were acquired for the area and time covered by the cruise track and the trajectories.

2.1 Eddy covariance measurements

The eddy covariance flux F (equation 1) is a product of the dry air density (ρ), the fluctuation of vertical wind speed (w') and the fluctuation of the mixing ratio (c').

$$F = \rho \cdot c'w' \quad (1)$$

We recorded DMS air mixing ratios at 5 Hz using an atmospheric pressure chemical ionization mass spectrometer (AP-CIMS) similar to that described by *Saltzman et al.* [2009]. The air was sampled from a mast at the bow of the ship (11 m asl) and pumped at 50-70 lpm ($Flow_{total}$) through a 1/2" diameter and 25 m long polytetrafluorethylen tube to a laboratory container where the AP-CIMS was placed. The air stream was dried using a Nafion membrane (Perma Pure) prior to analysis. For calibration, we continuously added a deuterated DMS standard (DMS-d3, 2.28 ppm C_{tank}) to the inlet at the rate of 2 mLmin⁻¹ ($Flow_{std}$). Using the ratio of the deuterated DMS counts ($Counts_{66}$) to the natural DMS counts ($Counts_{63}$), the concentration of atmospheric DMS (DMS_{air}) was calculated:

$$DMS_{air} = \frac{Flow_{std}}{Flow_{total}} * \frac{Counts_{63}}{Counts_{66}} * C_{tank} \quad (2)$$

Two ultrasonic anemometers (CSAT3), mounted next to the air-sample inlet, measured the 3D turbulent wind field. We determined the delay, between the passage of the air parcel at the inlet (CSAT3) and the measurement at the AP-CIMS, with a valve switch before each 1 h eddy covariance measurement run. A GPS and an inertial measurement unit (Landmark 10 by Gladiator Instruments), positioned next to the sonic anemometers provided the data for the motion correction of the 3D wind, which we performed based on *Miller et al.* [2008] and *Edson et al.* [1998], with an update by *Landwehr et al.* [2015]. We recorded a total of 130.15 h DMS air measurements. The data set was split into 477 running intervals (step size 10 min), each 29.6 min long. These intervals fulfilled the flow distortion relative wind direction criterion of $\pm 90^\circ$ degrees from the bow and the Landwehr requirement of steady wind direction. We screened the record for spikes, malfunctions, high and low frequency anomalies and proper time delay. 435 intervals were corrected for the high frequency loss in the tube. The high frequency correction was performed by fitting a

108 rectangular signal using a low-pass filter to the signal of an actual isotope standard valve
 109 switch. The loss in high frequency power of the isotope standard valve switch is equal to
 110 the loss in the 1/2" teflon tube. The loss displayed a linear relationship with 10 m neutral
 111 wind speed (u_{10}). The gain factor (G_{hf}), which is corrects for the tube's high frequency
 112 loss, is seen in equation 3.

$$113 \quad G_{hf} = 1.032 + 0.0021 \cdot u_{10} \quad (3)$$

114 **2.2 Bulk air and seawater measurements**

115 Seawater DMS and isoprene concentrations were measured using a purge and trap
 116 system attached to a gas chromatograph/mass spectrometer operating in single ion mode
 117 (GC/MS; Agilent 7890A/Agilent 5975C). We sampled the water from a constant stream
 118 out of the ship's moon pool at approximately 5 m depth and measured within 15 min of
 119 collection. The gases were purged from the water sample for 15 min and then dried us-
 120 ing potassium carbonate. The dried gas was preconcentrated in a trap cooled with liquid
 121 nitrogen and injected into the GC. We obtained a total of 162 DMS and isoprene sea sur-
 122 face concentration values (3 h sampling interval). At the same time and interval, we filled
 123 stainless steel canisters with air samples (25 m sampling height), which were analyzed for
 124 more than fifty gases, including DMS and isoprene, at the University of Miami.

125 We calculated isoprene fluxes using the bulk method (equation 4), where c_a and c_w
 126 are the respective air and water concentrations, H is the dimensionless form of Henry's
 127 law constant and k the gas transfer velocity by *Nightingale et al.* [2000].

$$128 \quad Flux = k \cdot \left(c_w - \frac{c_a}{H} \right) \quad (4)$$

129 Sea salt flux (F_{SSA} , billion particles ejected per m^2 per day [$Gpartm^{-2}d^{-1}$]) was parametrized
 130 using equation 5, which was proposed by *O'Dowd et al.* [2008]. The wind speed at 22 m
 131 u_{22} was calculated using the parametrization by *Hsu et al.* [1994].

$$132 \quad F_{SSA} = 1.854 \cdot 10^{-3} \cdot u_{22}^{2.706} \quad (5)$$

133 **2.3 Back- and forward trajectories**

134 For the trajectory calculations, we used the Lagrangian Particle Dispersion Model
 135 Flexpart Version 9.2 [*Stohl et al.*, 2005]. The model includes moist convection and tur-
 136 bulance parameterizations in the atmospheric boundary layer and free troposphere [*Stohl*
 137 *and Thomson*, 1999; *Forster et al.*, 2007]. We used Flexpart with the ECMWF (European

138 Centre for Medium-Range Weather Forecasts) reanalysis product ERA-Interim [Dee *et al.*,
139 2011] with a horizontal resolution of $1^\circ \times 1^\circ$ and 60 vertical model levels as meteorological
140 input fields with a 6 hourly temporal resolution. During the cruise we launched
141 radiosondes to improve meteorological reanalysis (e.g. ERA-Interim) for the later use in
142 the transport model [Fiehn *et al.*, 2017]. Flexpart was run with a synchronization interval
143 of 900 s and with a quarter of this time step in the atmospheric boundary layer to resolve
144 turbulent fluxes on short time scales. The model output was recorded hourly. An ensemble
145 of 10,000 forward and 1,000 backward trajectories are started at the positions and times
146 of the 435 direct DMS flux measurements and run for more than 2 days. From the hourly
147 trajectory positions we calculated the mean trajectory as an average of all ensemble mem-
148 bers. Trajectories reaching 24 h backwards and 24 h forwards were used in the correlation
149 calculation. Longer time spans up to 72 h were used to assess the possible influence of
150 land pollution.

151 **2.4 Remote sensing**

152 We obtained total column CCN and aerosol optical depth (AOD) data from the
153 MODIS instrument on board the Terra satellite. MODIS-Terra has a sun synchronous
154 orbit and an overpass time of 10:30 local time. The level-3 product can be found in the
155 MODIS-Terra 6 collection [Hubanks *et al.*, 2016] and is provided on a global $1^\circ \times 1^\circ$
156 grid. Additionally, total column (AOT) was obtained from the Visible Infrared Imaging
157 Radiometer Suite (VIIRS) instrument on board the Suomi-NPP satellite, which has a sun
158 synchronous orbit and an overpass time of 13:30 local time. The level-2 aerosol prod-
159 uct has a resolution of $0.25^\circ \times 0.25^\circ$. AOD and AOT both describe the degree to which
160 aerosols prevent the transmission of light by absorption or scattering of light. The name
161 difference has organizational non-scientific reasons. In total we obtained daily files from
162 27 June 2014 to 19 Aug 2014 for all products. All products have a daily resolution and
163 the output describes the aerosol properties at the time of the overpass. Using two different
164 satellites gives the opportunity to test the data with two independent systems. A cross-
165 check was done between the data from MODIS Aqua, MODIS-Terra and NPP-Suomi,
166 which shows consistent results (data shown in the supplement).

167 The satellite data was linearly interpolated to the specific location of each forward-
168 and backward trajectory output. If, due to missing values, the first interpolation was not
169 successful, following steps were carried out successively and stopped if one interpolation

170 returned a valid result: [1] a nearest interpolation (space and time) [2] linear interpolation
171 (space, at closest time step) [3] mean of nearest-neighbors (space, at closest time step).

172 The majority of missing values were caused by clouds.

173 2.5 Correlation

174 To link the oceanic sources to the aerosol products, we analyze the trend of the
175 aerosol properties in the downwind (forward trajectories) area. This approach has already
176 been established for volcanoes [*Mace and Abernathy, 2016; Eguchi et al., 2011; Yuan*
177 *et al., 2011*] and focuses on the absolute aerosol number or cloud density. We have im-
178 proved their method and, instead of a point source (volcano), we correlate all measured
179 fluxes from the cruise track with the satellite aerosol properties in the downwind area.
180 We hypothesize that a higher efflux of aerosol predecessor, such as DMS, isoprene, sea
181 salt, should lead to a higher value of satellite sensed aerosol values. Therefore a positive
182 correlation between aerosol source and aerosol product should be observed. We used the
183 Flexpart forward trajectories to pinpoint the downwind location of the directly measured
184 fluxes. For these positions we obtained the satellite based aerosol values for correlation.

185 We used Spearman's rank as correlation method, which describes a monotonically
186 increasing relationship between two variables. The bootstrap method was used to prove
187 the level of significance. A correlation coefficient of 0.2 is statistically significant with a
188 probability of 0.95.

189 3 Results and Discussion

190 The cruise took place during the Asian summer monsoon season, with prevailing
191 southeasterly winds south of the Equator and southwesterly winds north of the Equator.
192 The SO234-2/235 cruise track spanned a range of oceanic areas, traversing the Agulhas
193 current, the Antarctic circumpolar current (an area of high carbon dioxide drawdown), the
194 Indian Ocean Gyre, the South Equatorial Current, the Equatorial Countercurrent, and the
195 North Equatorial Current. Shallow areas (e.g. the Mascarene Plateau) and reef areas (e.g.
196 Maldives) were also traversed. We encountered an average oceanic mixed layer depth of
197 60 m, sea surface temperatures from 19°C to 25°C, salinity from 34 to 36 and generally
198 low nutrient levels (below 0.1 μmolL^{-1} for nitrate and below 0.2 μmolL^{-1} for phosphate).
199 Some areas of enhanced nutrients were encountered between 10° and 5° S. Chlorophyll
200 levels were also generally low. During the first leg (SO234-2), 30 min averaged wind

201 speed below 10 ms^{-1} was measured. North of Mauritius the wind speed increased to a
202 maximum of 16 ms^{-1} and then gradually declined towards the Maldives. Lower wind
203 speed prevailed closer to the Equator, which is in agreement with the monsoon circulation.
204 The average marine boundary layer heights were approximately 0.8 km, relative humid-
205 ity varied between 50 % and 90 %, and air temperatures ranged between 14°C and 30°C
206 [Fiehn *et al.*, 2017]. Precipitation was variable over the cruise tracks. Generally, the air
207 masses encountered were unpolluted and originated from over the ocean (Figure 2).

208 3.1 Seawater concentrations

209 Measured DMS surface seawater concentrations ranged from $0.4\text{-}5.19 \text{ nmolL}^{-1}$
210 (Figure 3). During the first leg (SO234-2), the concentrations stayed below 1.4 nmolL^{-1} ,
211 with one exception at 2.4 nmolL^{-1} at the southern tip of Madagascar, where a shallow
212 coastal area (Banc d'Etoile) was crossed. DMS values started increasing up to the max-
213 imum value of 5.19 nmolL^{-1} north of Mauritius in the area between 18°S and 5°S . Fur-
214 ther north, the values declined to sub 1 nmolL^{-1} levels. Two main features influenced the
215 DMS values north of Mauritius: [1] The Mascarene Plateau [Smythe-Wright *et al.*, 2005],
216 which is an extensive submarine plateau reaching a shallowness of up to 50 m. [2] As de-
217 scribed by Schott *et al.* [2009], during both monsoon seasons a southward Ekman transport
218 subducts underneath the equatorial roll. This leads to upwelling south of this roll in the
219 area between 10°S and 6°S , which elevates biological productivity and, as a result, also
220 the production of biogenically produced trace gases.

221 Isoprene water concentrations ranged from 0.36 pmolL^{-1} to a maximum of 64 pmolL^{-1}
222 (Figure 3). During SO234-2, from Durban to Mauritius, average values around 10 pmolL^{-1}
223 were observed. North of Mauritius the isoprene concentration steadily increased from sub
224 1 pmolL^{-1} just off Mauritius to around 30 pmolL^{-1} at the Maldives. The maximum val-
225 ues of isoprene were reached at 6.1°S and 64.45°E on day of year 2014 (DOY) 209.45
226 [Booge *et al.*, 2016].

227 3.2 Fluxes

228 Directly measured DMS fluxes ranged from $0.3\text{-}32.77 \text{ }\mu\text{molm}^{-2}\text{d}^{-1}$ (Figure 3). Dur-
229 ing SO234-2 from Durban to Mauritius and after DOY 214 the fluxes were low, which
230 can be attributed to low wind speed (below 10 ms^{-1}) and low water concentrations. Af-
231 ter Mauritius at DOY 205 a storm (wind speed maximum of 16 ms^{-1}) was encountered.

232 High wind speed in conjunction with high seawater concentrations were measured, lead-
233 ing to an increase of the flux. Wind speed steadily decreased as the cruise continued, but
234 seawater concentrations varied, causing the fluxes to vary accordingly in magnitude from
235 DOY 210 onwards. The lowest fluxes occurred on DOY 198 and the highest on DOY 207.
236 Isoprene fluxes ranged from 0-0.187 $\mu\text{molm}^{-2}\text{d}^{-1}$. Generally the isoprene fluxes of SO235
237 were higher, which is associated for the most part with the higher wind speed and sec-
238 ondly with the slightly higher water concentrations. The computed sea salt flux closely
239 resembles the measured wind speed (Figure 3).

240 3.3 Comparison to the Lana climatology and PMEL database

241 Generally the sea surface DMS concentrations throughout the cruise legs are lower
242 than those published in the Lana climatology and the PMEL database (Figure 1). A de-
243 scription of the PMEL database can be found in the supplement. The WTIO is heavily
244 under-sampled, especially in the months July and August. The only data available, and
245 therefore used, in the Lana climatology are 34 samples from two cruises [*Mihalopoulos*
246 *et al.*, 1992; *Smythe-Wright et al.*, 2005], diamonds in Figure 1. The influence of the Mas-
247 carene Plateau on biological productivity might be the reason for the general elevated val-
248 ues from both the PMEL database and the Lana climatology (background Figure 1), with
249 a maximum flux of 63.2 $\mu\text{molm}^{-2}\text{d}^{-1}$. As the database's seawater concentrations were
250 measured further west than our cruise track, they were located more directly in the region
251 impacted by the Mascarene Plateau and values up to 9 nmolL^{-1} were incorporated in the
252 climatology.

253 On a global scale the WTIO represents the DMS flux hotspot for July. Our maxi-
254 mum value of 32.77 $\mu\text{molm}^{-2}\text{d}^{-1}$ is of the same magnitude as the worldwide maximum
255 value (31.8 $\mu\text{molm}^{-2}\text{d}^{-1}$), excluding the Indian Ocean. The maximum value of the In-
256 dian Ocean from the Lana climatology is 63.2 $\mu\text{molm}^{-2}\text{d}^{-1}$ and is twice as much as mea-
257 sured during our cruise. Although larger than our measurements, this value is still plau-
258 sible because they it is located at 10° S 59° E and therefore more directly influenced by
259 the Mascarene Plateau. This supports the importance of the Indian Ocean as a source
260 of DMS during this season. Fluxes computed from the Lana climatology corresponding
261 to our cruise location and dates range between 2.22 and 34.78 $\mu\text{molm}^{-2}\text{d}^{-1}$. Lana's pre-
262 dicted fluxes are on average higher (Lana mean: 14.9 $\mu\text{molm}^{-2}\text{d}^{-1}$, this study mean: 9.1
263 $\mu\text{molm}^{-2}\text{d}^{-1}$, Figure 3). The reason for these differences is twofold. [1] The Lana clima-

264 tology uses higher DMS seawater concentrations than those we measured in situ. [2] The
265 air-sea flux parametrization (Equation 4) used in the climatology [Nightingale *et al.*, 2000]
266 has a quadratic dependence of the gas transfer velocity k on wind speed. However, our
267 directly measured fluxes and the associated gas transfer velocity appear to have a linear re-
268 lationship to wind speed. As the wind speed experienced during the cruise and the NCEP
269 derived wind speed used by the climatology were similar, the difference in a quadratic and
270 a linear dependence resulted in an increase of the Lana DMS flux.

271 **3.4 Correlations with aerosol properties**

272 Figure 4 shows a time series of the fluxes at the cruise track. Overlaid are the satel-
273 lite aerosol products from the location of the highest positive correlation within the 24
274 hour downwind period. The largest fluxes of DMS, in the top panel, are around DOY 207-
275 208. Additionally, at DOY 212-214, a secondary maximum, followed by a short decrease
276 and sudden increase, can be seen. Similar features are visible in all three satellite prod-
277 ucts. For isoprene, the highest fluxes occurred at DOY 209-211. Similar to DMS fluxes,
278 the isoprene fluxes at the end of the measurement period increase, decrease, then sharply
279 increase again. There is a general agreement in the distributions of the isoprene flux and
280 the aerosol products. The sea salt flux has its main feature at DOY 205, when the wind
281 speed was highest, and steadily decreases over the cruise track. The MODIS AOD product
282 distribution follows the sea salt flux source distribution, whereas the other aerosol satellite
283 product distributions do not appear similar to the trend of the sea salt flux distribution.

284 All three fluxes in Figure 4 have distinct features at different times, corresponding to
285 different features in the downwind aerosol product distributions. This allows us to quali-
286 tatively estimate the influence of each source on the satellite product. The aerosol product
287 distribution more closely resembles the trace gas fluxes than the sea salt flux distributions.
288 Nonetheless, there are also differences between the two trace gases, which are reflected
289 in the aerosol product distributions. For example, the spatial distribution of the isoprene
290 fluxes is anti-correlated with the DMS fluxes at DOY 212 and 214 and the maxima and
291 minima are offset for the two trace gas fluxes. A second example is the isoprene flux fea-
292 ture from DOY 209-211, which is not well represented in the downwind satellite product
293 distribution. The sea salt flux distribution, which starts high and then gradually decreases,
294 does not seem to have great influence on the satellite aerosol product distribution, which
295 does not mean that overall sea salt flux is not an aerosol precursor in this study region.

296 Generally, the correlations between all measured fluxes and their satellite aerosol values
297 are positive and significant. The maximum correlations are shown in the supplemental
298 material [supplement Figure S4-S7, table S3]. In addition, we correlated directly measured
299 CO₂ fluxes with the satellite aerosol products as a quality check on our analysis (supple-
300 ment S4-S7).

301 **4 Conclusion**

302 In this study, we observed that the WTIO during the summer monsoon period is
303 one of the world's largest DMS source regions to the atmosphere. We correlated our di-
304 rectly measured DMS, as well as calculated isoprene and sea salt fluxes, with satellite de-
305 rived aerosol products over the Indian Ocean during the summer monsoon. The maximum
306 correlations including regional transport, computed using trajectories from the Flexpart
307 model, were statistically significant. These results illustrate the regional coupling between
308 marine-derived precursors and aerosol products in the remote MBL, which is in opposition
309 to the arguments in the review paper by *Quinn and Bates* [2011]. Although we acknowl-
310 edge that correlation results do not always imply causation, the ensemble findings support
311 the idea that marine-derived biogenic trace gases, as well as sea salt, influence the CCN
312 number and aerosol properties on a regional scale.

313 **Acknowledgments**

314 The authors thank the crew of the RV Sonne (SO234-2/235). Tobias Steinhoff provided
315 help in measuring the CO₂ eddy covariance fluxes. E. Atlas acknowledges support from
316 the NASA UARP program and thanks Leslie Pope and Xiaorong Zhu for the canister
317 preparation. The authors acknowledge NASA and NOAA for providing the satellite data.
318 We thank the ECMWF for providing the ERA-Interim reanalysis data and the Flexpart
319 development team. This work was carried out under the Helmholtz Young Investigator
320 Group of C. Marandino, TRASE-EC (VH-NG-819), from the Helmholtz Association. The
321 cruise 234-2/235 and A. Fiehn were financed by the BMBF, 03G0235A. The authors de-
322 declare no competing financial interests. The data is stored at the data portal of GEOMAR
323 Kiel.

References

- Booge, D., C. A. Marandino, C. Schlundt, P. I. Palmer, M. Schlundt, E. L. Atlas, A. Bracher, E. S. Saltzman, and D. W. R. Wallace (2016), Can simple models predict large-scale surface ocean isoprene concentrations?, *Atmospheric Chemistry and Physics*, *16*(18), 11,807–11,821, doi:10.5194/acp-16-11807-2016.
- Charlson, R. J., J. E. Lovelock, M. O. Andreae, and S. G. Warren (1987), Oceanic phytoplankton, atmospheric sulphur, cloud albedo and climate, *Nature*, *326*(6114), 655–661, doi:10.1038/326655a0.
- Dee, D. P., S. M. Uppala, A. J. Simmons, P. Berrisford, P. Poli, S. Kobayashi, U. Andrae, M. A. Balmaseda, G. Balsamo, P. Bauer, P. Bechtold, A. C. M. Beljaars, L. van de Berg, J. Bidlot, N. Bormann, C. Delsol, R. Dragani, M. Fuentes, A. J. Geer, L. Haimberger, S. B. Healy, H. Hersbach, E. V. Holm, L. Isaksen, P. Kållberg, M. Köhler, M. Matricardi, A. P. McNally, B. M. Monge-Sanz, J. J. Morcrette, B. K. Park, C. Peubey, P. de Rosnay, C. Tavolato, J. N. Thepaut, and F. Vitart (2011), The era-interim reanalysis: configuration and performance of the data assimilation system, *Quarterly Journal of the Royal Meteorological Society*, *137*(656), 553–597, doi:10.1002/qj.828.
- Edson, J. B., A. A. Hinton, K. E. Prada, J. E. Hare, and C. W. Fairall (1998), Direct covariance flux estimates from mobile platforms at sea, *Journal of Atmospheric and Oceanic Technology*, *15*(2), 547–562, doi:10.1175/1520-0426(1998)015<0547:dcfefm>2.0.co;2.
- Eguchi, K., I. Uno, K. Yumimoto, T. Takemura, T. Y. Nakajima, M. Uematsu, and Z. Liu (2011), Modulation of cloud droplets and radiation over the north pacific by sulfate aerosol erupted from mount kilauea, *SOLA*, *7*, 77–80, doi:10.2151/sola.2011-020.
- Fiehn, A., B. Quack, H. Hepach, S. Fuhlbrügge, S. Tegtmeier, M. Toohey, E. Atlas, and K. Krüger (2017), Delivery of halogenated very short-lived substances from the west indian ocean to the stratosphere during asian summer monsoon, *Atmos. Chem. Phys. Discuss.*, *2017*, 1–40, doi:10.5194/acp-2017-8.
- Forster, C., A. Stohl, and P. Seibert (2007), Parameterization of convective transport in a lagrangian particle dispersion model and its evaluation, *Journal of Applied Meteorology and Climatology*, *46*(4), 403–422, doi:10.1175/jam2470.1.
- Green, T. K., and A. D. Hatton (2014), *The Claw Hypothesis: A New Perspective on the Role of Biogenic Sulphur in the Regulation of Global Climate*, pp. 315–336, Oceanogra-

- 357 phy and Marine Biology - An Annual Review, CRC Press, doi:10.1201/b17143-7.
- 358 Hsu, S. A., E. A. Meindl, and D. B. Gilhousen (1994), Determining the power-law wind-
359 profile exponent under near-neutral stability conditions at sea, *Journal of Applied Meteorology*, 33(6), 757–765, doi:10.1175/1520-0450(1994)033<0757:dtplwp>2.0.co;2.
- 360
361 Hubanks, P., S. Platnick, M. King, and B. Ridgway (2016), Modis atmosphere l3 gridded
362 product algorithm theoretical basis document for c6, *Tech. Rep. ATBD Reference Number: ATBD-MOD-30*, NASA.
- 363
364 Lana, A., T. G. Bell, R. Simo, S. M. Vallina, J. Ballabrera-Poy, A. J. Kettle, J. Dachs,
365 L. Bopp, E. S. Saltzman, J. Stefels, J. E. Johnson, and P. S. Liss (2011), An updated
366 climatology of surface dimethylsulfide concentrations and emission fluxes in the global
367 ocean, *Global Biogeochemical Cycles*, 25(1), n/a–n/a, doi:10.1029/2010GB003850.
- 368 Lana, A., R. Simo, S. M. Vallina, and J. Dachs (2012), Potential for a biogenic influence
369 on cloud microphysics over the ocean: a correlation study with satellite-derived data,
370 *Atmos. Chem. Phys.*, 12(17), 7977–7993, doi:10.5194/acp-12-7977-2012.
- 371 Landwehr, S., N. O’Sullivan, and B. Ward (2015), Direct flux measurements from mobile
372 platforms at sea: Motion and airflow distortion corrections revisited, *Journal of Atmospheric and Oceanic Technology*, 32(6), 1163–1178, doi:10.1175/jtech-d-14-00137.1.
- 373
374 Mace, G. G., and A. C. Abernathy (2016), Observational evidence for aerosol invigoration
375 in shallow cumulus downstream of mount kilauea, *Geophysical Research Letters*, 43(6),
376 2981–2988, doi:10.1002/2016GL067830, 2016GL067830.
- 377 Mihalopoulos, N., B. C. Nguyen, J. P. Putaud, and S. Belviso (1992), The oceanic source
378 of carbonyl sulfide (cos), *Atmospheric Environment. Part A. General Topics*, 26(8),
379 1383–1394, doi:10.1016/0960-1686(92)90123-3.
- 380 Miller, S. D., T. S. Hristov, J. B. Edson, and C. A. Friehe (2008), Platform motion effects
381 on measurements of turbulence and air–sea exchange over the open ocean, *Journal of Atmospheric and Oceanic Technology*, 25(9), 1683–1694, doi:10.1175/2008jtecho547.1.
- 382
383 Nightingale, P. D., G. Malin, C. S. Law, A. J. Watson, P. S. Liss, M. I. Liddicoat,
384 J. Boutin, and R. C. Upstill-Goddard (2000), In situ evaluation of air-sea gas exchange
385 parameterizations using novel conservative and volatile tracers, *Global Biogeochemical Cycles*, 14(1), 373–387, doi:10.1029/1999GB900091.
- 386
387 O’Dowd, C. D., B. Langmann, S. Varghese, C. Scannell, D. Ceburnis, and M. C. Facchini
388 (2008), A combined organic-inorganic sea-spray source function, *Geophysical Research Letters*, 35(1), n/a–n/a, doi:10.1029/2007GL030331.
- 389

- 390 Quinn, P. K., and T. S. Bates (2011), The case against climate regulation via oceanic phy-
391 toplankton sulphur emissions, *Nature*, 480(7375), 51–56, doi:10.1038/nature10580.
- 392 Rhoads, K. P., P. Kelley, R. R. Dickerson, T. P. Carsey, M. Farmer, D. L. Savoie, and
393 J. M. Prospero (1997), Composition of the troposphere over the indian ocean during
394 the monsoonal transition, *Journal of Geophysical Research: Atmospheres*, 102(D15),
395 18,981–18,995, doi:10.1029/97JD01078.
- 396 Saltzman, E. S., W. J. De Bruyn, M. J. Lawler, C. A. Marandino, and C. A. McCormick
397 (2009), A chemical ionization mass spectrometer for continuous underway shipboard
398 analysis of dimethylsulfide in near-surface seawater, *Ocean Sci.*, 5(4), 537–546, doi:
399 10.5194/os-5-537-2009.
- 400 Schott, F. A., S.-P. Xie, and J. P. McCreary (2009), Indian ocean circulation and climate
401 variability, *Reviews of Geophysics*, 47(1), n/a–n/a, doi:10.1029/2007RG000245.
- 402 Smythe-Wright, D., S. M. Boswell, C. H. Lucas, A. L. New, and M. S. Varney (2005),
403 Halocarbon and dimethyl sulphide studies around the mascarene plateau, *Philosophical*
404 *Transactions of the Royal Society A: Mathematical, Physical and Engineering Sciences*,
405 363(1826), 169–185, doi:10.1098/rsta.2004.1485.
- 406 Stohl, A., and D. J. Thomson (1999), A density correction for lagrangian par-
407 ticle dispersion models, *Boundary-Layer Meteorology*, 90(1), 155–167, doi:
408 10.1023/a:1001741110696.
- 409 Stohl, A., C. Forster, A. Frank, P. Seibert, and G. Wotawa (2005), Technical note: The la-
410 grangian particle dispersion model flexpart version 6.2, *Atmos. Chem. Phys.*, 5(9), 2461–
411 2474, doi:10.5194/acp-5-2461-2005.
- 412 Vallina, S. M., R. Simo, and S. Gasso (2006), What controls ccn seasonality in the south-
413 ern ocean? a statistical analysis based on satellite-derived chlorophyll and ccn and
414 model-estimated oh radical and rainfall, *Global Biogeochemical Cycles*, 20(1), n/a–n/a,
415 doi:10.1029/2005GB002597.
- 416 Yoder, J. A., C. R. McClain, G. C. Feldman, and W. E. Esaias (1993), Annual cycles of
417 phytoplankton chlorophyll concentrations in the global ocean: A satellite view, *Global*
418 *Biogeochemical Cycles*, 7(1), 181–193, doi:10.1029/93GB02358.
- 419 Yuan, T., L. A. Remer, and H. Yu (2011), Microphysical, macrophysical and radiative sig-
420 natures of volcanic aerosols in trade wind cumulus observed by the a-train, *Atmospheric*
421 *Chemistry and Physics*, 11(14), 7119–7132, doi:10.5194/acp-11-7119-2011.

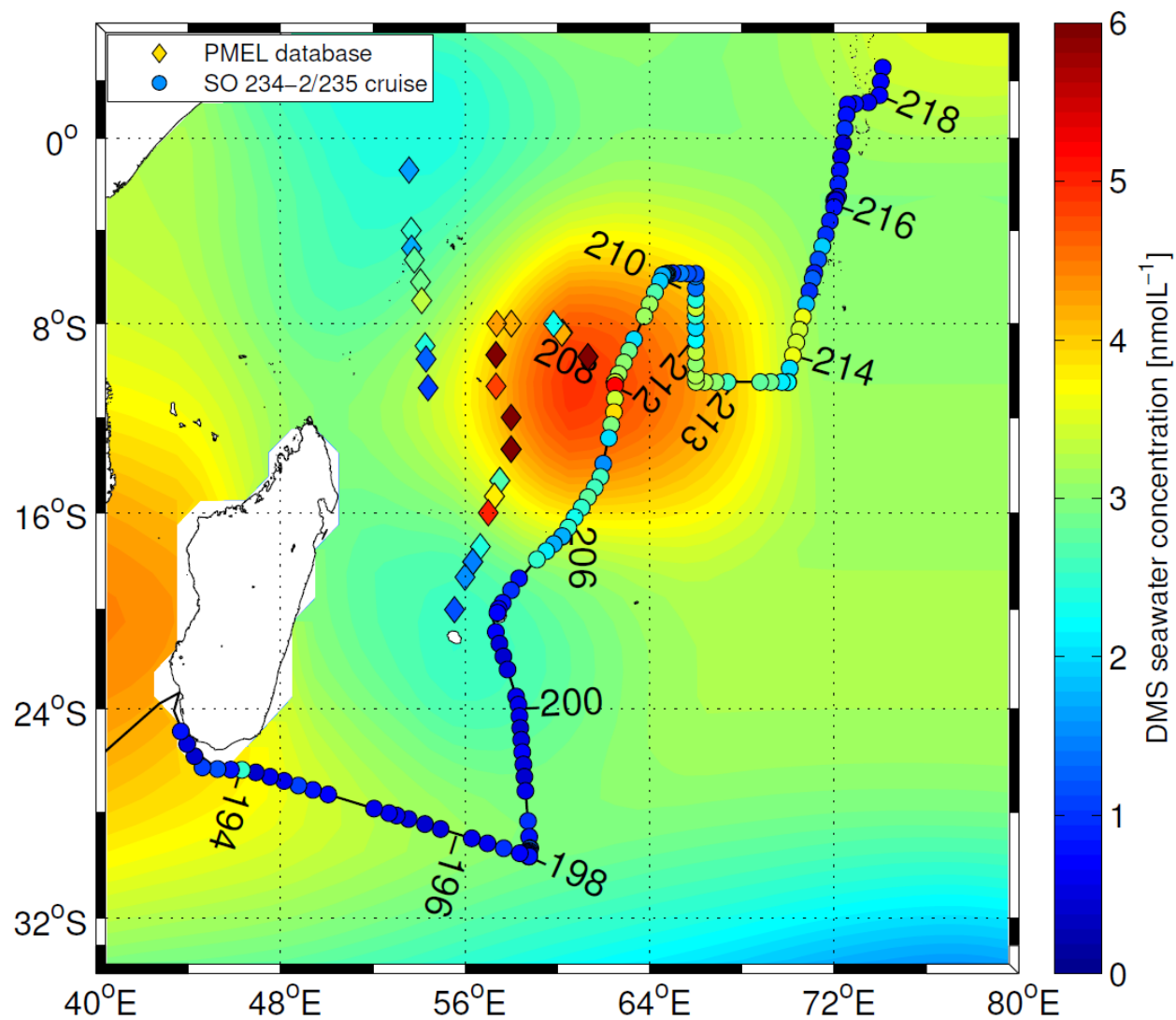


Figure 1: Cruise track (black solid line) of SO234-2/235. Circles are discrete sampled surface water DMS concentrations. Diamonds are all recorded DMS values within the PMEL database for July and August. July DMS surface concentrations from the Lana climatology are color coded in the background. The numbers indicate the Day of Year (DOY).

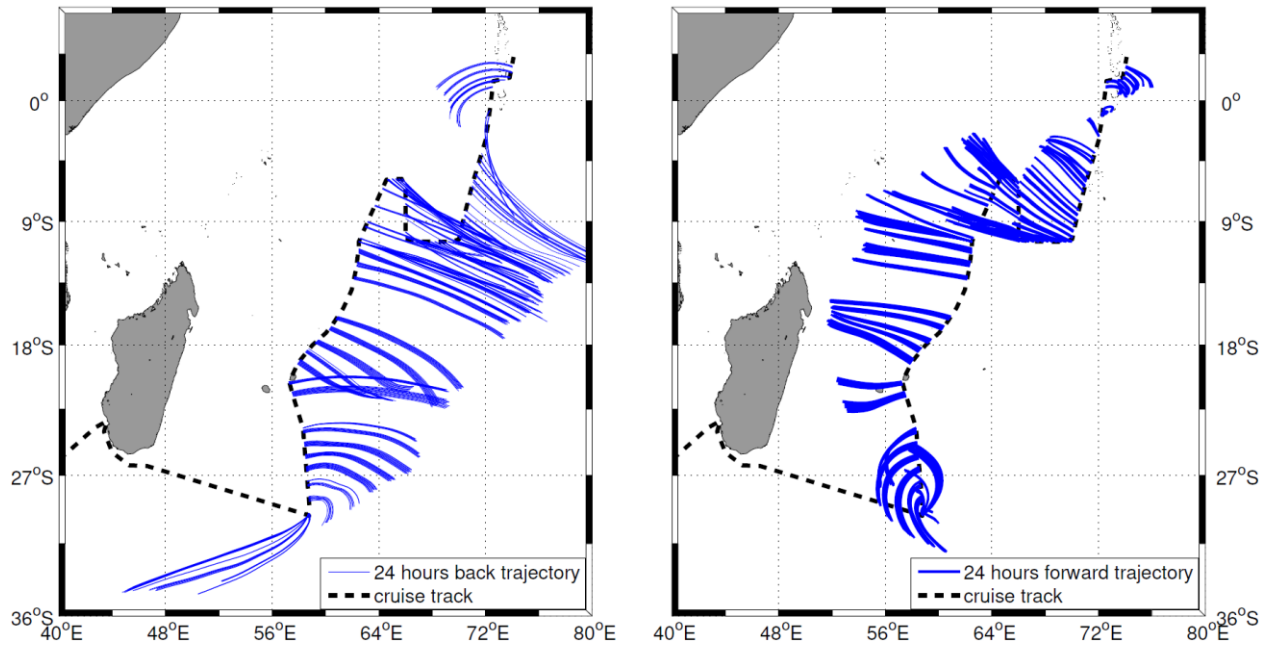


Figure 2: (Left) backward trajectories and (right) forward trajectories (24 hours) calculated using the Flexpart model. In total 435 back- and forward trajectories are shown.

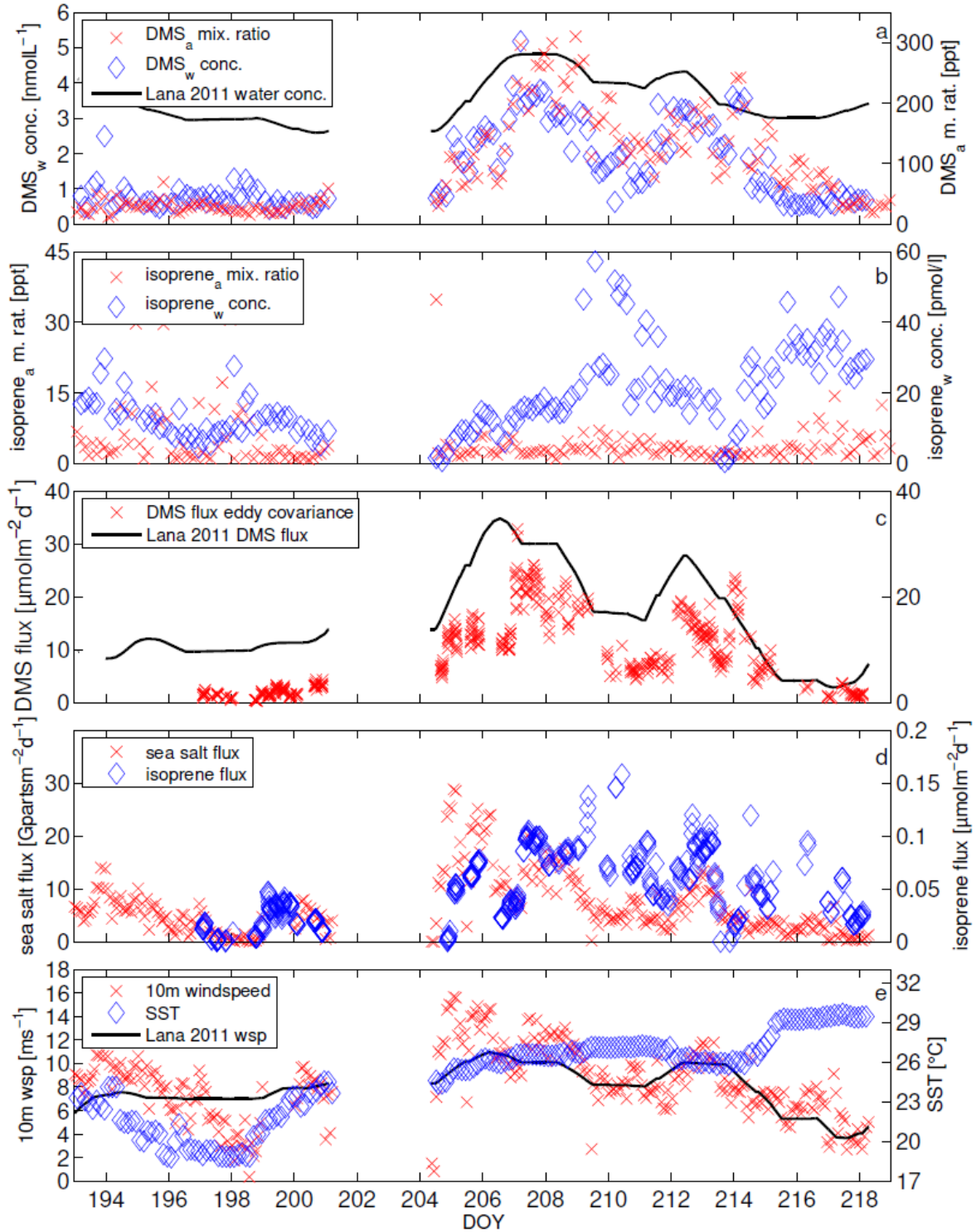


Figure 3: Time series along the cruise track (x-axis DOY 2014), a) DMS surface seawater concentration (diamonds) and the air mixing ratio (crosses), b) isoprene surface water concentrations (diamonds) and air mixing ratios (crosses), c) the measured DMS flux (crosses) and Lana’s climatological DMS flux (line), d) isoprene and the sea salt air-sea flux, e) sea surface temperature (SST, diamonds) and the 10 m wind speed along the cruise track, measured (crosses) and used by the Lana climatology (line).

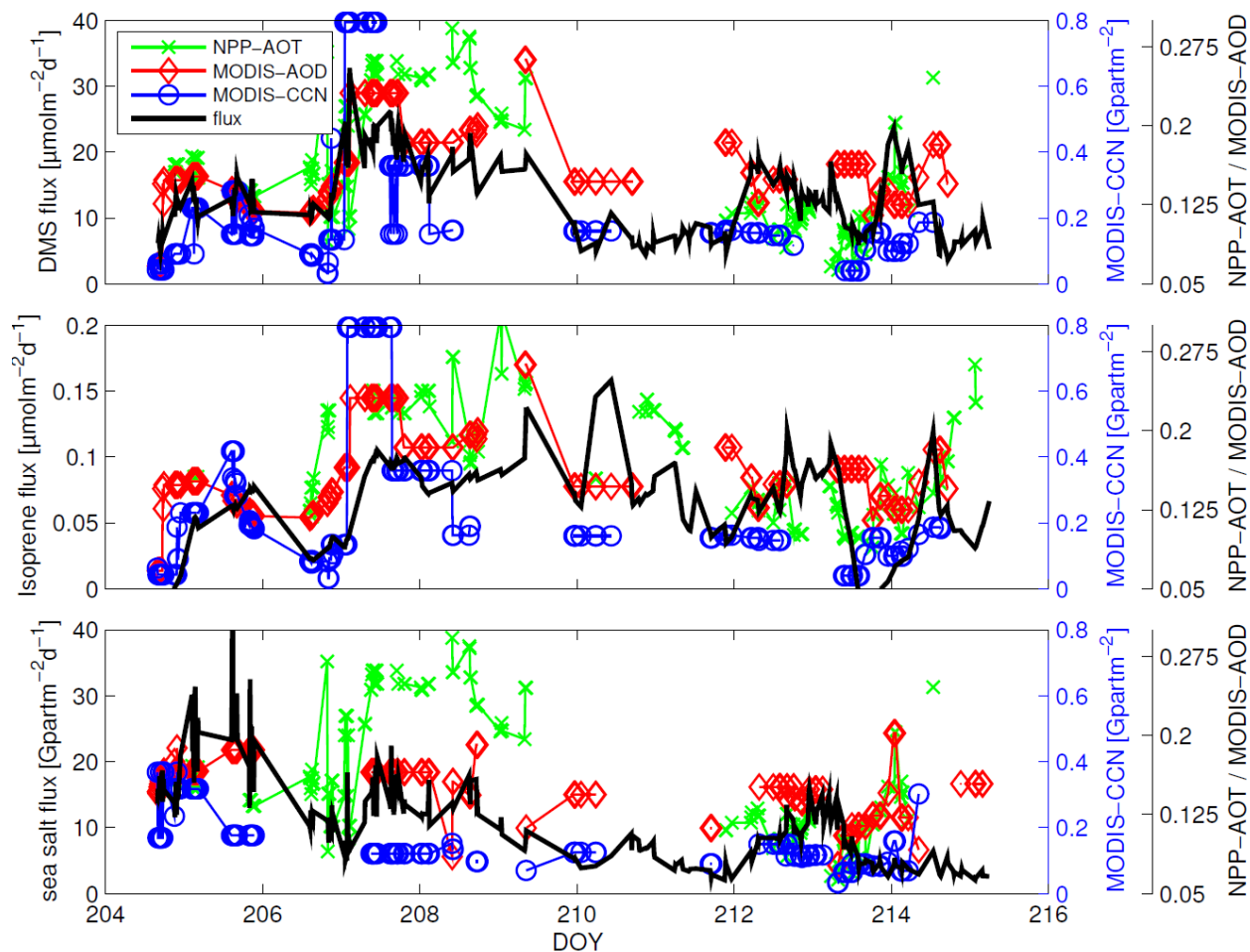


Figure 4: Time series of DMS flux (top panel), isoprene flux (middle panel) and sea salt flux (bottom panel) from DOY 204.66 to 215.25 shown together with the data from the Terra satellite (MODIS-CCN, MODIS-AOD) and the NPP satellite (NPP-AOT). The aerosol products shown are from the time of highest individual correlation.

3.3 Manuscript 3

Fiehn, A.; Quack, B.; Marandino, C. A.; Krüger, K.: Variability of VSLs transport from the West Indian Ocean to the stratosphere, under review at Journal of Geophysical Research: Atmospheres.

Variability of VSLs transport from the West Indian Ocean to the stratosphere

Alina Fiehn^{1,2}, Birgit Quack², Christa Marandino², Kirstin Krüger¹

¹Meteorology and Oceanography Section, Department of Geosciences, University of Oslo, Oslo, Norway

²GEOMAR Helmholtz Centre for Ocean Research Kiel, Kiel, Germany

Corresponding author: Kirstin Krüger (kkrueger@geo.uio.no)

Key Points:

- Transport of very short-lived substances (VSLs) from the West Indian Ocean to the stratosphere during 2000-2016 using FLEXPART/ERA-Interim.
- Stratospheric entrainment of VSLs shows a distinct annual cycle associated with the Asian monsoon.
- Interannual variability of stratospheric VSLs entrainment is influenced by West Indian Ocean sea surface temperatures, as well as by ENSO.

Abstract

Halogen- and sulfur-containing compounds are supersaturated in the surface ocean, which results in their emission to the atmosphere. These compounds can be transported to the stratosphere, where they impact ozone, the aerosol layer, and climate. In this study we calculate the seasonal and interannual variability of transport from the West Indian Ocean (WIO) surface to the stratosphere for 2000-2016 with the Lagrangian transport model FLEXPART using ERA-Interim meteorological fields. We investigate the transport relevant for very short-lived substances (VSLs) with tropospheric lifetimes corresponding to dimethylsulfide (DMS, 1 day), methyl iodide (CH_3I , 3.5 days), bromoform (CHBr_3 , 17 days), and dibromomethane (CH_2Br_2 , 150 days). The stratospheric entrainment of VSL tracers from the WIO shows a distinct annual cycle associated with the Asian monsoon. Over the 16 year time series, a slight increase in entrainment from the WIO to the stratosphere is found for all VSL tracers and during all seasons. The interannual variability shows a relationship with sea surface temperatures in the West Indian Ocean as well as the El Niño–Southern Oscillation (ENSO). During boreal spring of El Niño, enhanced stratospheric entrainment of VSLs from the tropical WIO is caused by positive sea surface temperature anomalies and enhanced vertical uplift above the WIO. During boreal fall of La Niña, stronger entrainment is related to enhanced atmospheric upward motion over the East Indian Ocean and a prolonged Indian summer monsoon season. Related physical mechanisms and uncertainties are discussed in this study.

1 Introduction

Halogens and sulfur in the stratosphere impact the ozone and Junge layers and can, thus, affect the radiation budget and climate [Solomon *et al.*, 1994; Dvortsov *et al.*, 1999; Myhre *et al.*, 2004; Solomon *et al.*, 2011]. Stratospheric halogen sources include halogenated very short-lived substances (VSLS) emitted from the oceans [Law *et al.*, 2006]. Model calculations suggest that marine dimethylsulfide (DMS) emissions contribute to the persistent stratospheric background aerosol layer or Junge layer [Marandino *et al.*, 2013]. Natural halogen and sulfur containing organic compounds originate from chemical and biological sources, such as phytoplankton and macro algae in the oceans [Moore and Zafiriou, 1994; Carpenter *et al.*, 1999; Stefels, 2000; Quack and Wallace, 2003]. Gases, that are emitted to the atmosphere, are defined as VSLS if they have atmospheric lifetimes of less than half a year [Law *et al.*, 2006]. In this study, we consider sulfuric and halogenated VSLS, namely DMS, methyl iodide (CH₃I), bromoform (CHBr₃), and dibromomethane (CH₂Br₂).

Estimates of VSLS emissions from the global oceans are subject to large uncertainties [Lana *et al.*, 2011; Carpenter *et al.*, 2014]. Global emission climatologies have been derived from observations and chemistry climate models (bottom-up approach) [Quack and Wallace, 2003; Butler *et al.*, 2007; Palmer and Reason, 2009; Lana *et al.*, 2011; Ziska *et al.*, 2013; Lennartz *et al.*, 2015], atmospheric abundances and chemistry climate models (the top-down approach) [Warwick *et al.*, 2006; Liang *et al.*, 2010; Ordóñez *et al.*, 2012], as well as biogeochemical ocean models [Kloster *et al.*, 2006; Hense and Quack, 2009; Stemmler *et al.*, 2015]. The delivery of these emissions to the stratosphere has been the topic of several modeling studies [Nielsen, 2001; Warwick *et al.*, 2006; Kerkweg *et al.*, 2008; Hossaini *et al.*, 2010; Liang *et al.*, 2010; Lennartz *et al.*, 2015; Sheng *et al.*, 2015]. While the main VSLS entrainment to the stratosphere occurs over the West Pacific Ocean [Aschmann *et al.*, 2009; Marandino *et al.*, 2013; Tegtmeier *et al.*, 2013], the Asian summer monsoon also is a significant transport pathway [Liang *et al.*, 2014; Hossaini *et al.*, 2016]. The few available measurements from the Indian Ocean showed strong VSLS emissions [Mihalopoulos *et al.*, 1992; Smythe-Wright *et al.*, 2005; Fiehn *et al.*, 2017]. Fiehn *et al.* [2017] underlined that halogenated VSLS emissions can reach the stratosphere during the summer monsoon season. In addition, the Indian Ocean is a region strongly affected by climate change: the West Indian Ocean (WIO) has been warming faster than any other tropical ocean over the last century [Roxy *et al.*, 2014]

causing a reduction in marine primary production [Roxy *et al.*, 2016], which influences seawater concentrations of DMS and halocarbons [Miles *et al.*, 2012; Hepach *et al.*, 2014].

In the atmosphere, current estimates of tropical tropospheric lifetimes are 1 day for DMS [Barnes *et al.*, 2006; Osthoff *et al.*, 2009], 3.5 days for CH₃I, 17 days for CHBr₃, and 150 days for CH₂Br₂ [Carpenter *et al.*, 2014]. The delivery of these compounds from the ocean surface to the stratosphere depends on emission strength and fast transport, because the chemical decay might be faster than the transport timescale. Stratospheric entrainment of VSLs is connected with fast and high reaching convection above the tropical oceans. The so-called “stratospheric fountain”, the region where tropospheric air enters the stratosphere, is located over the tropical West Pacific from November to March and over the Bay of Bengal and India during the summer monsoon [Newell and Gould-Stewart, 1981]. The stratospheric entrainment is most pronounced over the tropical Pacific and Maritime continent during boreal winter [Fueglistaler *et al.*, 2005; Krüger *et al.*, 2008; 2009], but the Indian summer monsoon is also efficient at transporting boundary layer air masses into the stratosphere [Park *et al.*, 2009; Randel *et al.*, 2010]. Several model studies of transport pathways toward the main stratospheric entrainment region of the summer monsoon have been carried out. Mostly anthropogenic continental boundary layer sources were accounted for with the Lagrangian chemical transport model CLAMS [Bergman *et al.*, 2013; Vogel *et al.*, 2015] and chemistry climate models [Orbe *et al.*, 2015]. Chen *et al.* [2012] calculated the Asian summer monsoon air mass transport pathways for 2001-2009 with the Lagrangian model FLEXPART and found the main stratospheric entrainment regions above the tropical central Indian Ocean, the Bay of Bengal, the South China Sea and West Pacific. With a chemistry climate model, Liang *et al.* [2014] simulated a VSLs bromine maximum above the tropical Indian Ocean at 355 K potential temperature (~13 km) using the emission scenario of Liang *et al.* [2010]. Based on observed emissions of halogenated VSLs from the WIO during July and August 2014 and the model FLEXPART, Fiehn *et al.* [2017] diagnosed stratospheric entrainment of CH₃I mainly above the equatorial Indian Ocean, while CHBr₃ and CH₂Br₂ reached the stratosphere in the southeastern part of the Asian monsoon anticyclone.

Influences on the transport above the Indian Ocean may originate from changes in the monsoon circulation and its convection. Fast vertical transport above the marine atmosphere, mostly realized through atmospheric deep convection, depends on the convective available potential energy and, thus, heat flux from the ocean connected to the

sea surface temperature (SST). Convective activity is often directly related to rainfall and has been used as a precipitation proxy since satellite data became available [Arkin and Ardanuy, 1989]. The Indian monsoon rainfall shows changes and variability in the monsoon circulation and convection strength. The leading mode of variability in Indian summer monsoon rainfall is connected with the influence of ENSO on the Walker Circulation [Walker, 1924; Webster and Yang, 1992; Wang *et al.*, 2001; Ding, 2007; Wang *et al.*, 2015]. The Asian monsoon system is also experiencing a long term change (1901-2012) due to greenhouse gas induced global warming, with a decrease in the land-sea thermal gradient and less summer monsoon rainfall over the central-east and northern regions of India [Roxy *et al.*, 2015], which may be related to reduced convection and VLS transport to the stratosphere through the summer monsoon.

The contribution of oceanic VLS to the stratospheric composition and their transport via the Asian monsoon circulation has hardly been studied. In order to better represent natural factors in global chemistry climate and transport models simulating the monsoon system, it is important to also investigate the role of oceanic trace gases, such as VLS, on atmospheric composition and chemistry. While the atmospheric abundances of many long-lived ozone depleting substances are declining due to the regulation through the Montreal protocol [WMO, 2014], natural VLS emissions [Ziska *et al.*, 2017] as well as their weighted stratospheric ozone depletion potential [Tegtmeier *et al.*, 2015] could increase in a future climate.

In a previous study, we investigated the stratospheric entrainment of halogenated VLS from the WIO during the summer monsoon season. We reported the first measurements of CHBr_3 and CH_2Br_2 from the Indian Ocean and calculated strong emissions of VLS from the WIO and their transport to the stratosphere along two pathways [Fiehn *et al.*, 2017]. In this follow-up study, we investigate the air mass transport relevant for VLS from the WIO to the stratosphere over the whole year, the seasonal transport cycle and interannual transport variability. A VLS tracer with a 1-day lifetime, DMS, was included in this study to investigate transport above the Indian Ocean for the shortest timescales, because the Indian Ocean is an emission hot spot for DMS [Lana *et al.*, 2011]. We determine the transport mechanisms and show the relationship between the transport variability above the WIO and the ENSO phase.

2 Methods

2.1 Trajectory Model and Meteorological Data

The air mass transport from the WIO to the stratosphere is calculated with the Lagrangian particle dispersion model FLEXPART Version 9.2 from the Norwegian Institute for Air Research [Stohl *et al.*, 2005]. The model includes parameterizations for convection [Forster *et al.*, 2007] and turbulence in the boundary layer and free troposphere [Stohl and Thomson, 1999]. The FLEXPART model is driven with the ECMWF (European Centre for Medium-Range Weather Forecasts) reanalysis product ERA-Interim [Dee *et al.*, 2011] based on a horizontal resolution of $1^\circ \times 1^\circ$ and 60 vertical model levels, providing 6 hourly air temperature, winds, and specific humidity. A preprocessor, which retrieves the meteorological fields from the ECMWF archives, calculates the vertical wind from spectral data in hybrid coordinates mass-consistently for the FLEXPART runs [Stohl *et al.*, 2005]. Similar to Fiehn *et al.* [2017], we start one trajectory per grid point from a $1^\circ \times 1^\circ$ grid at the sea surface within the release area in the tropical WIO (20°S - 10°N , 50°E - 80°E , Figure 16) once every day from January 1, 2000, until February 28, 2016 and calculate them for three months forward. The trajectory positions are recorded every 6 hours. First, we determine the path of these trajectories from the ocean surface to an entrainment height of 17 km, the approximate height of the tropical cold point tropopause over the Asian monsoon region [Munchak and Pan, 2014]. Based on the transit time from the sea surface to the stratosphere, the fraction of an artificial VLSL tracer that reaches the stratosphere on each trajectory is calculated using an exponential decay of the tracer assuming a tropical tropospheric lifetime for DMS, methyl iodide, bromoform, and dibromomethane of 1, 3.5, 17, and 150 days, respectively [Barnes *et al.*, 2006; Osthoff *et al.*, 2009; Carpenter *et al.*, 2014]. While the trajectories determine the transport of air masses, the VLSL tracers on the trajectories distinguish the transport on timescales of the individual VLSL lifetimes. The *transport efficiency* is defined as the percentage of entrained VLSL tracer and gives a measure of the strength of stratospheric entrainment depending on homogeneous VLSL fields at the ocean surface. It is allocated to the month in which the trajectories were initiated to infer the entrainment strength for oceanic sources at a certain time.

2.2 Climate Indices

In order to investigate the possible influences on seasonal and interannual variability in stratospheric entrainment of VLSL tracers from the WIO, we use different climate indices

(Figure 1) describing the state of the ocean, the atmospheric circulation, and different coupled ocean-atmosphere phenomena. We use ERA-Interim monthly mean sea surface temperature (SST) in our WIO release area (SST_{WIO}) to infer transport changes due to local SST anomalies. Above the Indian Ocean, the Indian monsoon circulation dominates the tropospheric circulation. The large scale Indian monsoon circulation is described by the Indian Monsoon Index (IMI), which is defined as the gradient of zonal wind at 850 hPa between a southern area over the northern WIO ($40^{\circ}\text{E}-80^{\circ}\text{E}$, $5^{\circ}\text{N}-15^{\circ}\text{N}$) and an area over northern India ($70^{\circ}\text{E}-90^{\circ}\text{E}$, $20^{\circ}\text{N}-30^{\circ}\text{N}$) [Wang and Fan, 1999; Wang et al., 2001]. Daily mean IMI data was provided by Yoshiyuki Kajikawa and Bin Wang on their Monsoon Monitoring Page (Supporting Information). The strength of the summer monsoon is often described by the amount of rainfall over India. All India Rainfall Index (AIRI) monthly data is provided by the Indian Institute for Tropical Meteorology for 1871-2014 (Supporting Information). The SST anomaly between the West and East Indian Ocean, the Indian Ocean Dipole (IOD), has been shown to influence convection and rainfall in the Indian Ocean region. The Dipole Mode Index (DMI) describes the status of the IOD and is defined as the difference between SST in the WIO ($50^{\circ}\text{E}-70^{\circ}\text{E}$, $10^{\circ}\text{S}-10^{\circ}\text{N}$) and the east Indian Ocean ($90^{\circ}\text{E}-110^{\circ}\text{E}$, $10^{\circ}\text{S}-0^{\circ}$, Figure 16) [Saji et al., 1999]. The DMI is provided by the National Oceanic and Atmospheric Administration (NOAA) State of the Ocean project (Supporting Information).

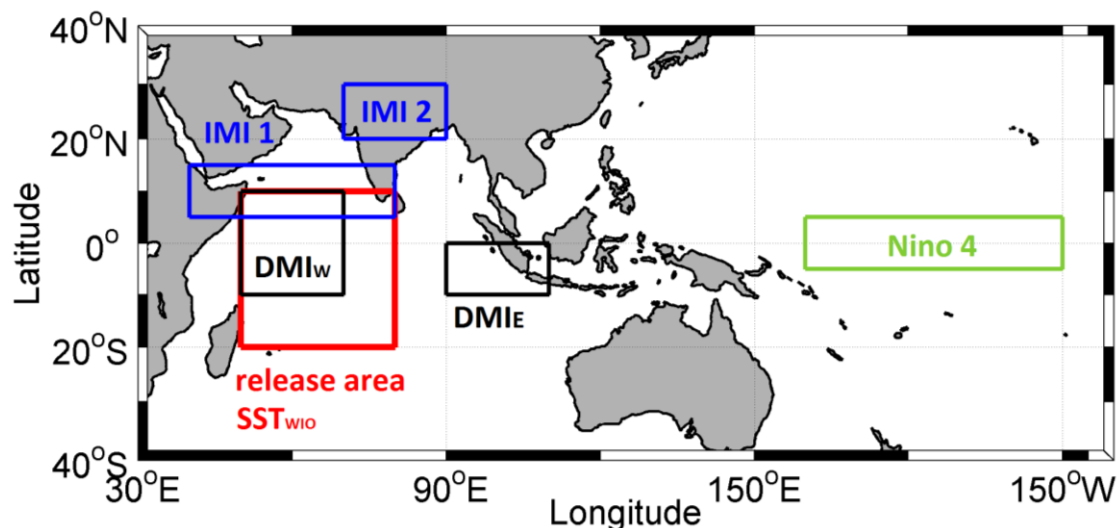


Figure 16: Areas for the definition of climate and circulation indices and the release area for the trajectories and SST_{WIO} . The indices are the Indian Monsoon Index ($IMI = IMI_1 - IMI_2$), Dipole Mode Index ($DMI = DMI_W - DMI_E$), and Nino 4 region.

We analyze the influence of ENSO on stratospheric entrainment from the WIO through the monthly $SST_{\text{Nino } 4}$ averaged over the Nino 4 region (160°E - 150°W , 5°N - 5°S , Figure 16) from ERA-Interim. We chose the central Pacific Nino 4 over the east Pacific Nino 3.4 region, because central Pacific ENSO events tend to have a greater influence on the Indian Ocean than those in the east Pacific [Kumar *et al.*, 2006].

2.3 Statistical analysis

We use different statistical analyses to infer trends, variability, and relationships from the considered time period. We detrended the interannual 16 year time series of transport efficiency from the WIO to the stratosphere for the calculations of interannual variability and correlations. Linear trends and their significance were computed with a permutation test (p-value).

The seasonal and interannual variability of transport from the WIO to the stratosphere is investigated with the coefficient of variation, which is defined as the standard deviation normalized by the mean. For seasonal variability, we calculate the seasonal coefficient of variation from 12 monthly transport efficiency values (Table 1). For interannual variability, we calculate the interannual coefficient of variation from 16 detrended annual values for the annual mean or seasonal means (Table 4). The values of transport efficiency for seasons were calculated from all trajectories started in the designated season. December to February (DJF, boreal winter) is allocated to the year of the starting month, thus trajectories for DJF₂₀₀₀ were released in December 2000, January 2001 and February 2001. The transport efficiency value of DJF₂₀₁₅ is the only value that includes the transport efficiency of January and February 2016; all other statistics are based on January 2000 to December 2015.

The correlation of annual cycles and detrended interannual variability of the transport efficiency to the stratosphere with different climate indices are calculated with the correlation coefficient r by *Pearson* [1895]. All data were tested for normal distribution. For the correlation of annual cycles, we first calculated the mean annual cycle of transport efficiency for each tracer and for the climate indices from 2000-2015 using monthly data. Then a time lag correlation was determined between each tracer's average annual cycle of transport efficiency and the average annual cycles of the climate indices IMI, AIRI, DMI, SST_{WIO} , and $SST_{\text{Nino } 4}$. We only show the average correlation over all four VLS tracers, because the individual correlations are similar. The interannual correlations between the detrended time series of VLS tracer transport

efficiency and climate indices were calculated for annual means as well as for seasonal means of each year. The significance of the correlations was determined with a permutation test (p-value).

We created maximum entrainment anomaly composites for all seasons. The five years (~30% of the time period) with maximum transport efficiency were determined from the detrended interannual values (Figure S5) and their average was subtracted from the climatological values for the whole 16 years.

3 Results

3.1 Case Study 2014

In a previous study we reported about the OASIS cruise in the WIO, which included observation based VLS emissions and their transport to the stratosphere during Asian summer monsoon [Fiehn *et al.*, 2017]. Here, we examine the transport during the whole 2014, the year of the OASIS cruise, to investigate the seasonality of transport from the same release area. The forward trajectories of the first 10 days for every month reflect the different circulation patterns during the seasons (Figure 17). From May to September, the summer monsoon circulation is clearly visible above the Indian Ocean. Most trajectories follow the southeast trade winds and the southwest monsoon winds towards the Indian subcontinent and Bay of Bengal. From October to April, the patterns are less organized. Over the whole year, trajectories released close to the ITCZ position experience rapid vertical uplift due to convective activity (Figure S1). The few north- and southbound trajectories are rarely lifted to the upper troposphere and lower stratosphere.

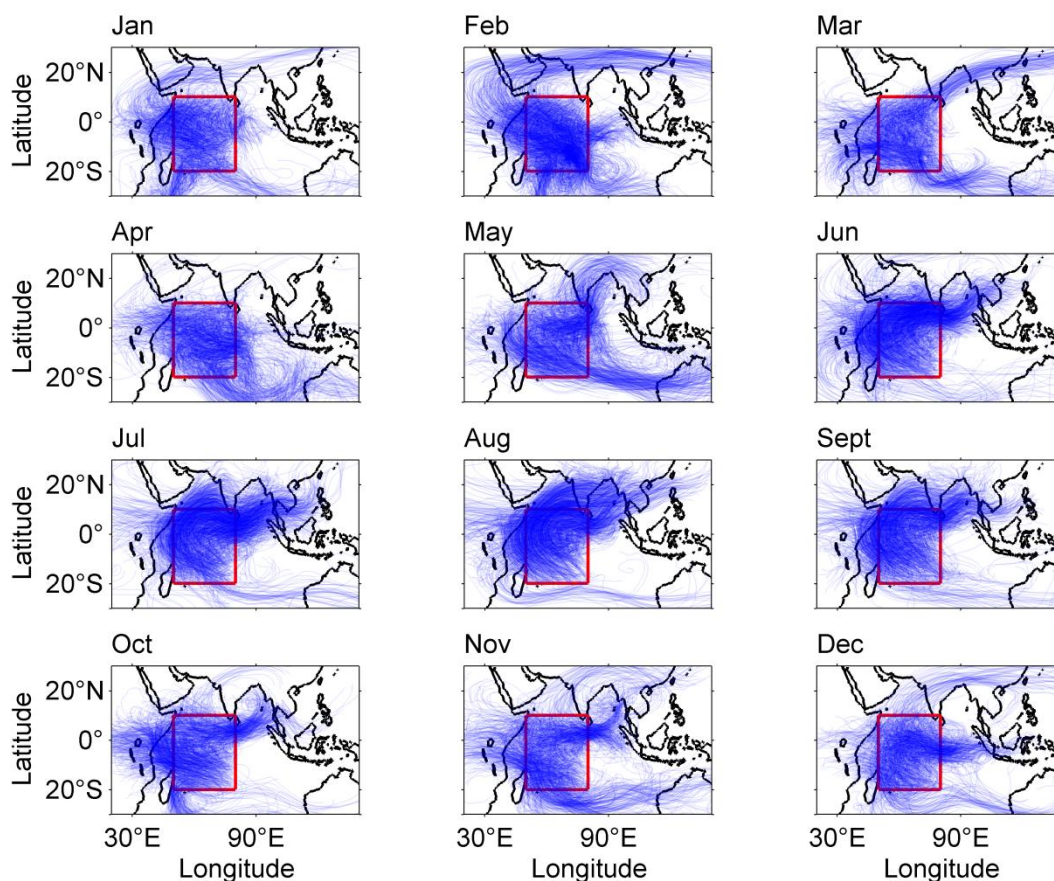


Figure 17: Ten-day forward trajectories released at the sea surface of the tropical WIO (red box) in 2014.

Figure 18 shows the latitude of maximum density of VSLs tracers at 8 km, mid-troposphere, and 15 km, upper-troposphere, for every month in 2014. Overall, the latitude of maximum density of trajectories reflects the annual cycle associated with the observed position of the ITCZ and connected precipitation [Schneider *et al.*, 2014]. In the mid-troposphere, the center of maximum density of trajectories moves from 5°S in boreal winter and spring to around 8°N in boreal summer and fall (Figure 18a). In the upper troposphere, the main tracer transport in boreal winter and spring is located as far as 10°S and moves to 20°N in boreal summer, depending on the lifetime of the tracer (Figure 18b). In July, the distance between the main pathways of the two longer-lived tracers (CHBr_3 and CH_2Br_2 , 20°N) and the two shorter-lived tracers (DMS and CH_3I , 8°N) in the upper troposphere is about 12° in latitude. This case study of the 2014 annual cycle confirms the two main transport pathways depending on the tracer lifetime found by Fiehn *et al.* [2017], and adds that they only exist during Asian summer monsoon. During the onset of the summer monsoon, in April and May, the CHBr_3 and CH_2Br_2 tracer pathways shift northwards about a month earlier than for the DMS and CH_3I tracers. After the end of the

summer monsoon in November the pathways of the two longer lived tracers shift southward a month earlier. This difference in the seasonal shift is not caused by the monsoon circulation, but is an effect of the different lifetimes and the assignment of the transport to the release time of the trajectories (Section 2.1). The trajectories released in April are influenced by the pre-monsoonal circulation in April if they have short lifetimes (DMS and CH₃I), but also by the onset of the monsoon in May if tracer lifetimes are longer (CHBr₃ and CH₂Br₂).

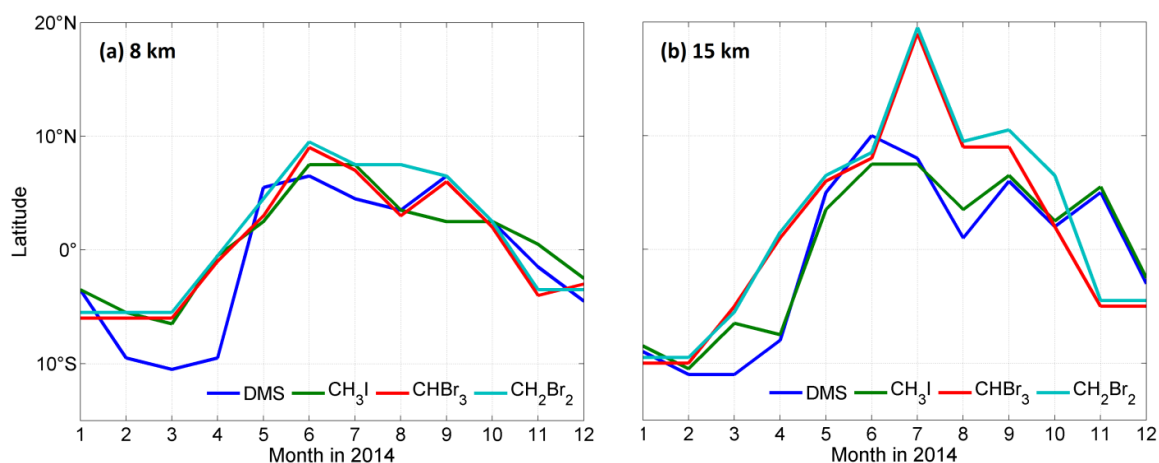


Figure 18: Annual cycle of latitude of maximum density of WIO to stratosphere transport at a) 8 km and b) 15 km altitude in 2014.

With the change in tropospheric circulation in the tropics over the year, the stratospheric entrainment region also varies. Figure 19 shows where the CHBr₃ tracer from the WIO first reaches 17 km for every month of 2014. Entrainment regions for DMS, CH₃I, and CH₂Br₂ tracers can be found in the supporting material (Figure S2-S4). From May to September 2014, during the summer monsoon, the stratospheric entrainment region lies above the Bay of Bengal, northern India and East Asia for CHBr₃ and CH₂Br₂. The DMS and CH₃I tracer summer monsoon entrainment at 17 km is further south at the northern edge of the release area, around 10°N. From October to April 2014, during the winter monsoon, the main stratospheric entrainment region of all tracers lies above the release box in the WIO. This is in accordance with their maximum transport density in the upper troposphere found in Figure 18b. During boreal summer (June-August, JJA) and fall (September-November, SON) 2014, the transport pathway from the WIO release area to the main uplift and entrainment region is much longer than during the rest of the year (Fig. S1). This leads to more decay of the VLSL-tracers and a minimum in transport efficiency in boreal summer and fall (Fig. 4, S2-S4). The maximum transport efficiency

from the WIO to the stratosphere for all tracers occurs during boreal spring (March-May, MAM) 2014.

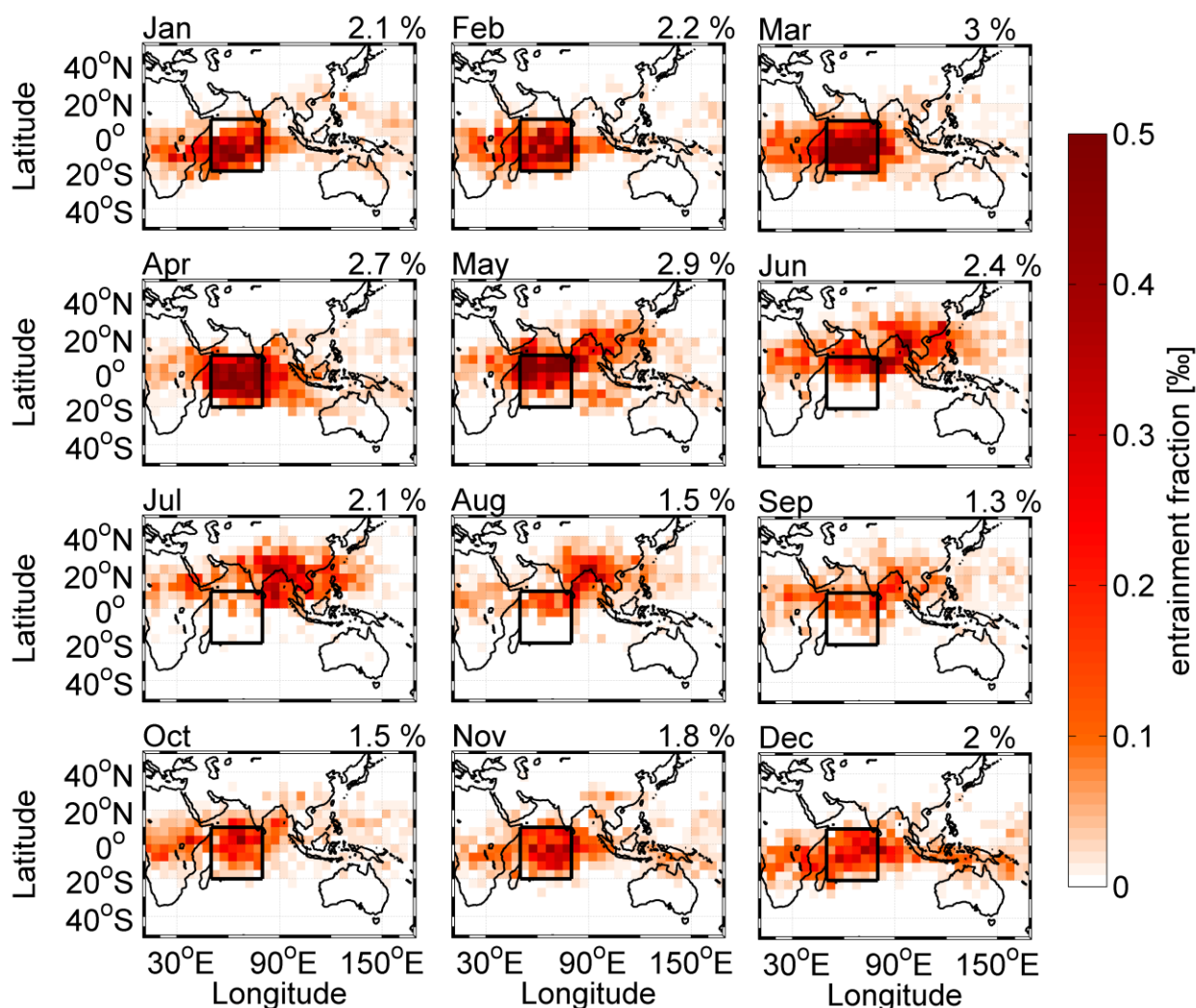


Figure 19: Stratospheric entrainment regions for CHBr_3 tracer released in 2014 shown as fraction of released tracer (in %) entrained in a $5^\circ \times 5^\circ$ grid. The black box shows the WIO release area. The transport efficiency (te), the fraction of released tracer (in %) reaching 17 km over the whole area, is noted in the top right for each month. DMS, CH_3I , and CH_2Br_2 entrainment regions are shown in the supporting material (Fig. S2-S4).

3.2 Climatology

The monthly transport efficiencies from 2000-2016 of the VSLs tracers from the WIO to the stratosphere show a distinct annual cycle, long-term changes as well as interannual variability (Figure 20). We analyze these phenomena in this section.

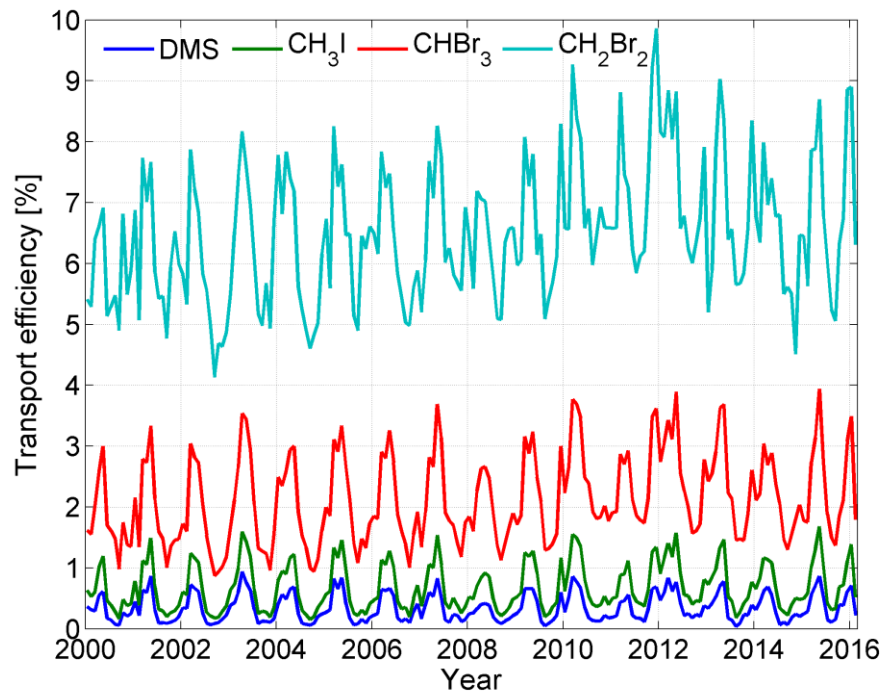


Figure 20: Monthly values of transport efficiency for VSL tracers (in %) from the Indian Ocean to the stratosphere from January 2000 to February 2016.

Annual Cycle

The climatological annual cycles of transport efficiency for all four VSL tracers, display maximum entrainment in boreal spring and minimum entrainment in boreal fall (Figure 6a). The climatological annual mean transport efficiency and their seasonal variation are summed up in Table 1. As expected, the climatological annual mean transport efficiency is highest for the longest-lived tracer, CH_2Br_2 , and lowest for the shortest-lived tracer, DMS. The seasonal coefficient of variation shows that the DMS annual cycle has the highest relative amplitude and the CH_2Br_2 cycle shows the smallest amplitude. There is, thus, an inverse relationship between the lifetime of tracers and the amplitude of their annual cycles.

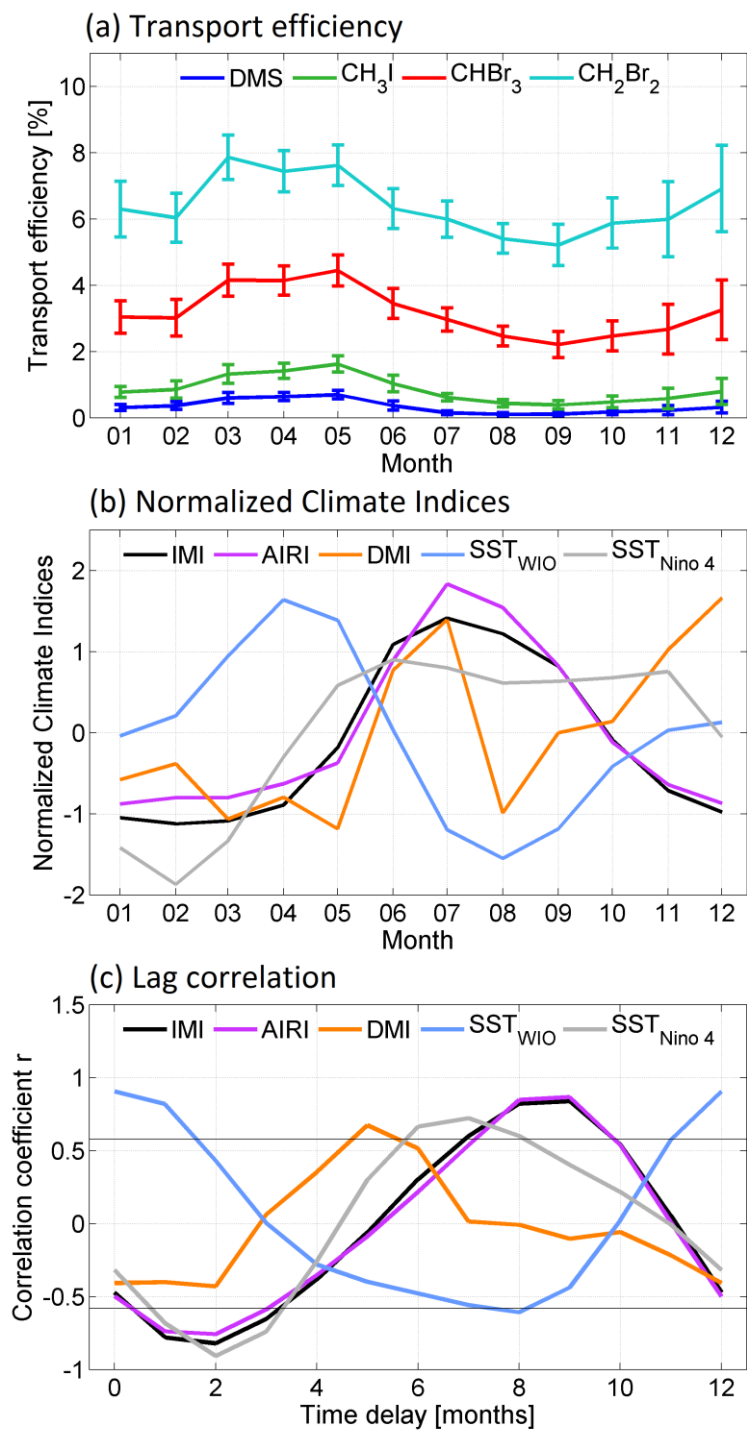


Figure 21: a) Climatological annual cycle of transport efficiency from the WIO to the stratosphere. b) Climatological normalized annual cycle of the Indian Monsoon Index (IMI), All India Rainfall Index (AIRI), Dipole Mode Index (DMI), SST in the WIO (SST_{WIO}), and the SST in the Nino 4 region (SST_{Nino 4}) for 2000-2015. c) Lag correlation of annual cycles of transport efficiency from the West Indian Ocean (WIO) to the stratosphere and the annual cycles of climate indices. Shown is the average for all four VSL tracers (Sect. 2.3). The grey line denotes the significance threshold for 95%.

Table 3: Climatological annual mean transport efficiency [%] and seasonal coefficient of variation for transport from the WIO to the stratosphere as displayed in Figure 21a.

	DMS	CH ₃ I	CHBr ₃	CH ₂ Br ₂
Climatological annual mean transport efficiency [%]	0.34	0.68	2.13	6.50
Seasonal coefficient of variation [unitless]	0.67	0.57	0.35	0.17

We conducted a time lag correlation between the climatological annual cycles of VLSL tracer transport efficiency (Figure 21a) and the climatological annual cycles of IMI, AIRI, DMI, SST_{WIO}, and SST_{Nino 4} climate indices (Figure 21b). The average time lag correlation coefficients for all VLSL tracers are displayed in Figure 21c. Without time lag, the correlation coefficient of transport efficiency with IMI, AIRI, DMI, and SST_{Nino 4} is between -0.3 to -0.5 with a significance threshold of -0.58. The SST_{WIO} shows a significant positive correlation of 0.8 without lag. For AIRI, IMI, and SST_{Nino 4}, we find significant maximum negative correlations with a time lag of two months, maximum positive correlations with a lag of seven to nine months. This means that the maximum (minimum) of entrainment occurs two months after the minimum (maximum) in monsoon circulation and rainfall over India. Significant correlations with DMI have a minimum without time lag and a maximum at five months, thus maximum stratospheric entrainment occurs at the time of year with the weakest DMI. The annual cycle of the SST_{WIO} has highest significant correlations to the stratospheric entrainment without time lag, and smallest correlations at eight months. Thus, the maximum stratospheric entrainment coincides with the time of highest SST in the WIO.

Long-term changes and interannual variability

The Asian monsoon circulation, as well as the convection strength over the Indian Ocean, is subject to long-term changes and interannual variability, which might be reflected in the VLSL transport efficiency from the WIO to the stratosphere (Figure 20 and Figure 22). Table 4 gives the climatological transport efficiency for the four tracers shown in Figure 22 as annual and seasonal means. The transport efficiency shows a slight increase over

the 16 years of our analysis for all VSLs tracers and seasons. The decadal increase in transport efficiency is noted in Table S1 in the supporting material. The detrended interannual time series of transport efficiency are shown as anomalies in Figure S5.

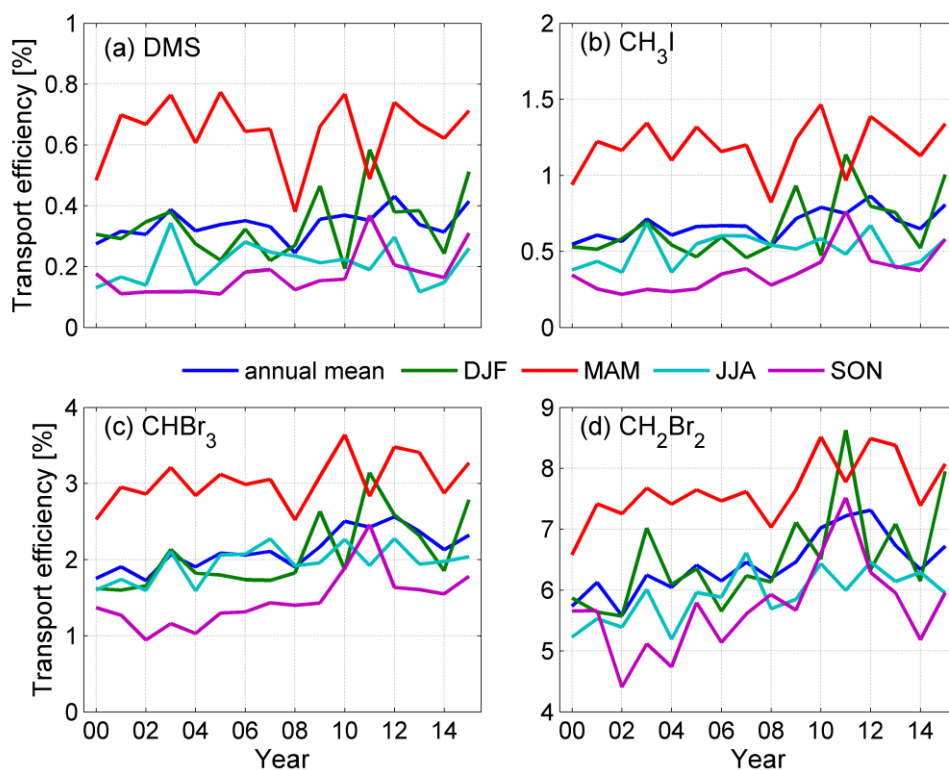


Figure 22: Interannual time series of the transport efficiency of VSLs tracers from the Indian Ocean to the stratosphere from 2000 to 2015. The color legend is provided in the figure.

To determine interannual variability of transport efficiency, we calculated the coefficient of variation from the detrended time series shown in the supporting material in Figure S5. The interannual coefficient of variation for the annual mean is less than for the seasonal means (Table 2). The seasons with high interannual variability are boreal fall and winter, while variability is lowest during maximum entrainment in boreal spring. There are differences between the VSLs tracers as well. The shortest-lived tracer (DMS) is most variable on interannual scales, with variability decreasing with lifetime. When comparing the interannual variability (Table 4) to the annual cycle (Table 3), we find that interannual variability is weaker than the amplitude of annual cycle.

Table 4: Climatological transport efficiency [%] from Figure 22 and interannual coefficient of variation for detrended transport efficiency values from Figure S5.

			DMS	CH ₃ I	CHBr ₃	CH ₂ Br ₂
Climatological transport efficiency [%]	Annual mean		0.34	0.68	2.13	6.50
	Seasonal means	DJF	0.34	0.66	2.07	6.52
		MAM	0.64	1.19	3.04	7.66
		JJA	0.21	0.51	1.96	5.91
		SON	0.17	0.37	1.47	5.70
Interannual coefficient of variation [unitless]	Annual mean		0.14	0.14	0.12	0.08
	Seasonal means	DJF	0.33	0.31	0.23	0.13
		MAM	0.17	0.15	0.10	0.07
		JJA	0.33	0.21	0.12	0.07
		SON	0.42	0.38	0.27	0.13

In order to investigate oceanic and atmospheric factors that influence interannual VLS transport variability, we calculated correlations between the detrended 16 year interannual time series of VLS tracer transport efficiency (Figure S5) and the climate indices (Section 2.2) describing the state of the ocean in the release area (SST_{WIO}), the Indian monsoon strength (IMI), the state of the Indian Ocean Dipole (DMI) and the central Pacific ENSO conditions (SST_{Nino4}) (Table 5). We discuss only those relationships that show a significant correlation (bold face in Table 5).

The SST_{WIO} in the WIO release area shows a positive interannual correlation with transport efficiency in MAM for all tracers, in DJF and JJA for DMS and CH₃I and for DMS in the annual mean. These positive correlations infer that higher SST in the release area during the mentioned seasons is connected with enhanced transport to the stratosphere. Correlations between IMI and the transport efficiency are low and not significant. The interannual correlations between the DMI and transport efficiency are only significant in JJA for DMS and CH₃I. The SST_{Nino4} has the strongest relationship with transport efficiency of CH₂Br₂ and CHBr₃ from the WIO to the stratosphere during

boreal fall, when negative SST anomalies in the central equatorial Pacific relate to enhanced stratospheric entrainment. In MAM positive correlation coefficients hint at a relationship between positive SST anomalies in the Nino 4 region and enhanced stratospheric entrainment from the WIO.

Table 5: Correlations between the detrended interannual transport efficiency from the WIO to the stratosphere as annual and seasonal means and SST in the WIO (SST_{WIO}), the Indian Monsoon Index (IMI), the Dipole Mode Index (DMI), and SST in the Nino 4 region ($SST_{Nino\ 4}$). Bold numbers are significant at the 95% level.

		Annual mean	Seasonal means			
			DJF	MAM	JJA	SON
SST_{WIO}	DMS	0.55	0.66	0.85	0.53	0.39
	CH ₃ I	0.44	0.60	0.85	0.55	0.28
	CHBr ₃	0.14	0.43	0.71	0.48	0.08
	CH ₂ Br ₂	-0.02	0.16	0.52	0.38	0.06
IMI	DMS	-0.12	-0.05	-0.44	-0.06	-0.16
	CH ₃ I	0.06	-0.02	-0.42	0.00	-0.01
	CHBr ₃	0.44	0.02	-0.26	0.17	0.25
	CH ₂ Br ₂	0.41	-0.01	-0.11	0.23	0.44
DMI	DMS	0.29	0.36	-0.24	0.75	0.48
	CH ₃ I	0.26	0.38	-0.14	0.68	0.28
	CHBr ₃	0.08	0.34	-0.12	0.41	-0.08
	CH ₂ Br ₂	0.17	0.10	-0.14	0.18	-0.25
$SST_{Nino\ 4}$	DMS	0.47	0.32	0.69	0.08	-0.20
	CH ₃ I	0.21	0.27	0.64	-0.04	-0.39
	CHBr ₃	-0.18	0.12	0.49	-0.18	-0.67
	CH ₂ Br ₂	-0.34	-0.08	0.38	-0.21	-0.72

Based on these interannual correlations, we calculated SST and vertical velocity anomaly composite maps for the five years with maximum transport efficiency after detrending (Figure 23). The maximum transport efficiency years for each season are listed in Table S2. The composites show anomalies that lead to more transport from the WIO to the stratosphere during these seasons. The DJF composite for SST illustrates positive and negative SST anomalies in the Indian Ocean, but a maximum anomaly in the equatorial Pacific. Vertical velocities also show up and downward anomalies over the Indian Ocean but upward anomalies over the central equatorial Pacific. The MAM composites reveal enhanced SST and upward air motion over the Indian Ocean, resulting in the significant MAM-SST_{WIO} correlation for all tracers in Table 5. In the Pacific Ocean, the composite indicates positive SST anomalies along the equator, resembling the positive correlation with SST_{Nino 4} in MAM.

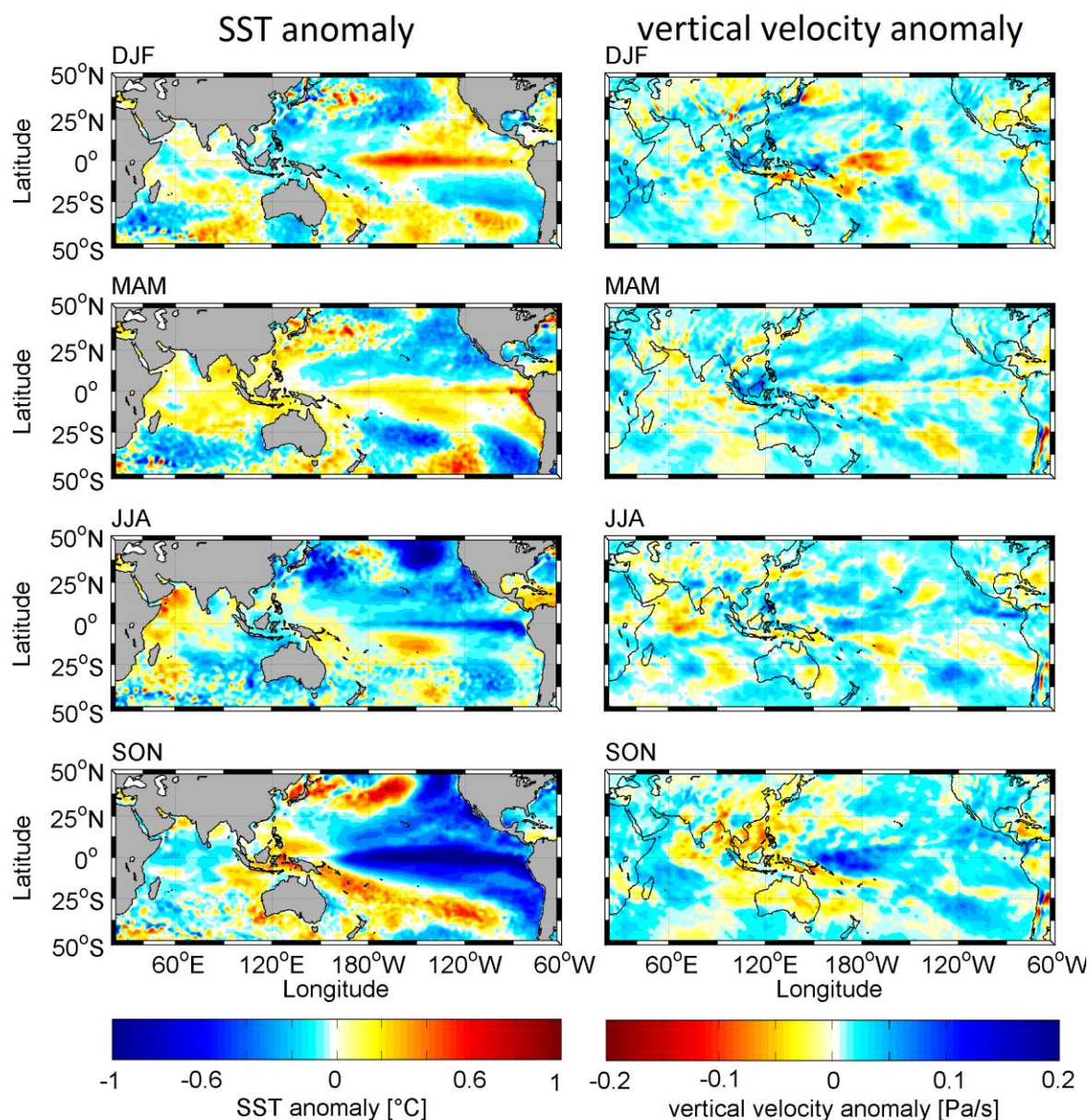


Figure 23: Composites of SST and vertical wind (at 200 hPa) anomaly for the detrended five maximum entrainment years (see Table S2) from ERA-Interim monthly means. Negative values of vertical velocities (in Pa/s) relate to enhanced uplift.

The JJA composites reflect the positive IOD pattern in the Indian Ocean, related to our positive correlation between DMI and transport efficiency for DMS and CH₃I. Vertical velocities show enhanced upward movement over the central Indian Ocean. In SON, the SST anomaly structure over the Indian Ocean is divided, with lower anomalies in the WIO and higher anomalies in the East Indian Ocean. The tropical and subtropical Pacific Ocean displays negative SST anomalies over a large region, reflecting the negative correlations of transport efficiency with SST_{Nino4} in Table 5. Vertical velocities in SON show enhanced uplift over the central tropical Indian Ocean, the Bay of Bengal,

Bangladesh, and the South China Sea. Overall, the derived maximum transport efficiency composites reflect the influence of ENSO events in particular for DJF and SON well (see Table S2).

4 Discussion

4.1 Annual Cycle

The transport of VSLs tracers from the WIO to the stratosphere experiences a distinct annual cycle modulated by the Indian monsoon winds, movement of convection connected with the ITCZ [Lawrence and Lelieveld, 2010; Schneider *et al.*, 2014], and the SST in the tropical WIO and Central Pacific Ocean (Figure 18). During boreal summer, the maximum density of transport at 8 km height (Figure 18a) occurs over southern India and the Bay of Bengal (10°N), farther south than the climatological position of the rainfall maximum. This can probably be explained by the center of our release area being located to the south of the equator. At 15 km height, the difference between the location of transport of DMS and CH₃I versus CHBr₃ and CH₂Br₂ (Figure 18b) in boreal summer can be related to their different lifetimes. The two shorter-lived tracers need very fast transport close to the release area to reach the stratosphere. The two longer-lived VSLs tracers survive long enough to be transported on a pathway farther to the north, with the Indian summer monsoon convection located over the Indian subcontinent. This transport pathway has been described previously by Fiehn *et al.* [2017] for 2014.

With the seasonal change of atmospheric circulation above the WIO, also the stratospheric entrainment regions change (Figure 19). For DMS and CH₃I, the main stratospheric entrainment region remains above the release area in the WIO all year, because these tracers' lifetimes are too short for long range horizontal transport and entrainment (Figures S2 and S3). The region of main entrainment of CHBr₃ and CH₂Br₂ tracers to the stratosphere (Figure 19 and S4) moves from the release area in DJF and MAM towards the Bay of Bengal, northern India and Southeast Asia in JJA and SON (Sect. 3). The convection over the Bay of Bengal, northern India and Bangladesh has previously been shown to be a major pathway from the Indian and Tibetan Plateau boundary layer to the stratosphere during boreal summer [Bergman *et al.*, 2013; Pan *et al.*, 2016]. Transport and stratospheric entrainment from the WIO with the summer monsoon circulation only play a role for VSLs with lifetimes on the order of CHBr₃ (17 days) or longer. Source regions closer to the monsoon convection, especially the Bay of Bengal,

would be more favored for fast delivery of DMS and CH₃I, but also CHBr₃ and CH₂Br₂, to the stratosphere during boreal summer.

The seasonal shift in tropospheric transport and stratospheric entrainment regions causes an annual cycle in the transport efficiency from the WIO to the stratosphere for all four VSLS tracers (Figure 20). The season of strongest stratospheric entrainment is boreal spring, because the strong vertical uplift is located directly above the WIO release area (Figure 18). Boreal summer and fall are the minimum transport seasons for all compounds, because the vertical uplift above the release area is weaker than during winter and spring. Furthermore, the fast vertical uplift of the Indian summer monsoon is farther away from the release area, causing longer transport pathways and more VSLS decay (Figure 18 and Figure 19). Our results are in contrast to two other studies investigating the annual cycle of VSLS transport from the boundary layer to the upper troposphere and lower stratosphere, which is probably due to differences in the models and tracer emission fields. *Liang et al.* [2014] derive the global atmospheric distribution of oceanic CHBr₃ and CH₂Br₂ using a chemistry climate model with top-down derived climatological emissions from the global ocean surface [*Liang et al.*, 2010]. They show seasonal maps of organic bromine (Br_y) and find a maximum at 355 K potential temperature (~14 km) above the tropical East Indian Ocean. This maximum is strongest for DJF and weakest for JJA, a seasonality, which is shifted by one season ahead of our results. They explain the seasonality with strong transport from the West Pacific boundary layer to the convective areas over the Indian Ocean in DJF. *Pan et al.* [2016], using a nudged Chemistry Climate Model, detect a maximum of a boundary layer tracer with a lifetime of 90 days in the Asian lower stratosphere from July to September due to monsoon vertical uplifting. This tracer is released globally and homogeneously, also close to the location of the Asian monsoon convection, and thus has an opposite annual cycle from our oceanic tracers with release regions farther away from the Asian summer monsoon convection.

The annual cycle of our transport efficiency can be related to the seasonality of SST in the WIO and the Indian monsoon circulation. This is supported by the significant positive correlation with the SST_{WIO} annual cycle without time lag and negative correlation with IMI and AIRI annual cycles with a time lag of only two months (Figure 21). *Chen et al.* [2012] diagnose Indian Ocean and West Pacific boundary layer to tropopause transport timescales for convective transport of 1-2 days. This relates to our SST_{WIO} annual cycle correlation without time lag and underlines that the SST in the WIO

has an immediate effect on the local convection and uplift and, thus, also the transport to the stratosphere. *Chen et al.* [2012] also find a large scale circulation transport timescale of 1-7 weeks, which fits the IMI/AIRI annual cycle correlation with a 2 month time lag. This time lag is caused by the time delay between the circulation change in the lower troposphere, where the indices are calculated, and the establishment of the transport pathway up to the stratosphere after the shift in the large scale atmospheric circulation pattern.

4.2 Interannual Variability and Long-Term Changes

The interannual variability is much smaller than the annual cycle (Sect. 3.2). Furthermore, the interannual variability for seasonal means is higher than for annual means, probably because temporal shifts in the pronounced annual cycle cause large variations from year to year (Table 4). An early onset or decline of the summer monsoon can cause transport shifts between the seasons, but the annual mean transport might remain the same.

Although *Hossaini et al.* [2016] did not find a global transport-driven long-term trend in stratospheric entrainment of VSLs bromine from 1993-2012, our transport efficiency shows a slight increase from 2000-2015 for all tracers and seasons (Figure 22). This is in agreement with *Tegtmeier et al.* [2015], who report overall no change for the updraught mass flux between 250 and 80 hPa of ERA-Interim data during 1979-2013, but an increase from 2000 onwards. Our time series is too short, however, to diagnose a trend, but detecting this for all seasons suggests a general circulation change in the Indian Ocean and Asian monsoon region during the 16-year time period. *Preethi et al.* [2016] detected a 2°-3° westward shift of the South Asian monsoon flow system between 1970 and 2015. This shift causes a weakening of the monsoon circulation over the Bay of Bengal, which would shorten the summer monsoon transport pathway and increase stratospheric entrainment of oceanic VSLs. Additionally, the increase in local WIO transport to the stratosphere diagnosed here could be caused by the fast warming of the tropical Indian Ocean [*Roxy et al.*, 2014] and subsequent enhancement of vertical uplift. In the future a continued trend of warming in the Indian Ocean could lead to increased vertical transport of VSLs source gases from the WIO to the stratosphere, according to the projected future increase of VSLs emissions [*Ziska et al.*, 2017], which may lead to more ozone depletion due to more direct VSLs source gas injections [*Tegtmeier et al.*, 2015].

The interannual variability of transport efficiency from the WIO to the stratosphere shows a strong relationship with tropical SST both in the Indian and in the Pacific Ocean (Table 5). The SST in the tropical WIO enhances the transport to the stratosphere for the shortest-lived tracers DMS and CH₃I during most seasons. For CHBr₃ and CH₂Br₂ the correlation is strongest in MAM, when the fast uplift is located over the equatorial WIO, but negligible in SON, when the main uplift of these tracers occurs above the Bay of Bengal far away from our WIO release region. The positive relationship between the local SST_{WIO} and transport efficiency reveals that the convective energy available from the warm ocean plays a role when the entrainment occurs directly above the release area. The positive DMI-transport efficiency correlation (impact of the IOD) for the two shortest-lived tracers in JJA supports this assumption, because a positive IOD also includes high SST anomalies in the WIO. Since DMS and CH₃I are not entrained via the Indian summer monsoon transport pathway (see Sect. 3.1 and *Fiehn et al.* [2017]) the local influence of the IOD on uplift plays a role.

In boreal spring, the SST_{Nino 4} in the equatorial central Pacific has a positive relationship with stratospheric entrainment suggesting that El Niño-like conditions enhance stratospheric entrainment from the WIO. Figure 24 depicts how El Niño events influence the SST and tropospheric vertical velocities above the Indian and Pacific Oceans through perturbations in the Walker circulation. SST warming in the central-to-east equatorial Pacific (El Niño) locally generates enhanced ascent of air, anomalous subsidence over the tropical East Indian and West Pacific Ocean, and enhanced uplift over the WIO [*Webster and Yang*, 1992; *Wang et al.*, 2001], which is the main entrainment region in boreal spring. Additionally, El Niño leads to a basin-wide warming of the Indian Ocean SST [*Ju and Slingo*, 1995; *Schott et al.*, 2009] and further enhanced uplift over the WIO [*Yu and Rienecker*, 1999; *Roxy et al.*, 2014]. In our study, El Niño conditions and a warm WIO surface increase the delivery of oceanic WIO VSL tracers to the stratosphere during boreal spring.

In boreal fall (SON), La Niña-like SST anomalies in the tropical central and East Pacific cause stronger than normal stratospheric entrainment over the East Indian Ocean (Table 5 and Figure 23). The main uplift and entrainment regions of sources from the WIO are above the central and northeast Indian Ocean (Figure 19) and La Niña-like SST anomalies in the east Pacific enhance upward movement in this region (Figure 24). Thus, La Niña events strengthen the monsoon convection and uplift over the Indian continent [*Wang et al.*, 2015]. The negative SST_{Nino 4} anomalies in boreal fall may extend the

summer monsoon season and its strong convection [Goswami and Xavier, 2005; Xavier *et al.*, 2007] bolstering and prolonging the established pathway by the Asian summer monsoon and enhancing stratospheric VSLs entrainment. This analysis highlights that the shift of stratospheric entrainment from the WIO in boreal spring to the central and northeast Indian Ocean in boreal fall causes opposing effects of El Niño and La Niña on transport efficiency during these seasons.

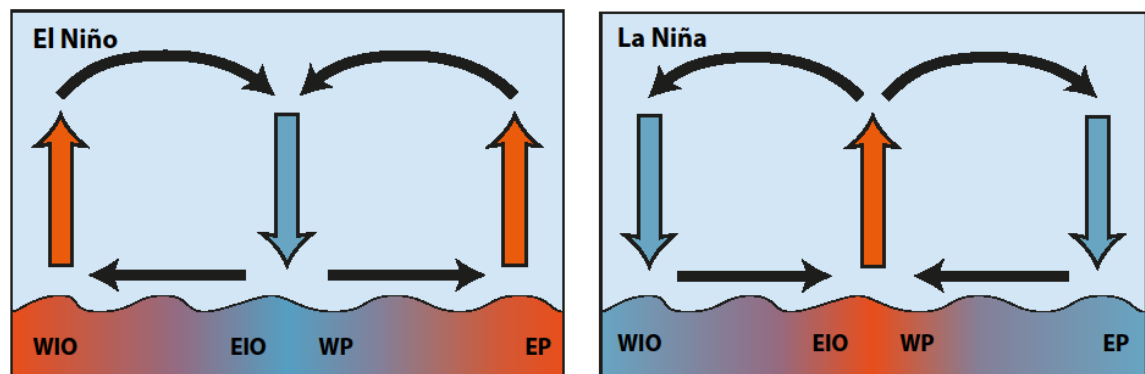


Figure 24: Schematic illustration of perturbations to the Walker circulation and tropical SST during El Niño and La Niña. Red stands for positive SST and vertical velocity anomalies, blue for negative anomalies. WIO: West Indian Ocean, EIO: East Indian Ocean, WP: West Pacific, EP: East Pacific.

4.3 Uncertainties

Our conclusions are subject to uncertainties resulting from the calculation and analysis of the trajectories and correlation methods used. The trajectory calculations depend on the Lagrangian model FLEXPART 9.2 and the reanalysis data ERA-Interim used to calculate the air mass transport. Convection generally takes place on scales smaller than the reanalysis model resolution. Therefore, FLEXPART uses a convection scheme to parameterize representative vertical displacement [Forster *et al.*, 2007]. Using also FLEXPART/ERA-Interim trajectory calculations, with observation based VSLs emissions, Tegtmeier *et al.* [2013] and Fuhlbrügge *et al.* [2016] were able to reproduce vertical VSLs distributions measured during several aircraft campaigns in the tropics, giving confidence in our approach.

The number of trajectories reaching the stratosphere depends on the definition of the boundary between troposphere and stratosphere. In the tropics, the cold point tropopause (CPT) is often used to describe this boundary [Carpenter *et al.*, 2014]. CPT

height lies around 17 km in the tropics and varies slightly with season and latitude [Munchak and Pan, 2014, and references therein]. During the OASIS campaign in the subtropical and tropical WIO, an average CPT height of 17 km was determined with daily several radiosonde launches [Fiehn *et al.*, 2017]. Here we use a static boundary of 17 km as a conservative estimate for the tropical tropopause. Upward trends in tropopause height [Seidel and Randel, 2006] could induce an increasing trend in stratospheric delivery of VSLS using a static boundary because a higher tropopause may lead to faster transport at a fixed height in the uppermost troposphere.

Our study is based on the homogeneous release of tracers from the ocean surface. In reality oceanic VSLS emissions exhibit both spatial and temporal variations [Lana *et al.*, 2011; Ziska *et al.*, 2013; Lennartz *et al.*, 2015]. Therefore our analysis only detects influences on the transport to the stratosphere but neglects influences on the strength of emissions or absolute delivery of VSLS to the stratosphere, which will be addressed in a follow-up study.

The deductions about the relationships between interannual variation of transport efficiency and SST in the Indian and Pacific Ocean depend on the considered time period. The 16 years time series is too short to detect significant long-term trends in the WIO transport to the stratosphere. However, this study is the longest transport time series calculated and analyzed for seasonal and interannual variability of Lagrangian transport from the WIO through the Asian Monsoon circulation to the stratosphere so far. The variability in conclusions on the development of transport to the stratosphere is large: Chen *et al.* [2012] calculated 9 years (2001-2009) of boreal summer air mass transport in the Asian monsoon region, but could not detect any significant correlations between boundary layer source variability and ENSO. Hossaini *et al.* [2016] did not find a transport-driven long-term trend in global stratospheric entrainment of bromine for the past period from 1993-2012, while Tegtmeier *et al.* [2015] suggest a future increase of the influence of CHBr₃ emissions on ozone depletion because of larger convective updraught mass flux in the upper troposphere and lower stratosphere. Since ENSO shows the strongest influence on transport efficiency from the WIO to the stratosphere, it is important to cover a period long enough to represent both ENSO phases well. Our chosen time period 2000-2016 is characterized by a clustering of La Niña events and a negative phase of the Pacific Decadal Oscillation (PDO) [Mantua and Hare, 2002]. The PDO has a very similar impact on the Indian summer monsoon rainfall to ENSO events, with a negative PDO phase related to an increase in summer monsoon rainfall and vice versa

[*Krishnan and Sugi, 2003*]. Thus, the reduced global climate variability due to the prevailing negative PDO phase might make it harder to find significant transport-climate variability relationships. A longer time series including more El Niño events and a positive PDO phase is needed for future studies.

5 Summary and Conclusions

A 16-year time series of transport from the tropical WIO to the stratosphere is analyzed using VSLS tracers with lifetimes corresponding to DMS (1 day), CH₃I (3.5 days), CHBr₃ (17 days), and CH₂Br₂ (150 days) applying homogenous oceanic sources. The transport efficiency, the amount of tracer entrained divided by the released amount, of all four VSLS tracers shows a distinct annual cycle with a maximum of entrainment in boreal spring and a minimum in boreal fall. This is caused by a seasonal change in the main transport pathway due to the reversal of lower tropospheric winds above the WIO connected to the Asian monsoon circulation. With the onset of the summer monsoon in May, the region of main upward transport of VSLS tracers moves from south of the equator to about 20°N. With the main vertical uplift, the main stratospheric entrainment region of the longer-lived VSLS tracer CHBr₃ and CH₂Br₂ shifts to the Bay of Bengal and northern India, elongating the transport pathway from the WIO to the stratosphere and causing a decrease in transport efficiency during boreal summer. The main entrainment of the shorter-lived tracers DMS and CH₃I remains over the tropical WIO, because their lifetimes are too short for entrainment through the summer monsoon circulation above northern India. Their transport efficiency also decreases in boreal summer due to weakened convection and vertical uplift above the WIO in comparison with spring. The annual cycle of stratospheric entrainment for DMS reveals the largest relative amplitude and CH₂Br₂ entrainment the smallest amplitude. This infers that the shorter the lifetime of a tracer, the stronger is the influence of the seasonal displacement of the main convection area and the strength of convection over the release area on stratospheric entrainment.

Over the 16 years of our time series from January 2000 to February 2016, we found an increase in VSLS tracer transport efficiency from the WIO to the stratosphere for all tracers and during all seasons, which may be related to the reported increasing SST in the WIO, a westward shift of the Asian monsoon circulation, and an upward trend in tropopause height. The interannual variability of transport efficiency is highest for the shortest-lived tracer, DMS. Regarding individual seasons, interannual variability for all

tracers is lowest during boreal spring, when the maximum transport occurs. The interannual variability of transport efficiency of all four VSLS tracers is influenced by the SST in the tropical WIO, as well as in the central equatorial Pacific. During boreal winter and spring, positive SST anomalies in the WIO and the Nino 4 region (El Niño) enhance stratospheric VSLS entrainment originating from the WIO. The warm Indian Ocean basin causes enhanced upward movement over the WIO, aiding the vertical transport to the stratosphere. During the summer monsoon, the transport of the two shortest-lived tracers for DMS and CH₃I is also influenced by high WIO SST anomalies and positive IOD events. In boreal fall, negative SST anomalies in the tropical Pacific (La Niña) cause stronger than normal stratospheric entrainment from the WIO through strengthening the monsoon flow from the Indian Ocean to the Indian subcontinent, and prolonging and bolstering the monsoon convection. A series of El Niño events may lead to more stratospheric entrainment above the WIO during boreal spring, while La Niña events enhance stratospheric entrainment of VSLS source gases above the central and northeast Indian Ocean during boreal fall.

In this study, we focus on variability and changes in the transport alone. Seasonal and interannual variability of oceanic emissions is not accounted for. In a follow-up study we will connect temporal and spatial variations in oceanic emissions from the whole Indian Ocean with the transport to the stratosphere to obtain a more holistic picture of stratospheric VSLS entrainment through the Asian monsoon circulation.

Acknowledgements and Data

This study was supported by BMBF grant SONNE-OASIS 03G0235A and the FP7 EU project StratoClim (603557). We thank the European Centre for Medium-Range Weather Forecasts (ECMWF) for the provision of ERA-Interim reanalysis data and the FLEXPART development team for the Lagrangian particle dispersion model used in this publication. Part of the FLEXPART simulations was performed on resources provided by UNINETT Sigma2 - the National Infrastructure for High Performance Computing and Data Storage in Norway and with support of the IT staff of University of Oslo. WCRP and University of Oslo's Industrial Liaison cooperation supported A. Fiehn's participation at the Training School on Monsoon Variability in a Changing Climate in January 2017. We thank Roxy Mathew Koll for the helpful advice on influences on Indian monsoon variability. We would like to thank Yoshiyuki Kajikawa and Bin Wang for updating the Indian Monsoon Index on their website. C. Marandino is funded by the Helmholtz Young Investigator Group TRASE-EC (VH-NG-819) at the GEOMAR Helmholtz Centre for Ocean Research Kiel.

The data used in this study can be obtained by inquiring to the authors directly. The authors declare that they have no conflict of interest.

References

- Arkin, P. A., and P. E. Ardanuy (1989), Estimating Climatic-Scale Precipitation from Space: A Review, *Journal of Climate*, 2(11), 1229-1238.
- Aschmann, J., B.-M. Sinnhuber, E. Atlas, and S. Schauffler (2009), Modeling the transport of very short-lived substances into the tropical upper troposphere and lower stratosphere, *Atmospheric Chemistry and Physics*, 9, 9237-9247.
- Barnes, I., J. Hjorth, and N. Mihalopoulos (2006), Dimethyl Sulfide and Dimethyl Sulfoxide and Their Oxidation in the Atmosphere, *Chemical Reviews*, 106(3), 940-975.
- Bergman, J. W., F. Fierli, E. J. Jensen, S. Honomichl, and L. L. Pan (2013), Boundary layer sources for the Asian anticyclone: Regional contributions to a vertical conduit, *Journal of Geophysical Research: Atmospheres*, 118(6), 2560-2575.
- Butler, J. H., D. B. King, J. M. Lobert, S. A. Montzka, S. A. Yvon-Lewis, B. D. Hall, N. J. Warwick, D. J. Mondeel, M. Aydin, and J. W. Elkins (2007), Oceanic distributions and emissions of short-lived halocarbons, *Global Biogeochemical Cycles*, 21(1), GB1023.
- Carpenter, L. J., W. T. Sturges, S. A. Penkett, P. S. Liss, B. Alicke, K. Hebestreit, and U. Platt (1999), Short-lived alkyl iodides and bromides at Mace Head, Ireland: Links to biogenic sources and halogen oxide production, *Journal of Geophysical Research: Atmospheres*, 104(D1), 1679-1689.
- Carpenter, L. J., S. Reimann, J. B. Burkholder, C. Clerbaux, B. D. Hall, R. Hossaini, J. C. Laube, and S. A. Yvon-Lewis (2014), Ozone-Depleting Substances (ODSs) and other gases of interest to the Montreal Protocol, in *Scientific Assessment of Ozone Depletion: 2014. Global Ozone Research and monitoring Project - Report N. 55*, edited, World Meteorological Organization, Geneva, Switzerland.
- Chen, B., X. Xu, S. Yang, and T. Zhao (2012), Climatological perspectives of air transport from atmospheric boundary layer to tropopause layer over Asian monsoon regions during boreal summer inferred from Lagrangian approach, *Atmospheric Chemistry and Physics*, 12(13), 5827-5839.
- Dee, D. P., et al. (2011), The ERA-Interim reanalysis: configuration and performance of the data assimilation system, *Quarterly Journal of the Royal Meteorological Society*, 137(656), 553-597.
- Ding, Y. (2007), The Variability of the Asian Summer Monsoon, *Journal of the Meteorological Society of Japan. Ser. II*, 85B, 21-54.
- Dvortsov, V. L., M. A. Geller, S. Solomon, S. M. Schauffler, E. L. Atlas, and D. R. Blake (1999), Rethinking reactive halogen budgets in the midlatitude lower stratosphere, *Geophysical Research Letters*, 26(12), 1699-1702.
- Fiehn, A., B. Quack, H. Hepach, S. Fuhlbrügge, S. Tegtmeier, M. Toohey, E. Atlas, and K. Krüger (2017), Delivery of halogenated very short-lived substances from the West Indian Ocean to the stratosphere during Asian summer monsoon, *Atmos. Chem. Phys. Discuss.*, 2017, 1-40.
- Forster, C., A. Stohl, and P. Seibert (2007), Parameterization of convective transport in a Lagrangian particle dispersion model and its evaluation, *Journal of Applied Meteorology and Climatology*, 46(4), 403-422.
- Fueglistaler, S., M. Bonazzola, P. H. Haynes, and T. Peter (2005), Stratospheric water vapor predicted from the Lagrangian temperature history of air entering the stratosphere in the tropics, *Journal of Geophysical Research: Atmospheres*, 110, D08107.
- Fuhlbrügge, S., B. Quack, S. Tegtmeier, E. Atlas, H. Hepach, Q. Shi, S. Raimund, and K. Krüger (2016), The contribution of oceanic halocarbons to marine and free tropospheric air over the tropical West Pacific, *Atmospheric Chemistry and Physics*, 16(12), 7569-7585.
- Goswami, B. N., and P. K. Xavier (2005), ENSO control on the south Asian monsoon through the length of the rainy season, *Geophysical Research Letters*, 32, L18717.
- Hense, I., and B. Quack (2009), Modelling the vertical distribution of bromoform in the upper water column of the tropical Atlantic Ocean, *Biogeosciences*, 6(4), 535-544.

- Hepach, H., B. Quack, F. Ziska, S. Fuhlbrügge, E. Atlas, K. Krüger, I. Peeken, and D. W. R. Wallace (2014), Drivers of diel and regional variations of halocarbon emissions from the tropical North East Atlantic, *Atmospheric Chemistry and Physics*, *14*(3), 1255-1275.
- Hossaini, R., M. P. Chipperfield, B. M. Monge-Sanz, N. A. D. Richards, E. Atlas, and D. R. Blake (2010), Bromoform and dibromomethane in the tropics: a 3-D model study of chemistry and transport, *Atmospheric Chemistry and Physics*, *10*, 719-735.
- Hossaini, R., et al. (2016), A multi-model intercomparison of halogenated very short-lived substances (TransCom-VSLS): linking oceanic emissions and tropospheric transport for a reconciled estimate of the stratospheric source gas injection of bromine, *Atmospheric Chemistry and Physics*, *16*(14), 9163-9187.
- Ju, J., and J. Slingo (1995), The Asian summer monsoon and ENSO, *Quarterly Journal of the Royal Meteorological Society*, *121*(525), 1133-1168.
- Kerkweg, A., P. Jöckel, N. Warwick, S. Gebhardt, C. A. M. Brenninkmeijer, and J. Lelieveld (2008), Consistent simulation of bromine chemistry from the marine boundary layer to the stratosphere – Part 2: Bromocarbons, *Atmos. Chem. Phys.*, *8*(19), 5919-5939.
- Kloster, S., J. Feichter, E. Maier-Reimer, K. Six, P. Stier, and P. Wetzel (2006), DMS cycle in the marine ocean-atmosphere system—a global model study, *Biogeosciences*, *3*, 29-51.
- Krishnan, R., and M. Sugi (2003), Pacific decadal oscillation and variability of the Indian summer monsoon rainfall, *Climate Dynamics*, *21*(3), 233-242.
- Krüger, K., S. Tegtmeier, and M. Rex (2008), Long-term climatology of air mass transport through the Tropical Tropopause Layer (TTL) during NH winter, *Atmospheric Chemistry and Physics*, *8*, 813–823.
- Krüger, K., S. Tegtmeier, and M. Rex (2009), Variability of residence time in the Tropical Tropopause Layer during Northern Hemisphere winter, *Atmospheric Chemistry and Physics*, *9*, 6717–6725.
- Kumar, K. K., B. Rajagopalan, M. Hoerling, G. Bates, and M. Cane (2006), Unraveling the Mystery of Indian Monsoon Failure During El Niño, *Science*, *314*(5796), 115-119.
- Lana, A., et al. (2011), An updated climatology of surface dimethylsulfide concentrations and emission fluxes in the global ocean, *Global Biogeochemical Cycles*, *25*, GB1004.
- Law, K. S., et al. (2006), Halogenated Very Short-Lived Substances, in *Scientific Assessment of Ozone Depletion: 2006. Global Ozone Research and Monitoring Project - Report N. 50*, edited, World Meteorological Organization, Geneva, Switzerland.
- Lawrence, M. G., and J. Lelieveld (2010), Atmospheric pollutant outflow from southern Asia: a review, *Atmospheric Chemistry and Physics*, *10*(4), 9463-9646.
- Lennartz, S. T., et al. (2015), Modelling marine emissions and atmospheric distributions of halocarbons and dimethyl sulfide: the influence of prescribed water concentration vs. prescribed emissions, *Atmospheric Chemistry and Physics*, *15*(20), 11753-11772.
- Liang, Q., E. Atlas, D. R. Blake, M. Dorf, K. Pfeilsticker, and S. Schauffler (2014), Convective transport of very short lived bromocarbons to the stratosphere, *Atmospheric Chemistry and Physics*, *14*(11), 5781-5792.
- Liang, Q., R. S. Stolarski, S. R. Kawa, J. E. Nielsen, A. R. Douglass, J. M. Rodriguez, D. R. Blake, E. Atlas, and L. E. Orr (2010), Finding the missing stratospheric Bry: a global modeling study of CHBr₃ and CH₂Br₂, *Atmospheric Chemistry and Physics*, 2269-2286.
- Mantua, N. J., and S. R. Hare (2002), The Pacific Decadal Oscillation, *Journal of Oceanography*, *58*(1), 35-44.
- Marandino, C. A., S. Tegtmeier, K. Krüger, C. Zindler, E. L. Atlas, F. Moore, and H. W. Bange (2013), Dimethylsulphide (DMS) emissions from the western Pacific Ocean: a potential marine source for stratospheric sulphur?, *Atmospheric Chemistry and Physics*, *13*(16), 8427-8437.
- Mihalopoulos, N., B. C. Nguyen, J. P. Putaud, and S. Belviso (1992), The oceanic source of carbonyl sulfide (COS), *Atmospheric Environment. Part A. General Topics*, *26*(8), 1383-1394.
- Miles, C. J., T. G. Bell, and P. Suntharalingam (2012), Investigating the inter-relationships between water attenuated irradiance, primary production and DMS(P), *Biogeochemistry*, *110*(1), 201-213.

- Moore, R. M., and O. C. Zafiriou (1994), Photochemical production of methyl iodide in seawater, *Journal of Geophysical Research: Atmospheres*, 99(D8), 16415-16420.
- Munchak, L. A., and L. L. Pan (2014), Separation of the lapse rate and the cold point tropopauses in the tropics and the resulting impact on cloud top-tropopause relationships, *Journal of Geophysical Research: Atmospheres*, 119(13), 7963-7978.
- Myhre, G., T. F. Berglen, C. E. L. Myhre, and I. S. A. Isaksen (2004), The radiative effect of the anthropogenic influence on the stratospheric sulfate aerosol layer, *Tellus B*, 56(3), 294-299.
- Newell, R. E., and S. Gould-Stewart (1981), A Stratospheric Fountain?, *Journal of the Atmospheric Sciences*, 38(12), 2789-2796.
- Nielsen, J. E. D., A.R. (2001), A simulation of bromoform's contribution to stratospheric bromine.
- Orbe, C., D. W. Waugh, and P. A. Newman (2015), Air-mass origin in the tropical lower stratosphere: The influence of Asian boundary layer air, *Geophysical Research Letters*, 42(10), 4240-4248.
- Ordóñez, C., J. F. Lamarque, S. Tilmes, D. E. Kinnison, E. L. Atlas, D. R. Blake, G. Sousa Santos, G. Brasseur, and A. Saiz-Lopez (2012), Bromine and iodine chemistry in a global chemistry-climate model: description and evaluation of very short-lived oceanic sources, *Atmospheric Chemistry and Physics*, 12(3), 1423-1447.
- Osthoff, H. D., et al. (2009), Regional variation of the dimethyl sulfide oxidation mechanism in the summertime marine boundary layer in the Gulf of Maine, *Journal of Geophysical Research: Atmospheres*, 114, D07301.
- Palmer, C. J., and C. J. Reason (2009), Relationships of surface bromoform concentrations with mixed layer depth and salinity in the tropical oceans, *Global Biogeochemical Cycles*, 23(2), GB2014.
- Pan, L. L., S. B. Honomichl, D. E. Kinnison, M. Abalos, W. J. Randel, J. W. Bergman, and J. Bian (2016), Transport of chemical tracers from the boundary layer to stratosphere associated with the dynamics of the Asian summer monsoon, *Journal of Geophysical Research: Atmospheres*, 121(23), 14,159-114,174.
- Park, M., W. J. Randel, L. K. Emmons, and N. J. Livesey (2009), Transport pathways of carbon monoxide in the Asian summer monsoon diagnosed from Model of Ozone and Related Tracers (MOZART), *Journal of Geophysical Research: Atmospheres*, 114, D08303.
- Pearson, K. (1895), Note on Regression and Inheritance in the Case of Two Parents, *Proceedings of the Royal Society of London*, 58, 240-242.
- Preethi, B., M. Mujumdar, R. H. Kripalani, A. Prabhu, and R. Krishnan (2016), Recent trends and tele-connections among South and East Asian summer monsoons in a warming environment, *Climate Dynamics*, 48(7), 2489-2505.
- Quack, B., and D. W. R. Wallace (2003), Air-sea flux of bromoform: Controls, rates, and implications, *Global Biogeochemical Cycles*, 17(1), 1023.
- Randel, W. J., M. Park, L. Emmons, D. Kinnison, P. Bernath, K. A. Walker, C. Boone, and H. Pumphrey (2010), Asian monsoon transport of pollution to the stratosphere, *Science*, 328(5978), 611-613.
- Roxy, M. K., K. Ritika, P. Terray, and S. Masson (2014), The Curious Case of Indian Ocean Warming, *Journal of Climate*, 27(22), 8501-8509.
- Roxy, M. K., K. Ritika, P. Terray, R. Murtugudde, K. Ashok, and B. N. Goswami (2015), Drying of Indian subcontinent by rapid Indian Ocean warming and a weakening land-sea thermal gradient, *Nature Communications*, 6, 7423.
- Roxy, M. K., A. Modi, R. Murtugudde, V. Valsala, S. Panickal, S. Prasanna Kumar, M. Ravichandran, M. Vichi, and M. Lévy (2016), A reduction in marine primary productivity driven by rapid warming over the tropical Indian Ocean, *Geophysical Research Letters*, 43(2), 826-833.
- Saji, N. H., B. N. Goswami, P. N. Vinayachandran, and T. Yamagata (1999), A dipole mode in the tropical Indian Ocean, *Nature*, 401(6751), 360-363.
- Schneider, T., T. Bischoff, and G. H. Haug (2014), Migrations and dynamics of the intertropical convergence zone, *Nature*, 513(7516), 45-53.

- Schott, F. A., S.-P. Xie, and J. P. McCreary (2009), Indian Ocean circulation and climate variability, *Reviews of Geophysics*, 47(1), RG1002.
- Seidel, D. J., and W. J. Randel (2006), Variability and trends in the global tropopause estimated from radiosonde data, *Journal of Geophysical Research: Atmospheres*, 111, D21101.
- Sheng, J.-X., D. K. Weisenstein, B.-P. Luo, E. Rozanov, A. Stenke, J. Anet, H. Bingemer, and T. Peter (2015), Global atmospheric sulfur budget under volcanically quiescent conditions: Aerosol-chemistry-climate model predictions and validation, *Journal of Geophysical Research: Atmospheres*, 120(1), 256-276.
- Smythe-Wright, D., S. M. Boswell, C. H. Lucas, A. L. New, and M. S. Varney (2005), Halocarbon and dimethyl sulphide studies around the Mascarene Plateau, *Philosophical transactions. Series A, Mathematical, physical, and engineering sciences*, 363(1826), 169-185.
- Solomon, S., R. R. Garcia, and A. R. Ravishankara (1994), On the role of iodine in ozone depletion, *Journal of Geophysical Research: Atmospheres*, 99(D10), 20491-20499.
- Solomon, S., J. S. Daniel, R. R. Neely, J. P. Vernier, E. G. Dutton, and L. W. Thomason (2011), The Persistently Variable “Background” Stratospheric Aerosol Layer and Global Climate Change, *Science*, 333(6044), 866.
- Stefels, J. (2000), Physiological aspects of the production and conversion of DMSP in marine algae and higher plants, *Journal of Sea Research*, 43(3), 183-197.
- Stemmler, I., I. Hense, and B. Quack (2015), Marine sources of bromoform in the global open ocean - global patterns and emissions, *Biogeosciences*, 12(6), 1967-1981.
- Stohl, A., and D. Thomson (1999), A density correction for Lagrangian particle dispersion models, *Boundary-Layer Meteorology*, 90(1), 155-167.
- Stohl, A., C. Forster, A. Frank, P. Seibert, and G. Wotawa (2005), Technical note: The Lagrangian particle dispersion model FLEXPART version 6.2, *Atmospheric Chemistry and Physics*, 5, 2461-2474.
- Tegtmeier, S., F. Ziska, I. Pisso, B. Quack, G. J. M. Velders, X. Yang, and K. Krüger (2015), Oceanic bromoform emissions weighted by their ozone depletion potential, *Atmos. Chem. Phys.*, 15(23), 13647-13663.
- Tegtmeier, S., et al. (2013), The contribution of oceanic methyl iodide to stratospheric iodine, *Atmospheric Chemistry and Physics*, 13(23), 11869-11886.
- Vogel, B., G. Günther, R. Müller, J. U. Grooß, and M. Riese (2015), Impact of different Asian source regions on the composition of the Asian monsoon anticyclone and on the extratropical lowermost stratosphere, *Atmospheric Chemistry and Physics*, 15(7), 13699-13716.
- Walker, G. T. (1924), Correlation in seasonal variations of weather, IX. A further study of world weather, *Memoirs of the India Meteorological Department*, 24(0), 275-333.
- Wang, B., and Z. Fan (1999), Choice of South Asian Summer Monsoon Indices, *Bulletin of the American Meteorological Society*, 80(4), 629-638.
- Wang, B., R. Wu, and K. M. Lau (2001), Interannual Variability of the Asian Summer Monsoon: Contrasts between the Indian and the Western North Pacific–East Asian Monsoons, *Journal of Climate*, 14(20), 4073-4090.
- Wang, B., J.-Y. Lee, and B. Xiang (2015), Asian summer monsoon rainfall predictability: a predictable mode analysis, *Climate Dynamics*, 44(1), 61-74.
- Warwick, N. J., J. A. Pyle, G. D. Carver, X. Yang, N. H. Savage, F. M. O'Connor, and R. A. Cox (2006), Global modeling of biogenic bromocarbons, *Journal of Geophysical Research: Atmospheres*, 111(D24), D24305.
- Webster, P. J., and S. Yang (1992), Monsoon and Enso: Selectively Interactive Systems, *Quarterly Journal of the Royal Meteorological Society*, 118(507), 877-926.
- WMO (2014), World Meteorological Organization, Global Ozone Research and Monitoring Project-Report No. 55, Scientific Assessment of Ozone Depletion: 2014, *Rep.*, 416 pp, World Meteorological Organization, Geneva, Switzerland.
- Xavier, P. K., C. Marzin, and B. N. Goswami (2007), An objective definition of the Indian summer monsoon season and a new perspective on the ENSO–monsoon relationship, *Quarterly Journal of the Royal Meteorological Society*, 133(624), 749-764.

- Yu, L., and M. M. Rienecker (1999), Mechanisms for the Indian Ocean warming during the 1997–98 El Niño, *Geophysical Research Letters*, 26(6), 735-738.
- Ziska, F., B. Quack, S. Tegtmeier, I. Stemmler, and K. Krüger (2017), Future emissions of marine halogenated very-short lived substances under climate change, *Journal of Atmospheric Chemistry*, 74(2), 245-260.
- Ziska, F., et al. (2013), Global sea-to-air flux climatology for bromoform, dibromomethane and methyl iodide, *Atmospheric Chemistry and Physics*, 13(17), 8915-8934.



Journal of Geophysical Research

Supporting Information for

Variability of VSLs transport from the West Indian Ocean to the stratosphere

Alina Fiehn^{1,2}, Birgit Quack², Christa Marandino², Kirstin Krüger¹

¹ Meteorology and Oceanography Section, Department of Geosciences, University of Oslo, Oslo, Norway

² GEOMAR Helmholtz Centre for Ocean Research Kiel, Kiel, Germany

Corresponding author: Kirstin Krüger (kkrueger@geo.uio.no)

Contents of this file

Text S1

Table S1 to S2

Figures S1 to S5

Introduction

The supporting information contains the download web addresses for the climate indices used in the publication. Supporting information on the increase of transport efficiency from Section 3.3 is shown in Table S1. The supporting figures (S1-S5) include a latitudinal view of FLEXPART trajectories mentioned in Section 3.1 of the main publication, stratospheric entrainment regions for DMS, CH₃I and CH₂Br₂ similar to Figure 4, and the detrended interannual time series of transport efficiency.

Text S1: Download addresses of the climate indices:

IMI: <http://apdrc.soest.hawaii.edu/projects/monsoon/seasonal-monidx.html>

AIRI: http://www.tropmet.res.in/static_page.php?page_id=53

DMI: <http://stateoftheocean.osmc.noaa.gov/sur/ind/dmi.php>

Table S1: Increase of transport efficiency from the West Indian Ocean to the stratosphere during 2000-2015 (in % per decade) for annual and seasonal means. Bold numbers mark significant trends at 95% level.

	Annual mean	DJF	MAM	JJA	SON
DMS	0.01	0.01	0.00	0.00	0.01
CH ₃ I	0.01	0.01	0.01	0.01	0.02
CHBr ₃	0.04	0.07	0.03	0.03	0.05
CH ₂ Br ₂	0.08	0.10	0.07	0.06	0.08

Table S2: The five maximum transport efficiency years after detrending from Figure S5 used for the composites in Figure 8 in the main text. ENSO events based on the Ocean Niño Index from NCEP/CPC are highlighted with red for El Niño and blue for La Niña; note that “DJF 2002” stands for D2002-JF2003 ff.

	1	2	3	4	5
DJF	2002	2003	2009	2011	2015
MAM	2001	2003	2005	2010	2012
JJA	2003	2006	2007	2010	2012
SON	2000	2001	2007	2010	2011

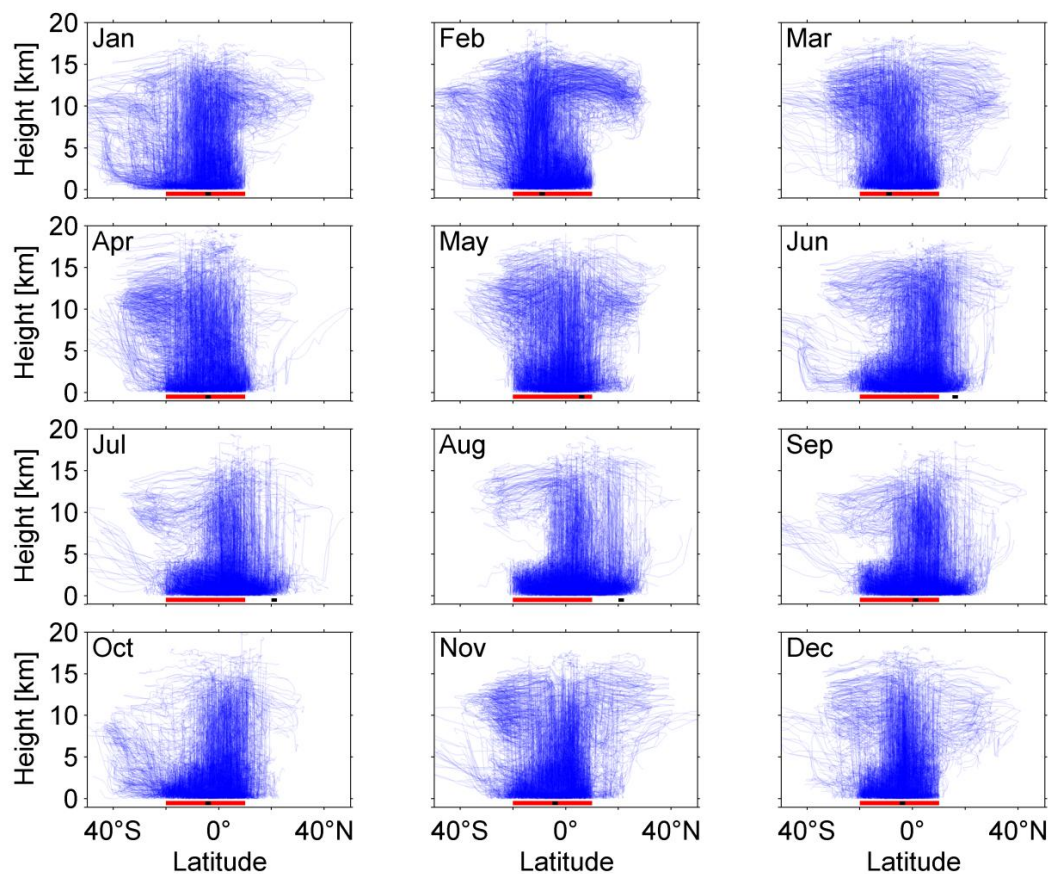


Figure S25: Latitude-height cross sections of ten day forward trajectories from the WIO release region (red) during 2014 and climatological position of ITCZ in the Indian monsoon region (black square) from 1998-2012 taken from Schneider et al. [2014].

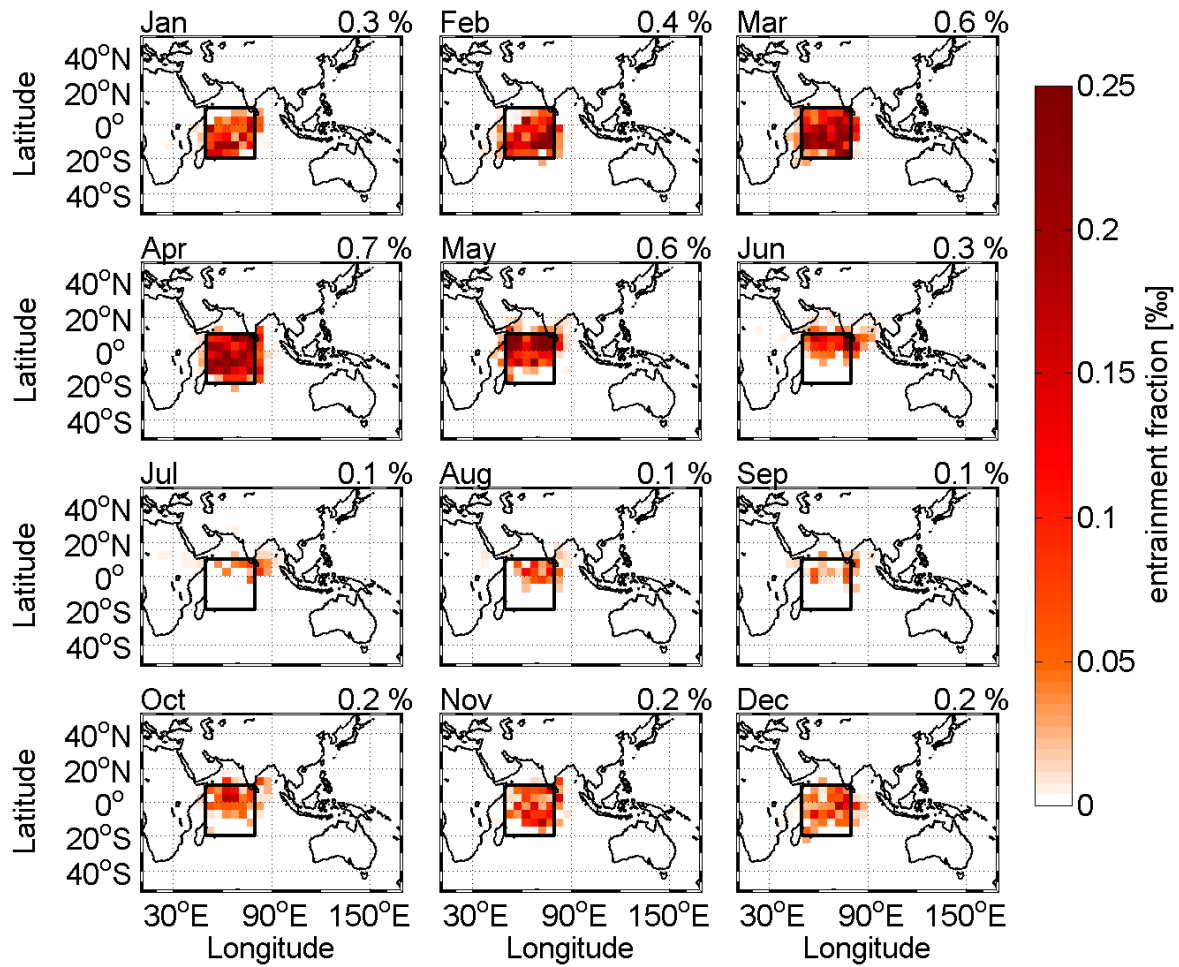


Figure S26: Stratospheric entrainment regions for DMS tracer released in 2014 shown as fraction of released tracer (in %) entrained in a 5°x5° grid. The black box shows the WIO release area. The transport efficiency (t_e), noted on the upper right, is the fraction of released tracer (in %) reaching 17 km over the whole area.

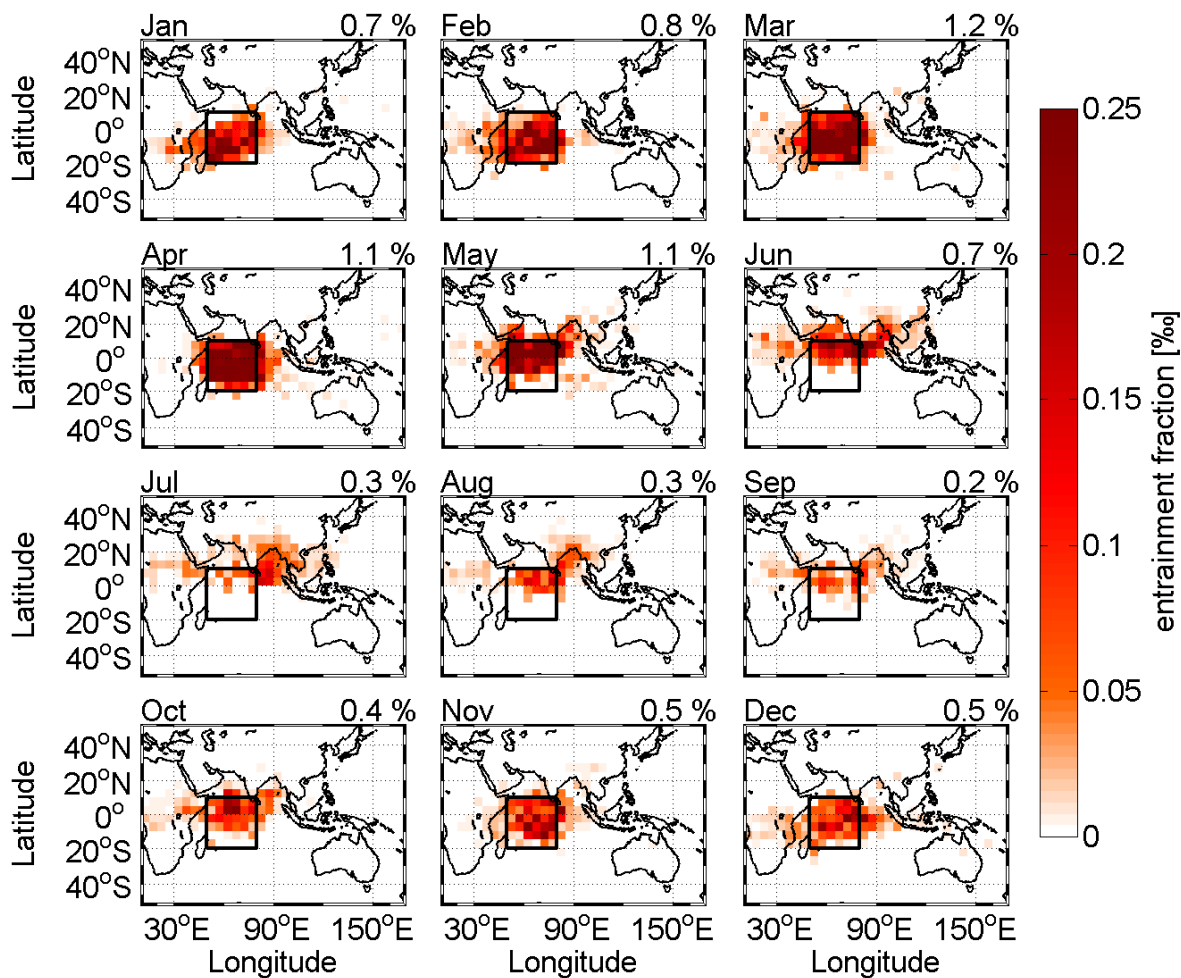


Figure S27: As Figure S2 for the CH₃I tracer.

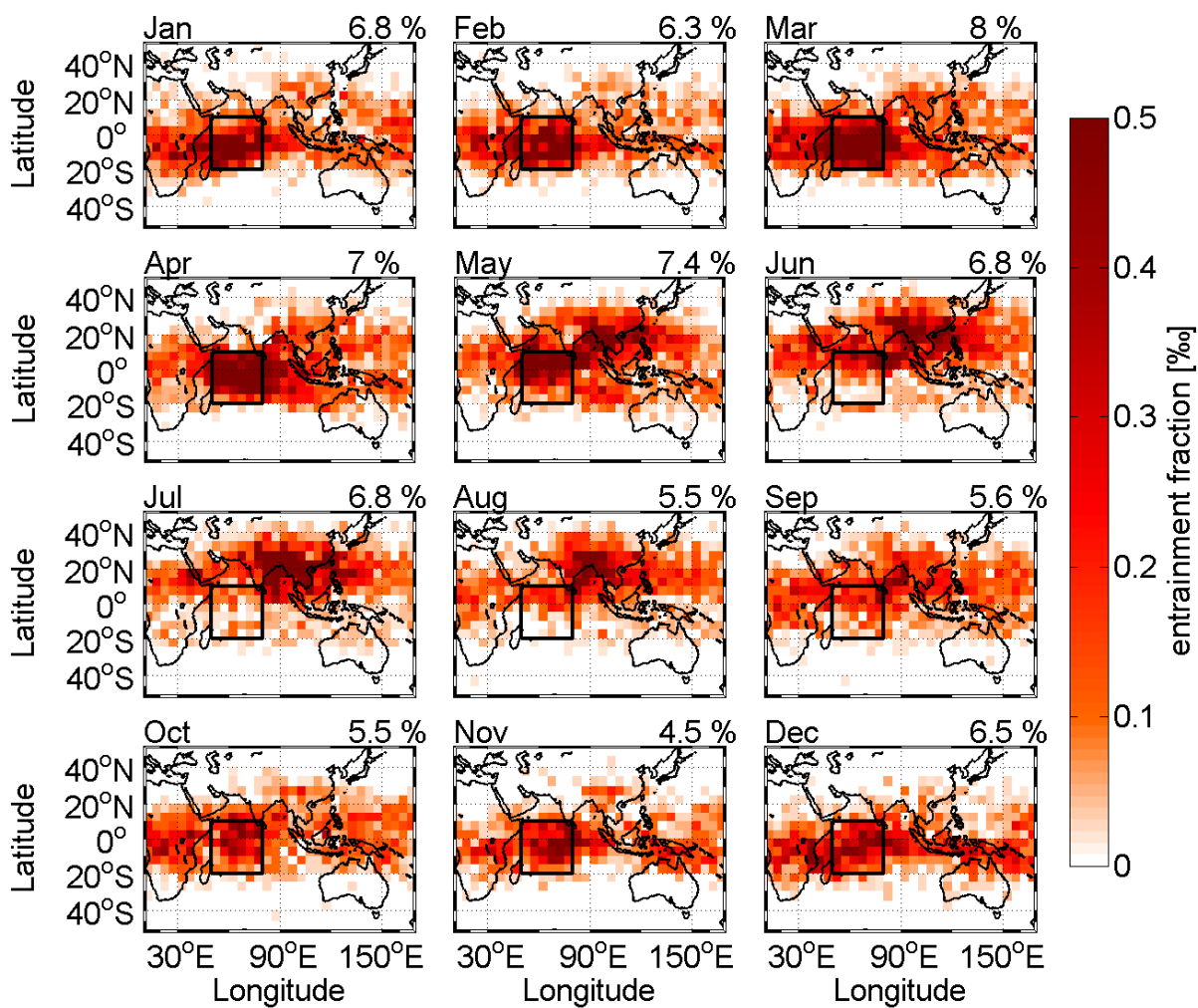


Figure S28: As Figure S2 for the CH_2Br_2 tracer.

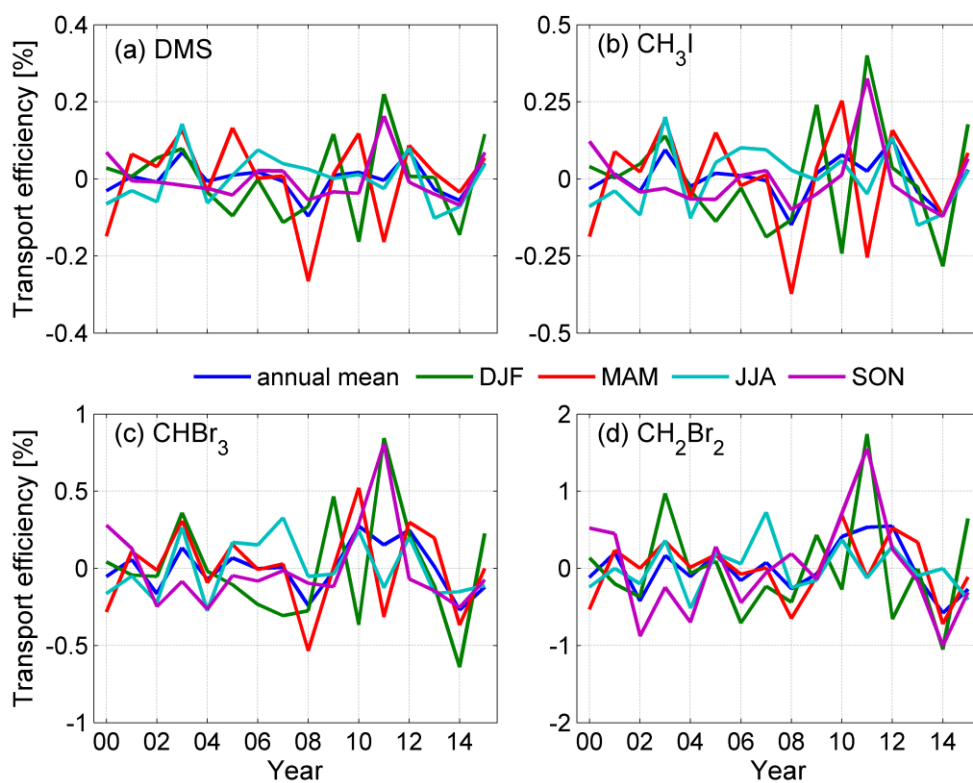


Figure S29: Detrended interannual time series of the annual and seasonal mean anomalies of transport efficiency of VSL tracers from the West Indian Ocean to the stratosphere.

References

Schneider, T., T. Bischoff, and G. H. Haug (2014), Migrations and dynamics of the intertropical convergence zone, *Nature*, 513(7516), 45-53.

3.4 Manuscript 4

Fiehn, A.; Quack, B.; Stemmler, I.; Ziska, F.; and Krüger, K.: Influence of seasonally resolved emissions on the transport of bromoform from the Indian Ocean to the stratosphere, in preparation for Atmos. Chem. Phys. Diss..

Importance of seasonally resolved oceanic emissions for VSLs delivery from the Indian Ocean to the stratosphere

Alina Fiehn^{1,2}, Birgit Quack², Irene Stemmler³, Franziska Ziska^{2,*}, Kirstin Krüger¹

¹ *Meteorology and Oceanography Section, Department of Geosciences, University of Oslo, Oslo, Norway*

² *GEOMAR Helmholtz Centre for Ocean Research Kiel, Kiel, Germany*

³ *Max Planck Institute for Meteorology, Hamburg, Germany*

**now at: Deutscher Wetterdienst, Hamburg, Germany*

Alina Fiehn: alina.fiehn@geo.uio.no

Birgit Quack: bquack@geomar.de

Irene Stemmler: irene.stemmler@mpimet.mpg.de

Franziska Ziska: fziska@geomar.de

Kirstin Krüger: kkrueger@geo.uio.no (corresponding author)

Abstract

Oceanic very short-lived substances (VSLs), such as bromoform (CHBr_3), contribute to stratospheric halogen loading and, thus, to ozone depletion. However, the amount, timing, and region of bromine delivery to the stratosphere through one of the main entrance gates, the Asian monsoon circulation, are still uncertain. In this study, we created bromoform emission inventories in the tropical Indian and west Pacific Oceans based on new in situ bromoform measurements and novel ocean biogeochemistry modeling with annual and monthly resolutions. Using these emissions, the mass transport and atmospheric mixing ratios of bromoform were modeled with the particle dispersion model FLEXPART driven by ERA-Interim reanalysis. Using monthly resolved emissions, main oceanic source regions for the stratosphere include the tropical west Pacific Ocean in boreal winter and the Arabian Sea and Bay of Bengal in boreal summer. The main stratospheric entrainment occurs over the southern tip of India, associated with local oceanic sources and strong convection of the Indian summer monsoon. The use of different temporal resolutions of emissions leads to changes in the season with maximum atmospheric mixing ratios at the tropopause: Monthly emissions result in highest mixing ratios above the central Indian Ocean in boreal winter and within the Asian monsoon anticyclone in boreal summer, while annual emissions display a maximum above the west Indian Ocean in boreal spring. However, the total annual entrainment of bromoform to the tropical stratosphere is the same in our Lagrangian calculations whether using monthly or annual emissions. Our results underline that the seasonal and regional stratospheric bromine loading for the Indian Ocean region critically depends on the seasonality in the VSLs emissions.

1 Introduction

Halogenated very short-lived substances (VSLS) contribute to the stratospheric halogen burden, take part in ozone depletion and, thus, impact climate (Law et al., 2006). They are of oceanic origin and their transport to the stratosphere depends on deep convection in the tropics. The contribution of oceanic VSLS is estimated to be 10-40 % of the ~20 ppt total stratospheric bromine (Carpenter et al., 2014). Uncertainties result mainly from the tropospheric degradation and removal, transport processes, and especially from the spatial and temporal variability of halogenated VSLS emissions (Carpenter et al., 2014; Hossaini et al., 2016). In this study, we focus on the influence of seasonal variations of emissions.

Bromoform (CHBr_3), next to dibromomethane (CH_2Br_2), is the largest contributor to bromine from VSLS ($\text{Br}_y^{\text{VSLS}}$) in the stratosphere (Hossaini et al., 2012) due to its large oceanic emissions (Quack and Wallace, 2003), moderate lifetime of 15-17 days in the tropics (Carpenter et al., 2014), and because it contains three bromine atoms. The bromoform surface concentration in the ocean is spatially and temporally variable and depends on its chemical and biological production (Carpenter et al., 1999; Quack and Wallace, 2003). Enhanced emissions coincide with biologically active equatorial and coastal upwelling regions (Quack et al., 2007) and the distribution of macro algae and anthropogenic sources along the coasts (Carpenter and Liss, 2000; Quack and Wallace, 2003). There have been different approaches in creating global bromoform emission inventories. As a bottom-up approach, emissions have been extrapolated from marine and atmospheric observations (Quack and Wallace, 2003; Butler et al., 2007; Palmer and Reason, 2009; Ziska et al., 2013) or surface water observations with a chemistry climate model coupled to an air-sea exchange module (Lennartz et al., 2015). The top-down approach uses chemistry climate models (Warwick et al., 2006; Liang et al., 2010), also in combination with biological activity in the ocean (Ordóñez et al., 2012), to infer possible emission distributions that reproduce observed atmospheric abundances of VSLS. Recently, a biogeochemical model inferred oceanic bromoform distributions and emissions from observational atmospheric data and assumptions on the marine production (Hense and Quack, 2009; Stemmler et al., 2015).

Overall, large differences between bromoform emissions exist. The bottom-up emission inventories (Ziska et al., 2013; Stemmler et al., 2015) estimate lower global bromoform emissions than the top-down inventories (Warwick et al., 2006; Liang et al., 2010; Ordóñez et al., 2012). The emission inventories of Warwick et al. (2006), Liang et

al. (2010), Ordóñez et al. (2012), and Ziska et al. (2013) have been compared and evaluated by Hossaini et al. (2013). The observation based bromoform emissions of Ziska et al. (2013) led to the best agreement with atmospheric measurements of atmospheric mixing ratios in the tropics. Some emission inventories contain climatological annual means (Warwick et al., 2006; Liang et al., 2010) and other inventories include a seasonality of emissions (Ordóñez et al., 2012; Ziska et al., 2013; Stemmler et al., 2015). The use of these inventories in atmospheric modeling is described later.

In the atmosphere VLS are defined as having a lifetime of less than half a year. They degrade through photolysis or reaction with the hydroxyl radical (OH) into soluble substances, which can then be washed out. The injection of oceanic VLS source gases to the stratosphere implies fast transport, because the degradation occurs on the same timescales as the transport. Thus, stratospheric delivery of VLS is connected to fast and high-reaching convection and ascent of air masses through the tropical tropopause layer (TTL) into the stratosphere (Gettelman et al., 2009). The main regions of entrainment of tropospheric air masses into the stratosphere lie over the west Pacific Ocean in boreal winter and the Indian monsoon region in boreal summer (Newell and Gould-Stewart, 1981).

The Pacific Ocean VLS emissions, atmospheric mixing ratios, and transport to the stratosphere has been measured and modeled in various studies (Tegtmeier et al., 2012; Tegtmeier et al., 2013; Hossaini et al., 2016; and data listed therein), but the Indian Ocean emissions and their contribution to stratospheric bromine are still very uncertain (Liang et al., 2014). The Indian Ocean emissions could be quite high based on the few measurements in the marginal seas (Yamamoto et al., 2001; Roy et al., 2011), as well as extrapolations from other oceans (Ziska et al., 2013) and top-down source estimates (Liang et al., 2010). They have the potential to significantly contribute to stratospheric bromine (Liang et al., 2014; Hossaini et al., 2016). Based on first measurements of enhanced surface concentrations of bromoform and CH_2Br_2 from the subtropical and tropical west Indian Ocean in 2014, (Fiehn et al., 2017) calculated strong emissions and diagnosed stratospheric entrainment of these two VLS in the southeastern part of the Asian monsoon anticyclone in July and August 2014 with the FLEXPART model. VLS tracers with different lifetimes reveal a strong seasonality in the transport strength from the tropical west Indian Ocean to the stratosphere, with maximum transport in boreal spring, when the main uplift occurs over the release area (Fiehn et al., under review).

The atmospheric distribution and the delivery of bromoform to the stratosphere have been the topic of several chemistry transport and climate modeling studies. These studies used different approaches to constrain the input of VSLs from the ocean to the atmosphere: fixed VSLs mixing ratios in the boundary layer (Hossaini et al., 2010; Hossaini et al., 2012) or at the convective detrainment location (Aschmann et al., 2011; Aschmann and Sinnhuber, 2013), prescribed emissions as homogeneous fields (Dvortsov et al., 1999; Nielsen, 2001) or one of the inventories described above (Warwick et al., 2006; Hossaini et al., 2013; Liang et al., 2014; Tegtmeier et al., 2015; Hossaini et al., 2016), or prescribed water concentrations and the online calculation of emissions (Lennartz et al., 2015). Only Lennartz et al. (2015), Tegtmeier et al. (2015), and Hossaini et al. (2016) included seasonally varying emissions in their models.

The necessity or influences of the implementation of seasonally varying emissions is not clear yet. The seasonality of surface mixing ratios is influenced by the varying emissions as well as chemical degradation and transport processes. Liang et al. (2010) could reproduce the seasonality of atmospheric bromoform mixing ratios in the lower troposphere using annual mean emissions, because the seasonality was mainly determined by chemical loss and tropospheric transport. On the other hand, Lennartz et al. (2015) were not able to match the observed seasonality in atmospheric bromoform mixing ratios at all stations, even with seasonally varying emissions.

Furthermore, the studies show a disagreement on the main stratospheric entrainment season and location over the Asian continent and Indian Ocean area. Liang et al. (2014) modeled the highest upper tropospheric mixing ratios above the Indian Ocean during boreal winter based on the emission estimate by Liang et al. (2010). Calculating ozone depletion potential (ODP)-weighted emissions of bromoform, Tegtmeier et al. (2015) used monthly emissions from Ziska et al. (2013) and inferred maximum ODP-weighted emissions from the Indian Ocean during boreal summer. Hossaini et al. (2016) conducted a multi-model intercomparison study using different emission inventories and chemistry transport and chemistry climate models and compared with measurements to infer inter-model differences due to emissions and transport processes. The model intercomparison study uses three different emission inventories (Liang et al., 2010; Ordóñez et al., 2012; Ziska et al., 2013) of which only one (Ordóñez et al., 2012) was used with seasonality. The models agree on the seasonality of volume mixing ratio (VMR) at the cold point tropopause (CPT), but the absolute values vary within a factor of three. The locations of the VMR maxima at the CPT above the tropical west Pacific in DJF and

the northern Indian Ocean in JJA are model consistent, but model differences in the strength of the Asian monsoon signature are high and strongly dependent on the parameterization of mixing in the boundary layer and convection in the free troposphere (Hossaini et al., 2016). They detect no differences caused by the seasonality in the Ordóñez et al. (2012) emissions. The influence of seasonally varying emissions on the seasonality at the CPT and the impact of the Asian monsoon transport has not been investigated. The combination of detailed marine emissions and high resolution atmospheric transport will help to answer the question of where and when the main marine bromine delivery to the stratosphere occurs.

In this study, we investigate the influence of seasonally varying bromoform emissions for the Indian and west Pacific Ocean on the stratospheric entrainment of bromoform and mixing ratios in the TTL. Our research questions for this study are: What is the influence of seasonal bromoform emissions on stratospheric entrainment through the Asian Monsoon? Which is the main stratospheric entrainment region and season for bromoform above the Indian Ocean? What is the difference between using annual or monthly emissions?

In Sect. 2, we describe the bromoform emission scenarios that we applied in our transport simulations and the FLEXPART model set up. In Sect. 3, we present and discuss the created emission inventories Ziska Updated and Stemmler Scaled for annual and monthly emission scenarios (Sect. 3.1). We compare the model simulations with available observations (Sect. 3.2) and describe the delivery of bromoform from its oceanic source regions to the stratosphere (Sect. 3.3). In Sect. 3.4 and 3.5, we analyze the differences between stratospheric entrainment using annual and monthly emissions and discuss these. Uncertainties in our studies are addressed in Sect. 4 and Sect. 5 contains the conclusions.

2 Data and Methods

2.1 Emission inventories

We created two bromoform emission inventories for the Indian Ocean and the west Pacific in 2014 from existing publications. The emission inventories are based on the publications from Ziska et al. (2013) and Stemmler et al. (2015) and have annual and monthly resolution of emissions. An overview is given in Table 6. These will be used in FLEXPART to determine the transport of bromoform from the Indian Ocean to the

stratosphere in 2014, which is the year of the west Indian Ocean measurement data from the OASIS cruise on RV Sonne in July and August 2014 (Fiehn et al., 2017).

Table 6: Emission inventories (header) and scenarios (first column) used in this study.

	Ziska Updated	Stemmler Scaled
Annual emissions	x	x
Monthly emissions	x	x

The calculation is based on oceanic concentrations and atmospheric mixing ratios of bromoform. We calculated monthly emission fields for 2014 using the parameterization of air-sea gas exchange by Nightingale et al. (2000). Details of the calculation are given by Fiehn et al. (2017). We used ERA-Interim $1^\circ \times 1^\circ$ monthly mean 10 m wind speed, sea level pressure and sea surface temperature fields. The climatological annual mean sea surface salinity field was taken from the World Ocean Atlas 2009. From these monthly emission fields we also created an annual mean emission field with the same total annual emissions as the monthly fields.

As a first inventory, the Ziska et al. (2013) inventory was updated with new oceanic and atmospheric measurements. This emission inventory will be called *Ziska Updated* in the following. The Ziska et al. (2013) emission inventory is a data-based global sea-to-air flux estimate of bromoform, dibromomethane and methyl iodide, calculated from oceanic and atmospheric surface concentrations within the Halocarbons in the Ocean and Atmosphere (HalOcAt) database. The available surface data was classified as coastal, shelf or open ocean data. The open ocean data was further divided into 21 regions according to the physical and geochemical characteristics of ocean and atmosphere. Data points were interpolated on a $1^\circ \times 1^\circ$ grid and extrapolated within the regions using longitude and latitude regressions. The most relevant addition for this study are observations in the west Indian Ocean in July and August 2014 (Fiehn et al., 2017), which are the first measurements in the tropical Indian Ocean. The original Ziska climatology was based on measurements from other ocean basins (Ziska et al., 2013). The global fields of bromoform oceanic concentration and atmospheric mixing ratios were updated using the same method as in Ziska et al. (2013) creating annual mean climatological fields.

As a second emission inventory, we scaled the bromoform emission fields that Stemmler et al. (2015) calculated with a biogeochemical ocean model. This emission inventory will be called *Stemmler Scaled* in the following. Stemmler et al. (2015) used a global three-dimensional ocean biogeochemistry model (MPIOM-HAMOCC) to simulate bromoform cycling in the ocean and emission to the atmosphere. They used the Ziska et al. (2013) atmospheric concentration as upper boundary for their air-sea flux calculations. In general, the Stemmler et al. (2015) oceanic concentrations and air-sea fluxes were lower than previous estimates. The low emissions might be caused by the use of the fixed atmospheric mixing ratios, which might not be consistent with the state of the ocean and atmosphere and have been shown to generally decrease bromoform emissions (Lennartz et al., 2015). In this study, we scaled the oceanic bromoform concentrations of the Stemmler et al. (2015) Dia experiment, which showed the most realistic emission distribution, according to oceanic measurements from the OASIS cruise in the Indian Ocean (Fiehn et al., 2017) and the TransBrom transit across the west Pacific Ocean (Krüger and Quack, 2013). For every measurement point of bromoform concentration in the ocean during these campaigns, the model concentration in that grid box during the respective months was selected and a scaling factor was calculated, to obtain the measured value order to match the observations. The average scaling factor of 3.48 was homogeneously applied to the modeled sea surface bromoform concentrations of Stemmler et al. (2015). For our Stemmler Scaled inventory, we use a constant atmospheric bromoform mixing ratio of 1 ppt, which is the average atmospheric mixing ratio of bromoform from the OASIS and TransBrom campaigns.

For this study we only consider air-sea fluxes from the Indian Ocean and west Pacific (IO/WP). We define a release area in this region from 30°N - 30°S and 30°E - 160°E, which we use for the calculation of annual fields and for the particle releases in the FLEXPART simulations (Sect. 2.2).

2.2 FLEXPART calculations

For our transport calculations, we use the Lagrangian particle dispersion model Flexpart of the Norwegian Institute for Air Research in the Atmosphere and Climate Department (Stohl et al., 2005), which has been evaluated in previous studies (Stohl et al., 1998; Stohl and Trickl, 1999). The model includes moist convection and turbulence parameterizations in the atmospheric boundary layer and free troposphere (Stohl and Thomson, 1999; Forster et al., 2007). In this study, we employ version 9.2 of Flexpart. This version has

been modified to incorporate lifetime profiles for the decay of transported VSLS. We use the ECMWF reanalysis product ERA-Interim (Dee et al., 2011) with a horizontal resolution of $1^\circ \times 1^\circ$ and 60 vertical model levels as meteorological input fields, providing air temperature, winds, boundary layer height, specific humidity, as well as convective and large scale precipitation with a 3-hourly temporal resolution. The vertical winds in hybrid coordinates were calculated mass-consistently from spectral data by the pre-processor (Stohl et al., 2005). We record the transport model output every 12 hours.

We ran the Flexpart model using the annual emission field and monthly emission fields for each of the Ziska Updated and Stemmler Scaled scenarios described above. According to these emission scenarios, we calculated the mass of bromoform released from each $1^\circ \times 1^\circ$ grid cell during one day. We released one particle per day and grid cell from the IO/WP release area ($30^\circ\text{N} - 30^\circ\text{S}$, $30^\circ\text{E} - 160^\circ\text{E}$) with the released mass attached. The exponential decay is realized through the application of the lifetime profile of bromoform from Hossaini et al. (2010). For stratospheric entrainment we consider particles that reach above the CPT. The CPT is calculated online based on the ERA-Interim data. The seasonal mean CPT height is displayed in Fig. S1. We define the stratospheric *transport efficiency* as the mass of bromoform entrained to the stratosphere divided by the emitted mass. FLEXPART also provides the VMR of bromoform. The displayed monthly fields are an average of the 12 hourly output fields. We only calculate source gas injection and not the absolute delivery of $\text{Br}_y^{\text{VSLS}}$ from bromoform to the stratosphere.

3 Results and Discussion

3.1 Bromoform emissions from the Indian Ocean/ West Pacific

The 2014 annual mean bromoform air-sea flux maps for the Ziska Updated and the Stemmler Scaled emission inventories in the IO/WP release area are shown in Figure 30. These emission distributions are used in the annual emission scenario in FLEXPART. The Stemmler Scaled bromoform emission inventory shows emission hot spots at the Horn of Africa ($2000 \text{ pmol m}^{-2} \text{ h}^{-1}$), south of the Oman coast ($1700 \text{ pmol m}^{-2} \text{ h}^{-1}$), and in the Torres Strait north of the Cape York Peninsula of Australia (up to $5000 \text{ pmol m}^{-2} \text{ h}^{-1}$). The Ziska Updated bromoform emission inventory features high emissions along the northern hemispheric coastlines ($1500\text{-}3000 \text{ pmol m}^{-2} \text{ h}^{-1}$) and in the central Bay of Bengal (up to $5000 \text{ pmol m}^{-2} \text{ h}^{-1}$). An area of high emissions is the southern tropical IO

(1000 pmol m⁻² h⁻¹), while the flux from the northern tropical WP is negative, meaning that the ocean takes up bromoform from the atmosphere. This is caused by the low oceanic production and the cold water, which can take up more gas from the atmosphere (Krüger and Quack, 2013). The two emission inventories are similar in their main emission regions, the Arabian Sea and the Bay of Bengal, but show two significant differences: The coastal emissions and the tropical northern WP emissions. The bromoform module implemented into HAMOCC (Stemmler et al., 2015) does not account for bromoform production by macro algae and anthropogenic influences near the coastline. Therefore, near the coast the Stemmler Scaled emissions are much lower than the Ziska Updated emission, which uses separate regions for coast and shelf areas. The second difference concerns the air-sea fluxes in the west Pacific Ocean. While Stemmler Scaled emissions are small, but positive, in the west Pacific, the Ziska Updated includes negative fluxes north of 20°N and in some other parts of the WP.

The seasonal mean emission fields show the intraannual variability of bromoform emissions (Fig. 1). Emissions are high in boreal fall (December-February, DJF) and summer (June-August, JJA) and lower in boreal spring (March-May, MAM) and fall (September-November, SON) for both inventories. For the Stemmler Scaled inventory, strong emissions in JJA are located in the Arabian Sea, Bay of Bengal, the equatorial and tropical southern Indian Ocean, and a hot spot north of Australia. This hot spot results from the high phytoplankton productivity in the biogeochemical model (Stemmler et al., 2015). High emissions of Ziska Updated are concentrated along the northern Indian Ocean coastline, the central Bay of Bengal and the tropical southern Indian Ocean.

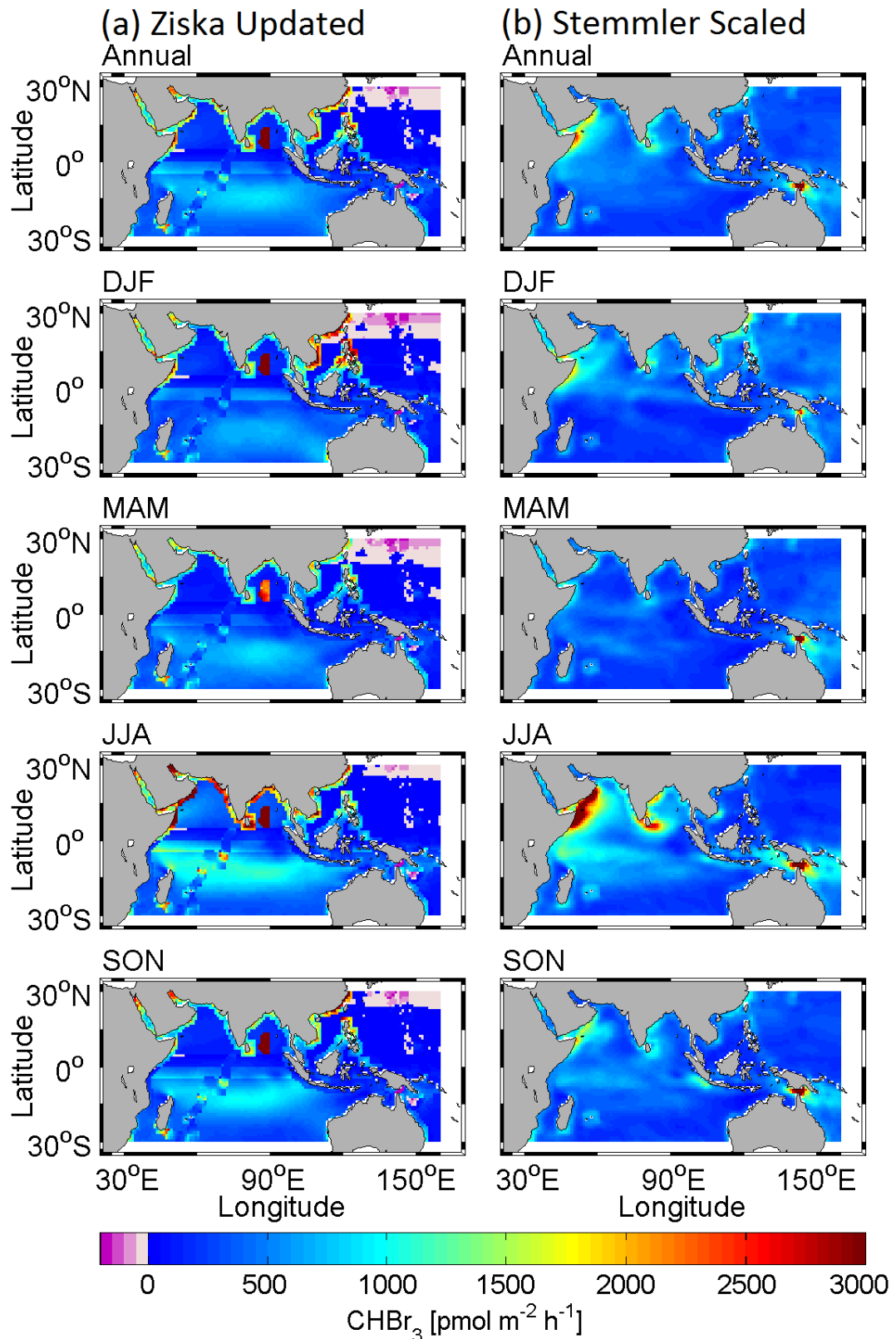


Figure 30: Annual and seasonal mean bromoform emissions from the Indian Ocean and west Pacific release area based on the inventories Ziska Updated (a) and Stemmler Scaled (b).

We compare the annual mean emissions of the two created emission inventories with their progenitors and two top-down inventories (Table 7). In Ziska Updated, the emission distribution has changed compared to Ziska et al. (2013), while the Stemmler Scaled bromoform emission inventory mainly differs from Stemmler et al. (2015) in the total amount of bromoform emitted. The Ziska Updated inventory incorporates new measurements in the west Indian Ocean compared to Ziska et al. (2013). Overall, the Ziska annual bromoform emission from the IO/WP increased from $670 \text{ Mmol Br yr}^{-1}$ (Ziska et al., 2013, OLS) to $750 \text{ Mmol Br yr}^{-1}$ (Ziska Updated). The Stemmler Scaled emissions from the IO/WP release area are $760 \text{ Mmol Br yr}^{-1}$, while Stemmler et al. (2015) modeled only $43 \text{ Mmol Br yr}^{-1}$. The distribution has mainly remained the same for this inventory. Slight differences in emission distribution result from the applied homogenous atmospheric mixing ratios and the ERA-Interim meteorological fields instead of the NCEP data used in Stemmler et al. (2015). The Ziska Updated and Stemmler Scaled inventories show similarities in the IO/WP region with previously published top-down bromoform emission inventories of Liang et al. (2010) and Ordóñez et al. (2012). Comparing spatial features, all six inventories display high emissions in the tropics, while Liang et al. (2010) have the highest open ocean emissions incorporating a large area in the tropics. The emission strength for coastal and open ocean emissions from the Indian Ocean for the annual mean of six emission inventories is given in Table 7. The coastal emissions are similar for all inventories, except Stemmler et al. (2015) which is much lower, due to the lack of coastal macroalgal production. The high emissions along the coast of Somalia and the Oman in the Stemmler Scaled inventory are caused by high wind speeds during boreal summer and coastal upwelling, entailing bromoform production (Figure 30).

The annual cycles of emission for Ziska Updated and Stemmler Scaled are very similar with a maximum in July and a secondary maximum in January and minima in April and November (Fig. 2). While the Ziska Updated inventory applies mean annual oceanic concentrations, the Stemmler Scaled inventory uses monthly concentrations tied to phytoplankton production (Stemmler et al., 2015). Both scenarios show the highest emissions in summer, which has the highest wind speed, an important driver of air-sea gas exchange besides the oceanic concentration. We calculated the correlation between the annual cycles of emission from the IO/WP release area with each of the other variables (Table 3). Strongest correlations of the emission cycle exist with the wind speed and the SST. The correlation between emissions and oceanic concentrations for Stemmler

Scaled are weak. Thus the annual cycle of emissions in the Indian Ocean is mainly driven by the wind speed, which varies strongly over the year changing between the weak northeast (winter) and strong southwest (summer) monsoon winds.

Table 7: Coastal and open Indian Ocean emissions for different bromoform emission inventories.

Inventory	Coastal emissions pmol m ⁻² h ⁻¹	Open Indian Ocean emissions pmol m ⁻² h ⁻¹
Liang et al. (2010)	1500	150 – 1100
Ordóñez et al. (2012)	~ 950	~350
Stemmler et al. (2015)	0 – 300	0 – 130
Ziska et al. (2013)	500 – 3000	-300 – 800
Ziska Updated (this study)	300 – 2500	-300 – 800
Stemmler Scaled (this study)	300 – 2300	200 – 800

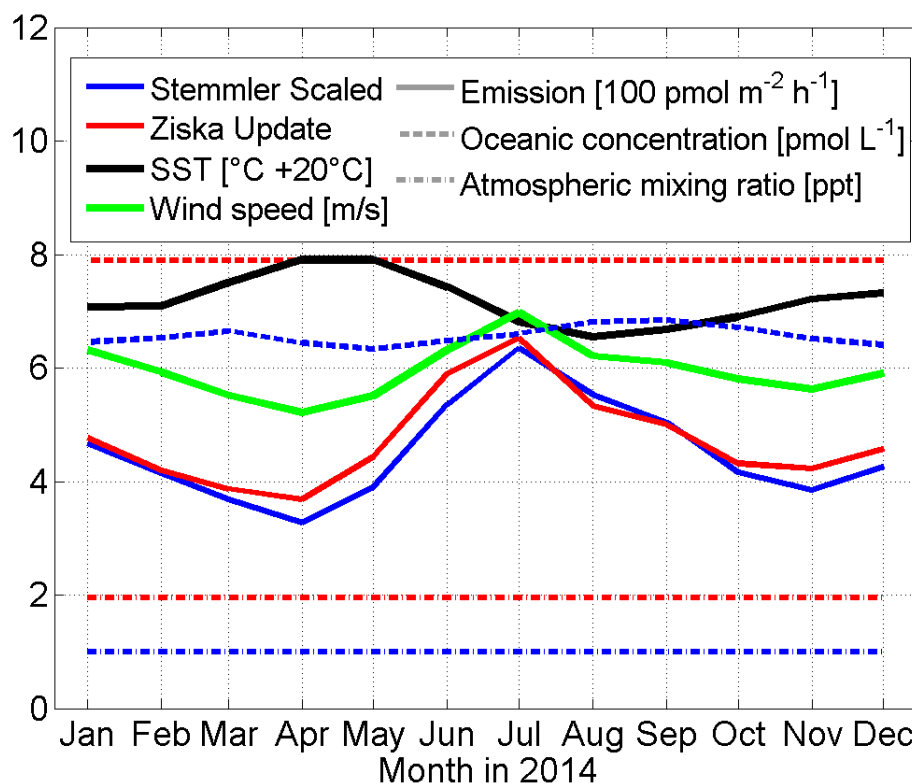


Figure 31: Annual cycle of average emission, surface water concentration, and atmospheric mixing ratio of bromoform, as well as wind speed and SST, in the IO/WP release area in 2014 for the two inventories.

Table 8: Correlation between the annual cycle of emission and surface water concentration, wind speed and SST from Figure 31 using Spearman rank correlation.

Variable	Stemmler Scaled	Ziska Updated
Surface water concentration	0.36	-
Wind speed	0.92	0.86
SST	-0.71	-0.55

3.2 Comparison with observations

To validate our FLEXPART/ERA-Interim calculations, we compare the modeled VMR with observations from available ship and aircraft campaigns. A comparison of modeled and observed VMR may also determine which sources the different emission inventories account for and where sources might be missing or have been overestimated. In the

boundary layer, we compare the modeled VMR with the tropical ship cruise observations from OASIS in the west Indian Ocean (Fiehn et al., 2017), SHIVA in the South China and Sulu Seas (Fuhlbrügge et al., 2016), and TransBrom across the west Pacific (Krüger and Quack, 2013; Fiehn et al., 2017). In the free troposphere, we compare modeled VMR with observations from the CARIBIC aircraft observatory at around 11 km height (Wisher et al., 2014) and average tropical profiles modeled by Liang et al. (2014).

In the atmospheric boundary layer, which extends from the surface to about 1 km, the VMR mainly reflects the emission hotspots. For both emission inventories, the modeled VMR at 1 km height are highest above the Indian Ocean (Fig. S2). Beside their different coastal/open ocean distribution of emissions, they display the same hotspots in JJA and SON in the Arabian Sea and the Bay of Bengal, caused by high emissions in these basins during the summer monsoon season due to high wind speeds.

The mean VMR values and their standard deviation for the three research cruises are summed up in Table 9. A scatter plot of the monthly emission scenario VMR comparison is displayed in the supplement (Fig. S3). Note that we modeled the VMR for 2014, and thus higher deviations are expected for SHIVA (2011) and TransBrom (2009) than for OASIS (2014). We sample the model during the month of the cruise and around the location of the measurement. As expected, the modeled VMR are lower than the measurements, due to the model set up of including the IO/WP only. Thus, very likely important sources from the central Pacific are missing (see Fig. 7 in Liang et al., 2014). In the Indian Ocean, the Ziska Updated inventory is closer to observations than the Stemmler Scaled inventory, probably because the OASIS cruise data was included directly into the Ziska Updated inventory. In the South China Sea, emissions from both inventories are similar, but far lower than the coastal SHIVA cruise observations, probably because of underestimation of coastal emissions in both inventories (Table 9). In the West Pacific, the Stemmler Scaled inventory has a smaller deviation from the observations than the Ziska Updated, because of the low emissions during TransBrom included in Ziska Updated, while Stemmler Updated has higher emissions from the open West Pacific Ocean. This comparison reveals that, especially in boreal summer, the monthly emissions are necessary to account for the measured VMR above the Indian Ocean. It also hints at missing coastal emissions and an uncertainty in the West Pacific emissions.

Table 9: Mean bromoform volume mixing ratios (VMR) observed during the research cruises and modeled with FLEXPART at 100 m height for the same location and month as the observation, but for the year 2014.

VMR [ppt]		West Pacific		South China Sea	Indian Ocean
	Emission inventory	Emission scenario	Oct	Nov	July
Observation		in situ	0.92*	2.02 ^Δ	1.18 [°]
Modeled for 2014	Ziska Updated	annual	0.12	0.52	0.72
		monthly	0.10	0.41	1.01
for 2014	Stemmler Scaled	annual	0.35	0.44	0.44
		monthly	0.30	0.35	0.63

* TransBrom 2008 , ^Δ SHIVA 2010 (Fuhlbrügge et al., 2016), [°] OASIS 2014 (Fiehn et al., 2017)

For comparison with aircraft observations, there are a few measurements available from the CARIBIC observatory at around 11 km altitude between November 2012 and February 2013 (Wisher et al., 2014). The range and latitudinal gradient of FLEXPART VMR compare well with the aircraft measurements made between 15°N and 30°N (Fig. S4). At low latitudes and farthest north our simulation delivers less bromoform into the South Asian region than observed. We suspect the reason for this to be the missing oceanic emissions from the central and east Pacific west of 160°E. The assumption is supported by the fact that at low latitudes mixing ratios calculated with Ziska Updated are lower than those calculated with Stemmler Scaled and so are the emissions from the west Pacific for this inventory.

The modeled annual mean mixing ratio profiles of bromoform up to 20 km height are largest over the Indian Ocean and lowest over the West Pacific (Figure 32a). Although mixing ratios are highest above the Indian Ocean, the above comparison with CARIBIC showed that also here contributions from the central Pacific are important. Thus, the missing emissions from the central and East Pacific result in low modeled VMR in the West Pacific, where their contribution is even higher than above the Indian Ocean.

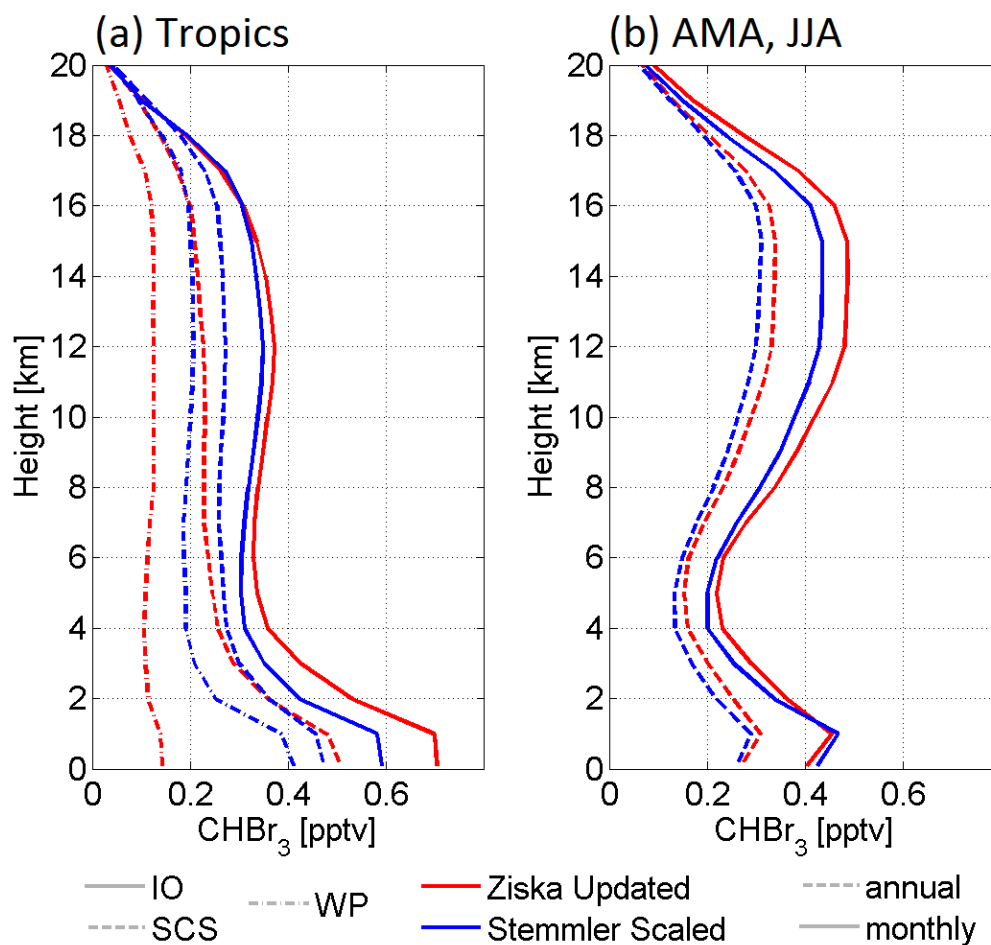


Figure 32: (a) Average tropical (20°S-20°N) VMR profiles of bromoform over the Indian Ocean (IO: 40°E-90°E), the South China Sea (SCS: 90°E-130°E), and the West Pacific (WP: 130°E-160°E) from the Ziska Updated and Stemmler Scaled inventories with monthly emissions. (b) Bromoform VMR profiles in the Asian monsoon anticyclone region (AMA: 10°N-40°N, 20°E-90°E) from both inventories with annual and monthly emissions in JJA.

3.3 Ocean-to-stratosphere transport of bromoform

In this section we analyze the main oceanic source regions and stratospheric entrainment regions for bromoform from the Indian Ocean and the west Pacific. Here, we focus on emission scenarios with monthly variation.

Oceanic source regions

Figure 4 shows the transport efficiency to the stratosphere and the oceanic source regions of bromoform delivered to the stratosphere according to the two emission inventories. The spatial distribution of transport efficiency is per definition independent of the emission distribution and strength. It shows which fraction of a bromoform mass released at a certain location reaches the stratosphere. The distribution of bromoform mass delivered to the stratosphere at the oceanic release locations depicts the oceanic source regions (Fig. 4b and c) and result from a combination of the air-sea fluxes (Fig. 2) and the transport efficiency (Fig. 4a).

The transport efficiency maps (Fig. 4a) show that the west Pacific is the most efficient region at transporting bromoform from the ocean to the stratosphere in the annual mean. The maximum efficiency shifts from the WP equator in DJF toward the north in JJA and SON. In MAM the transport efficiency is more evenly distributed between the Indian Ocean and the west Pacific. In JJA the Bay of Bengal also displays elevated transport efficiencies. For both emission inventories (Fig. 4b and c) the most important source regions for bromoform to the stratosphere are the Asian coast and the Arabian Sea and Bay of Bengal, especially in JJA. During this season, the emissions from these regions are high (Fig. 1) providing bromoform to the Indian summer monsoon convection over India and the Bay of Bengal. For the Ziska Updated inventory (Fig. 4b), the southern tropical Indian Ocean is also an important source region, while the open west Pacific delivers hardly any bromoform to the stratosphere. This is visible for all seasons. Using the Stemmler Scaled inventory (Fig. 4c), the equatorial west Pacific Ocean provides a secondary bromoform source to the stratosphere, which is strongest in DJF.

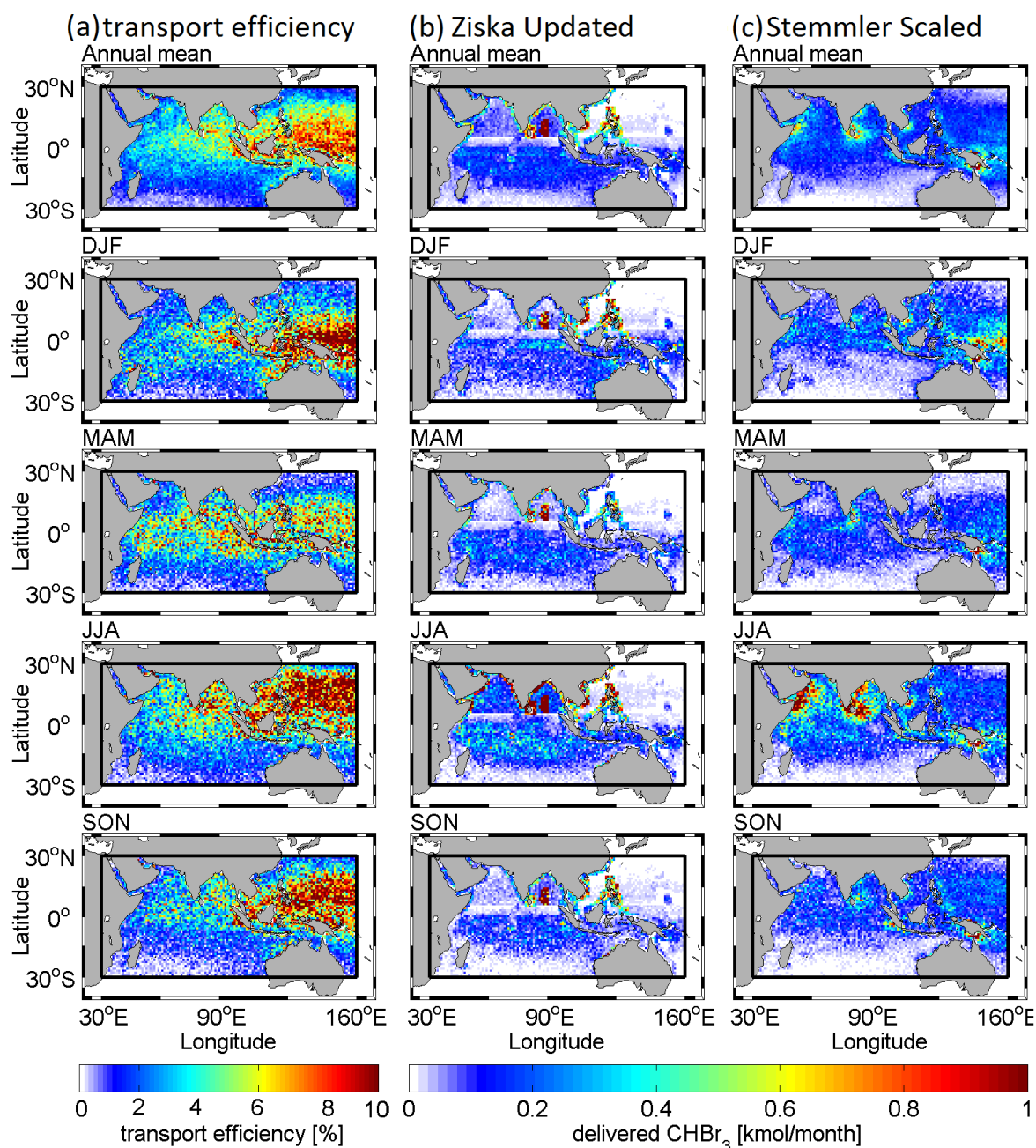


Figure 33: (a) Transport efficiency for bromoform to the CPT. (b) Oceanic source regions of bromoform delivered to the CPT for the Ziska Updated inventory with monthly emissions. (c) Like (b) but for Stemmler Scaled. The black box depicts the Indian Ocean/West Pacific release area.

When comparing emissions (Fig. 1), transport efficiency (Fig. 4a), and delivered mass (Fig. 4b and c) we can determine the oceanic regions where the stratospheric delivery is determined by the emissions and those where the transport dominates stratospheric entrainment. If important source regions coincide with high emissions, the stratospheric entrainment from this region is mainly emission-driven; if important source regions coincide with high transport efficiency and corresponding emissions are low, then

the stratospheric delivery is transport-driven. Analyzing the annual mean, the Arabian Sea and the Bay of Bengal are emission-driven source regions for the stratosphere: These ocean basins are not very efficient source regions (2% - 5%), but due to the high emissions they deliver maximum bromoform to the stratosphere. The west Pacific is a transport-driven source region: It contributes to stratospheric delivery through the generally high transport efficiency (6% - 9%) despite low emissions in this region in both the Ziska Updated and the Stemmler Scaled inventories. This also means that small changes in the VSLs emissions in the west Pacific will have a strong influence on the total mass delivered to the stratosphere, which makes it important to better constrain current and future emissions from this region.

Important bromoform source regions have been identified by Tegtmeier et al. (2015). They used a combination of bromoform emissions from Ziska et al. (2013) and ODP calculations (Pisso et al., 2010) to infer the importance of different oceanic regions for stratospheric ozone depletion, including an emission seasonality and the future development of emissions. The Maritime Continent significantly contributed to ODP-weighted emissions all year round. In accordance with our results, the main contribution in boreal summer comes from the Asian coastal areas and the Indian Ocean.

Stratospheric entrainment regions

The modeled stratospheric entrainment regions for Ziska Updated and Stemmler Scaled inventories with monthly emissions are depicted in Figure 34. In the annual mean, the entrainment maximum for both inventories occurs over the southern tip of India (Fig. 5a/b, top row). This maximum results from the strong emissions in JJA and the fast uplift with the Asian summer monsoon circulation. The Stemmler Scaled inventory also shows a secondary entrainment maximum over the equatorial west Pacific, which the Ziska Updated lacks. It is present in all seasons, but most pronounced in DJF. It results from the stronger emissions from the west Pacific Ocean in Stemmler Scaled compared to Ziska Updated as discussed above. The stronger stratospheric entrainment above the west Pacific from Stemmler Scaled is the most obvious pattern throughout all seasons and in the annual mean of the difference between the two inventories (Fig. 5c). The Ziska Updated inventory, on the other hand, displays stronger entrainment above the Bay of Bengal, caused by the strong coastal and central-Bay of Bengal emissions in this inventory.

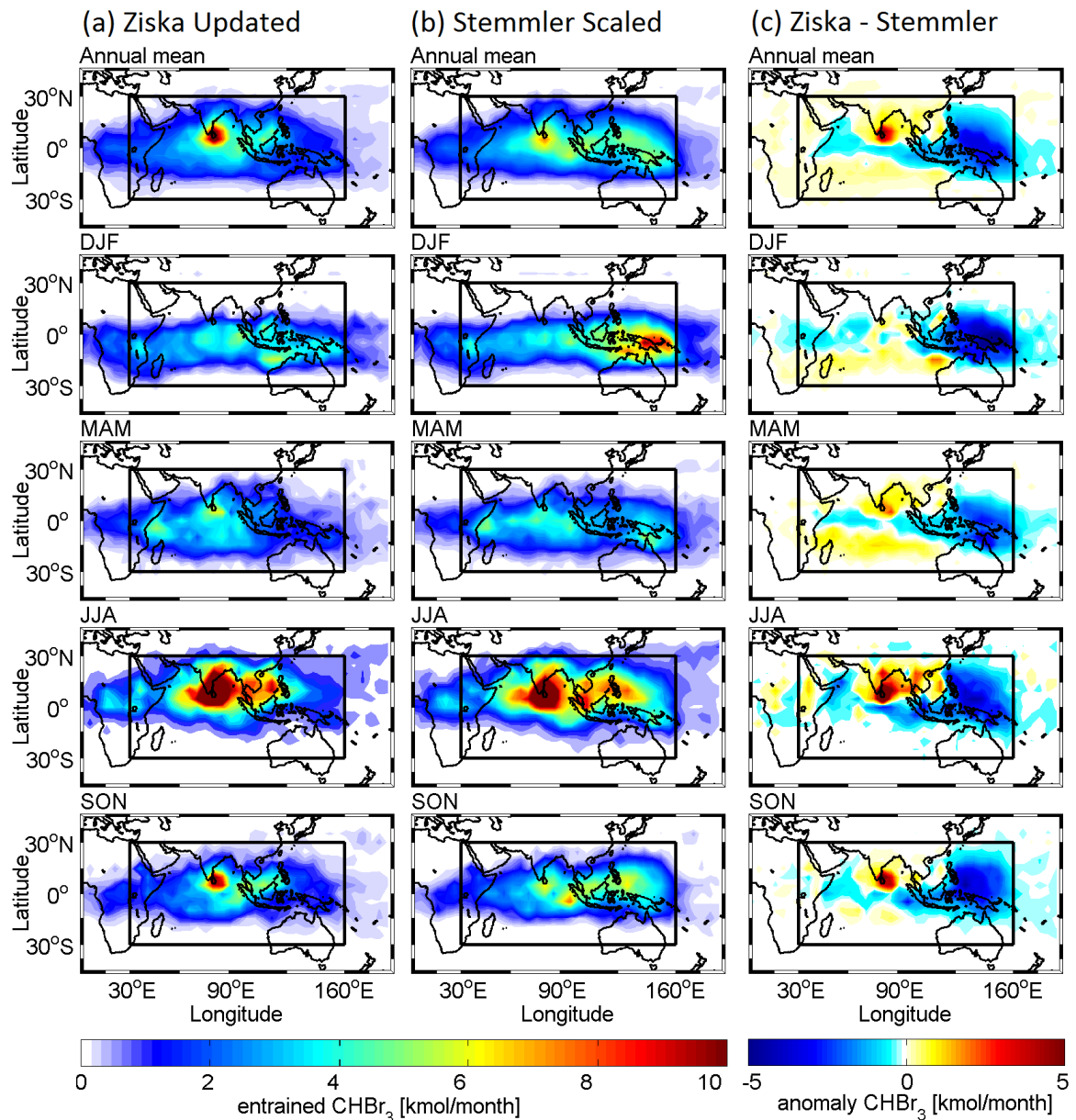


Figure 34: CPT entrainment for monthly bromoform emissions for (a) Ziska Updated and (b) Stemmler Scaled emission inventories. (c) Difference in entrainment between the two inventories (a) - (b). The black box depicts the Indian Ocean/West Pacific release area.

3.4 Annual vs. monthly bromoform emissions

For this study, we calculated the ocean to stratosphere transport of bromoform for annual and monthly emission fields for 2014. This enables us to detect the differences between the two experimental set ups and to find out which season and region delivers most bromoform to the stratosphere above the Indian Ocean.

Figure 6 shows the annual cycle of bromoform emissions, transport efficiency, and entrainment comparing the annual and monthly emission scenarios of Ziska Updated and Stemmler Scaled calculations plotted at the time of particle release from the ocean. The annual cycles of monthly emissions (Fig. 6a) display maxima in January and July and minimum emissions in April and November. Monthly emissions are higher than the annual mean from June to September. The annual cycle of bromoform transport efficiency to the stratosphere displays two maximum seasons: May-July and January-February (Fig. 6b). Generally, the transport efficiency is higher for the Stemmler Scaled than for the Ziska Updated emissions, because Stemmler Scaled has higher emissions in the west Pacific, which is the most efficient source region for the stratosphere (Fig. 4a). The combination of the emission cycles and transport efficiency results in the annual cycles of stratospheric entrainment (Fig. 6c). Using annual emissions, the annual cycle of stratospheric entrainment has the same seasonality and amplitude as the transport efficiency and a maximum from May to July. Using monthly emissions, the annual cycle of entrainment is amplified due to the similar seasonality in emissions and transport efficiency. The very high emissions in JJA combined with highest transport efficiencies result in the season with most stratospheric entrainment using monthly emissions. There is, thus, a shift in the maximum entrainment season between the annual and monthly emission scenarios.

The total annual entrainment of bromoform to the stratosphere is similar whether we use annual or monthly emissions (Table 10). The similar sums mean that the difference in the seasonality of entrainment between annual and monthly emissions (Fig. 6c) does not influence the total annual mass entrained in our experimental set up. Nonetheless, the consideration of seasonally varying emissions should, through the influence of the annual cycle, also influence the regions of VLSL entrainment to the stratosphere.

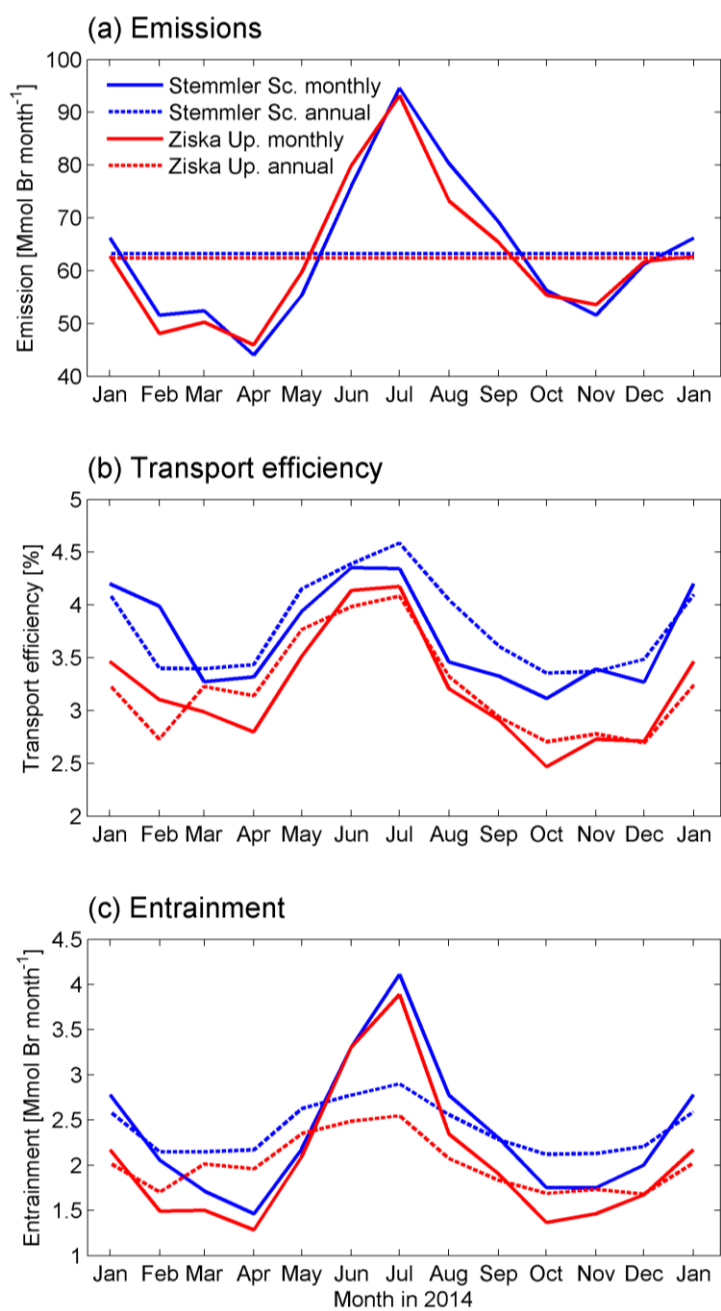


Figure 35: Annual cycles of bromoform (a) emission, (b) transport efficiency, and (c) entrainment above the CPT in 2014 for the Ziska Updated and Stemmler Scaled annual and monthly bromoform emission scenarios for the time of particle release.

Table 10: Total annual stratospheric entrainment of bromoform emitted from the IO/WP region.

	Stemmler Scaled	Ziska Updated
	[Mmol Br yr ⁻¹]	[Mmol Br yr ⁻¹]
Annual emissions	28.7	24.2
Monthly emissions	28.2	24.5

We distinguish these spatial differences in the stratospheric entrainment of bromoform between the annual and monthly emission scenarios of the Ziska Updated inventory by examining the atmospheric VMR at 17 km altitude (Figure 36). This height is a good approximation for the tropical CPT height, although it can be even higher in the Asian monsoon anticyclone (Munchak and Pan, 2014). High VMRs generally represent regions with enhanced uplift of bromoform from the ocean, but additionally indicate if the compound is accumulated in a certain region. Using annual emissions (Fig. 7a), the maximum VMR region covers the tropical west and central Indian Ocean in the annual mean. This maximum is strongest for this scenario in MAM. For the monthly emission scenario (Fig. 7b), the region of highest VMR at 17 km is also located above the tropical west and central Indian Ocean. The season with highest VMR is JJA, when the maximum region is shifted to the north and east from its annual mean position. We, thus, discover different maximum VMR seasons using annual vs. monthly emissions. The differences between VMR for the two scenarios are visible in Fig. 7c. In the annual mean, the VMR is lower north of 15°N and higher south of 15°N using annual emissions than with monthly emissions. In DJF the differences are less clear, while in MAM the annual emissions deliver much more bromoform to 17 km height than monthly emissions. This is reversed in JJA and SON, when monthly emissions lead to higher VMR in the Asian monsoon anticyclone region in JJA and across the whole Indian Ocean/Asian area in SON. The respective figure for the Stemmler Scaled emission inventory shows very similar patterns (Fig. S5). Furthermore, the differences in the entrainment regions of bromoform mass at the CPT between the two scenarios also show a similar pattern (Fig. S6), except for SON when the entrainment shows a positive anomaly, which we try to explain in Sect. 3.5.

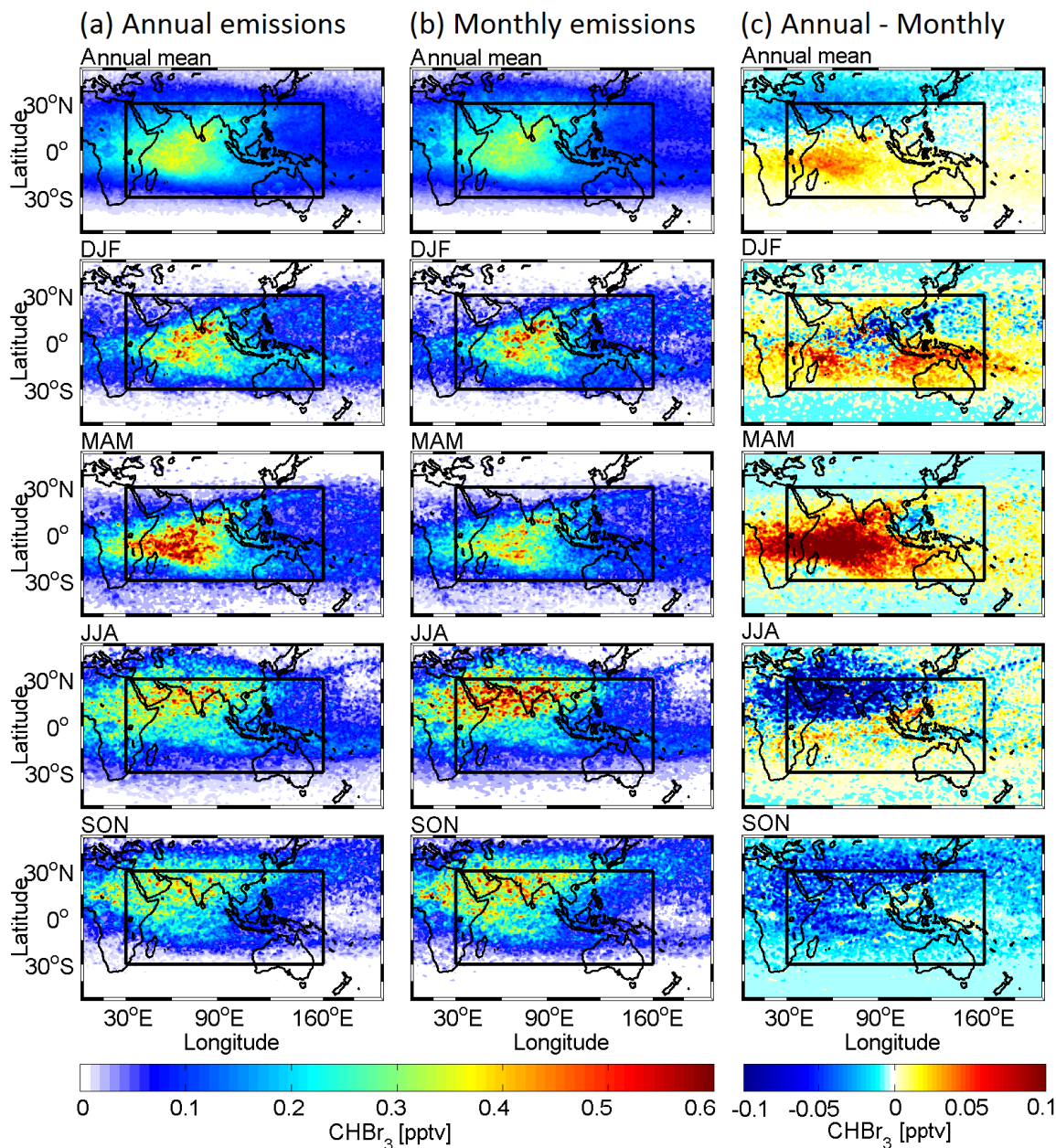


Figure 36: Bromoform volume mixing ratios (VMR) at 17 km for the Ziska Updated (a) annual emissions, (b) monthly emissions, and (c) the difference between the two scenarios. The black box depicts the IO/WP release area.

3.5 Discussion

The spatial differences in the VMR at 17 km can be explained by the annual cycle of emissions and transport from the Indian Ocean. In DJF, the monthly emissions are around the annual mean (Fig. 6a), causing only small differences in VMR at the tropopause. In MAM, monthly emissions are lower than the annual mean (Fig. 6a), causing higher VMR for annual than monthly emissions in the central Indian Ocean (Fig. 7c), which is the region of maximum entrainment during this season (Fig. 5a). In JJA, monthly emissions reach their maximum, which are much higher than the annual mean emissions (Fig. 6a), and the transport efficiency through the Asian summer monsoon convection is also maximized (Fig. 6b). The Asian monsoon anticyclone in the upper troposphere and lower stratosphere (UTLS) region is known to confine lifted boundary layer air masses within its circulation (Park et al., 2007; Fiehn et al., 2017). The high monthly emissions show a distinct negative anomaly in the JJA difference between annual and monthly emissions (Fig. 7c). In SON, the monthly emissions are lower than the annual emissions (Fig. 6a). These lower monthly emissions, however, lead to higher VMR around the CPT than annual emissions, shown by negative anomalies throughout the whole region (Fig. 7c). We suspect that the bromoform, which has been accumulating in the anticyclone during JJA, spreads throughout the region and causes the negative anomaly in SON. The lifetime of bromoform in the TTL region is around 25 to 30 days (Hossaini et al., 2010), which is long enough to be distributed across the region. The spreading of air masses from the anticyclone across the northern and also into the southern hemisphere during the breakup of the anticyclone in September has been observed for trace gases like CO, H₂O, and O₃ with satellites (Santee et al., 2017) and also modeled with a chemistry transport model (Vogel et al., 2016). In the annual mean, the representation of monthly resolved emissions results in less bromoform around the equator and in the southern hemisphere UTLS and more in the UTLS north of 15°N in the Asian region, especially in the Asian monsoon anticyclone, because of the different main entrainment seasons: JJA using monthly emissions and MAM using annual emissions.

The difference in atmospheric bromoform mixing ratios in the Asian summer monsoon anticyclone between the annual and monthly emissions is also visible in the VMR profiles in this region (Fig. 3b). At the level of main convective outflow (~14 km), the monthly emissions produce mixing ratios that are more than 40 % higher than from

annual emissions. This large difference in a circulation regime with pronounced delivery to stratosphere has a significant impact on stratospheric $\text{Br}_y^{\text{VSLs}}$.

Our results help to interpret the discrepancy of modeled seasonality of bromoform VMR above the Indian Ocean between Liang et al. (2014) and Hossaini et al. (2016). Both studies use global emissions of bromoform and show results only of annual emission scenarios. While Liang et al. (2014) simulated a VMR maximum for bromoform above the Indian Ocean using a chemistry climate model for 1960-2010 in DJF, the set of chemistry climate and transport models from Hossaini et al. (2016) find that the Asian monsoon in JJA is the most important pathway for bromoform to the stratosphere. They add that the contribution of this pathway is highly uncertain, because of the large spread in the signal from model to model. The importance of DJF as season of enhanced entrainment is connected with the high transport efficiency in the West Pacific during that season and, thus, the emissions in that region. The bromoform emissions inventory of Liang et al. (2010) used in Liang et al. (2014) generally has high tropical emissions in the West Pacific, which are transported towards the Indian Ocean region. The emission inventory of Ziska et al. (2013), which is used for some models in Hossaini et al. (2016), has low emissions in the West Pacific and high emissions in the Indian Ocean, resulting in a maximum of bromoform VMR above the Indian Ocean in JJA. We find that the stratospheric entrainment seasonality does depend on the distribution of emissions. Using seasonal emissions in these simulations would generally increase the importance of the JJA entrainment through the monsoon.

4 Uncertainties

This study presents an estimate of bromoform entrainment to the stratosphere over the Indian Ocean and Asia. Uncertainties in the analysis result from the emission inventories, the FLEXPART model with the ERA-Interim reanalysis fields.

The Ziska et al. (2013) inventory was updated in this study by including new observations. Available oceanic and atmospheric VSLs observations contain a mixture of measurements from different seasons and years, which are used to calculate an annual climatology. The seasonality in monthly emissions from Ziska Updated results from the seasonality in wind speed, SST, and sea surface pressure in the parameterization. The Indian Ocean has a pronounced seasonality in ocean currents and upwelling regions (Schott et al., 2009) affecting the biological productivity, surface bromoform

concentrations, and emissions (Quack et al., 2004; Hepach et al., 2015). Stemmler et al. (2015) include seasonality in oceanic bromoform concentrations from phytoplankton growth. The study was designed to assess processes that drive large scale patterns of bromoform emissions from the open ocean and was carried out as climatological steady state simulation. Thus, deviations from observations arise, for example, through the missing bromoform production from macroalgae along the coasts and unresolved temporal variability patterns caused e.g. by ENSO (Stemmler et al., 2015). Although the model resolution is low, the MPI model shows the most realistic circulation of all CMIP 5 models in the Indian Ocean (Roxy et al., 2016). Furthermore, our Stemmler Scaled inventory uses a temporally and spatially uniform atmospheric bromoform mixing ratio to calculate the emissions. However, since the annual cycle of emissions results mainly from the changes in surface wind speed for both inventories (Sect. 3.1), we conclude that in an oversaturated tropical ocean, as is mostly the case for bromoform (Ziska et al., 2013), the annual cycle of oceanic concentrations plays only a secondary role in determining the emission cycle. In a previous publication we have shown a good agreement of surface wind speed of ERA-Interim with ship-bound and radiosonde measurements over the Indian Ocean (Fiehn et al., 2017). Furthermore, the parameterization for the air-sea flux itself, is estimated to introduce an uncertainty of a factor of two (Lennartz et al., 2015).

The emissions and transport of VSLs in this study strongly depend on the ERA-Interim meteorological reanalysis data and the boundary layer and convective parameterizations in the FLEXPART model. In most atmospheric models, convection, which occurs on scales smaller than the grid scale, is parameterized. The FLEXPART convection scheme was described and evaluated by Forster et al. (2007). FLEXPART has previously been used to simulate VSLs transport and good agreement with aircraft measurements of bromoform, dibromomethane, and methyl iodide up to 11 km above the tropical West Pacific (Fuhlbrügge et al., 2016) and methyl iodide in the UTLS (Tegtmeier et al., 2013) was achieved.

If we want to infer the total delivery of $\text{Br}_y^{\text{VSLs}}$ to the stratosphere, we have to consider the oceanic source gases, but also the possible entrainment of their soluble product gases. Here we only consider the gases directly released from the ocean. The source gas injection is generally enhanced with enhanced vertical uplift (Hossaini et al., 2010). Product gas injection depends on the occurrence of precipitation and washout processes, which are modeled with high uncertainties (Montzka et al., 2010; Carpenter et

al., 2014). Liang et al. (2014) simulated that product gas injection of bromine has a contrary relationship with convection, because more convection causes enhanced scavenging of the soluble product gases. This effect was stronger than the enhancement of source gas injection, causing an overall reduction in halogen entrainment for scenarios with stronger convection. Thus, large uncertainties remain with regard to modeling product gas injection.

5 Summary and Conclusions

For this study, we compiled two new bromoform emission inventories for the Indian Ocean and west Pacific (IO/WP) in 2014: An update (this study) of the Ziska et al. (2013) inventory including new measurements in the west Indian Ocean (Fiehn et al., 2017) and an inventory using monthly surface water concentrations modeled by Stemmler et al. (2015) and scaled with measurements from the Indian Ocean and west Pacific. We added seasonality through the calculation of emissions using annual and monthly oceanic concentrations and fixed annual mean atmospheric mixing ratios with monthly mean wind speed, SST, SSS, and sea level pressure data. The resulting seasonality in bromoform emissions in the IO/WP is mainly driven by the wind speed. The annual cycle of emissions for both inventories displays maximum emissions in boreal summer located in the Bay of Bengal, Arabian Sea, and the tropical southern Indian Ocean.

We modeled the ocean-to-stratosphere transport for 2014 with FLEXPART based on ERA-Interim fields using annual and monthly emission scenarios for both inventories to detect the influence of seasonally varying emissions on stratospheric entrainment of VSLs. A comparison of modeled VMR with observations from aircraft and ship observations from the Indian Ocean, the South China Sea, and the west Pacific displays that modeled mixing ratios were generally lower than observations due to our regionally restricted model set up. It is also caused by low coastal emissions in our inventories and missing sources from the central and east Pacific Ocean.

The oceanic source regions for stratospheric Br_y from bromoform and the entrainment regions to the stratosphere for monthly emissions were analyzed. For both emission inventories, most stratospheric bromoform originates from the Arabian Sea and Bay of Bengal in boreal summer and from the tropical west Pacific in boreal winter. The annual mean main entrainment to the stratosphere occurs above the southern tip of India

and results from the strong emissions from the Bay of Bengal and Arabian Sea and the efficient uplift with the monsoon convection during boreal summer.

We studied the influence of annual vs. monthly emissions on the stratospheric entrainment and VMR of bromoform above the IO/WP region in 2014. We simulated similar total annual bromoform delivery to the stratosphere whether applying annual or monthly emissions. However, monthly emissions led to less entrainment above the IO in boreal spring and more in boreal summer than annual emissions. This causes up to 40% higher VMR in the Asian monsoon anticyclone using monthly emissions and a change in the season with maximum VMR at 17 km height above the Indian Ocean: Annual emissions lead to highest VMR in MAM, while monthly emissions cause high VMR in JJA. In the annual mean, the monthly emissions induce higher VMR at the tropopause north of 15°N and lower VMR around the equatorial and southern hemisphere tropopause, probably caused by the enhanced entrainment through the Asian summer monsoon in the northern hemisphere.

Most surface-to-stratosphere transport above the Indian Ocean and Asia occurs in the Asian monsoon anticyclone during the summer monsoon and during its decline. The use of annual bromoform emissions, the most common practice of previous studies, underestimates oceanic emissions, volume mixing ratios, and stratospheric source gas delivery of bromoform and, thus, the stratospheric bromine loading during this season. Although the total annual bromoform delivery did not vary in our 2014 study, the region and season of stratospheric entrainment determines the bromine pathway and impact in the stratosphere. Therefore, we recommend using seasonally resolved emissions for the Indian and west Pacific Ocean and Asian monsoon region, if a process study or comparison to observations is intended. This study was conducted for bromoform, but the impact of representing seasonally resolved oceanic emissions for delivery from the Indian Ocean to the stratosphere also applies for other oceanic VSLs.

Data availability

The created bromoform emission inventory data and the FLEXPART model output can be inquired from the authors.

Author contribution

K. Krüger and A. Fiehn developed the idea for this paper. F. Ziska updated the Ziska et al. (2013) bottom-up oceanic concentration and atmospheric mixing ratio climatology. I. Stemmler scaled the Stemmler et al. (2015) oceanic concentrations with the ship measurements. A. Fiehn created the emission fields with valuable advice from B. Quack. A. Fiehn, K. Krüger, B. Quack, and I. Stemmler designed the model experiments and A. Fiehn carried out the FLEXPART calculations. A. Fiehn analyzed the model output and wrote the manuscript with contributions from all co-authors.

Competing interests

The authors declare that they have no conflict of interest.

Acknowledgements

A. Fiehn was funded through the EU FP7 project StratoClim (603557). We thank the European Centre for Medium-Range Weather Forecasts (ECMWF) for the provision of ERA-Interim reanalysis data and the Flexpart development team for the Lagrangian particle dispersion model used in this publication. The Flexpart simulations were performed on resources provided by UNINETT Sigma2 - the National Infrastructure for High Performance Computing and Data Storage in Norway.

References

- Aschmann, J., Sinnhuber, B. M., Chipperfield, M. P., and Hossaini, R.: Impact of deep convection and dehydration on bromine loading in the upper troposphere and lower stratosphere, *Atmos. Chem. Phys.*, 11, 2671-2687, 10.5194/acp-11-2671-2011, 2011.
- Aschmann, J., and Sinnhuber, B. M.: Contribution of very short-lived substances to stratospheric bromine loading: uncertainties and constraints, *Atmos. Chem. Phys.*, 13, 1203-1219, 10.5194/acp-13-1203-2013, 2013.
- Butler, J. H., King, D. B., Lobert, J. M., Montzka, S. A., Yvon-Lewis, S. A., Hall, B. D., Warwick, N. J., Mondeel, D. J., Aydin, M., and Elkins, J. W.: Oceanic distributions and emissions of short-lived halocarbons, *Global Biogeochemical Cycles*, 21, GB1023, 10.1029/2006gb002732, 2007.
- Carpenter, L. J., Sturges, W. T., Penkett, S. A., Liss, P. S., Alicke, B., Hebestreit, K., and Platt, U.: Short-lived alkyl iodides and bromides at Mace Head, Ireland: Links to biogenic sources and halogen oxide production, *Journal of Geophysical Research: Atmospheres*, 104, 1679-1689, 10.1029/98jd02746, 1999.
- Carpenter, L. J., and Liss, P. S.: On temperate sources of bromoform and other reactive organic bromine gases, *Journal of Geophysical Research: Atmospheres*, 105, 20539-20547, 10.1029/2000jd900242, 2000.
- Carpenter, L. J., Reimann, S., Burkholder, J. B., Clerbaux, C., Hall, B. D., Hossaini, R., Laube, J. C., and Yvon-Lewis, S. A.: Ozone-Depleting Substances (ODSs) and other gases of interest to the Montreal Protocol, in: *Scientific Assessment of Ozone Depletion: 2014. Global Ozone Research and monitoring Project - Report N. 55*, World Meteorological Organization, Geneva, Switzerland, 2014.
- Dvortsov, V. L., Geller, M. A., Solomon, S., Schauffler, S. M., Atlas, E. L., and Blake, D. R.: Rethinking reactive halogen budgets in the midlatitude lower stratosphere, *Geophysical Research Letters*, 26, 1699-1702, 10.1029/1999gl900309, 1999.
- Fiehn, A., Quack, B., Hepach, H., Fuhlbrügge, S., Tegtmeier, S., Toohey, M., Atlas, E., and Krüger, K.: Delivery of halogenated very short-lived substances from the west Indian Ocean to the stratosphere during the Asian summer monsoon, *Atmos. Chem. Phys.*, 17, 6723-6741, 10.5194/acp-17-6723-2017, 2017.
- Fiehn, A., Quack, B., Marandino, C. A., and Krüger, K.: Variability of VLS transport from the Indian Ocean to the stratosphere, *Journal of Geophysical Research: Atmospheres*, under review.
- Forster, C., Stohl, A., and Seibert, P.: Parameterization of convective transport in a Lagrangian particle dispersion model and its evaluation, *Journal of Applied Meteorology and Climatology*, 46, 403-422, 10.1175/JAM2470.1, 2007.
- Fuhlbrügge, S., Quack, B., Tegtmeier, S., Atlas, E., Hepach, H., Shi, Q., Raimund, S., and Krüger, K.: The contribution of oceanic halocarbons to marine and free tropospheric air over the tropical West Pacific, *Atmos. Chem. Phys.*, 16, 7569-7585, 10.5194/acp-16-7569-2016, 2016.
- Gottelman, A., Lauritzen, P. H., Park, M., and Kay, J. E.: Processes regulating short-lived species in the tropical tropopause layer, *Journal of Geophysical Research: Atmospheres*, 114, D13303, 10.1029/2009jd011785, 2009.
- Hense, I., and Quack, B.: Modelling the vertical distribution of bromoform in the upper water column of the tropical Atlantic Ocean, *Biogeosciences*, 6, 535-544, 10.5194/bg-6-535-2009, 2009.
- Hepach, H., Quack, B., Raimund, S., Fischer, T., Atlas, E. L., and Bracher, A.: Halocarbon emissions and sources in the equatorial Atlantic Cold Tongue, *Biogeosciences*, 12, 6369-6387, 2015.
- Hossaini, R., Chipperfield, M. P., Monge-Sanz, B. M., Richards, N. A. D., Atlas, E., and Blake, D. R.: Bromoform and dibromomethane in the tropics: a 3-D model study of chemistry and transport, *Atmos. Chem. Phys.*, 10, 719-735, 2010.

- Hossaini, R., Chipperfield, M. P., Feng, W., Breider, T. J., Atlas, E., Montzka, S. A., Miller, B. R., Moore, F., and Elkins, J.: The contribution of natural and anthropogenic very short-lived species to stratospheric bromine, *Atmos. Chem. Phys.*, 12, 371-380, 10.5194/acp-12-371-2012, 2012.
- Hossaini, R., Mantle, H., Chipperfield, M. P., Montzka, S. A., Hamer, P., Ziska, F., Quack, B., Krüger, K., Tegtmeier, S., Atlas, E., Sala, S., Engel, A., Bönisch, H., Keber, T., Oram, D., Mills, G., Ordóñez, C., Saiz-Lopez, A., Warwick, N., Liang, Q., Feng, W., Moore, F., Miller, B. R., Marécal, V., Richards, N. A. D., Dorf, M., and Pfeilsticker, K.: Evaluating global emission inventories of biogenic bromocarbons, *Atmos. Chem. Phys.*, 13, 11819-11838, 10.5194/acp-13-11819-2013, 2013.
- Hossaini, R., Patra, P. K., Leeson, A. A., Krysztofiak, G., Abraham, N. L., Andrews, S. J., Archibald, A. T., Aschmann, J., Atlas, E. L., Belikov, D. A., Bönisch, H., Carpenter, L. J., Dhomse, S., Dorf, M., Engel, A., Feng, W., Fuhlbrügge, S., Griffiths, P. T., Harris, N. R. P., Hommel, R., Keber, T., Krüger, K., Lennartz, S. T., Maksyutov, S., Mantle, H., Mills, G. P., Miller, B., Montzka, S. A., Moore, F., Navarro, M. A., Oram, D. E., Pfeilsticker, K., Pyle, J. A., Quack, B., Robinson, A. D., Saikawa, E., Saiz-Lopez, A., Sala, S., Sinnhuber, B. M., Taguchi, S., Tegtmeier, S., Lidster, R. T., Wilson, C., and Ziska, F.: A multi-model intercomparison of halogenated very short-lived substances (TransCom-VSLS): linking oceanic emissions and tropospheric transport for a reconciled estimate of the stratospheric source gas injection of bromine, *Atmos. Chem. Phys.*, 16, 9163-9187, 10.5194/acp-16-9163-2016, 2016.
- Krüger, K., and Quack, B.: Introduction to special issue: the TransBrom Sonne expedition in the tropical West Pacific, *Atmos. Chem. Phys.*, 13, 9439-9446, 10.5194/acp-13-9439-2013, 2013.
- Law, K. S., Sturges, W. T., Blake, D. R., Blake, N. J., Burkeholder, J. B., Butler, J. H., Cox, R. A., Haynes, P. H., Ko, M. K. W., Kreher, K., Mari, C., Pfeilsticker, K., Plane, J. M. C., Salawitch, R. J., Schiller, C., Sinnhuber, B. M., von Glasow, R., Warwick, N. J., Wuebbles, D. J., and Yvon-Lewis, S. A.: Halogenated Very Short-Lived Substances, in: *Scientific Assessment of Ozone Depletion: 2006. Global Ozone Research and Monitoring Project - Report N. 50*, World Meteorological Organization, Geneva, Switzerland, 2006.
- Lennartz, S. T., Krysztofiak, G., Marandino, C. A., Sinnhuber, B. M., Tegtmeier, S., Ziska, F., Hossaini, R., Krüger, K., Montzka, S. A., Atlas, E., Oram, D. E., Keber, T., Bönisch, H., and Quack, B.: Modelling marine emissions and atmospheric distributions of halocarbons and dimethyl sulfide: the influence of prescribed water concentration vs. prescribed emissions, *Atmos. Chem. Phys.*, 15, 11753-11772, 10.5194/acp-15-11753-2015, 2015.
- Liang, Q., Stolarski, R. S., Kawa, S. R., Nielsen, J. E., Douglass, A. R., Rodriguez, J. M., Blake, D. R., Atlas, E., and Orr, L. E.: Finding the missing stratospheric Bry: a global modeling study of CHBr_3 and CH_2Br_2 , *Atmos. Chem. Phys.*, 2269-2286, 2010.
- Liang, Q., Atlas, E., Blake, D. R., Dorf, M., Pfeilsticker, K., and Schauffler, S.: Convective transport of very short lived bromocarbons to the stratosphere, *Atmos. Chem. Phys.*, 14, 5781-5792, 2014.
- Montzka, S., Reimann, S., Engel, A., Kruger, K., Sturges, W., Blake, D., Dorf, M., Fraser, P., Froidevaux, L., and Jucks, K.: *Scientific assessment of ozone depletion: 2010*, Global Ozone Research and Monitoring Project-Report No. 51, 2010.
- Munchak, L. A., and Pan, L. L.: Separation of the lapse rate and the cold point tropopauses in the tropics and the resulting impact on cloud top-tropopause relationships, *Journal of Geophysical Research: Atmospheres*, 119, 7963-7978, 10.1002/2013jd021189, 2014.
- Newell, R. E., and Gould-Stewart, S.: A Stratospheric Fountain?, *Journal of the Atmospheric Sciences*, 38, 2789-2796, 10.1175/1520-0469(1981)038<2789:ASF>2.0.CO;2, 1981.
- Nielsen, J. E. D., A.R.: A simulation of bromoform's contribution to stratospheric bromine, 2001.
- Nightingale, P., Malin, G., Law, C., Watson, A., Liss, P., Liddicoat, M., Boutin, J., and Upstill-Goddard, R.: In situ evaluation of air-sea gas exchange parameterizations using novel conservative and volatile tracers, *Global Biogeochemical Cycles*, 14, 373-387, 10.1029/1999GB900091, 2000.

- Ordóñez, C., Lamarque, J. F., Tilmes, S., Kinnison, D. E., Atlas, E. L., Blake, D. R., Sousa Santos, G., Brasseur, G., and Saiz-Lopez, A.: Bromine and iodine chemistry in a global chemistry-climate model: description and evaluation of very short-lived oceanic sources, *Atmos. Chem. Phys.*, 12, 1423-1447, 10.5194/acp-12-1423-2012, 2012.
- Palmer, C. J., and Reason, C. J.: Relationships of surface bromoform concentrations with mixed layer depth and salinity in the tropical oceans, *Global Biogeochemical Cycles*, 23, GB2014, 10.1029/2008gb003338, 2009.
- Park, M., Randel, W. J., Gettelman, A., Massie, S. T., and Jiang, J. H.: Transport above the Asian summer monsoon anticyclone inferred from Aura Microwave Limb Sounder tracers, *Journal of Geophysical Research*, 112, D16309, 10.1029/2006jd008294, 2007.
- Pisso, I., Haynes, P. H., and Law, K. S.: Emission location dependent ozone depletion potentials for very short-lived halogenated species, *Atmos. Chem. Phys.*, 10, 12025-12036, 10.5194/acp-10-12025-2010, 2010.
- Quack, B., and Wallace, D. W. R.: Air-sea flux of bromoform: Controls, rates, and implications, *Global Biogeochemical Cycles*, 17, 1023, 10.1029/2002gb001890, 2003.
- Quack, B., Atlas, E., Petrick, G., Stroud, V., Schauffler, S., and Wallace, D. W. R.: Oceanic bromoform sources for the tropical atmosphere, *Geophysical Research Letters*, 31, L23S05, 10.1029/2004gl020597, 2004.
- Quack, B., Atlas, E., Petrick, G., and Wallace, D. W. R.: Bromoform and dibromomethane above the Mauritanian upwelling: Atmospheric distributions and oceanic emissions, *Journal of Geophysical Research*, 112, D09312, 10.1029/2006jd007614, 2007.
- Roxy, M. K., Modi, A., Murtugudde, R., Valsala, V., Panickal, S., Prasanna Kumar, S., Ravichandran, M., Vichi, M., and Lévy, M.: A reduction in marine primary productivity driven by rapid warming over the tropical Indian Ocean, *Geophysical Research Letters*, 43, 826-833, 10.1002/2015gl066979, 2016.
- Roy, R., Pratihary, A., Narvenkar, G., Mochamadkar, S., Gauns, M., and Naqvi, S. W. A.: The relationship between volatile halocarbons and phytoplankton pigments during a *Trichodesmium* bloom in the coastal eastern Arabian Sea, *Estuarine, Coastal and Shelf Science*, 95, 110-118, 10.1016/j.ecss.2011.08.025, 2011.
- Santee, M. L., Manney, G. L., Livesey, N. J., Schwartz, M. J., Neu, J. L., and Read, W. G.: A comprehensive overview of the climatological composition of the Asian summer monsoon anticyclone based on 10 years of Aura Microwave Limb Sounder measurements, *Journal of Geophysical Research: Atmospheres*, 122, 5491-5514, 10.1002/2016jd026408, 2017.
- Schott, F. A., Xie, S.-P., and McCreary, J. P.: Indian Ocean circulation and climate variability, *Reviews of Geophysics*, 47, RG1002, 10.1029/2007rg000245, 2009.
- Stemmler, I., Hense, I., and Quack, B.: Marine sources of bromoform in the global open ocean - global patterns and emissions, *Biogeosciences*, 12, 1967-1981, 10.5194/bg-12-1967-2015, 2015.
- Stohl, A., Hittenberger, M., and Wotawa, G.: Validation of the Lagrangian particle dispersion model FLEXPART against large-scale tracer experiment data, *Atmospheric Environment*, 32, 4245-4264, 10.1016/S1352-2310(98)00184-8, 1998.
- Stohl, A., and Thomson, D.: A density correction for Lagrangian particle dispersion models, *Boundary-Layer Meteorology*, 90, 155-167, 10.1023/A:1001741110696, 1999.
- Stohl, A., and Trickl, T.: A textbook example of long-range transport: Simultaneous observation of ozone maxima of stratospheric and North American origin in the free troposphere over Europe, *Journal of Geophysical Research: Atmospheres*, 104, 30445-30462, 10.1029/1999JD900803, 1999.
- Stohl, A., Forster, C., Frank, A., Seibert, P., and Wotawa, G.: Technical note: The Lagrangian particle dispersion model FLEXPART version 6.2, *Atmos. Chem. Phys.*, 5, 2461-2474, 2005.
- Tegtmeier, S., Krüger, K., Quack, B., Atlas, E. L., Pisso, I., Stohl, A., and Yang, X.: Emission and transport of bromocarbons: from the West Pacific ocean into the stratosphere, *Atmos. Chem. Phys.*, 12, 10633-10648, 10.5194/acp-12-10633-2012, 2012.

- Tegtmeier, S., Krüger, K., Quack, B., Atlas, E., Blake, D. R., Boenisch, H., Engel, A., Hepach, H., Hossaini, R., Navarro, M. A., Raimund, S., Sala, S., Shi, Q., and Ziska, F.: The contribution of oceanic methyl iodide to stratospheric iodine, *Atmos. Chem. Phys.*, 13, 11869-11886, 10.5194/acp-13-11869-2013, 2013.
- Tegtmeier, S., Ziska, F., Pisso, I., Quack, B., Velders, G. J. M., Yang, X., and Krüger, K.: Oceanic bromoform emissions weighted by their ozone depletion potential, *Atmos. Chem. Phys.*, 15, 13647-13663, 10.5194/acp-15-13647-2015, 2015.
- Vogel, B., Günther, G., Müller, R., Groß, J. U., Afchine, A., Bozem, H., Hoor, P., Krämer, M., Müller, S., Riese, M., Rolf, C., Spelten, N., Stiller, G. P., Ungermann, J., and Zahn, A.: Long-range transport pathways of tropospheric source gases originating in Asia into the northern lower stratosphere during the Asian monsoon season 2012, *Atmos. Chem. Phys.*, 16, 15301-15325, 10.5194/acp-16-15301-2016, 2016.
- Warwick, N. J., Pyle, J. A., Carver, G. D., Yang, X., Savage, N. H., O'Connor, F. M., and Cox, R. A.: Global modeling of biogenic bromocarbons, *Journal of Geophysical Research: Atmospheres*, 111, D24305, 10.1029/2006jd007264, 2006.
- Wisher, A., Oram, D. E., Laube, J. C., Mills, G. P., van Velthoven, P., Zahn, A., and Brenninkmeijer, C. A. M.: Very short-lived bromomethanes measured by the CARIBIC observatory over the North Atlantic, Africa and Southeast Asia during 2009–2013, *Atmos. Chem. Phys.*, 14, 3557-3570, 10.5194/acp-14-3557-2014, 2014.
- Yamamoto, H., Yokouchi, Y., Otsuki, A., and Itoh, H.: Depth profiles of volatile halogenated hydrocarbons in seawater in the Bay of Bengal, *Chemosphere*, 45, 371-377, 10.1016/S0045-6535(00)00541-5, 2001.
- Ziska, F., Quack, B., Abrahamsson, K., Archer, S. D., Atlas, E., Bell, T., Butler, J. H., Carpenter, L. J., Jones, C. E., Harris, N. R. P., Hepach, H., Heumann, K. G., Hughes, C., Kuss, J., Krüger, K., Liss, P., Moore, R. M., Orlikowska, A., Raimund, S., Reeves, C. E., Reifenhäuser, W., Robinson, A. D., Schall, C., Tanhua, T., Tegtmeier, S., Turner, S., Wang, L., Wallace, D., Williams, J., Yamamoto, H., Yvon-Lewis, S., and Yokouchi, Y.: Global sea-to-air flux climatology for bromoform, dibromomethane and methyl iodide, *Atmos. Chem. Phys.*, 13, 8915-8934, 10.5194/acp-13-8915-2013, 2013.

Supplement Manuscript 4

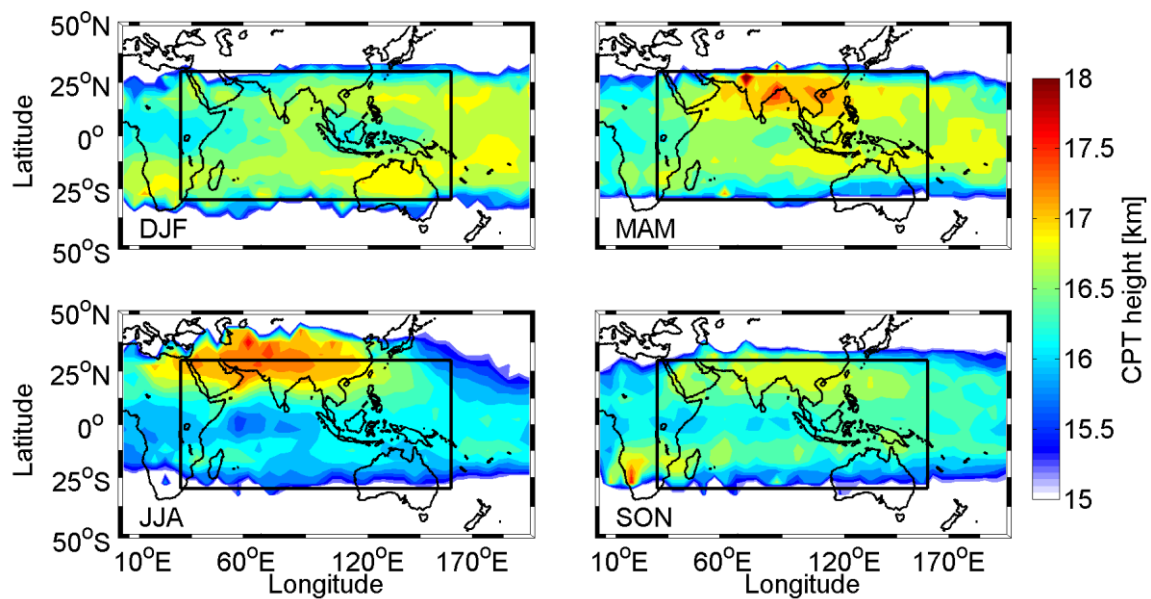


Figure S1: Height of the cold point tropopause (CPT) in 2014 from ERA-Interim data used in FLEXPART.

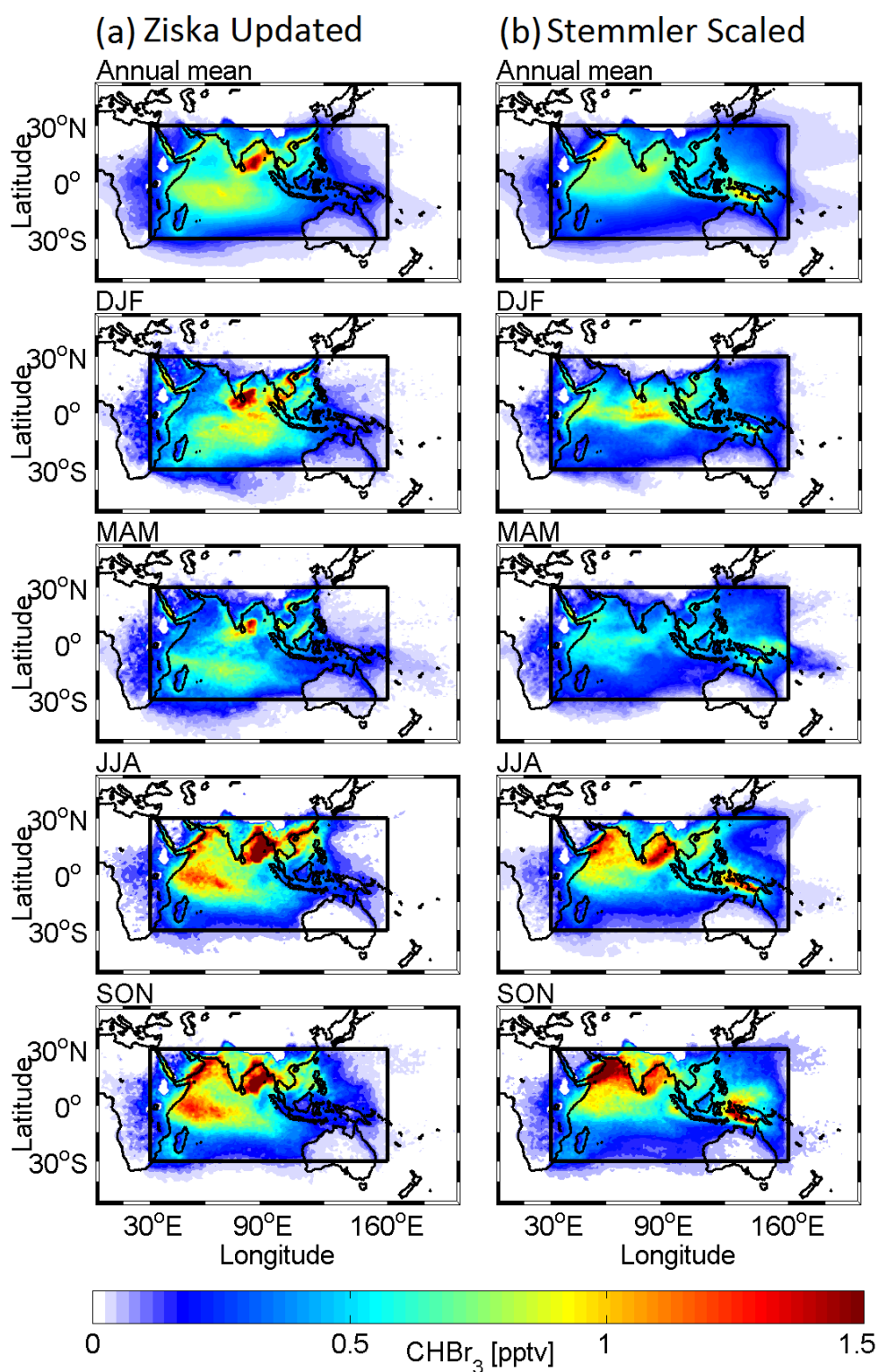


Figure S2: Bromoform volume mixing ratios (VMR) at 1 km for monthly emissions from (a) Ziska Updated and (b) Stemmler Scaled inventories. The black box depicts the IO/WP release area.

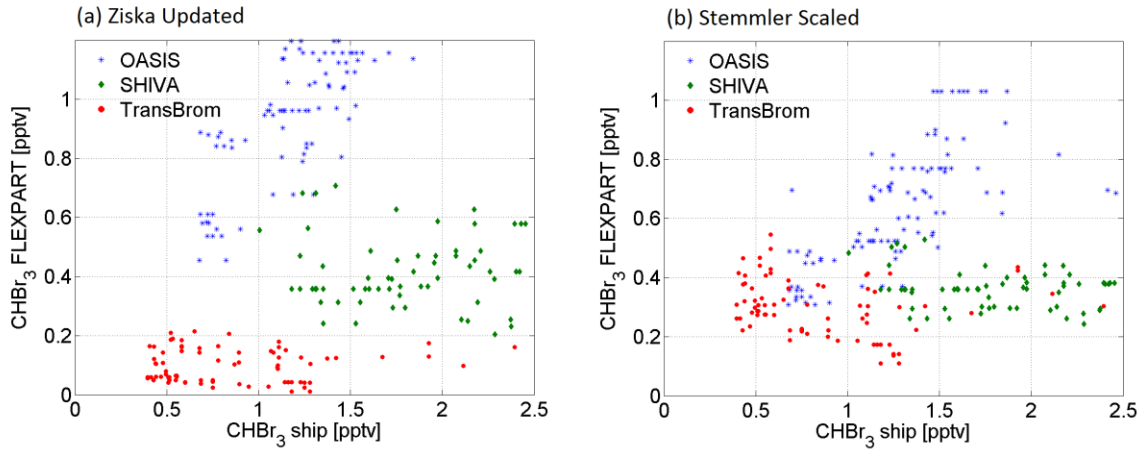


Figure S3: Comparison of bromoform volume mixing ratios at 1 km height from monthly emissions and ship cruise measurements in the Indian Ocean (OASIS), the South China and Sulu Seas (SHIVA), and the west Pacific (TransBrom). The Flexpart output was sampled in the grid cell of the observation during the month of the cruise, but in 2014.

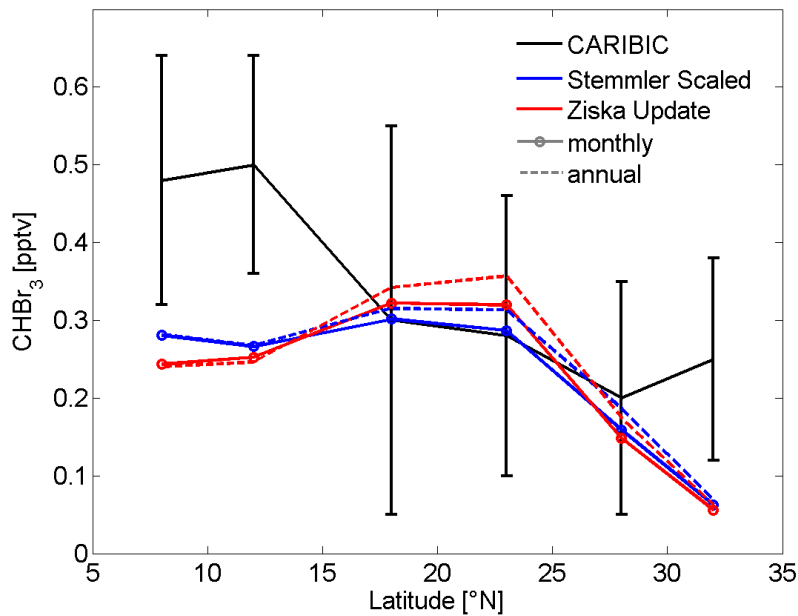


Figure S4: CARIBIC aircraft measurements of bromoform on Southeast Asian flights for November and December 2012 and February 2013 at about 11 km height averaged in 5° latitude bins taken from Wisher et al. (2014). Stemmler Scaled and Ziska Update CHBr₃ mixing ratio at 11 km averaged in 5°x5° boxes around the measurement locations in February, November, and December of 2014.

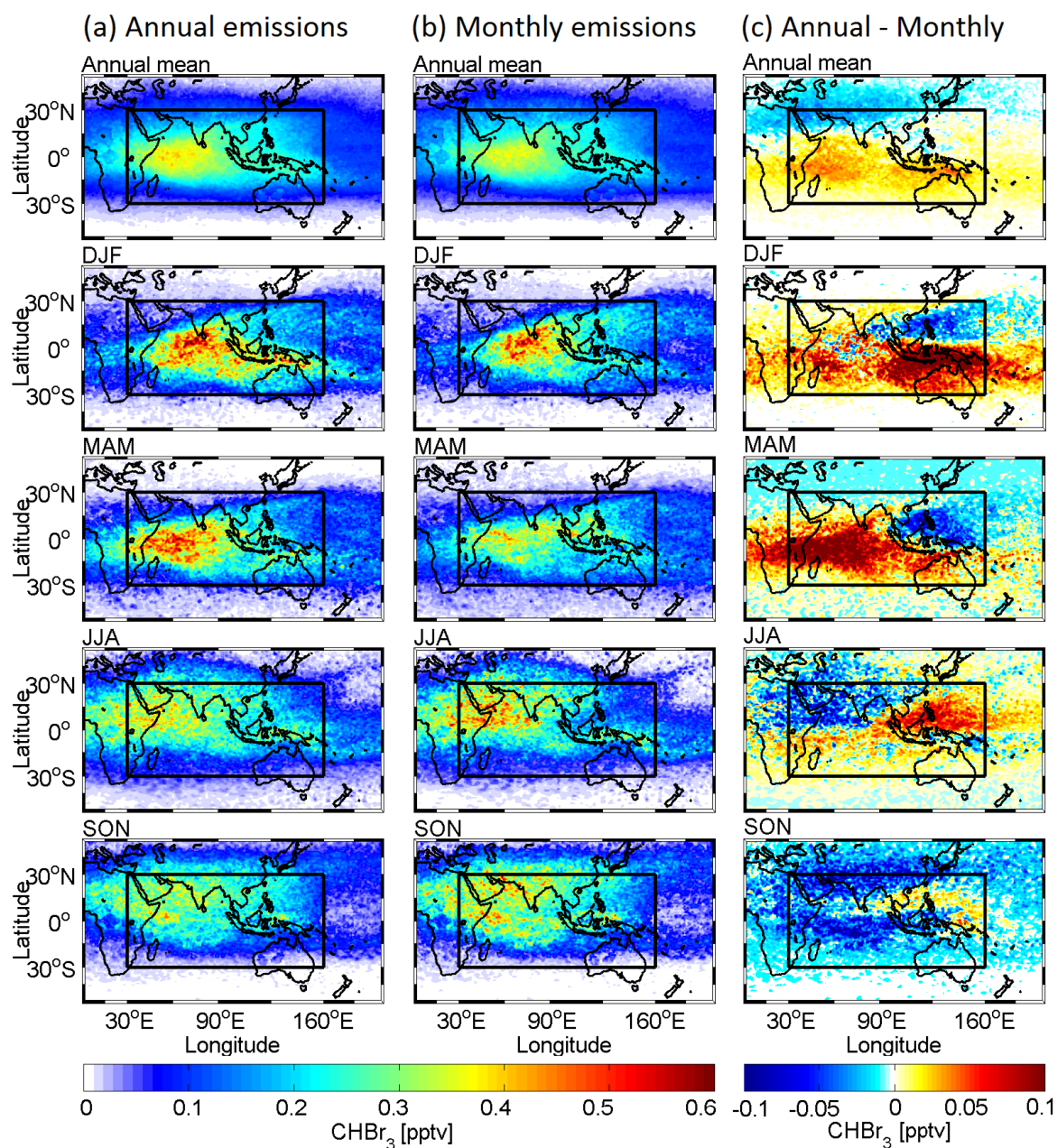


Figure S5: Bromoform volume mixing ratios (VMR) at 17 km for the Stemmler Scaled (a) annual emissions and (b) monthly emissions and (c) the difference between the two scenarios. The black box depicts the IO/WP release area.

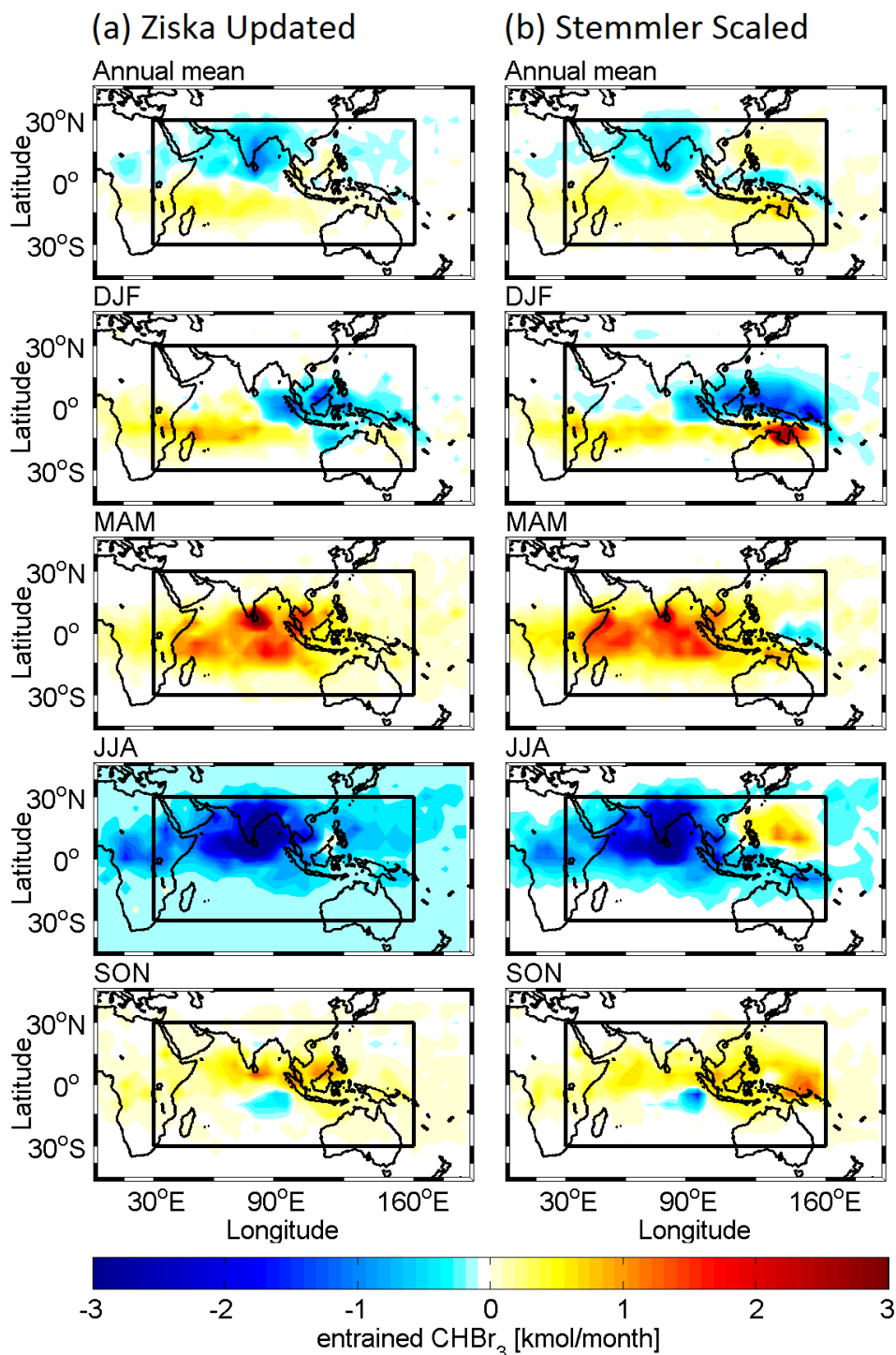


Figure S6: Bromoform entrainment anomalies at the CPT between annual and monthly emissions for (a) Ziska Updated and (b) Stemmler Scaled inventories.

Wisher, A., Oram, D. E., Laube, J. C., Mills, G. P., van Velthoven, P., Zahn, A., and Brenninkmeijer, C. A. M.: Very short-lived bromomethanes measured by the CARIBIC observatory over the North Atlantic, Africa and Southeast Asia during 2009–2013, *Atmos. Chem. Phys.*, 14, 3557–3570, 10.5194/acp-14-3557-2014, 2014.

4 Summary, Conclusions, and Outlook

Summary

Seven questions were addressed in this thesis and their answers, summarized from the manuscripts, are given in the following.

1. How strong are VSLs emissions from the West Indian Ocean (WIO)?

During the OASIS cruise in the subtropical and tropical WIO in July and August 2014, oceanic concentrations and atmospheric mixing ratios of the four VSLs CHBr_3 , CH_2Br_2 , CH_3I , and DMS were measured and emissions were calculated with an air-sea gas exchange parameterization. DMS direct fluxes were also observed with the eddy-covariance technique. For CHBr_3 and CH_2Br_2 these were the first measurements in the southern subtropical and tropical West Indian Ocean. The emissions of CHBr_3 were at the upper end of previous tropical measurements and estimates, while CH_2Br_2 emissions were the highest emissions reported so far. CH_3I emissions were in the range of previously published datasets. Eddy-covariance derived DMS emissions confirmed that the Indian Ocean is a hot spot emission region during boreal summer despite the emissions being lower than in the climatology from Lana et al. (2011) (Zavarsky et al., under review at GRL). We identified the coastal upwelling southeast of Madagascar and the open ocean upwelling of the Chagos-Seychelles thermocline ridge as a biologically productive region with enhanced VSLs production and emissions.

2. What are the transport pathways in the atmosphere above the West Indian Ocean during summer monsoon?

The transport of VSLs emissions was modeled with the Lagrangian particle dispersion model FLEXPART using ERA-Interim reanalysis meteorological fields. The Asian summer monsoon transport from the tropical West Indian Ocean to the stratosphere during 2014 occurs along two pathways: Either via local convection around the equator, or with the monsoon circulation towards India and the Bay of Bengal close to the surface and from there upwards with the summer monsoon convection into the Asian monsoon anticyclone. The first pathway is fast (0-2 days) and, therefore, more important for the shorter-lived VSLs' CH_3I and DMS, while the second pathway takes more time (4-12 days) and is more relevant for the transport of the longer-lived VSLs CHBr_3 and CH_2Br_2 .

3. How large is the intra- and interannual variability of VSLs transport from the WIO to the stratosphere?

The transport of artificial “VSLs tracers” applying lifetimes of DMS, CH₃I, CHBr₃, and CH₂Br₂ on air mass transport from a large area of the tropical WIO to the stratosphere from 2000-2015 using FLEXPART and ERA-Interim was investigated. The strength of transport was described through the transport efficiency, defined as the amount of VSLs tracer entrained to the stratosphere divided by the amount released from the ocean. The most important characteristic of transport variability from the WIO is the pronounced annual cycle. The interannual variability of transport to the stratosphere is less pronounced than the annual cycle. Interannual variability is strongest during boreal fall and winter. The intra- and interannual variability is larger the shorter the lifetime of the VSLs tracer.

4. Which is the main stratospheric entrainment season from the West Indian Ocean?

The transport efficiency from the West Indian Ocean displays a maximum during boreal winter and spring, when the convection resides over the release locations in the ocean. The transport efficiency is minimal during summer monsoon and boreal fall, when the convection is farther away from the release area. The seasonality strongly depends on the location of the emission region and is different when investigating emissions from the whole tropical Indian Ocean.

5. What causes the variability of VSLs transport to the stratosphere above the Indian Ocean?

The strong annual cycle of VSLs tracer transport efficiency from the WIO to the stratosphere is driven by the annual reversal of winds and displacement of deep convection by the Indian Monsoon and the local ocean heat content. It correlates well with the annual cycle of the Indian Monsoon Index and the All-India Rainfall Index, as well as the sea surface temperature (SST) in the WIO release area. The time series of transport efficiency displays a small increase over the 16 year period, which might be driven by the long-term changes of the Asian monsoon. A weakening of the monsoon circulation shortens the summer monsoon transport pathway and warming SST in the WIO enhances vertical uplift, which both increases stratospheric entrainment of VSLs. The interannual variability of transport efficiency is influenced by the SST in the WIO and equatorial Pacific. High local SST enhances the transport to the stratosphere,

especially in boreal spring, when the deep convection is directly above the WIO. During boreal winter and spring, stratospheric entrainment of the VSLS tracers from the WIO is also enhanced by positive SST anomalies in the equatorial Pacific, an El Niño. The relatively warm SST in the East Pacific influences the Walker circulation and the SST in the IO, which both enhance uplift over the WIO. During boreal summer and fall, negative SST anomalies in the Pacific Ocean, a La Niña, increase VSLS tracer delivery from the WIO to the stratosphere, because the Walker circulation strengthens the monsoon flow from the Indian Ocean to the Indian subcontinent, prolonging and bolstering the monsoon convection and VSLS transport pathways to the stratosphere.

6. Which are the main oceanic source regions in the Indian Ocean for stratospheric CHBr_3 and where do they enter the stratosphere?

Annual and monthly CHBr_3 emission fields for the tropical Indian Ocean and West Pacific (IO/WP) were compiled based on the new OASIS observations. With the help of FLEXPART/ERA-Interim, the transport of these emissions to the stratosphere was calculated for the year 2014. The highest transport efficiency is simulated for the tropical North West Pacific, but the Bay of Bengal and Arabian Sea are also efficient during June to August (JJA). Comparing the delivery of CHBr_3 to the stratosphere, the Bay of Bengal and the Arabian Sea are the most important source regions, because of the high emissions in these basins driven by the monsoon winds and the Somali Jet during boreal summer. In our calculations, the tropical West Pacific delivers less CHBr_3 to the stratosphere due to the low assumed emissions in this region. The main stratospheric entrainment region of CHBr_3 from IO/WP lies above the southern tip of the Indian subcontinent where maximum entrainment occurs during JJA. There is secondary entrainment maximum over the tropical West Pacific, but its strength strongly depends on the underlying emissions in the emission inventory.

7. What is the influence of annual vs. monthly representation of CHBr_3 emissions on stratospheric entrainment through the Asian monsoon?

For this question, CHBr_3 emission fields with annual and monthly temporal resolution were used. Monthly emissions display an absolute maximum in July and a local maximum in January. The annual cycle of transport efficiency shows almost the same seasonality as the oceanic emissions. Together this results in a stronger seasonality in the stratospheric entrainment of CHBr_3 for the calculations with monthly emissions than

annual emissions. The total annual amount of CHBr_3 entrained to the stratosphere is similar for both emission scenarios. The different seasonality is also reflected in the differing distribution of CHBr_3 at the tropopause. Monthly emissions lead to higher CHBr_3 volume mixing ratios in the Asian monsoon anticyclone during JJA and north of 15°N in the annual mean and lower mixing ratios at the equatorial and southern hemispheric tropopause than annual emissions. In the Asian monsoon region, the seasons and regions of CHBr_3 emissions from the ocean play a large role in the temporal and spatial distribution of stratospheric entrainment.

Through this thesis and the incorporated four manuscripts, I contributed to the scientific understanding of VSLS emissions from the Indian Ocean and their transport to the stratosphere through the Asian monsoon. First measurements of CHBr_3 and CH_2Br_2 were conducted and CH_3I and DMS observations were added to the sparse data coverage in the Indian Ocean (Manuscripts 1 & 2). These observations confirmed the expected strong VSLS sources from the subtropical and tropical West Indian Ocean with regional hot spots during boreal summer. Furthermore, this thesis advanced the understanding of VSLS transport through the Asian monsoon in various aspects. Manuscript 1 identified transport pathways during the Asian summer monsoon and showed that for the shorter-lived VSLS CH_3I and DMS the co-occurrence of convection at the location of strong emission is important for stratospheric delivery. The pronounced Asian monsoon circulation during summer, thus, transports mainly longer-lived VSLS, such as CHBr_3 and CH_2Br_2 , from a large area of the tropical Indian Ocean and West Pacific to the stratosphere. While previous air mass transport studies mainly focused on the Asian summer monsoon, this thesis investigated the strong annual cycle of VSLS transport from the tropical West Indian Ocean to the stratosphere in Manuscript 3. A 16-year time series of interannual transport variability for VSLS through the Asian monsoon was compiled. A modulation of stratospheric VSLS entrainment strength by ENSO was shown. For Manuscript 4, available emission inventories were updated with the new observations from the subtropical and tropical West Indian Ocean. While some VSLS transport studies already use seasonally resolved oceanic VSLS emissions (Tegtmeier et al., 2015; Hossaini et al., 2016), Manuscript 4 is the first study investigating the differences between annual and monthly bromoform emissions on stratospheric entrainment.

Conclusions

The results from this thesis help determining the importance of the Indian Ocean as a VSLs source for the atmosphere and the efficiency of the Asian monsoon in transporting VSLs to the stratosphere. Now, I can use my studies to answer the overarching research question:

How important are oceanic VSLs emissions from the Indian Ocean for their stratospheric loading?

To infer the Indian Ocean contribution to global VSLs emissions, I use the update of the annual halogenated VSLs emission climatology from Ziska et al. (2013), created for Manuscript 4 as “Ziska Update”, and the Lana et al. (2011) monthly DMS emission inventory (Table 11). I define the tropical Indian Ocean area investigated here as all ocean surface inside 30°S-30°N and 30°E-100°E, which is $3.37 \cdot 10^{13} \text{ m}^2$ large. Compared to the area of the global oceans this is 9.4 %, compared to the tropical oceans (30°S-30°N) it is 17.7 %. I added this comparison between Indian Ocean and tropical ocean contribution, because the emissions in the tropics are more important for stratospheric entrainment than emissions at higher latitudes. The Indian Ocean (IO) contribution is the IO emissions divided by the global/tropical emissions. According to the above mentioned emission inventories, the Indian Ocean represents an important region for VSLs flux from the ocean to the atmosphere (Table 11). Emissions from the IO contribute significantly to the global and tropical CHBr_3 emissions, with 27% and 31%, respectively.

Table 11: VSLs emissions from the annual mean update of the climatology from Ziska et al. (2013) for the halocarbons and from Lana et al. (2011) monthly emissions for DMS. Total annual emissions are given for the Indian Ocean (IO: 30°S-30°N, 30°E-100°E), the global oceans, and the tropical oceans. The IO global contribution is the IO emission divided by global emission and the IO tropical contribution is the IO emission divided by the tropical emission.

VSLs	Unit	IO emission	Global emission	IO global contrib.	Tropical emission	IO tropical contribution
Ocean area	m^2	$3.37 \cdot 10^{13}$	$3.6 \cdot 10^{14}$	9.4%	$1.9 \cdot 10^{14}$	17.7 %
CHBr_3	Mmol Br yr^{-1}	502	1840	27 %	1620	31 %
CH_2Br_2	Mmol Br yr^{-1}	146	957	15 %	575	25 %
CH_3I	Mmol I yr^{-1}	101	1319	8 %	652	15 %
DMS	Gmol S yr^{-1}	118	886	13 %	473	25 %

CH_2Br_2 and DMS emission contribution from the Indian Ocean are also larger than the area fraction of the Indian Ocean towards both global and tropical oceans. This means that the Indian Ocean emissions are higher than the average global and tropical emissions. Only CH_3I emissions are lower than the global and tropical averages, probably because CH_3I emissions are highest in the subtropics and midlatitudes and do not have a tropical maximum (Ziska et al., 2013). The Indian Ocean has the potential to influence the stratosphere more than other oceanic regions, if the atmospheric transport efficiently delivers the high VSLS emissions to the stratosphere.

Next, I compare the transport of VSLS from the Indian Ocean region to the stratosphere with the global stratospheric VSLS delivery (Table 12). I use the trajectories calculated with FLEXPART/ERA-Interim for the year 2014 in Manuscript 4. The climatological emissions for CHBr_3 , CH_2Br_2 , and CH_3I from the Ziska Update (Fiehn et al., to be submitted) and for DMS from Lana et al. (2011) from the above mentioned IO area are attached to the trajectories and exponentially reduced with lifetimes of 1day (DMS), 3.5 days (CH_3I), 17 days (CHBr_3), and 150 days (CH_2Br_2), as in Manuscript 3. The annual entrained mass of VSLS is given by the trajectories reaching above the CPT. Calculated transport efficiencies for the whole Indian Ocean are similar to the transport efficiencies for the West Indian Ocean (WIO) release area (Table 1 in Manuscript 3). Marandino et al. (2013) modelled a DMS transport efficiency of 0.48 % in the tropical West Pacific, which is a high estimate because boreal winter is the season with most convection in that region. I determine the volume mixing ratio of the mass entrained from the Indian Ocean into the global stratosphere by dividing through the number of particles in the entire stratosphere of $2.7 \cdot 10^{19}$ mol (Jacob, 1999). The global VMR is taken from literature values (Carpenter et al., 2014; Sheng et al., 2015; Hossaini et al., 2016) and represents the stratospheric volume mixing ratio from global emissions. The IO contribution to the global entrainment is the ratio between the calculated IO and global VMR and gives the contribution of the Indian Ocean to the stratospheric abundances of bromine, iodine, and sulfur from VSLS estimated with this rough estimate.

Table 12: VSLS emissions from the Indian Ocean from Table 11 and their mass entrained above the CPT between 30°S and 30°N in 2014 calculated with FLEXPART/ERA-Interim plus the transport efficiency. The IO VMR is the IO entrainment converted into VMR using the total number of particles in the stratosphere. The global VMR are from literature. The IO contribution is the IO VMR divided by the global VMR.

Comp.	IO emiss.	IO entrainm.	Transport efficiency	IO VMR [pptv]	Global VMR [pptv]	IO contrib.
CHBr ₃	502 ¹	11.6 ¹	2.3 %	0.43	0.60 ^o	72 %
CH ₂ Br ₂	146 ¹	9.2 ¹	6.6 %	0.34	1.46 ^o	23 %
Br _y ^{VSLS}	648 ¹	20.8 ¹	3.2 %	0.77	0.7-3.4*	23-110 %
CH ₃ I	101 ²	0.6 ²	0.6 %	0.02	<0.05*	40 %
DMS	118 ³	164 ⁴	0.1 %	6.07	5.07 ^Δ	120 %

¹ Mmol Br yr⁻¹, ² Mmol I yr⁻¹, ³ Gmol S yr⁻¹, ⁴ Mmol S yr⁻¹, ^o (Hossaini et al., 2016), * (Carpenter et al., 2014),

^Δ converted from global DMS entrainment of 4.4 Gg S yr⁻¹ (Sheng et al., 2015)

The Indian Ocean contribution to stratospheric VMR can be compared to the Indian Ocean area ratio with the tropical oceans of 17.7% (Table 11) to determine the importance of emissions and entrainment from the Indian Ocean. According to my entrainment estimates the Indian Ocean emissions contribute around 72 % to stratospheric CHBr₃. From the combined VSLS source gases CHBr₃ and CH₂Br₂ (Br_y^{VSLS}), 23 % to 110% of total stratospheric bromine originate from the Indian Ocean and methyl iodide from the Indian Ocean contributes with 40%. This depicts that the emissions and transport to the stratosphere from the Indian Ocean through the Asian monsoon is more efficient than on average over the whole tropics. The contribution of DMS from the Indian Ocean is higher than the total global entrained DMS. This might result from the high Indian Ocean emissions in the Lana et al. (2011) inventory compared to our in-situ measurements (Manuscript 2), the overestimation of transport efficiency of our FLEXPART/ERA-Interim calculations, or the uncertainty in the stratospheric entrainment of DMS. It shows that the Indian Ocean is probably an important contributor to stratospheric sulfur from DMS source gas injection.

In conclusion, I determine that the Indian Ocean is an important source region for VSLS delivery to the stratosphere and that the Asian Monsoon circulation efficiently

transports VSLS into the stratosphere. The combination of both phenomena makes the Indian Ocean an important source region, especially during the summer monsoon when high wind speeds maximize emissions and the upward transport through the monsoon convection and the Asian monsoon anticyclone is most pronounced.

Outlook

This thesis newly combines two scientific fields: the contribution of oceanic VSLS to stratospheric loading of bromine, iodine, and sulfur, and the Asian monsoon transport to the stratosphere and its variability. The results of this work reduce the uncertainties of oceanic VSLS emissions from the undersampled region of the Indian Ocean through novel observations. The combination of new emission inventories with a Lagrangian dispersion model enables us to identify efficient oceanic source regions and transport pathways. This thesis also depicts where uncertainties still exist and on what future research should focus. Since the contribution of the Indian Ocean to stratospheric VSLS is significant, it is important to reduce existing uncertainties in emissions and transport pathways from the tropical Indian Ocean and West Pacific to the stratosphere.

The trajectory simulations for the Indian Ocean and West Pacific (Manuscript 4) determined that the tropical West Pacific is the most efficient region at transporting CHBr_3 from the ocean surface to the stratosphere. At the same time the available emission inventories show large differences in this region (range: -300 to $1100 \text{ pmol m}^{-2} \text{ h}^{-1}$, from Table 2 in Manuscript 4) (Liang et al., 2010; Ziska et al., 2013; Stemmler et al., 2015), which significantly impacts the amount and distribution of CHBr_3 entrained to the stratosphere. Future research should try to constrain the emission estimate for this important source region through in situ ship and aircraft measurement during different seasons and years. Main source regions for the Asian summer monsoon convection, as an efficient pathway for VSLS to the stratosphere, are the Bay of Bengal and the Arabian Sea, where VSLS emissions are likewise uncertain. Future observations in this region during boreal summer would be very profitable. The general poor coverage with observations in time and space could be addressed through permanent monitoring stations for VSLS emissions.

Chemistry climate and transport model uncertainties in the UTLS mixing ratios are large and do not only result from differences between the emission inventories (Hossaini et al., 2016). There is great need for observations in the Asian tropopause layer and lower

stratosphere to verify model calculations. My thesis adds a first estimate of the contribution of Indian Ocean emissions to the VSLS mixing ratios in the Asian monsoon anticyclone, which has been identified as important transport pathway from the land surface to the stratosphere (Randel et al., 2010; Pan et al., 2016). The thesis results will be available for comparison with aircraft campaigns, such as the recent StratoClim campaign, which took place over Nepal and India during boreal summer 2017 and focused on atmospheric composition in the Asian monsoon anticyclone.

In this thesis, I investigated source gas injection of VSLS only. There is also a contribution to the stratospheric VSLS abundances from VSLS product gases. A next step in modeling these would be to include chemical reactions and microphysics in FLEXPART. Then, an estimate of both source and product gas injection and the attribution of sources, chemical products, entrainment regions, and ozone depletion would be possible. This will further improve the understanding of the contribution of oceanic VSLS emissions to the stratospheric halogen and sulfur loading.

5 References

- Abrahamsson, K., A. Lorén, A. Wulff, and S.-Å. Wängberg: Air–sea exchange of halocarbons: the influence of diurnal and regional variations and distribution of pigments, *Deep Sea Research Part II: Topical Studies in Oceanography*, 51, 2789-2805, <https://doi.org/10.1016/j.dsr2.2004.09.005>, 2004.
- Amachi, S., Y. Kamagata, T. Kanagawa, and Y. Muramatsu: Bacteria mediate methylation of iodine in marine and terrestrial environments, *Applied and environmental microbiology*, 67, 2718-2722, 10.1128/AEM.67.6.2718-2722.2001, 2001.
- Aschmann, J., B.-M. Sinnhuber, E. Atlas, and S. Schauffler: Modeling the transport of very short-lived substances into the tropical upper troposphere and lower stratosphere, *Atmos. Chem. Phys.*, 9, 9237-9247, 2009.
- Aschmann, J., B. M. Sinnhuber, M. P. Chipperfield, and R. Hossaini: Impact of deep convection and dehydration on bromine loading in the upper troposphere and lower stratosphere, *Atmos. Chem. Phys.*, 11, 2671-2687, 10.5194/acp-11-2671-2011, 2011.
- Aschmann, J., and B. M. Sinnhuber: Contribution of very short-lived substances to stratospheric bromine loading: uncertainties and constraints, *Atmos. Chem. Phys.*, 13, 1203-1219, 10.5194/acp-13-1203-2013, 2013.
- Ashok, K., Z. Guan, and T. Yamagata: Impact of the Indian Ocean dipole on the relationship between the Indian monsoon rainfall and ENSO, *Geophysical Research Letters*, 28, 4499-4502, 10.1029/2001gl013294, 2001.
- Barnes, I., K. H. Becker, and I. Patroescu: The tropospheric oxidation of dimethyl sulfide: A new source of carbonyl sulfide, *Geophysical Research Letters*, 21, 2389-2392, 10.1029/94gl02499, 1994.
- Barnes, I., J. Hjorth, and N. Mihalopoulos: Dimethyl Sulfide and Dimethyl Sulfoxide and Their Oxidation in the Atmosphere, *Chemical Reviews*, 106, 940-975, 10.1021/cr020529+, 2006.
- Bates, T. S., R. P. Kiene, G. V. Wolfe, P. A. Matrai, F. P. Chavez, K. R. Buck, B. W. Blomquist, and R. L. Cuhel: The cycling of sulfur in surface seawater of the northeast Pacific, *Journal of Geophysical Research: Oceans*, 99, 7835-7843, 10.1029/93jc02782, 1994.
- Behera, S. K., R. Krishnan, and T. Yamagata: Unusual ocean-atmosphere conditions in the tropical Indian Ocean during 1994, *Geophysical Research Letters*, 26, 3001-3004, 10.1029/1999gl010434, 1999.
- Bell, N., L. Hsu, D. J. Jacob, M. G. Schultz, D. R. Blake, J. H. Butler, D. B. King, J. M. Lobert, and E. Maier-Reimer: Methyl iodide: Atmospheric budget and use as a tracer of marine convection in global models, *Journal of Geophysical Research: Atmospheres*, 107, ACH 8-1-ACH 8-12, 10.1029/2001jd001151, 2002.
- Bergman, J. W., E. J. Jensen, L. Pfister, and Q. Yang: Seasonal differences of vertical-transport efficiency in the tropical tropopause layer: On the interplay between tropical deep convection, large-scale vertical ascent, and horizontal circulations, *Journal of Geophysical Research: Atmospheres*, 117, D05302, 10.1029/2011jd016992, 2012.
- Bergman, J. W., F. Fierli, E. J. Jensen, S. Honomichl, and L. L. Pan: Boundary layer sources for the Asian anticyclone: Regional contributions to a vertical conduit, *Journal of Geophysical Research: Atmospheres*, 118, 2560-2575, 10.1002/jgrd.50142, 2013.
- Bjerknes, J.: Atmospheric teleconnections from the equatorial Pacific, *Monthly Weather Review*, 97, 163-172, 10.1175/1520-0493(1969)097<0163:atftpe>2.3.co;2, 1969.
- Blomquist, B. W., C. W. Fairall, B. J. Huebert, D. J. Kieber, and G. R. Westby: DMS sea-air transfer velocity: Direct measurements by eddy covariance and parameterization based on the NOAA/COARE gas transfer model, *Geophysical Research Letters*, 33, L07601, 10.1029/2006gl025735, 2006.
- Bösch, H., C. Camy-Peyret, M. P. Chipperfield, R. Fitzenberger, H. Harder, U. Platt, and K. Pfeilsticker: Upper limits of stratospheric IO and OIO inferred from center-to-limb-darkening-corrected balloon-borne solar occultation visible spectra: Implications for total

- gaseous iodine and stratospheric ozone, *Journal of Geophysical Research: Atmospheres*, 108, D154455, 10.1029/2002jd003078, 2003.
- Bourassa, A. E., A. Robock, W. J. Randel, T. Deshler, L. A. Rieger, N. D. Lloyd, E. J. Llewellyn, and D. A. Degenstein: Large Volcanic Aerosol Load in the Stratosphere Linked to Asian Monsoon Transport, *Science*, 337, 78-81, 10.1126/science.1219371, 2012.
- Braesicke, P., J. Keeble, X. Yang, G. Stiller, S. Kellmann, N. L. Abraham, A. Archibald, P. Telford, and J. A. Pyle: Circulation anomalies in the Southern Hemisphere and ozone changes, *Atmos. Chem. Phys.*, 13, 10677-10688, 10.5194/acp-13-10677-2013, 2013.
- Brewer, A. W.: Evidence for a world circulation provided by the measurements of helium and water vapour distribution in the stratosphere, *Quarterly Journal of the Royal Meteorological Society*, 75, 351-363, 10.1002/qj.49707532603, 1949.
- Brinckmann, S., A. Engel, H. Bönisch, B. Quack, and E. Atlas: Short-lived brominated hydrocarbons—observations in the source regions and the tropical tropopause layer, *Atmos. Chem. Phys.*, 12, 1213-1228, 2012.
- Bruce, J. G.: Large-scale variations of the Somali current during the southwest monsoon, 1970, *Deep Sea Research and Oceanographic Abstracts*, 20, 837-846, [https://doi.org/10.1016/0011-7471\(73\)90005-3](https://doi.org/10.1016/0011-7471(73)90005-3), 1973.
- Butler, J. H., D. B. King, J. M. Lobert, S. A. Montzka, S. A. Yvon-Lewis, B. D. Hall, N. J. Warwick, D. J. Mondeel, M. Aydin, and J. W. Elkins: Oceanic distributions and emissions of short-lived halocarbons, *Global Biogeochemical Cycles*, 21, GB1023, 10.1029/2006gb002732, 2007.
- Butz, A., H. Bösch, C. Camy-Peyret, M. P. Chipperfield, M. Dorf, S. Kreycky, L. Kritten, C. Prados-Román, J. Schwärzle, and K. Pfeilsticker: Constraints on inorganic gaseous iodine in the tropical upper troposphere and stratosphere inferred from balloon-borne solar occultation observations, *Atmos. Chem. Phys.*, 9, 7229-7242, 10.5194/acp-9-7229-2009, 2009.
- Carpenter, L. J., W. T. Sturges, S. A. Penkett, P. S. Liss, B. Alicke, K. Hebestreit, and U. Platt: Short-lived alkyl iodides and bromides at Mace Head, Ireland: Links to biogenic sources and halogen oxide production, *Journal of Geophysical Research: Atmospheres*, 104, 1679-1689, 10.1029/98jd02746, 1999.
- Carpenter, L. J., and P. S. Liss: On temperate sources of bromoform and other reactive organic bromine gases, *Journal of Geophysical Research: Atmospheres*, 105, 20539-20547, 10.1029/2000jd900242, 2000.
- Carpenter, L. J., C. Jones, R. Dunk, K. Hornsby, and J. Woeltjen: Air-sea fluxes of biogenic bromine from the tropical and North Atlantic Ocean, *Atmos. Chem. Phys.*, 9, 1805-1816, 2009.
- Carpenter, L. J., S. Reimann, J. B. Burkholder, C. Clerbaux, B. D. Hall, R. Hossaini, J. C. Laube, and S. A. Yvon-Lewis: Ozone-Depleting Substances (ODSs) and other gases of interest to the Montreal Protocol, in: *Scientific Assessment of Ozone Depletion: 2014. Global Ozone Research and monitoring Project - Report N. 55*, World Meteorological Organization, Geneva, Switzerland, 2014.
- Charlson, R. J., J. E. Lovelock, M. O. Andreae, and S. G. Warren: Oceanic phytoplankton, atmospheric sulphur, cloud albedo and climate, *Nature*, 326, 655-661, 1987.
- Chatfield, R. B., and P. J. Crutzen: Sulfur dioxide in remote oceanic air: Cloud transport of reactive precursors, *Journal of Geophysical Research: Atmospheres*, 89, 7111-7132, 10.1029/JD089iD05p07111, 1984.
- Chen, B., X. Xu, S. Yang, and T. Zhao: Climatological perspectives of air transport from atmospheric boundary layer to tropopause layer over Asian monsoon regions during boreal summer inferred from Lagrangian approach, *Atmos. Chem. Phys.*, 12, 5827-5839, 2012.
- Christensen, J. H., K. K. Kumar, E. Aldrian, S.-I. An, I. F. A. Cavalcanti, M. d. Castro, W. Dong, P. Goswami, A. Hall, J. K. Kanyanga, A. Kitoh, J. Kossin, N.-C. Lau, J. Renwick, D. B. Stephenson, S.-P. Xie, and T. Zhou: Climate Phenomena and their Relevance for Future Regional Climate Change, *Climate Change 2013: The Physical Science Basis. Contribution of Working Group I to the Fifth Assessment Report of the*

- Intergovernmental Panel on Climate Change, edited by: Stocker, T. F., D. Qin, G.-K. Plattner, M. Tignor, S.K. Allen, J. Boschung, A. Nauels, Y. Xia, V. Bex and P.M. Midgley, Cambridge University Press, Cambridge, United Kingdom and New York, NY, USA, 2013.
- Chubachi, S.: Preliminary result of ozone observations at Syowa Station from February 1982 to January 1983, *Memoirs of National Institute of Polar Research*. Special issue, 34, 13-19, 1984.
- Crutzen, P. J.: The possible importance of CSO for the sulfate layer of the stratosphere, *Geophysical Research Letters*, 3, 73-76, 10.1029/GL003i002p00073, 1976.
- De Bruyn, W. J., E. Swartz, J. H. Hu, J. A. Shorter, P. Davidovits, D. R. Worsnop, M. S. Zahniser, and C. E. Kolb: Henry's law solubilities and Setchenow coefficients for biogenic reduced sulfur species obtained from gas-liquid uptake measurements, *Journal of Geophysical Research: Atmospheres*, 100, 7245-7251, 10.1029/95jd00217, 1995.
- Devasthale, A., and S. Fueglistaler: A climatological perspective of deep convection penetrating the TTL during the Indian summer monsoon from the AVHRR and MODIS instruments, *Atmos. Chem. Phys.*, 10, 4573-4582, 10.5194/acp-10-4573-2010, 2010.
- Dobson, G. M. B.: Origin and Distribution of the Polyatomic Molecules in the Atmosphere, *Proceedings of the Royal Society of London. Series A, Mathematical and Physical Sciences*, 236, 187-193, 1956.
- Donner, L. J., L. W. Horowitz, A. M. Fiore, C. J. Seman, D. R. Blake, and N. J. Blake: Transport of radon-222 and methyl iodide by deep convection in the GFDL Global Atmospheric Model AM2, *Journal of Geophysical Research: Atmospheres*, 112, D17303, 10.1029/2006jd007548, 2007.
- Dorf, M., J. H. Butler, A. Butz, C. Camy-Peyret, M. P. Chipperfield, L. Kritten, S. A. Montzka, B. Simmes, F. Weidner, and K. Pfeilsticker: Long-term observations of stratospheric bromine reveal slow down in growth, *Geophysical Research Letters*, 33, L24803, 10.1029/2006gl027714, 2006.
- Dunkerton, T. J.: Evidence of meridional motion in the summer lower stratosphere adjacent to monsoon regions, *Journal of Geophysical Research: Atmospheres*, 100, 16675-16688, 10.1029/95jd01263, 1995.
- Farman, J. C., B. G. Gardiner, and J. D. Shanklin: Large losses of total ozone in Antarctica reveal seasonal ClO_x/NO_x interaction, *Nature*, 315, 207-210, 1985.
- Fernandez, R. P., D. E. Kinnison, J. F. Lamarque, S. Tilmes, and A. Saiz-Lopez: Impact of biogenic very short-lived bromine on the Antarctic ozone hole during the 21st century, *Atmos. Chem. Phys.*, 17, 1673-1688, 10.5194/acp-17-1673-2017, 2017.
- Fiehn, A., B. Quack, H. Hepach, S. Fuhlbrügge, S. Tegtmeier, M. Toohey, E. Atlas, and K. Krüger: Delivery of halogenated very short-lived substances from the west Indian Ocean to the stratosphere during the Asian summer monsoon, *Atmos. Chem. Phys.*, 17, 6723-6741, 10.5194/acp-17-6723-2017, 2017.
- Fiehn, A., B. Quack, I. Stemmler, and K. Krüger: Importance of seasonally resolved oceanic emissions for VSLs delivery from the Indian Ocean to the stratosphere, *Atmos. Chem. Phys. Discuss.*, to be submitted.
- Fiehn, A., B. Quack, C. A. Marandino, and K. Krüger: Variability of VSLs transport from the Indian Ocean to the stratosphere, *Journal of Geophysical Research: Atmospheres*, under review.
- Fogelqvist, E., B. Josefsson, and C. Roos: Halocarbons as tracer substances in studies of the distribution patterns of chlorinated waters in coastal areas, *Environmental Science & Technology*, 16, 479-482, 1982.
- Fogelqvist, E., and M. Krysell: Naturally and anthropogenically produced bromoform in the Kattegatt, a semi-enclosed oceanic basin, *Journal of Atmospheric Chemistry*, 13, 315-324, 10.1007/bf00057749, 1991.
- Folkens, I., M. Loewenstein, J. Podolske, S. J. Oltmans, and M. Proffitt: A barrier to vertical mixing at 14 km in the tropics: Evidence from ozonesondes and aircraft measurements, *Journal of Geophysical Research: Atmospheres*, 104, 22095-22102, 10.1029/1999jd900404, 1999.

- Folkins, I., and R. V. Martin: The Vertical Structure of Tropical Convection and Its Impact on the Budgets of Water Vapor and Ozone, *Journal of the Atmospheric Sciences*, 62, 1560-1573, 10.1175/jas3407.1, 2005.
- Fueglistaler, S., M. Bonazzola, P. H. Haynes, and T. Peter: Stratospheric water vapor predicted from the Lagrangian temperature history of air entering the stratosphere in the tropics, *Journal of Geophysical Research: Atmospheres*, 110, D08107, 10.1029/2004jd005516, 2005.
- Fueglistaler, S., A. E. Dessler, T. J. Dunkerton, I. Folkins, Q. Fu, and P. W. Mote: Tropical tropopause layer, *Reviews of Geophysics*, 47, 10.1029/2008rg000267, 2009.
- Garny, H., and W. J. Randel: Transport pathways from the Asian monsoon anticyclone to the stratosphere, *Atmos. Chem. Phys.*, 16, 2703-2718, 10.5194/acp-16-2703-2016, 2016.
- Gettelman, A., and P. M. d. F. Forster: A Climatology of the Tropical Tropopause Layer, *Journal of the Meteorological Society of Japan. Ser. II*, 80, 911-924, 10.2151/jmsj.80.911, 2002.
- Glasow, R. v., and P. Crutzen: Model study of multiphase DMS oxidation with a focus on halogens, *Atmos. Chem. Phys.*, 4, 589-608, 10.5194/acp-4-589-2004, 2004.
- Gschwend, P. M., J. K. Macfarlane, and K. A. Newman: Volatile Halogenated Organic Compounds Released to Seawater from Temperate Marine Macroalgae, *Science*, 227, 1033, 10.1126/science.227.4690.1033, 1985.
- Hepach, H., B. Quack, F. Ziska, S. Fuhlbrügge, E. Atlas, K. Krüger, I. Peeken, and D. W. R. Wallace: Drivers of diel and regional variations of halocarbon emissions from the tropical North East Atlantic, *Atmos. Chem. Phys.*, 14, 1255-1275, 10.5194/acp-14-1255-2014, 2014.
- Hepach, H., B. Quack, S. Raimund, T. Fischer, E. L. Atlas, and A. Bracher: Halocarbon emissions and sources in the equatorial Atlantic Cold Tongue, *Biogeosciences*, 12, 6369-6387, 2015.
- Hoffmann, E. H., A. Tilgner, R. Schrödner, P. Bräuer, R. Wolke, and H. Herrmann: An advanced modeling study on the impacts and atmospheric implications of multiphase dimethyl sulfide chemistry, *Proceedings of the National Academy of Sciences*, 113, 11776-11781, 10.1073/pnas.1606320113, 2016.
- Holton, J. R., P. H. Haynes, M. E. McIntyre, A. R. Douglass, R. B. Rood, and L. Pfister: Stratosphere-troposphere exchange, *Reviews of Geophysics*, 33, 403-439, 10.1029/95rg02097, 1995.
- Hossaini, R., M. P. Chipperfield, B. M. Monge-Sanz, N. A. D. Richards, E. Atlas, and D. R. Blake: Bromoform and dibromomethane in the tropics: a 3-D model study of chemistry and transport, *Atmos. Chem. Phys.*, 10, 719-735, 2010.
- Hossaini, R., M. P. Chipperfield, W. Feng, T. J. Breider, E. Atlas, S. A. Montzka, B. R. Miller, F. Moore, and J. Elkins: The contribution of natural and anthropogenic very short-lived species to stratospheric bromine, *Atmos. Chem. Phys.*, 12, 371-380, 10.5194/acp-12-371-2012, 2012.
- Hossaini, R., H. Mantle, M. P. Chipperfield, S. A. Montzka, P. Hamer, F. Ziska, B. Quack, K. Krüger, S. Tegtmeier, E. Atlas, S. Sala, A. Engel, H. Bönisch, T. Keber, D. Oram, G. Mills, C. Ordóñez, A. Saiz-Lopez, N. Warwick, Q. Liang, W. Feng, F. Moore, B. R. Miller, V. Marécal, N. A. D. Richards, M. Dorf, and K. Pfeilsticker: Evaluating global emission inventories of biogenic bromocarbons, *Atmos. Chem. Phys.*, 13, 11819-11838, 10.5194/acp-13-11819-2013, 2013.
- Hossaini, R., M. P. Chipperfield, S. A. Montzka, A. Rap, S. Dhomse, and W. Feng: Efficiency of short-lived halogens at influencing climate through depletion of stratospheric ozone, *Nature Geoscience*, 8, 186-190, 10.1038/ngeo2363, 2015.
- Hossaini, R., P. K. Patra, A. A. Leeson, G. Krysztofiak, N. L. Abraham, S. J. Andrews, A. T. Archibald, J. Aschmann, E. L. Atlas, D. A. Belikov, H. Bönisch, L. J. Carpenter, S. Dhomse, M. Dorf, A. Engel, W. Feng, S. Fuhlbrügge, P. T. Griffiths, N. R. P. Harris, R. Hommel, T. Keber, K. Krüger, S. T. Lennartz, S. Maksyutov, H. Mantle, G. P. Mills, B. Miller, S. A. Montzka, F. Moore, M. A. Navarro, D. E. Oram, K. Pfeilsticker, J. A. Pyle, B. Quack, A. D. Robinson, E. Saikawa, A. Saiz-Lopez, S. Sala, B. M. Sinnhuber, S. Taguchi, S. Tegtmeier, R. T. Lidster, C. Wilson, and F. Ziska: A multi-model intercomparison of halogenated very short-lived substances (TransCom-VSLS): linking

- oceanic emissions and tropospheric transport for a reconciled estimate of the stratospheric source gas injection of bromine, *Atmos. Chem. Phys.*, 16, 9163-9187, 10.5194/acp-16-9163-2016, 2016.
- Hughes, C., D. J. Franklin, and G. Malin: Iodomethane production by two important marine cyanobacteria: *Prochlorococcus marinus* (CCMP 2389) and *Synechococcus* sp. (CCMP 2370), *Marine Chemistry*, 125, 19-25, 10.1016/j.marchem.2011.01.007, 2011.
- Hughes, C., M. Johnson, R. Utting, S. Turner, G. Malin, A. Clarke, and P. S. Liss: Microbial control of bromocarbon concentrations in coastal waters of the western Antarctic Peninsula, *Marine Chemistry*, 151, 35-46, 10.1016/j.marchem.2013.01.007, 2013.
- Jacob, D. J.: *Introduction to atmospheric chemistry*, Princeton University Press, Princeton, New Jersey, U.S., 1999.
- Jenner, H. A., C. J. L. Taylor, M. van Donk, and M. Khalanski: Chlorination by-products in chlorinated cooling water of some European coastal power stations, *Marine Environmental Research*, 43, 279-293, 10.1016/S0141-1136(96)00091-8, 1997.
- Ju, J., and J. Slingo: The Asian summer monsoon and ENSO, *Quarterly Journal of the Royal Meteorological Society*, 121, 1133-1168, 10.1002/qj.49712152509, 1995.
- Junge, C. E., C. W. Chagnon, and J. E. Manson: Stratospheric Aerosols, *Journal of Meteorology*, 18, 81-108, 10.1175/1520-0469(1961)018<0081:sa>2.0.co;2, 1961.
- Kerkweg, A., P. Jöckel, N. Warwick, S. Gebhardt, C. A. M. Brenninkmeijer, and J. Lelieveld: Consistent simulation of bromine chemistry from the marine boundary layer to the stratosphere – Part 2: Bromocarbons, *Atmos. Chem. Phys.*, 8, 5919-5939, 10.5194/acp-8-5919-2008, 2008.
- Kloster, S., J. Feichter, E. Maier-Reimer, K. Six, P. Stier, and P. Wetzel: DMS cycle in the marine ocean-atmosphere system—a global model study, *Biogeosciences*, 3, 29-51, 2006.
- Ko, M. K. W., and G. Poulet: Very Short-Lived Halogen and Sulfur Substances, in: *Scientific Assessment of Ozone Depletion: 2002. Global Ozone Research and monitoring Project - Report N. 47*, World Meteorological Organization, Geneva, Switzerland, 2003.
- Interannual Variations of Indian Summer Monsoon:
<http://www.tropmet.res.in/~kolli/MOL/Monsoon/> Historical/air.html, access: 14.09.2017, 2016.
- Kremser, S., L. W. Thomason, M. von Hobe, M. Hermann, T. Deshler, C. Timmreck, M. Toohey, A. Stenke, J. P. Schwarz, R. Weigel, S. Fueglistaler, F. J. Prata, J.-P. Vernier, H. Schlager, J. E. Barnes, J.-C. Antuña-Marrero, D. Fairlie, M. Palm, E. Mahieu, J. Notholt, M. Rex, C. Bingen, F. Vanhellefont, A. Bourassa, J. M. C. Plane, D. Klocke, S. A. Carn, L. Clarisse, T. Trickl, R. Neely, A. D. James, L. Rieger, J. C. Wilson, and B. Meland: Stratospheric aerosol—Observations, processes, and impact on climate, *Reviews of Geophysics*, 54, 278-335, 10.1002/2015rg000511, 2016.
- Krishnamurti, T. N., L. Stefanova, and V. Misra: Monsoons, in: *Tropical Meteorology: An Introduction*, Springer New York, New York, NY, 75-119, 2013.
- Krishnan, R., and M. Sugi: Pacific decadal oscillation and variability of the Indian summer monsoon rainfall, *Climate Dynamics*, 21, 233-242, 10.1007/s00382-003-0330-8, 2003.
- Krüger, K., S. Tegtmeier, and M. Rex: Variability of residence time in the Tropical Tropopause Layer during Northern Hemisphere winter, *Atmos. Chem. Phys.*, 9, 6717-6725, 10.5194/acp-9-6717-2009, 2009.
- Lana, A., T. G. Bell, R. Simó, S. M. Vallina, J. Ballabrera-Poy, A. J. Kettle, J. Dachs, L. Bopp, E. S. Saltzman, J. Stefels, J. E. Johnson, and P. S. Liss: An updated climatology of surface dimethylsulfide concentrations and emission fluxes in the global ocean, *Global Biogeochemical Cycles*, 25, GB1004, 10.1029/2010gb003850, 2011.
- Latif, M., F. S. Syed, and A. Hannachi: Rainfall trends in the South Asian summer monsoon and its related large-scale dynamics with focus over Pakistan, *Climate Dynamics*, 1-17, 10.1007/s00382-016-3284-3, 2016.
- Law, K. S., W. T. Sturges, D. R. Blake, N. J. Blake, J. B. Burkholder, J. H. Butler, R. A. Cox, P. H. Haynes, M. K. W. Ko, K. Kreher, C. Mari, K. Pfeilsticker, J. M. C. Plane, R. J. Salawitch, C. Schiller, B. M. Sinnhuber, R. von Glasow, N. J. Warwick, D. J. Wuebbles, and S. A. Yvon-Lewis: Halogenated Very Short-Lived Substances, in: *Scientific*

- Assessment of Ozone Depletion: 2006. Global Ozone Research and Monitoring Project - Report N. 50, World Meteorological Organization, Geneva, Switzerland, 2006.
- Lennartz, S. T., G. Krysztofciak, C. A. Marandino, B. M. Sinnhuber, S. Tegtmeier, F. Ziska, R. Hossaini, K. Krüger, S. A. Montzka, E. Atlas, D. E. Oram, T. Keber, H. Bönisch, and B. Quack: Modelling marine emissions and atmospheric distributions of halocarbons and dimethyl sulfide: the influence of prescribed water concentration vs. prescribed emissions, *Atmos. Chem. Phys.*, 15, 11753-11772, 10.5194/acp-15-11753-2015, 2015.
- Levine, J. G., P. Braesicke, N. R. P. Harris, N. H. Savage, and J. A. Pyle: Pathways and timescales for troposphere-to-stratosphere transport via the tropical tropopause layer and their relevance for very short lived substances, *Journal of Geophysical Research: Atmospheres*, 112, D04308, 10.1029/2005jd006940, 2007.
- Li, J., and Q. Zeng: A new monsoon index and the geographical distribution of the global monsoons, *Adv. Atmos. Sci.*, 20, 299-302, 10.1007/s00376-003-0016-5, 2003.
- Liang, Q., R. S. Stolarski, S. R. Kawa, J. E. Nielsen, A. R. Douglass, J. M. Rodriguez, D. R. Blake, E. Atlas, and L. E. Orr: Finding the missing stratospheric Br: a global modeling study of CHBr₃ and CH₂Br₂, *Atmos. Chem. Phys.*, 2269-2286, 2010.
- Liang, Q., E. Atlas, D. R. Blake, M. Dorf, K. Pfeilsticker, and S. Schauffler: Convective transport of very short lived bromocarbons to the stratosphere, *Atmos. Chem. Phys.*, 14, 5781-5792, 2014.
- Liss, P. S., and P. G. Slater: Flux of Gases across the Air-Sea Interface, *Nature*, 247, 181-184, 10.1038/247181a0, 1974.
- Liss, P. S., C. A. Marandino, E. E. Dahl, D. Helmig, E. J. Hints, C. Hughes, M. T. Johnson, R. M. Moore, J. M. C. Plane, B. Quack, H. B. Singh, J. Stefels, R. von Glasow, and J. Williams: Short-Lived Trace Gases in the Surface Ocean and the Atmosphere, in: *Ocean-Atmosphere Interactions of Gases and Particles*, edited by: Liss, P. S., and Johnson, M. T., Springer Berlin Heidelberg, Berlin, Heidelberg, 1-54, 2014.
- Liu, C., and E. J. Zipser: Global distribution of convection penetrating the tropical tropopause, *Journal of Geophysical Research: Atmospheres*, 110, D23104, 10.1029/2005jd006063, 2005.
- Liu, Y., S. A. Yvon-Lewis, L. Hu, J. E. Salisbury, and J. E. O'Hern: CHBr₃, CH₂Br₂, and CHClBr₂ in U.S. coastal waters during the Gulf of Mexico and East Coast Carbon cruise, *Journal of Geophysical Research: Oceans*, 116, C10004, 10.1029/2010jc006729, 2011.
- Lovelock, J. E.: Natural halocarbons in the air and in the sea, *Nature*, 256, 193-194, 10.1038/256193a0, 1975.
- Mantua, N. J., and S. R. Hare: The Pacific Decadal Oscillation, *Journal of Oceanography*, 58, 35-44, 10.1023/a:1015820616384, 2002.
- Marandino, C. A., W. J. De Bruyn, S. D. Miller, and E. S. Saltzman: Eddy correlation measurements of the air/sea flux of dimethylsulfide over the North Pacific Ocean, *Journal of Geophysical Research: Atmospheres*, 112, D03301, 10.1029/2006jd007293, 2007.
- Marandino, C. A., S. Tegtmeier, K. Krüger, C. Zindler, E. L. Atlas, F. Moore, and H. W. Bange: Dimethylsulphide (DMS) emissions from the western Pacific Ocean: a potential marine source for stratospheric sulphur?, *Atmos. Chem. Phys.*, 13, 8427-8437, 10.5194/acp-13-8427-2013, 2013.
- McGillis, W. R., J. B. Edson, J. E. Hare, and C. W. Fairall: Direct covariance air-sea CO₂ fluxes, *Journal of Geophysical Research: Oceans*, 106, 16729-16745, 10.1029/2000jc000506, 2001.
- McGivern, W. S., J. S. Francisco, and S. W. North: Investigation of the Atmospheric Oxidation Pathways of Bromoform: Initiation via OH/Cl Reactions, *The Journal of Physical Chemistry A*, 106, 6395-6400, 10.1021/jp0255886, 2002.
- Meehl, G. A.: The Tropics and Their Role in the Global Climate System, *The Geographical Journal*, 153, 21-36, 10.2307/634469, 1987.
- Meehl, G. A., and J. M. Arblaster: The Tropospheric Biennial Oscillation and Asian–Australian Monsoon Rainfall, *Journal of Climate*, 15, 722-744, 10.1175/1520-0442(2002)015<0722:ttboaa>2.0.co;2, 2002.

- Miller, S., C. Marandino, W. de Bruyn, and E. S. Saltzman: Air-sea gas exchange of CO₂ and DMS in the North Atlantic by eddy covariance, *Geophysical Research Letters*, 36, L15816, 10.1029/2009gl038907, 2009.
- Molina, M. J., and F. S. Rowland: Stratospheric sink for chlorofluoromethanes: chlorine atom-catalysed destruction of ozone, *Nature*, 249, 810-812, 1974.
- Montzka, S., S. Reimann, A. Engel, K. Kruger, W. Sturges, D. Blake, M. Dorf, P. Fraser, L. Froidevaux, and K. Jucks: Scientific assessment of ozone depletion: 2010, Global Ozone Research and Monitoring Project-Report No. 51, 2010.
- Moore, R. M., and O. C. Zafiriou: Photochemical production of methyl iodide in seawater, *Journal of Geophysical Research: Atmospheres*, 99, 16415-16420, 10.1029/94jd00786, 1994.
- Moore, R. M., C. E. Geen, and V. K. Tait: Determination of Henry's Law constants for a suite of naturally occurring halogenated methanes in seawater, *Chemosphere*, 30, 1183-1191, 10.1016/0045-6535(95)00009-W, 1995a.
- Moore, R. M., R. Tokarczyk, V. K. Tait, M. Poulin, and C. Geen: Marine phytoplankton as a natural source of volatile organohalogens, in: *Naturally-Produced Organohalogens*, edited by: Grimvall, A., and de Leer, E. W. B., Springer Netherlands, Dordrecht, 283-294, 1995b.
- Moore, R. M., M. Webb, R. Tokarczyk, and R. Wever: Bromoperoxidase and iodoperoxidase enzymes and production of halogenated methanes in marine diatom cultures, *Journal of Geophysical Research: Oceans*, 101, 20899-20908, 10.1029/96jc01248, 1996.
- Mossop, S. C.: Volcanic Dust Collected at an Altitude of 20 KM, *Nature*, 203, 824-827, 1964.
- Müller, S., P. Hoor, H. Bozem, E. Gute, B. Vogel, A. Zahn, H. Bönisch, T. Keber, M. Krämer, C. Rolf, M. Riese, H. Schlager, and A. Engel: Impact of the Asian monsoon on the extratropical lower stratosphere: trace gas observations during TACTS over Europe 2012, *Atmos. Chem. Phys.*, 16, 10573-10589, 10.5194/acp-16-10573-2016, 2016.
- Myhre, G., T. F. Berglen, C. E. L. Myhre, and I. S. A. Isaksen: The radiative effect of the anthropogenic influence on the stratospheric sulfate aerosol layer, *Tellus B*, 56, 294-299, 10.1111/j.1600-0889.2004.00106.x, 2004.
- Myhre, G., D. Shindell, F.-M. Bréon, W. Collins, J. Fuglestedt, J. Huang, D. Koch, J.-F. Lamarque, D. Lee, and B. Mendoza: Anthropogenic and natural radiative forcing, *Climate change*, 423, 658-740, 2013.
- Newell, R. E., and S. Gould-Stewart: A Stratospheric Fountain?, *Journal of the Atmospheric Sciences*, 38, 2789-2796, 10.1175/1520-0469(1981)038<2789:ASF>2.0.CO;2, 1981.
- Nightingale, P., G. Malin, C. Law, A. Watson, P. Liss, M. Liddicoat, J. Boutin, and R. Upstill-Goddard: In situ evaluation of air-sea gas exchange parameterizations using novel conservative and volatile tracers, *Global Biogeochemical Cycles*, 14, 373-387, 10.1029/1999GB900091, 2000.
- O'Dowd, C. D., J. L. Jimenez, R. Bahreini, R. C. Flagan, J. H. Seinfeld, K. Hameri, L. Pirjola, M. Kulmala, S. G. Jennings, and T. Hoffmann: Marine aerosol formation from biogenic iodine emissions, *Nature*, 417, 632-636, 2002.
- Oberlander, P. E.: Indian Ocean Dipole, *Oceanus Magazine*, Online edition, 2017.
- Oman, L. D., A. R. Douglass, R. J. Salawitch, T. P. Canty, J. R. Ziemke, and M. Manyin: The effect of representing bromine from VSLS on the simulation and evolution of Antarctic ozone, *Geophysical Research Letters*, 43, 9869-9876, 10.1002/2016gl070471, 2016.
- Ordóñez, C., J. F. Lamarque, S. Tilmes, D. E. Kinnison, E. L. Atlas, D. R. Blake, G. Sousa Santos, G. Brasseur, and A. Saiz-Lopez: Bromine and iodine chemistry in a global chemistry-climate model: description and evaluation of very short-lived oceanic sources, *Atmos. Chem. Phys.*, 12, 1423-1447, 10.5194/acp-12-1423-2012, 2012.
- Osthoff, H. D., T. S. Bates, J. E. Johnson, W. C. Kuster, P. Goldan, R. Sommariva, E. J. Williams, B. M. Lerner, C. Warneke, J. A. de Gouw, A. Pettersson, T. Baynard, J. F. Meagher, F. C. Fehsenfeld, A. R. Ravishankara, and S. S. Brown: Regional variation of the dimethyl sulfide oxidation mechanism in the summertime marine boundary layer in the Gulf of Maine, *Journal of Geophysical Research: Atmospheres*, 114, D07301, 10.1029/2008jd010990, 2009.

- Pan, L. L., S. B. Honomichl, D. E. Kinnison, M. Abalos, W. J. Randel, J. W. Bergman, and J. Bian: Transport of chemical tracers from the boundary layer to stratosphere associated with the dynamics of the Asian summer monsoon, *Journal of Geophysical Research: Atmospheres*, 121, 14,159-114,174, 10.1002/2016jd025616, 2016.
- Park, M., W. J. Randel, L. K. Emmons, and N. J. Livesey: Transport pathways of carbon monoxide in the Asian summer monsoon diagnosed from Model of Ozone and Related Tracers (MOZART), *Journal of Geophysical Research: Atmospheres*, 114, D08303, 10.1029/2008JD010621, 2009.
- Parthasarathy, B., A. A. Munot, and D. R. Kothawale: All-India monthly and seasonal rainfall series: 1871–1993, *Theoretical and Applied Climatology*, 49, 217-224, 10.1007/bf00867461, 1994.
- Penkett, S. A., B. M. R. Jones, M. J. Rycroft, and D. A. Simmons: An interhemispheric comparison of the concentrations of bromine compounds in the atmosphere, *Nature*, 318, 550-553, 1985.
- Ploeger, F., P. Konopka, R. Müller, S. Fueglistaler, T. Schmidt, J. C. Manners, J. U. Groö, G. Günther, P. M. Forster, and M. Riese: Horizontal transport affecting trace gas seasonality in the Tropical Tropopause Layer (TTL), *Journal of Geophysical Research: Atmospheres*, 117, D09303, 10.1029/2011jd017267, 2012.
- Ploeger, F., P. Konopka, K. Walker, and M. Riese: Quantifying pollution transport from the Asian monsoon anticyclone into the lower stratosphere, *Atmos. Chem. Phys.*, 17, 7055-7066, 10.5194/acp-17-7055-2017, 2017.
- Pommereau, J.-P.: Troposphere-to-stratosphere transport in the tropics, *Comptes Rendus Geoscience*, 342, 331-338, 10.1016/j.crte.2009.10.015, 2010.
- Preethi, B., M. Mujumdar, R. H. Kripalani, A. Prabhu, and R. Krishnan: Recent trends and teleconnections among South and East Asian summer monsoons in a warming environment, *Climate Dynamics*, 48, 2489–2505, 10.1007/s00382-016-3218-0, 2016.
- Pyle, J. A., M. J. Ashfold, N. R. P. Harris, A. D. Robinson, N. J. Warwick, G. D. Carver, B. Gostlow, L. M. O'Brien, A. J. Manning, S. M. Phang, S. E. Yong, K. P. Leong, E. H. Ung, and S. Ong: Bromoform in the tropical boundary layer of the Maritime Continent during OP3, *Atmos. Chem. Phys.*, 11, 529-542, 10.5194/acp-11-529-2011, 2011.
- Quack, B., and D. W. R. Wallace: Air-sea flux of bromoform: Controls, rates, and implications, *Global Biogeochemical Cycles*, 17, 1023, 10.1029/2002gb001890, 2003.
- Quack, B., E. Atlas, G. Petrick, V. Stroud, S. Schauffler, and D. W. R. Wallace: Oceanic bromoform sources for the tropical atmosphere, *Geophysical Research Letters*, 31, L23S05, 10.1029/2004gl020597, 2004.
- Quack, B., I. Peeken, G. Petrick, and K. Nachtigall: Oceanic distribution and sources of bromoform and dibromomethane in the Mauritanian upwelling, *Journal of Geophysical Research: Oceans*, 112, C10006, 10.1029/2006jc003803, 2007.
- Ramage, C. S.: *Monsoon Meteorology*, International Geophysics Series, Academic Press, San Diego, California, 296 pp., 1971.
- Randel, W. J., M. Park, L. Emmons, D. Kinnison, P. Bernath, K. A. Walker, C. Boone, and H. Pumphrey: Asian monsoon transport of pollution to the stratosphere, *Science*, 328, 611-613, 10.1126/science.1182274, 2010.
- Rex, M., I. Wohltmann, T. Ridder, R. Lehmann, K. Rosenlof, P. Wennberg, D. Weisenstein, J. Notholt, K. Krüger, V. Mohr, and S. Tegtmeier: A tropical West Pacific OH minimum and implications for stratospheric composition, *Atmos. Chem. Phys.*, 14, 4827-4841, 10.5194/acp-14-4827-2014, 2014.
- Richardson, K., J. Bendtsen, T. Kragh, and E. A. Mousing: Constraining the Distribution of Photosynthetic Parameters in the Global Ocean, *Frontiers in Marine Science*, 3, 10.3389/fmars.2016.00269, 2016.
- Roxy, M. K., K. Ritika, P. Terray, and S. Masson: The Curious Case of Indian Ocean Warming, *Journal of Climate*, 27, 8501-8509, 10.1175/jcli-d-14-00471.1, 2014.
- Roxy, M. K., K. Ritika, P. Terray, R. Murtugudde, K. Ashok, and B. N. Goswami: Drying of Indian subcontinent by rapid Indian Ocean warming and a weakening land-sea thermal gradient, *Nature Communications*, 6, 7423, 10.1038/ncomms8423, 2015.

- Roxy, M. K., A. Modi, R. Murtugudde, V. Valsala, S. Panickal, S. Prasanna Kumar, M. Ravichandran, M. Vichi, and M. Lévy: A reduction in marine primary productivity driven by rapid warming over the tropical Indian Ocean, *Geophysical Research Letters*, 43, 826-833, 10.1002/2015gl066979, 2016.
- Roy, R., A. Pratihary, G. Narvenkar, S. Mochamadkar, M. Gauns, and S. W. A. Naqvi: The relationship between volatile halocarbons and phytoplankton pigments during a *Trichodesmium* bloom in the coastal eastern Arabian Sea, *Estuarine, Coastal and Shelf Science*, 95, 110-118, 10.1016/j.ecss.2011.08.025, 2011.
- Saiz-Lopez, A., J. M. C. Plane, A. R. Baker, L. J. Carpenter, R. von Glasow, J. C. Gómez Martín, G. McFiggans, and R. W. Saunders: Atmospheric Chemistry of Iodine, *Chemical Reviews*, 112, 1773-1804, 10.1021/cr200029u, 2012.
- Saji, N. H., B. N. Goswami, P. N. Vinayachandran, and T. Yamagata: A dipole mode in the tropical Indian Ocean, *Nature*, 401, 360-363, 1999.
- Salawitch, R. J., D. K. Weisenstein, L. J. Kovalenko, C. E. Sioris, P. O. Wennberg, K. Chance, M. K. W. Ko, and C. A. McLinden: Sensitivity of ozone to bromine in the lower stratosphere, *Geophysical Research Letters*, 32, L05811, 10.1029/2004gl021504, 2005.
- Scarratt, M. G., and R. M. Moore: Production of chlorinated hydrocarbons and methyl iodide by the red microalga *Porphyridium purpureum*, *Limnology and Oceanography*, 44, 703-707, 10.4319/lo.1999.44.3.0703, 1999.
- Schneider, T., T. Bischoff, and G. H. Haug: Migrations and dynamics of the intertropical convergence zone, *Nature*, 513, 45-53, 10.1038/nature13636, 2014.
- Schott, F. A., S.-P. Xie, and J. P. McCreary: Indian Ocean circulation and climate variability, *Reviews of Geophysics*, 47, RG1002, 10.1029/2007rg000245, 2009.
- Sheng, J.-X., D. K. Weisenstein, B.-P. Luo, E. Rozanov, A. Stenke, J. Anet, H. Bingemer, and T. Peter: Global atmospheric sulfur budget under volcanically quiescent conditions: Aerosol-chemistry-climate model predictions and validation, *Journal of Geophysical Research: Atmospheres*, 120, 256-276, 10.1002/2014jd021985, 2015.
- Shi, Q., C. Marandino, G. Petrick, B. Quack, and D. Wallace: A time series of incubation experiments to examine the production and loss of CH₃I in surface seawater, *Journal of Geophysical Research: Oceans*, 119, 8242-8254, 10.1002/2014jc010223, 2014.
- Sikka, D. R., and S. Gadgil: On the Maximum Cloud Zone and the ITCZ over Indian, Longitudes during the Southwest Monsoon, *Monthly Weather Review*, 108, 1840-1853, 10.1175/1520-0493(1980)108<1840:otmzca>2.0.co;2, 1980.
- Simó, R., S. D. Archer, C. Pedrós-Alió, L. Gilpin, and C. E. Stelfox-Widdicombe: Coupled dynamics of dimethylsulfoniopropionate and dimethylsulfide cycling and the microbial food web in surface waters of the North Atlantic, *Limnology and Oceanography*, 47, 53-61, 10.4319/lo.2002.47.1.0053, 2002.
- Sinnhuber, B.-M., and S. Meul: Simulating the impact of emissions of brominated very short lived substances on past stratospheric ozone trends, *Geophysical Research Letters*, 42, 2449-2456, 10.1002/2014gl062975, 2015.
- Sinnhuber, B. M., and I. Folkins: Estimating the contribution of bromoform to stratospheric bromine and its relation to dehydration in the tropical tropopause layer, *Atmos. Chem. Phys.*, 6, 4755-4761, 10.5194/acp-6-4755-2006, 2006.
- Sinnhuber, B. M., N. Sheode, M. Sinnhuber, M. P. Chipperfield, and W. Feng: The contribution of anthropogenic bromine emissions to past stratospheric ozone trends: a modelling study, *Atmos. Chem. Phys.*, 9, 2863-2871, 10.5194/acp-9-2863-2009, 2009.
- Smythe-Wright, D., S. M. Boswell, C. H. Lucas, A. L. New, and M. S. Varney: Halocarbon and dimethyl sulphide studies around the Mascarene Plateau, *Philosophical transactions. Series A, Mathematical, physical, and engineering sciences*, 363, 169-185, 10.1098/rsta.2004.1485, 2005.
- Solomon, S., R. R. Garcia, and A. R. Ravishankara: On the role of iodine in ozone depletion, *Journal of Geophysical Research: Atmospheres*, 99, 20491-20499, 10.1029/94jd02028, 1994.

- Solomon, S., J. S. Daniel, R. R. Neely, J. P. Vernier, E. G. Dutton, and L. W. Thomason: The Persistently Variable “Background” Stratospheric Aerosol Layer and Global Climate Change, *Science*, 333, 866, 2011.
- Solomon, S., D. Kinnison, J. Bandoro, and R. Garcia: Simulation of polar ozone depletion: An update, *Journal of Geophysical Research: Atmospheres*, 120, 7958-7974, 10.1002/2015jd023365, 2015.
- Stefels, J.: Physiological aspects of the production and conversion of DMSP in marine algae and higher plants, *Journal of Sea Research*, 43, 183-197, 10.1016/S1385-1101(00)00030-7, 2000.
- Stemmler, I., M. Rothe, I. Hense, and H. Hepach: Numerical modelling of methyl iodide in the eastern tropical Atlantic, *Biogeosciences*, 10, 4211-4225, 10.5194/bg-10-4211-2013, 2013.
- Stemmler, I., I. Hense, and B. Quack: Marine sources of bromoform in the global open ocean - global patterns and emissions, *Biogeosciences*, 12, 1967-1981, 10.5194/bg-12-1967-2015, 2015.
- Takahashi, H., and Z. J. Luo: Characterizing tropical overshooting deep convection from joint analysis of CloudSat and geostationary satellite observations, *Journal of Geophysical Research: Atmospheres*, 119, 112-121, 10.1002/2013jd020972, 2014.
- Tegtmeier, S., K. Krüger, B. Quack, E. Atlas, D. R. Blake, H. Boenisch, A. Engel, H. Hepach, R. Hossaini, M. A. Navarro, S. Raimund, S. Sala, Q. Shi, and F. Ziska: The contribution of oceanic methyl iodide to stratospheric iodine, *Atmos. Chem. Phys.*, 13, 11869-11886, 10.5194/acp-13-11869-2013, 2013.
- Tegtmeier, S., F. Ziska, I. Pisso, B. Quack, G. J. M. Velders, X. Yang, and K. Krüger: Oceanic bromoform emissions weighted by their ozone depletion potential, *Atmos. Chem. Phys.*, 15, 13647-13663, 10.5194/acp-15-13647-2015, 2015.
- Tokarczyk, R., and R. M. Moore: Production of volatile organohalogenes by phytoplankton cultures, *Geophysical Research Letters*, 21, 285-288, 10.1029/94gl00009, 1994.
- Trenberth, K. E., D. P. Stepaniak, and J. M. Caron: The Global Monsoon as Seen through the Divergent Atmospheric Circulation, *Journal of Climate*, 13, 3969-3993, 10.1175/1520-0442(2000)013<3969:tgmast>2.0.co;2, 2000.
- Tzella, A., and B. Legras: A Lagrangian view of convective sources for transport of air across the Tropical Tropopause Layer: distribution, times and the radiative influence of clouds, *Atmos. Chem. Phys.*, 11, 12517-12534, 10.5194/acp-11-12517-2011, 2011.
- Van der Leun, J. C., X. Tang, and M. Tevini: Environmental effects of ozone depletion: 1994 assessment, *Ambio*, 24, 138-142, 1995.
- Vernier, J. P., J. P. Pommereau, L. W. Thomason, J. Pelon, A. Garnier, T. Deshler, J. Jumelet, and J. K. Nielsen: Overshooting of clean tropospheric air in the tropical lower stratosphere as seen by the CALIPSO lidar, *Atmos. Chem. Phys.*, 11, 9683-9696, 10.5194/acp-11-9683-2011, 2011.
- Vogel, B., G. Günther, R. Müller, J. U. Groß, and M. Riese: Impact of different Asian source regions on the composition of the Asian monsoon anticyclone and on the extratropical lowermost stratosphere, *Atmos. Chem. Phys.*, 15, 13699-13716, 10.5194/acpd-15-13699-2015, 2015.
- Vogt, R., R. Sander, R. von Glasow, and P. J. Crutzen: Iodine Chemistry and its Role in Halogen Activation and Ozone Loss in the Marine Boundary Layer: A Model Study, *Journal of Atmospheric Chemistry*, 32, 375-395, 10.1023/a:1006179901037, 1999.
- Walker, G. T.: Correlation in seasonal variations of weather, IX. A further study of world weather, *Memoirs of the India Meteorological Department*, 24, 275-333, 1924.
- Wang, B., and Z. Fan: Choice of South Asian Summer Monsoon Indices, *Bulletin of the American Meteorological Society*, 80, 629-638, 10.1175/1520-0477(1999)080<0629:cosasm>2.0.co;2, 1999.
- Wang, B., R. Wu, and K. M. Lau: Interannual Variability of the Asian Summer Monsoon: Contrasts between the Indian and the Western North Pacific–East Asian Monsoons, *Journal of Climate*, 14, 4073-4090, 10.1175/1520-0442(2001)014<4073:ivotas>2.0.co;2, 2001.

- Wang, B., and Q. Ding: Changes in global monsoon precipitation over the past 56 years, *Geophysical Research Letters*, 33, n/a-n/a, 10.1029/2005gl025347, 2006.
- Wanninkhof, R., W. E. Asher, D. T. Ho, C. Sweeney, and W. R. McGillis: Advances in Quantifying Air-Sea Gas Exchange and Environmental Forcing, *Annual Review of Marine Science*, 1, 213-244, 10.1146/annurev.marine.010908.163742, 2009.
- Warwick, N. J., J. A. Pyle, G. D. Carver, X. Yang, N. H. Savage, F. M. O'Connor, and R. A. Cox: Global modeling of biogenic bromocarbons, *Journal of Geophysical Research: Atmospheres*, 111, D24305, 10.1029/2006jd007264, 2006.
- Webster, P. J.: The elementary monsoon, *Monsoons*, edited by: Fein, J. S., and Stephens, P. L., John Wiley & Sons, 1987.
- Webster, P. J., and S. Yang: Monsoon and Enso: Selectively Interactive Systems, *Quarterly Journal of the Royal Meteorological Society*, 118, 877-926, 10.1002/qj.49711850705, 1992.
- Webster, P. J., and J. Fasullo: Monsoon: Dynamical Theory, *Encyclopedia of Atmospheric Sciences*, edited by: Holton, J., and Curry, J., Academic Press, 1370-1391 pp., 2003.
- WMO: Scientific Assessment of Ozone Depletion: 2014, World Meteorological Organization, Global Ozone Research and Monitoring Project - Report No. 55, Geneva, Switzerland, 416 pp., 2014.
- Wofsy, S. C., M. B. McElroy, and Y. L. Yung: The chemistry of atmospheric bromine, *Geophysical Research Letters*, 2, 215-218, 10.1029/GL002i006p00215, 1975.
- Wright, J. S., R. Fu, S. Fueglistaler, Y. S. Liu, and Y. Zhang: The influence of summertime convection over Southeast Asia on water vapor in the tropical stratosphere, *Journal of Geophysical Research: Atmospheres*, 116, D12302, 10.1029/2010jd015416, 2011.
- Yamamoto, H., Y. Yokouchi, A. Otsuki, and H. Itoh: Depth profiles of volatile halogenated hydrocarbons in seawater in the Bay of Bengal, *Chemosphere*, 45, 371-377, 10.1016/S0045-6535(00)00541-5, 2001.
- Yang, M., R. Beale, T. Smyth, and B. Blomquist: Measurements of OVOC fluxes by eddy covariance using a proton-transfer-reaction mass spectrometer – method development at a coastal site, *Atmos. Chem. Phys.*, 13, 6165-6184, 10.5194/acp-13-6165-2013, 2013.
- Yang, X., R. A. Cox, N. J. Warwick, J. A. Pyle, G. D. Carver, F. M. O'Connor, and N. H. Savage: Tropospheric bromine chemistry and its impacts on ozone: A model study, *Journal of Geophysical Research: Atmospheres*, 110, D23311, 10.1029/2005jd006244, 2005.
- Yang, X., N. L. Abraham, A. T. Archibald, P. Braesicke, J. Keeble, P. J. Telford, N. J. Warwick, and J. A. Pyle: How sensitive is the recovery of stratospheric ozone to changes in concentrations of very short-lived bromocarbons?, *Atmos. Chem. Phys.*, 14, 10431-10438, 10.5194/acp-14-10431-2014, 2014.
- Yokouchi, Y., F. Hasebe, M. Fujiwara, H. Takashima, M. Shiotani, N. Nishi, Y. Kanaya, S. Hashimoto, P. Fraser, D. Toom-Sauntry, H. Mukai, and Y. Nojiri: Correlations and emission ratios among bromoform, dibromochloromethane, and dibromomethane in the atmosphere, *Journal of Geophysical Research: Atmospheres*, 110, D23309, 10.1029/2005jd006303, 2005.
- Zavarsky, A., D. Booge, A. Fiehn, K. Krüger, E. Atlas, and C. A. Marandino: The influence of air-sea fluxes on atmospheric aerosols during the summer monsoon over the Indian Ocean, *Geophysical Research Letters*, under review at GRL.
- Zindler, C., A. Bracher, C. A. Marandino, B. Taylor, E. Torrecilla, A. Kock, and H. W. Bange: Sulphur compounds, methane, and phytoplankton: interactions along a north-south transit in the western Pacific Ocean, *Biogeosciences*, 10, 3297-3311, 10.5194/bg-10-3297-2013, 2013.
- Ziska, F., B. Quack, K. Abrahamsson, S. D. Archer, E. Atlas, T. Bell, J. H. Butler, L. J. Carpenter, C. E. Jones, N. R. P. Harris, H. Hepach, K. G. Heumann, C. Hughes, J. Kuss, K. Krüger, P. Liss, R. M. Moore, A. Orlikowska, S. Raimund, C. E. Reeves, W. Reifenhäuser, A. D. Robinson, C. Schall, T. Tanhua, S. Tegtmeier, S. Turner, L. Wang, D. Wallace, J. Williams, H. Yamamoto, S. Yvon-Lewis, and Y. Yokouchi: Global sea-to-air flux climatology for bromoform, dibromomethane and methyl iodide, *Atmos. Chem. Phys.*, 13, 8915-8934, 10.5194/acp-13-8915-2013, 2013.

Ziska, F., B. Quack, S. Tegtmeier, I. Stemmler, and K. Krüger: Future emissions of marine halogenated very-short lived substances under climate change, *Journal of Atmospheric Chemistry*, 74, 245-260, 10.1007/s10874-016-9355-3, 2017.

6 List of Figures

Figure 1: Schematic of the Hadley circulation.	6
Figure 2: Annual range and global monsoon domain after the definition of Wang et al. (2006).	7
Figure 3: Schematic of the major circulation of the surface winds, the Hadley cell, and the jets of the Indian summer monsoon (after Meehl, 1987).	8
Figure 4: ERA-Interim monthly fields for July 2014 at 100 hPa for (a) geopotential height anomaly with wind arrows and (b) zonal wind speed with geopotential height anomaly contours.	9
Figure 5: Annual shift of main rainfall and surface winds over the Indian Ocean. The red line marks the ITCZ (Schneider et al., 2014).	9
Figure 6: (a) West Pacific SST, Walker cell and upwelling during ENSO neutral conditions. (b) West Pacific SST anomalies, Walker cells and reduced upwelling during El Niño conditions (Christensen et al., 2013).	11
Figure 7: Time series of All-Indian Summer (JJA) monsoon rainfall and ENSO events (Kothawale et al., 2016).	12
Figure 8: Sea surface temperature anomalies and rainfall patterns during positive and negative Indian Ocean Dipole events (Illustration by Paul E. Oberlander, 2017, Woods Hole Oceanographic Institution).	13
Figure 9: Schematic of vertical transport pathways in the tropics (Bergman et al., 2012).	15
Figure 10: The vertical conduit of boundary layer air masses to the Asian monsoon anticyclone (after Bergman et al., 2013).	16
Figure 11: Indian Ocean currents during boreal summer partaking in the equatorial roll circulation and areas of upwelling (green) and downwelling (blue) (Schott et al., 2009).	17
Figure 12: Two layer model of air-sea gas exchange from Liss et al. (1974), displayed in Wanninkhof et al. (2009).	20
Figure 13: Annual tropical ($\pm 20^\circ$) atmospheric lifetime profiles of (a) CHBr_3 and (b) CH_2Br_2 calculated from a chemistry transport model (Hossaini et al., 2010).	24
Figure 14: The contribution of different chlorinated and brominated source gases to stratospheric halogen for 1996 and 2012 (WMO, 2014).	27
Figure 15: Total stratospheric bromine measurements and estimated contribution of CH_3Br , Halons, and VSLs bromine (update from Dorf et al., 2006; in Carpenter et al., 2014).	28

7 List of Tables

Table 1: Tropical atmospheric lifetimes of VSLS at different altitudes for halogenated VSLS (Carpenter et al., 2014) and for DMS (Barnes et al., 2006; Osthoff et al., 2009).	24
Table 2: Delivery of bromine, iodine, and sulfur from VSLS to the stratosphere.....	25
Table 3: VSLS emissions from the annual mean update of the climatology from Ziska et al. (2013) for the halocarbons and from Lana et al. (2011) monthly emissions for DMS.....	177
Table 4: VSLS emissions from the Indian Ocean from Table 3 and their mass entrained above the CPT between 30°S and 30°N in 2014 calculated with FLEXPART/ERA-Interim plus the transport efficiency.....	179

8 List of Abbreviations

AIRI	All-India Rainfall Index
AMA	Asian monsoon anticyclone
BrO	Bromine monoxide
Bry	Reactive bromine
BRyVLSL	Reactive bromine from VLSL
c_a	Concentration in air
CFC	Chlorofluorocarbon
CHBr ₃	Bromoform
CHBrCl ₂	Bromodichloromethane
CHBr ₂ Cl	Dibromochloromethane
CH ₂ Br ₂	Dibromomethane
CH ₂ BrCl	Bromochloromethane
CH ₂ I	Iodomethanide radical
CB _{r2} O	Carbonyl dibromide
CHBrO	Formyl bromide
CH ₃ Br	Methyl bromide
CH ₃ Cl	Methyl chloride
CH ₃ I	Methyl iodide
Chl <i>a</i>	Chlorophyll a
CO ₂	Carbon dioxide
c_w	Concentration in water
DMI	Dipole Mode Index
DMS	Dimethylsulfide
DMSP	dimethylsulfoniopropiate
DOAS	Doppler Optical Absorption Spectroscopy
EACC	East African Coastal Current
EIMR	Extended Indian Monsoon Rainfall

ENSO	El Niño – Southern Oscillation
F	Flux
H	Henry's constant
HBr	Hydrobromic acid
HOBr	Hypobromous acid
H ₂ SO ₄	Sulfuric acid
IMI	Indian Monsoon Index
IOD	Indian Ocean Dipole
IO	Iodine oxide
IOx	Reactive Iodine
ITF	Indonesian Throughflow
ITCZ	Intertropical Convergence Zone
<i>k</i>	Transfer velocity
<i>k_w</i>	Transfer velocity from water side
<i>k₆₀₀</i>	Transfer velocity for a Schmidt Number of 600
MSA	Methyl sulfonic acid
NEMC	Northeast Madagascar Current
OCS	Carbonyl sulfide
ODS	Ozone depleting substance
OH	Hydroxyl radical
OVOC	Oxygenated volatile organic compounds
PDO	Pacific Decadal Oscillation
PGI	Product gas injection
Sc	Schmidt Number
SC	Somali Current
SE	Southeast
SEC	South Equatorial Current
SECC	South Equatorial Counter Current
SEMC	Southeast Madagascar Current

SGI	Source gas injection
SJ	Subtropical Jet
SO ₂	Sulfur dioxide
SST	Sea surface temperature
SW	Southwest
TBO	Tropical Biennial Oscillation
TEJ	Tropical Easterly Jet
TTL	Tropical tropopause layer
UTLS	Upper troposphere-lower stratosphere
UV	ultraviolet
U10	Horizontal wind speed at 10m
VSLs	Very short-lived substance
WMO	World Meteorological Organization
WYI	Webster-Yang Index

Curriculum Vitae

Alina Fiehn

25.03.1989, Kiebitzweg 10, 30900 Wedemark, Germany
+4917699330849, alina.fiehn@gmail.com, Deutsch

Education

- 2014 – 2017 **Ph.D. student in Meteorology**
University of Oslo, Norway, and
GEOMAR Helmholtz-Centre for Ocean Research together with
Christian-Albrechts-University Kiel, both Germany
- 2012 - 2014 **Meteorology (M.Sc.)**
Leibniz University Hannover, Germany
- 2008 - 2012 **Meteorology (B.Sc.)**
Leibniz University Hannover, Germany
- 2008 **Abitur**, Gymnasium Mellendorf, Niedersachsen, Germany

Research Cruises

- 10/2015 SO243 ASTRA-OMZ, RV Sonne
Guayaquil (Ecuador) – Antofagasta (Chile)
- 07-08/2014 SO235 OASIS, RV Sonne
Pt. Louis (Mauritius) – Malé (Maldives)
- 07/2014 SO234-2 SPACES, RV Sonne
Durban (South Africa) – Pt. Louis (Mauritius)

List of Publications

Peer- reviewed

Fuhlbrügge, S., B. Quack, E. Atlas, **A. Fiehn**, H. Hepach, K. Krüger: Meteorological constraints on oceanic halocarbons above the Peruvian upwelling; Atmos. Chem. Phys., 16, 12205-12217, doi:10.5194/acp-16-12205-2016, 2016.

Fiehn, A., B. Quack, H. Hepach, S. Tegtmeier, S. Fuhlbrügge, M. Toohey, E. Atlas, K. Krüger: Delivery of halogenated very short-lived substances from the west Indian Ocean to the stratosphere during the Asian summer monsoon; Atmos. Chem. Phys., 17, 6723-6741, <https://doi.org/10.5194/acp-17-6723-2017>, 2017.

Under review

Zavarsky, A.; Booge, D.; **Fiehn, A.**; Krüger, K.; Atlas, E.; and Marandino, C.: The influence of air-sea fluxes on atmospheric aerosols during the summer monsoon over the Indian Ocean, under review at Geophysical Research Letters.

Fiehn, A.; Quack, B.; Marandino, C. A.; Krüger, K.: Variability of VSLS transport from the West Indian Ocean to the stratosphere, under review at Journal of Geophysical Research: Atmospheres.

In preparation

Fiehn, A.; Quack, B.; Stemmler, I.; Ziska, F.; and Krüger, K.: Influence of seasonally resolved emissions on the transport of bromoform from the Indian Ocean to the stratosphere, Atmos. Chem. Phys., in preparation.

Danksagung

Zuallererst möchte ich meinen Betreuerinnen Prof. Dr. Kirstin Krüger und Dr. Birgit Quack für die Möglichkeit danken, dieses spannende wissenschaftliche Thema zu bearbeiten. Euch habe ich die Teilnahme an zwei Forschungsfahrten auf FS Sonne, fünf internationalen Konferenzen, einem Lehrgang in Korea und damit verbundene Reisen auf vier Kontinente zu verdanken. Ihr habt mich auf dem ganzen Weg begleitet, vom Konzipieren der Experimente, über das Ausarbeiten der Ergebnisse bis zum Verfassen der Manuskripte. Besonders Kicki gilt mein Dank für den Aufbau der Kooperation zwischen den Universitäten in Kiel und Oslo, die mir ein erlebnisreiches Jahr im wundervollen Oslo ermöglicht hat. Danke außerdem an Prof. Dr. Christa Marandino, meiner Betreuerin an der Uni Kiel, für ihren hilfreichen Beitrag zu den ISOS-Treffen mit Kicki und Birgit, die Beantwortung meiner Fragen zu DMS und das Lesen und Bewerten der Doktorarbeit. Weiterhin danke ich Dr. Susann Tegtmeier für die Hilfe bei der Flexpart Installation, Anpassung, und Auswertung der Daten, Dr. Steffen Fuhlbrügge für Tipps und Matlab-Skripte zu Radio-, Ozonsonden und ERA-Interim Daten, Dr. Irene Stemmler für die Skalierung und Bereitstellung von Modelldaten und Dr. Helmke Hepach für Beratung über Halocarbons und den Ozean. Danke an die Mannschaft und die Wissenschaftler der Sonne Expeditionen SPACES, OASIS, und ASTRA-OMZ.

Für mein soziales Wohlergehen muss ich zuallererst den „Freunden der Sonne“ danken. Alex, Dennis, Gesa, Helmke, Matthias, Sinikka und Steffen haben mich auf unserem OASIS-Abenteuer sofort in ihre Mitte aufgenommen und seitdem vergeht kaum ein Tag ohne neue Nachrichten in unserer WhatsApp-Gruppe. Durch euch habe ich mich in Kiel sofort heimisch gefühlt und konnte mir sicher sein, immer jemanden für Superbowl, Grillen, Segeln, Yoga, Strand, Rugby, das Freitagsbier und gemeinsame Spieleabende zu finden. Danke auch an die noch nicht erwähnten Bürogefährten aus der HPA (Annette, Cathleen, Meike und Nils) und ihre Kinder, Männer und Frauen für Urlaube, Nudelabende, Kindergeburtstage und viele schöne Stunden. Ich danke der gesamten Chemischen Ozeanografie Abteilung des GEOMAR Kiel für zwei gesellige Jahre an der Kieler Förde und der Section for Meteorology and Oceanography an der Uni Oslo für das angenehme Arbeitsklima.

Some more girls have to be thanked: Jen for sharing the apartment in Kiel and Sara for sharing offices in Oslo, as well as Moa, Marta, Ada, Eli, Inger-Helene, and Christine for “fika”-breaks and “Kasbah”-evenings. I enjoyed living and working with awesome and inspiring people like you. Thanks to geo-football for lots of fun on and off the court.

I would like to thank the IT support of Geomar and UiO, the FLEXPART development team, ECMWF, Notur/Norstore and the projects I received funding from: OASIS and StratoClim.

Schlussendlich gilt mein Dank meiner Familie und Nils: Danke, dass ich mich immer auf eure Unterstützung, eure Hilfe und euren Glauben an mich verlassen konnte.

Eidesstattliche Erklärung

Hiermit erkläre ich, dass ich die vorliegende Dissertation, abgesehen von der Beratung durch meine Betreuer, unter Einhaltung der Regeln guter wissenschaftlicher Praxis der Deutschen Forschungsgemeinschaft selbstständig und ohne Zuhilfenahme unerlaubter Hilfsmittel erarbeitet und verfasst habe. Alle wörtlichen und inhaltlichen Zitate wurden als solche gekennzeichnet.

Diese Arbeit hat weder ganz noch in Teilen an anderer Stelle im Rahmen eines Prüfungsverfahrens vorgelegen.

Kiel, Oktober 2017

(Alina Fiehn)